UNIVERSITÀ DEGLI STUDI DI GENOVA

Dipartimento di Neuroscienze, Riabilitazione, Oftalmologia, Genetica e Scienze Materno-Infantili (DINOGMI)

Dottorato di Ricerca in

SCIENZE PEDIATRICHE

Curriculum

MALATTIE MUSCOLARI, NEURODEGENERATIVE E METABOLICHE DELL'ETÀ EVOLUTIVA

Ciclo XXXIV

The role of inflammation on disease progression in alpha sarcolgycan-related limb girdle muscular dystrophy (LGMDR3): new insights from human histological analysis and *in vivo* studies on Sgca-null mice.

Candidato:

Dott.ssa Chiara Panicucci

Relatore:

Prof. Claudio Bruno

Summary

Summary

Limb Girdle Muscular Dystrophy R3 (LGMDR3), previously known as LGMD2D, is a rare autosomal recessive primary myopathy, clinically characterized by progressive involvement of the pelvic and shoulder girdles, and genetically by mutations in the α-sarcoglycan gene (*SGCA*) coding for α-sarcoglycan (SG). The clinical course of LGMDR3 presents a great variability, ranging from severe form with onset in the first decade of life and rapid progression, to milder form with later onset.

Currently, physical therapy and prevention of secondary cardiac, pulmonary or orthopedic complications are the only possible care interventions and no disease-specific therapies are yet available.

As other muscular dystrophies, LGMDR3 muscle histology is characterized by myofiber necrosis and regeneration, reactive fibrosis, and inflammatory infiltrates. However, to date, no data exploring the role of immune response on disease progression have been published.

The primary objective of this PhD thesis was therefore to deepen the contribution of inflammatory processes to the severity of α-sarcoglycanopathy.

AIM1. -to correlate the inflammatory infiltrates extension with the age at onset, the clinical severity, and the muscle involvement at MRI, in a cohort of patients followed at Istituto Giannina Gaslini, Genova

In a cohort of 8 LGMDR3 patients, we characterized the clinical course, the MRI muscle pattern, and the histological parameters, focusing on inflammatory features. Overall, our data on muscle biopsies showed a high variable degree of the immune response, and a correlation was found between the degree of inflammation and the severity of the disease.

AIM2.-to immunophenotype the composition of muscular immune infiltrates in different sarcoglycanopathies and verify whether differences would be detectable between distinct subtypes of sarcoglycan-related LGMDs

In a multicenter study involving Italian tertiary centers for neuromuscular disorders, we analysed muscle expression of inflammatory markers in two forms of sacoglycanopathies LGMDR3 and LGMDR5, the latter due to deficiency of γ-sarcoglycan. A consistent involvement of the immune response was detected in both the diseases, that shared an abnormal expression of MHCI, and a comparable composition of the muscular

immune infiltrates.

AIM3.-to study the *in vivo* effect of anti-purinergic molecules on disease progression in the Sgca null mouse

In two pre-clinical studies, we explored the role of the P2X7 receptor, a ionotrophic receptor involved in the inflammasome pathway which mediates the release of pro-inflammatory cytokines, in a mouse model lacking the α-sarcoglycan gene (Sgca-null). Mice treated with two different molecules that antagonize P2X7 receptor activity, showed improvements in functional muscle performance, biochemical, and histological parameters, by reducing muscle fibrosis and inflammation.

In sum, from these studies, inflammation emerges as a crucial player of α-sarcoglycanopathy disease progression, and we therefore suggest that a fine-tune immunomodulatory regimen should be offered to LGMDR3 patients, especially considered the emerging disease specific gene-therapy. In this scenario, selective P2X7 antagonists could represent candidates for a combination therapy to endorse the efficacy of gene therapy by dampening the basal muscular inflammation.

Sommario

La Distrofia Muscolare dei Cingoli da difetto di alfa-sarcoglicano (LGMD2D) è una rara malattia muscolare ad ereditarietà autosomica recessiva, caratterizzata da una progressiva debolezza ed ipotrofia della muscolatura dei cingoli, e geneticamente da mutazioni nel gene alfa-sarcoglicano (*SGCA*), che codifica per l'omonima proteina (α-SG). Il quadro clinico è molto variabile, con uno spettro fenotipico che comprende sia casi ad esordio precoce e progressione rapida, che casi più lievi. Al momento attuale le uniche terapie utilizzabili sono terapie di supporto volte alla prevenzione di complicanze secondarie di tipo cardiologico, respiratorio ed ortopedico, ed una cura specifica per la patologia non è disponibile.
Come in altre distrofie muscolari, il quadro istologico della LGMDR3 è caratterizzato dalla presenza di necrosi e rigenerazione delle fibre muscolari, fibrosi e infiltrazione del tessuto muscolare da parte di cellule infiammatorie. Tuttavia il ruolo della componente infiammatoria nella progressione della LGMDR3 non è noto.

Scopo principale di questa Tesi di Dottorato è stato indagare la rilevanza della risposta immunitaria nel determinare la gravità e la progressione di malattia nella sarcoglicanopatia da deficit di α-sarcoglicano.

AIM1. – correlare l'estensione degli infiltrati infiammatori a livello muscolare con l'età di esordio della malattia, la severità clinica e il pattern di interessamento muscolare alla RMN, in una coorte di pazienti LGMDR3 afferenti all'Isituto Giannina Gaslini di Genova

In una coorte di LGMDR3, abbiamo caratterizzato la severità clinica della malattia, il grado del coinvolgimento muscolare misurato con RMN, e la gravità del quadro bioptico, focalizzando l'attenzione su parametri istologici di infiammazione. L'analisi istologica, ha evidenziato una grande variabilità della risposta infiammatoria, ed è stato possibile identificare una correlazione tra l'entità dell'infiltrato infiammatorio e la severità clinica.
AIM2.- caratterizzare la composizione degli infiltrati infiammatori in due tipi di sarcoglicanopatia (LGMDR3 e LGMDR5), evidenziando eventuali differenze tra le diverse forme

Nell'ambito di uno studio multicentrico che ha coinvolto differenti centri neuromuscolari italiani di terzo livello, abbiamo analizzato l'espressione di alcuni

marcatori di infiammazione a livello muscolare in due forme di sarcoglicanopatia. Abbiamo trovato un consistente coinvolgimento della risposta infiammatoria in entrambe le patologie, LGMD R3 e R5, che condividono una aumentata espressione di molecole MHC di classe 1 e una simile composizione degli infiltrati infiammatori muscolari.
AIM3.-verifica dell'efficacia di molecole antagoniste dei recettori purinergici, ad azione anti infiammatoria, sull'andamento della malattia nel modello animale di LGMDR3 (Sgca null)

Abbiamo esplorato il ruolo del recettore purinergico P2X7, un recettore ionotropico coinvolto nell'attivazione del pathway dell'inflammasoma e nel rilascio finale di citochine pro-infiammatorie, in un modello animale di LGMDR3 (Sgca null). Il trattamento con due differenti antagonisti del P2X7 ha dimostrato la loro efficacia nel migliorare misure di outcome funzionale, aspetti biochimici e parametri istologici, riducendo la fibrosi e l'infiammazione muscolare.

In conclusione, questi studi dimostrano come l'infiammazione giochi un ruolo cruciale nella progressione della distrofia muscolare da deficit di α-sarcoglicano, suggerendo che i pazienti affetti da questa forma di distrofia potrebbero beneficiare di un regime immunomodulatorio, soprattutto in previsione di trial di terapia genica dedicati alla LGMDR3. In questo contesto, gli antagonisti del recettore P2X7 potrebbero rappresentare una strategia terapeutica per aumentare l'efficacia della terapia genica, grazie ad un miglioramento dell'omeostasi muscolare dovuto alla loro azione antinfiammatoria.

1. Introduction

1.1 Limb girdle muscular dystrophy due to alpha-sarcoglycan gene deficiency (LGMD R3)

Clinical features

Muscular dystrophies are rare, genetically inherited disorders, characterized by a wide spectrum of clinical presentations. Duchenne Muscular Dystrophy (DMD), a severe muscular dystrophy leading to loss of ambulation within the first decade, was the first muscular dystrophy described in 1852 [1, 2] and, in association with its milder form, Becker Muscular Dystrophy (DMB), accounts for the two-thirds of muscular dystrophies.

About a century later, other primary myopathies, described as Duchenne-like muscular dystrophies, were reported, affecting both males and females, and with an autosomal inheritance [3].

The identification of pathogenic mutations on the dystrophin (*DYS*) gene as the genetic cause for DMD and DMB [4], shed light to the definition of a dystrophin associated protein complex (DAPC) (Figure 1). Further analysis of the DAPC components led to the identification of the four sarcoglycan proteins, the α-, β-, δ- and ɣ-sarcoglycan, encoded respectively by four different sarcoglycan genes, *SGCA*, *SGCB, SGCD* and *SGCG*. Pathological mutations in α- sarcoglycan [5], β- sarcoglycan [6], δ- sarcoglycan [7], and ɣ-sarcoglycan [8], have been firstly reported in the 1990s, associated to autosomal recessive proximal muscular dystrophies, thus identifying the sarcoglycanopathies as a clinical entity.

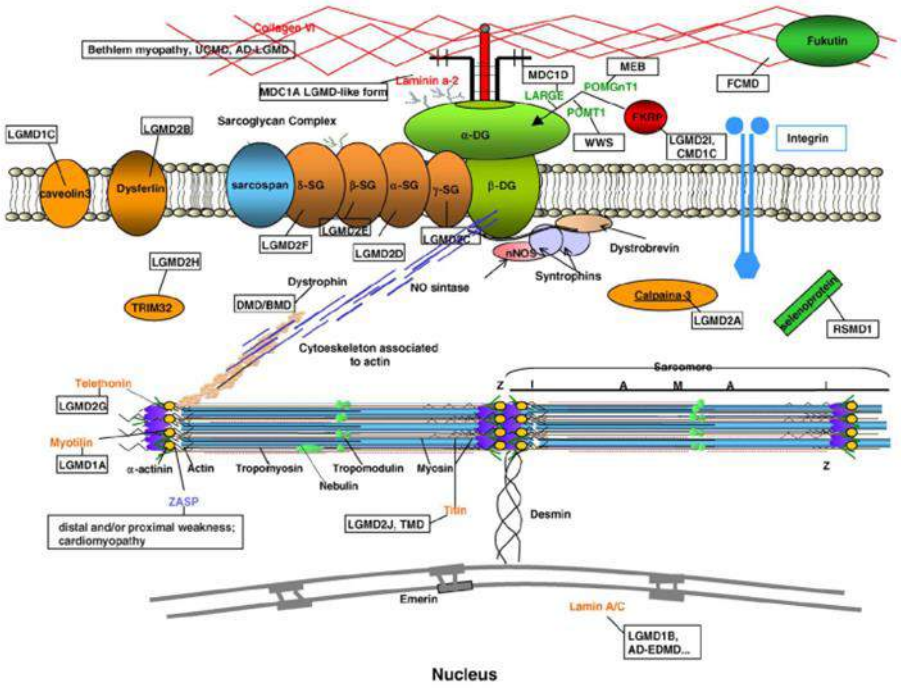

Figure 1. Molecular organisation of the dystrophin-associated glycoprotein complex (DAPC) in skeletal muscle. Dystrophin binds to cytoskeletal F-actin and associates with several proteins of the DGC, including the sarcoglycan complex. The DAPC stabilises the cell membrane during cycle of muscle contraction and relaxation.

Sarcoglycanopathies (LGMDR3–6; LGMD2D–F), as a group, represent the third most common cause of recessive muscular dystrophies after calpainopathies and dysferlinopathies [9-11].

The prevalence of the different subtypes of sarcoglycanopathy varies according to geographic region. LGMD2D/LGMD R3 α-sarcoglycan-related is the most common sarcoglycanopathy in US, Brazil, Europe, and China, with a prevalence per 100000 abitants ranging from 0.07 to 0.13, whereas the second common sarcoglycanopathy is variably represented by LGMD2C/LGMD R5-y-sarcoglycan- or LGMD2E/LGMD R4 β-sarcoglycan-related depending on different series reports [11-13]. Contrarily with the above, in the Iranian and Indian populations, LGMD2E/LGMD R4 β-sarcoglycan- and the LGMD2C/LGMD R5 y-sarcoglycan-related respectively are the most frequent sarcoglycanopathies [14, 15]. LGMD2F/LGMD R6 δ-sarcoglycan-related is the less frequent sarcoglycanopathy in all series, despite the region and etnicity.

Since sarcoglycans were discovered in 1990s, several studies reported the clinical features in cohorts of sarcoglycan deficient patients [16-20]. The clinical presentation of sarcoglycanopathies is characterized by a progressive muscle weakness, that primarily

affects the proximal skeletal muscles, and the clinical course ranges from cases with a severe childhood-onset, resulting in loss of ambulation in the first decades, to rarer cases of asymptomatic hyperCKemia or exercise-induced myalgia and myoglobinuria [11-13, 21-25] (Figure 2).

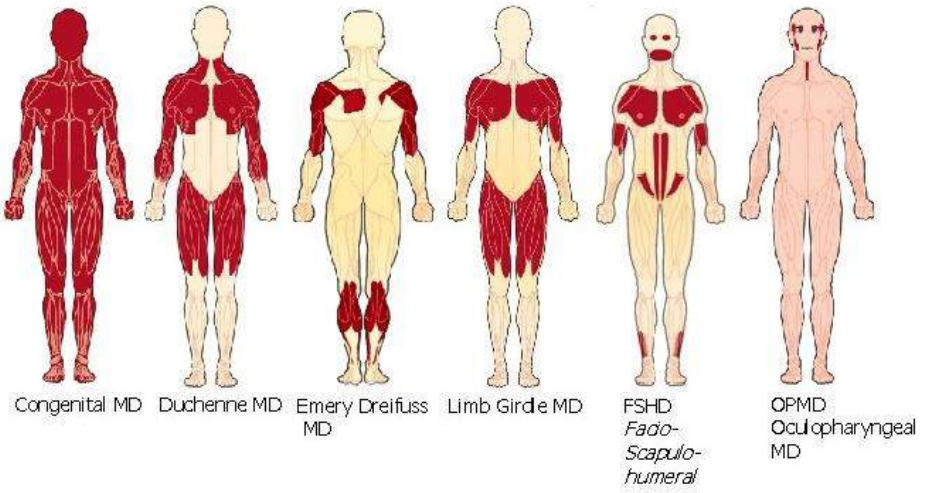

11 34

Figure 2. Patterns of initial muscular weakness in different muscular dystrophies. In Limb Girdle Muscular Dystrophies, girdle muscles are primarly affected.

A correlation between reduction of sarcoglycans level and disease severity was observed in LGMDR3–6 patients, indicating that disease severity may be predicted by residual sarcolgycan expression at muscle biopsy in these patients [17] (further explored in the following paragraph "Histological Findings").

Within sarcoglycanopathies, LGMD2D/LGMDR3 α-sarcoglycan-related (henceforth LGMDR3) represents the most clinically heterogeneous form, and it is often reported as the mildest sarcoglycanopathy [13, 16-18]. The age at onset in LGMDR3 patients, around the 10th year of age, is later than in other sarcolgycanopathies (5.8 years for LGMDR4 and R5) [13, 26]. In LGMD R3 patients, the most common symptom at onset is proximal lower legs (44%) or upper limbs weakness (18%), or hyperckemia (20%), and loss of ambulation (LOA) occurs at a median age of 18 years. An earlier LOA, before the age of 18, has been associated with a precocious onset of the disease, earlier than 10 years. Cardiac involvement is described in 10% of patients at an average age of 34 years and respiratory support is required in 27% of LGMDR3 patients at a median age of 29 years [13].

A specific muscular MRI pattern has been identified in sarcoglycanopathies, although it

was not possible to highlight differencies among the different subtypes of sarcoglycan deficiencies [27]. MRI data in LGMDR3s reflected the clinical heterogeneity of this disorder, with 13% presenting normal lower limb MRI and 5% showing only minor changes. In patients with overt muscle MRI abnormalities, the overall involvement was symmetrical. Adductor magnus was the most frequently and severely affected muscle, followed by adductor longus, vastus intermedius, biceps femoris long head and semimembranosus. In the posterior thigh, semitendinosus was more affected than semimembranosus only in two patients. Among the vasti muscles, vastus intermedius was the most severely involved, followed by vastus medialis and lateralis. Sartorius and gracilis were the most spared muscles. Lower leg was not significantly involved until loss of ambulation occurs, and it was always less affected than pelvis and thigh. The sparing of the distal quadriceps also seemed to be very specific for LGMDR5–R6 and not reported elsewhere (Figure 3).

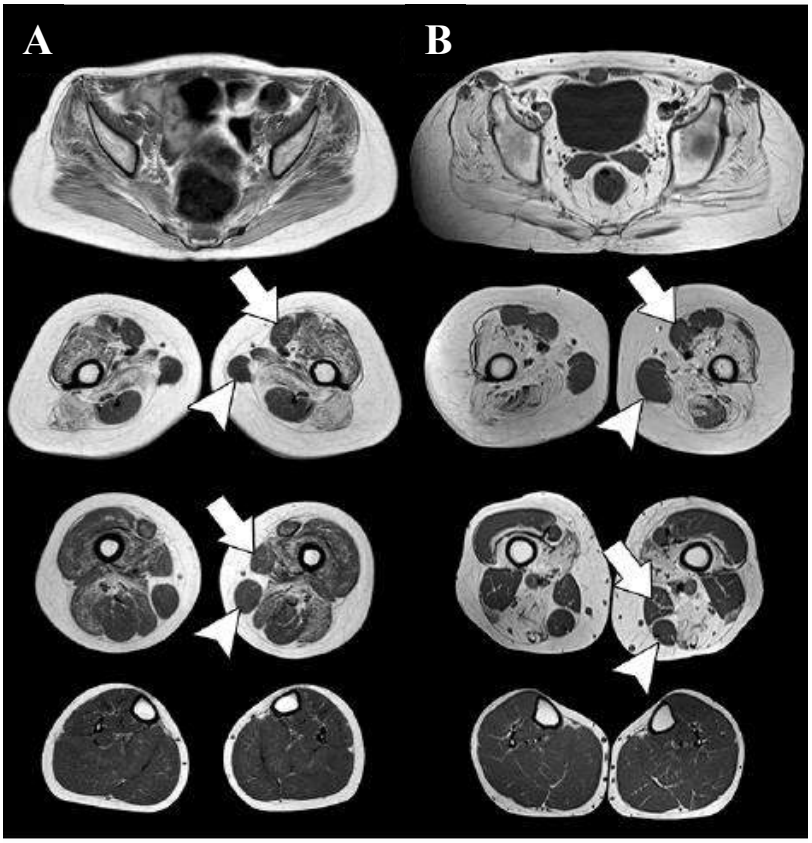

Figure 3. Representative T1-weighted muscle MRI performed in LGMDR3 patients at 11 and 34 years of age. Glutei muscles are involved, as well as proximal quadriceps and posterior thigh. Lower leg remains spared even when the thigh and pelvis are significantly affected, and sartorius and gracilis (arrow and arrowhead) may show relative hypertrophy. Adapted from [27].

Histological features

The four sarcoglycan proteins (SG), form a tetrameric complex on the sarcolemma. Together with other two complexes, (i) syntrophin, nNOS, and dystrobrevin, and (ii) α-dystroglycan and β-dystroglycan [28, 29], sarcoglycans take part to the DAPC, that sustains sarcolemmal integrity during muscle contraction, providing a molecular link between the actin cytoskeleton and the extracellular matrix in muscle cells. Mutations in any of the DAPC member, including sarcoglycans, induce a disruption of the whole DAPC, thereby producing a common histological pattern, "dystrophic pattern", i.e. wide range variation in fiber size (10-100um), excess internal nuclei, muscle fiber necrosis, inflammation and replacement of muscle with fibro-adipose tissue (Figura 4). Depending on the missing protein, the relative abundance of these features can vary, as well as the severity and the extension of the histological changes.

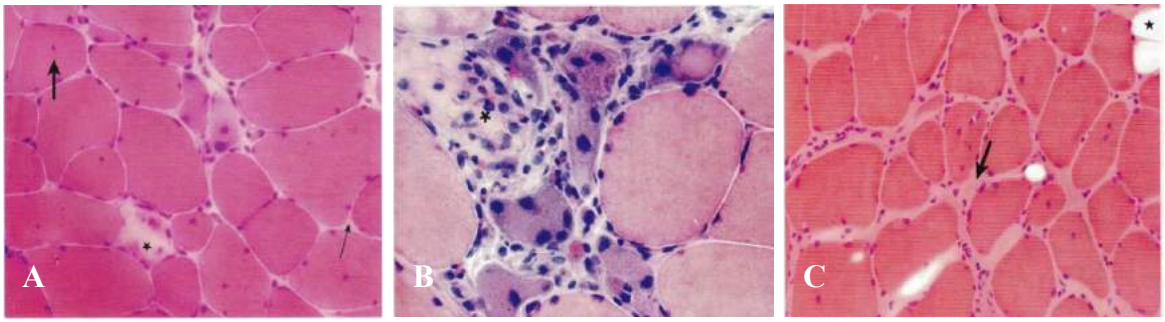

Figure 4. Haematoxylin and eosin (H&E) representative images from a quadriceps biopsy in a patient with limb-girdle dystrophy aged 39 years. (A) shows a wide range in fiber size (10-100 um), with necrosis (*), excess internal nuclei (large arrow) and little endomysial connective tissue (small arrow); in (B) a necrotic fiber invaded by immune cells (*) and a cluster of regenerating basophilic fibers (mean diameter 30 um) with large and surrounded by mononucleas cella of various type. In (C) most fibers are surrounded by endomisial connective tissue (arrow), note also a little adipocyte (*). Adapted from Dubowitz.

A correlation between reduction of sarcoglycans level and disease severity was observed in LGMDR3–6 patients in several studies and with different techniques. In details, an immunohistochemistry study on 18 muscle biopsies from LGMDR3 patients showed a highly variable expression of α-SG, ranging from the complete absence to a mild reduction, to some cases with normal α-SG expression [12], and a statistically significant positive correlation between reduction of α-SG levels and disease severity was observed, indicating that disease severity may be predicted by α-SG expression in these patients.

Similar results were obtained by a western blot study, detecting α-SG residual protein expression by Western Blot (WB) in 55 LGMDR3 patients. The age of onset, the age of loss of ambulation and the time from onset of symptoms to being wheelchair-bound, were significantly different between patients with no α-SG expression, patients with <30% expression, and those patients with expression >30% compared to controls (Figure 5). The authors obtained the same results for other sarcoglycanopathies, as they also performed WB studies on 20 biopsies from LGMDR4 and 35 from LGMDR5.

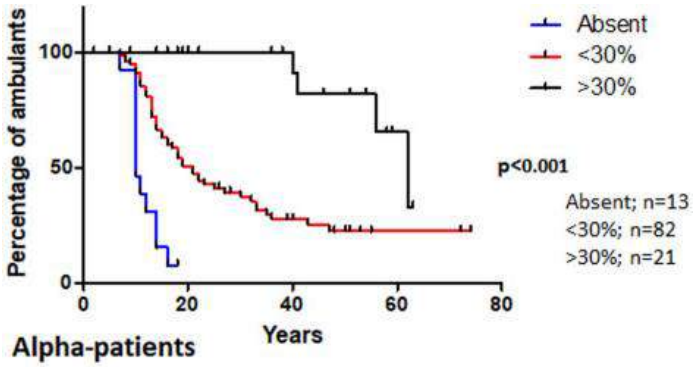

Figure 5. Kaplan-Meier estimates influence of residual protein expression in age at wheelchair LGMDR3 (alpha patients). Patients were stratified into three groups: no protein expression (absent), remaining protein expression lower than 30% (<30%) and remaining protein expression higher than 30% (>30%). Adapted from [13].

Immunohistochemistry has also shown that the sarcoglycans act as a complex, such that a defect in one gene causes variable secondary reduction in protein expression of the whole complex (Figure 6).

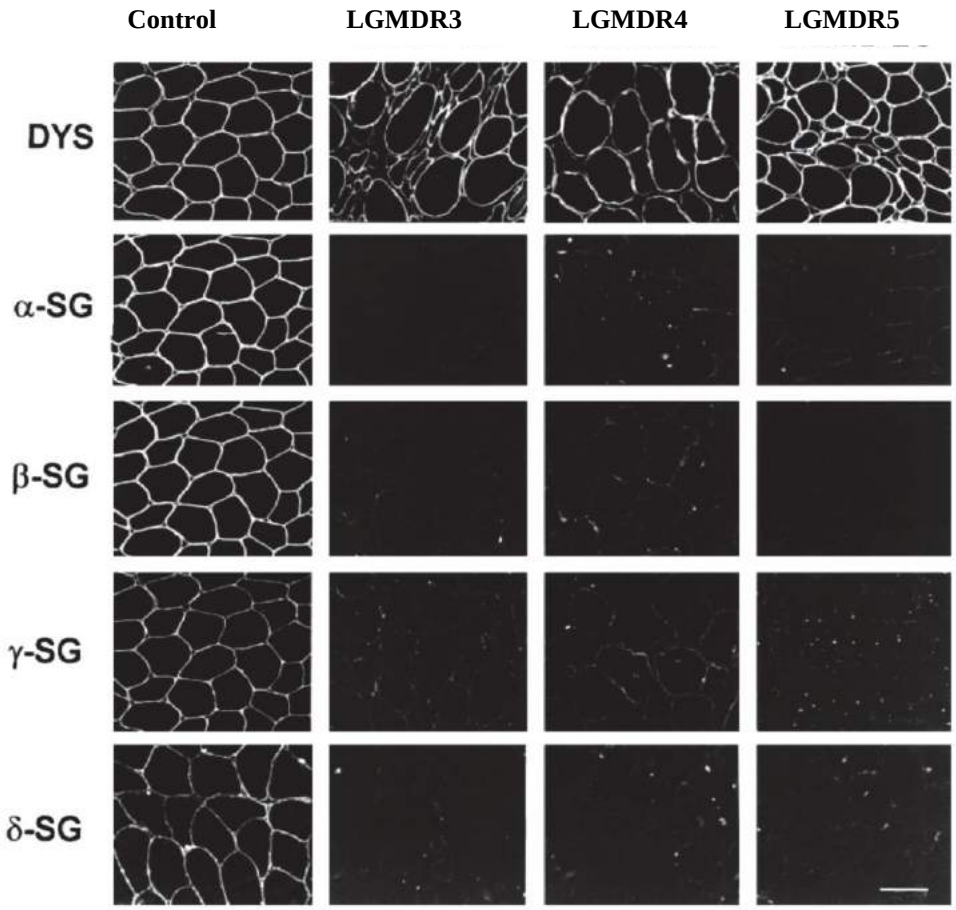

Figure 6. Representative images of immunofluorescence analysis of dystrophin (DYS) and sarcoglycans (α-, β-, γ-, δ-SG) in control subject and LGMD due to defects in α-, β-, and γ-SG (LGMDR3, R4 and R5 respectively). Normal control subject showed positive staining of the four sarcoglycans; LGMDR3, R4 and R5 patients showed a variable reductio-to absent expression in all the four sarcoglycans, despite their genetic background.

Genetic features

The nomenclature of the α-sarcoglycan has changed and developed over the years. Originally, in 1993, Roberds et al. cloned a cDNA sequence encoding for the 50-kD Dystrophin-associated Glycoprotein (50-DAG) from rabbit skeletal and cardiac muscle, the terminology reflected the molecular mass of the protein and its membership of the DAG complex [30]. The deduced amino acid sequence predicted a protein of 387-amino acid with a 17-amino acid signal sequence, 1 transmembrane domain, and 2 potential sites of N-linked glycosylation. Since the 50-DAG was firstly involved in the pathogenesis of a severe childhood autosomal recessive muscular dystrophy (SCARMD), with a high prevalence in Arabic countries, Roberds et al. suggested to re-name the protein "50-DAG" with "adhalin", which derives from the Arabic word "adhal" for muscle. In 1994, the same group isolated human adhalin cDNA from a human skeletal muscle library and determined the adhalin gene sequence (now known as *SGCA*) [31]. The gene is located on the 17q21 chromosome and encompasses 10 exons.

To date, 413 variants in SGCA gene have been reported (UniProt, ClinVar, VarSome and PubMed), 135 being pathogenic, 181 with uncertain significance and 97 bening [VarSome.com search engine, 32]. Most of the pathogenic variants were missense mutations (50%), followed by frameshift (28%), splice junction loss (11%), and nonsense mutations (9.6%).

A large study on 159 LGMDR3 European patients, pointed out that most of the patients carried two missense mutations (74.8%), while only 3.1% carried two frameshift or nonsense mutations [13]. Frequency analysis of mutations in the study population showed that 60% of LGMDR3 patients carried one of the following mutations, either in a homozygous or heterozygous: c.229C4T, p.(Arg77Cys), that was present in at least one allele in 75 patients (47.2% of all LGMDR3), c.850C4T, p.(Arg284Cys), present in 30 patients (18.9%), and c.739G4A, p.(Val247Met) found in 26 patients (16.4%) (Figure 7, adapted from Alonso-Pèrez J. et al, 2020). Among the most common SGCA variants, the c.229C>T, p.(Arg77Cys), causes protein aggregation in the Endoplasmic Reticulum, thus preventing the formation of the sarcoglycan complex [33], and leading to a very reduced muscular residual protein expression, always <30%, with a consequent worse prognosis, characterized by early onset of symptoms, more rapid progression and early loss of ambulation [13]. In contrast, c.850C4T, p.(Arg284Cys) and c.739G4A, p.(Val247Met) have been associated with a higher protein expression and a better prognosis.

Moreover, it has been suggested that LGMDR3 patients carrying two missense mutations

had milder forms of disease compared to subjects harboring null mutations (splicing, nonsense, initiation codon loss, large deletion or duplication, and frameshift mutations) in at least one of the mutated alleles [12, 24, 34].

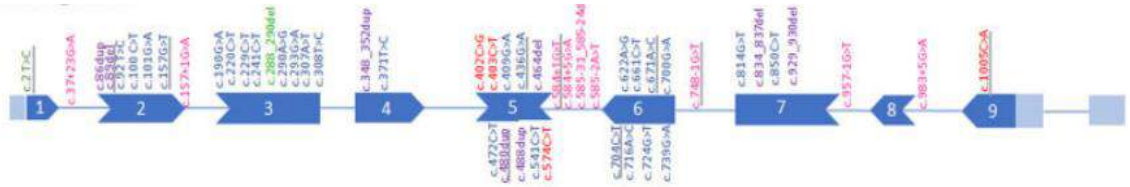

Figure 7. Distribution of the pathogenic variants found in a large cohort of European patients in the SGCA gene. The graph shows the distribution of the pathogenic variants throughout the different exons. Adapted from [13].

Animal models

The first experimental model for the study of LGMDR3 was generated by Duclos et al in 1998 [35], a null mutant mouse that helped to further define the biological role of the sarcoglycans. The authors showed that the absence of the sarcoglycan–sarcospan complex due to a null mutation in the Sgca gene causes dissociation of the DAPC, contributing to progressive muscle degeneration in LGMDR3. The mouse model developed dystrophic histopathological features shortly after birth, showing fiber degeneration until the 9th month of age.

Almost twenty years later, two studies explored the disease progression in Sgca-null mice at different time points (at 8-16-24 and 34 weeks) [36, 37]. As a result, muscle function was already impaired at 8 weeks of age and showed a rapid decline with age. Histological analyses showed severe dystrophic features in all examined muscles, including fibrosis, inflammation and necrosis at all ages. Contrarily to LGMDR3 progression in patients, muscle pathology in Sgca-null mice did not show a drastic increase in severity with age, as in the mouse model for Duchenne Muscular Dystrophy (the *mdx* mouse). Different hypothesis suggested that mouse muscle regeneration capacity might be more efficient, and that mouse muscles might be less stressed due to the reduced muscles load considered their small body size and, the load distribution on the four limbs.

Current therapeutic strategies

Current therapeutic strategies under development for LGMDR3 patients can be divided in two groups: the gene therapy and other approaches, small molecule correctors aiming to guide the folding of the α-SG protein, and cell therapy [38].

Gene replacement therapy (GRT)

The first Phase I clinical trial for α-SG deficient patients was completed almost a decade ago (NCT00494195) [39, 40], with the main objective of testing doses, assessing adverse effects, and proving efficacy in term of expression of the missing α-SG protein. In details, a small group of LGMDR3 patients was treated with local intramuscular (i.m.) gene delivery mediated by adeno-associated virus (AAV), under control of a muscle-specific promoter (tMCK). The rAAV1.tMCK.hSGCA vector (3.25×10^{11} vg) was delivered to the extensor digitorum brevis muscle (EDB) muscle and the α-SG expression tested at 6 weeks or 3 months (in 3 subjects) [39], and at 6 months (3 subjects) [40]. These encouraging proof of principle trials, proving sustained muscular gene expression without overt immune response to α-SG or AAV1 capsid, led 10 years later, to a Phase II clinical trial (NCT01976091). The latter aimed both to test ascending doses and safety (primary outcomes) and to assess meaningful motor achievement in terms of Change in Six-Minute-Walk-Test (6MWT) distance (secondary outcome) [41]. Six LGMDR3 patients received 10^{12} vg/kg or 3×10^{12} vg/kg of scAAVrh74.tMCK.hSGCA via isolated limb infusion (ILI) through percutaneous access to the femoral artery. The rational for ILI gene delivery was based on targeting gene delivery to the predominant area of muscle weakness. Moreover, at the time of the study, concerns around high-dose of AAV gene for systemic delivery remained, and ILI offered an alternative route using less viral load compared to systemic delivery. ILI delivery of AAVrh74.tMCK.hSGCA was effective at producing SGCA protein (Figure 8) that correlated with local functional improvement restricted to targeted muscles, while the 6MWT decreased or remained unchanged [41].

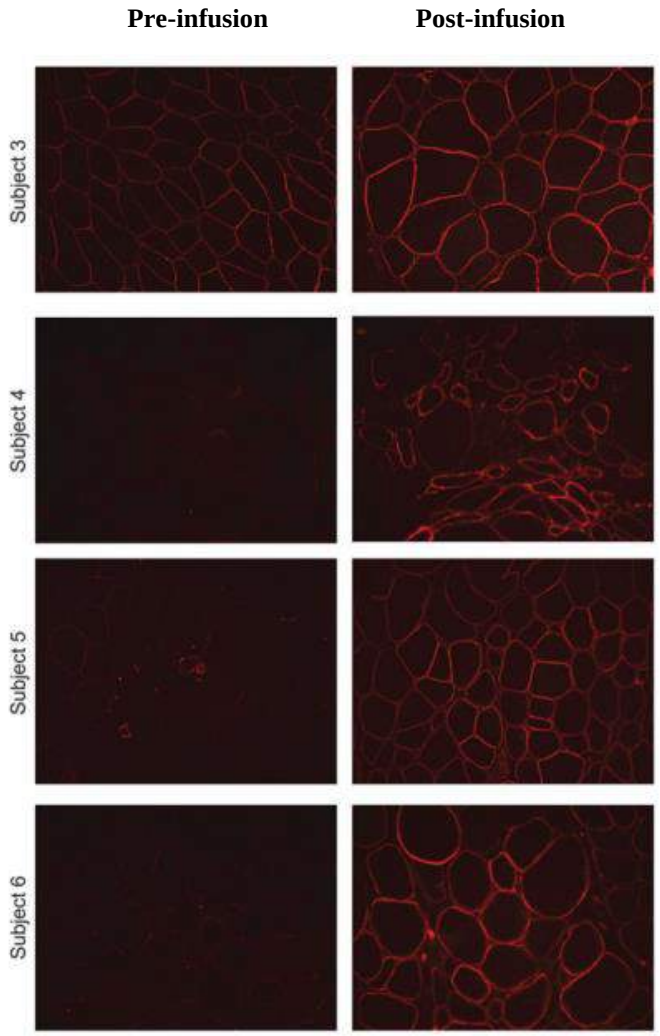

Figure 8. SGCA expression following isolated limb infusion (ILI) demonstrated by immunofluorescence alpha-sarcoglycan (a-SG) antibody staining of muscle biopsies taken pre and post gene transfer for subject for subjects 3–6 (quadriceps). Membrane staining intensity post gene transfer showed increased intensity. Adapted from [41].

Recently, a systemic approach was tested in a pre-clinical study on sgca-null (sgca-/-) mice, a mouse model that recapitulates the clinical phenotype of patients with LGMDR3, including dystrophic features, elevated serum creatine kinase (CK), and reduction in the generation of muscle force and locomotor activity [42]. In sgca-/- mice, scAAVrh74.tMCK.hSGCA administration resulted in a significantly increased expression of α-SG at sarcolemma of skeletal muscle cells, together with an improvement of histopathological parameter, and a significant increase of locomotor activity.

Taken into account these data, and the emerging gene therapy clinical trials for other neuromuscular disorders, such as DMD and X-linked myotubular myopathy, as well as, the

already approved onasemnogene abeparvovec-xioi (Zolgensma) for the treatment of spinal muscle atrophy (SMA), a systemic delivery of scAAVrh74.tMCK.hSGCA in a clinical setting for the treatment of LGMDR3 might be available soon.

Small molecules

Small molecule correctors application for LGMDR3 treatment aim to guide the correct folding of the protein in the route from the endoplasmic reticulum (ER) to the membrane final localization. Sarcoglycans are transmembrane proteins that mature in the endoplasmic reticulum (ER), where reach their native conformation through the activity of a quality control (QC) system. The majority of the SGCA disease-causing defects are missense mutations, often resulting in misfolded α-SG proteins, recognised by the QC system, are translocated back to the cytosol for proteasomal degradation through the ER-associated protein degradation (ERAD) pathway [43, 44]. Thereby, interventions targeting the correct protein folding emerged as potential novel therapeutic targets. With this respect, drugs used in other genetic diseases sharing a similar primary pathogenic event, i.e. Cystic Fibrosis (CF) determined by mutations in the *CFTR* gene, have been re-purposed for the treatment of α-sarcolgycanopathy in *in vitro* studies, proving efficacy in recovering missense mutants of α-SG [45, 46]. Recently, Sandonà and co-authors, further explored the efficacy of C17, the most promising CFTR corrector, with a pre-clinical *in vivo* study that proved a significant improve at both histological, molecular, and functional levels, without signs of toxicity (Figure 9) [47].

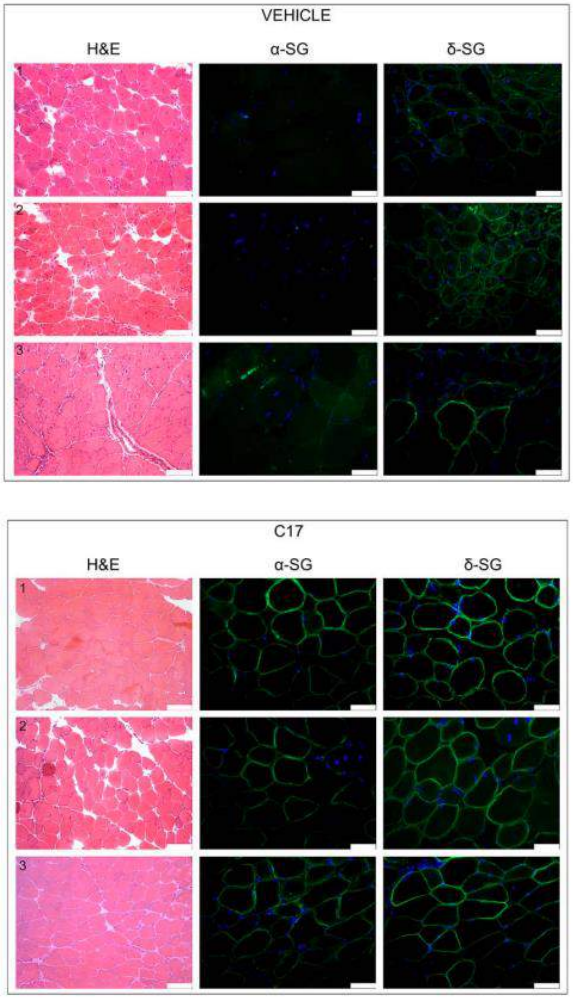

Figure 9. H&E staining and IF analysis of representative TA muscle cryo-sections of mice expressing the R98H-α-SG treated for 5 weeks with either VEHICLE (3 mice, marked as 1-2-3) or corrector C17 (3 mice, marked as 1-2-3). A significant increase in sarcoglycans muscle expression was detected in mice treated with the corrector C17. Adapted from [47].

Cell Therapy

Experiments with autologous muscle stem cells transplantation are also ongoing in a pre-clinical phase [48]. Human muscle cells from two patients, harboring the c.157G>A mutation on the *SGCA* gene, were gene-edited through the Adenine base editing (ABE), rescuing the defect with > 90% efficiency, and leading to α- sarcoglycan expression (Figure 10). The cells were then transplanted in a xenograft model mouse via i.m. injection, boosting regenerative pathways acting on the Pax7+ satellite cell compartment in skeletal muscles. These data provide a proof-of-principle for routine generation of gene-repaired primary MuSC to use in a clinical setting, although further studies are needed to adapt the gene delivery methods, and to avoid off-target effects.

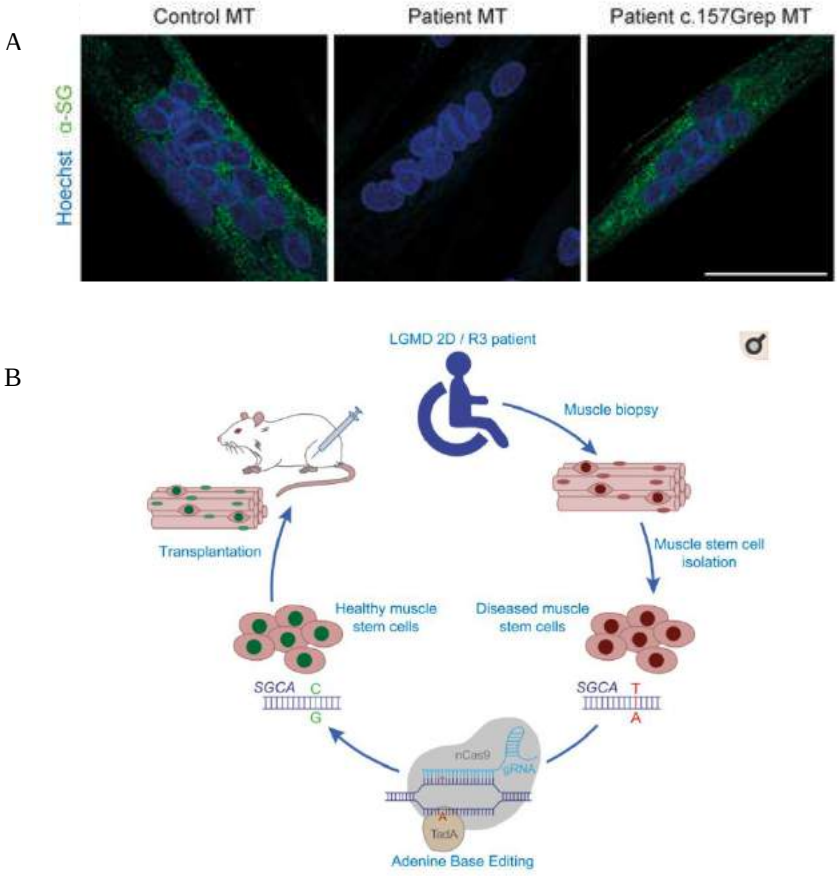

Figure 10. (A) α-Sarcoglycan immunostaining in control myotubes (Control MT), as well as untreated (Patient MT) and in gene-edited patients myotubes (c.157Grep MT). Compared to untreated Patietns MT, the gene-edited c.157Grep MT express α-SG. (B) graphical abstract of the study. Human muscle stem cells were isolated from 2 donors, with the common SGCA c.157G>A mutation, inducing skipping of 2 coregulated exons. Using adenine base editing, we corrected the mutation in the cells from both donors with > 90% efficiency, thereby rescuing the splicing defect and α-sarcoglycan expression. Base-edited patient cells regenerated muscle and contributed to the Pax7+ satellite cell compartment in vivo in mouse xenografts. Adapted from [48].

1.2 The role of inflammation in the pathogenesis of LGMDR3

In physiological conditions, skeletal muscle is considered a privileged immunological site, with few immune cells, poorly able to generate a local immune response. Conversely, during acute muscle damage, i.e. muscle trauma or muscle invasions by myotrophic infectious organisms, the immune system takes part in muscle repair and regenerative processes. Inflammatory cells are rapidly mobilized to the injured site, where they drive mechanisms such as necrotic debris removing, finally leading to a complete muscle repair.

In muscular dystrophies, the absence or reduction of structural membrane proteins, such as DAPC components, makes the sarcolemma weak and leaking, inducing the release of molecules known as danger-associated-molecular-patterns (DAMPs) in the extracellular space [49]. This provokes a chronic and self-renewing activation of inflammatory pathways that fail to complete an efficient tissue repair, contributing to muscle fibrosis as a downstream consequence.The dystrophic-associated immune response involves both innate immunity, with myeloid cells (neurtrophils and macrophages) as the primary populations infiltrating muscles, and the acquired immune system, with central role of cytotoxic T cells ($CD8^+$) and helper T cells ($CD4^+$), that not only increases muscle fiber death through direct cytolysis, but also amplifies the innate immune response [50]. Different subsets of inflammatory infiltrates follow one another in a well-orchestrated sequence. First neutrophils infiltrate the necrotic area, followed by M1 macrophages and $CD4^+$/$CD8^+$ T cells with a pro-inflammatory phenotype, gradually replaced by M2 macrophages and T regulatory cells with a pro-regenerative activity (Figure 11**)**. These interactions between damaged myofibers with the immune system resolve quickly with return of function in normal muscle [51], while in the chronic muscle injury that occurs in muscular dystrophies, immune response often contribute to amplify rather than resolve the pathology.

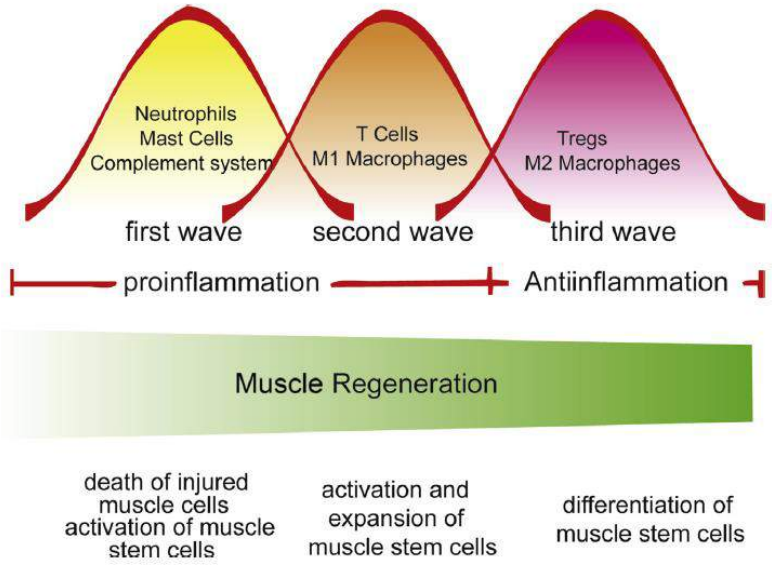

Figure 11. Inflammation and muscle regeneration. Three waves of immune cells were recruited to the muscle injury site orderly. The recruitment of various types of immune cells regulates the activation, expansion and differentiation of muscle stem cells to facilitate muscle regeneration. Adapted from [50].

Most of the data on the immunobiology of muscular dystrophies have been generated from studies on dystrophinopathies and dysferlin-related LGMD (LGMDR2), and relatively few groups explored the role of inflammation on disease progression in LGMDR3 [52]. Nevertheless, a common process of inflammatory events could be assumed in LGMDR3, considered that much of the pathology is attributable to the loss of mechanical functions served by the DAPC, with subsequent DAMPs release in the extracellular space and immune system activation.

Among DAMPs, the extracellular ATP (eATP) becomes an important signal, triggering inflammatory response binding the P2X7 receptor, an ionotropic receptor involved in the induction of the inflammasome, one of the most relevant pathway for innate immune response [49, 53], leading to interleukin-1 (IL-1) release by mononuclear and polymorphonuclear phagocytes [54-57]. P2X7 is also over-expressed in dystrophic muscle cells [58, 59], where it contributes to exacerbate myofiber injury by increasing sarcolemma permeability, and participates in the amplification of the inflammatory process by releasing IL-1 (Figure 12**)**.

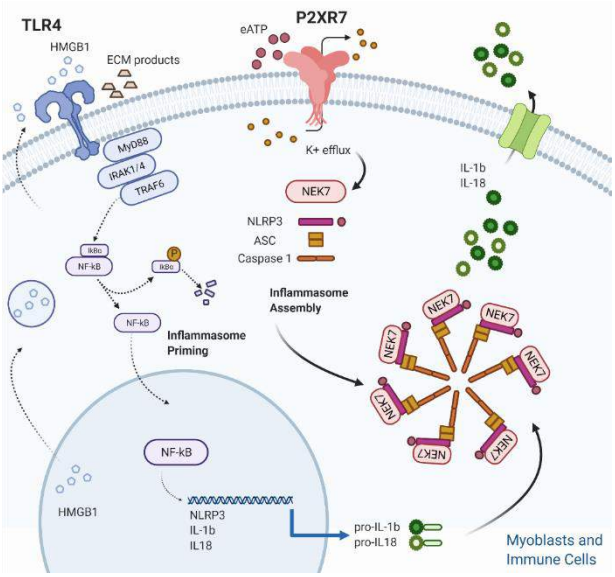

Figure 12. NLRP3 inflammasome activation in skeletal muscle. Skeletal muscle cells are equipped with a functional inflammasome pathway and actively participate to the inflammatory response upon P2X7R stimulation.Adapted from [60].

We and others already proved that interfering with P2X7 receptor activity, by genetic ablation or pharmacological inhibition, determined an improvement of functional, biochemical, and histological muscle features in the mouse model for Duchenne Muscular Dystrophy (the *mdx* mouse) [61-63].

The regulation of the eATP/P2X7R axis might be even more complex in sarcoglycanopathies: indeed, eATP concentration is regulated by extracellular hydrolyzing enzymes (nucleotidases) [64]. Importantly, 25% of eATP degradation in muscles is performed by the muscle-specific ATP hydrolase α-sarcoglycan [65, 66] (Figure 13). Thus, in LGMDR3-R6, where α-SG can be reduced or absent, an impaired hydrolysis of eATP might lead to further activation of the aATP/P2XR axis.

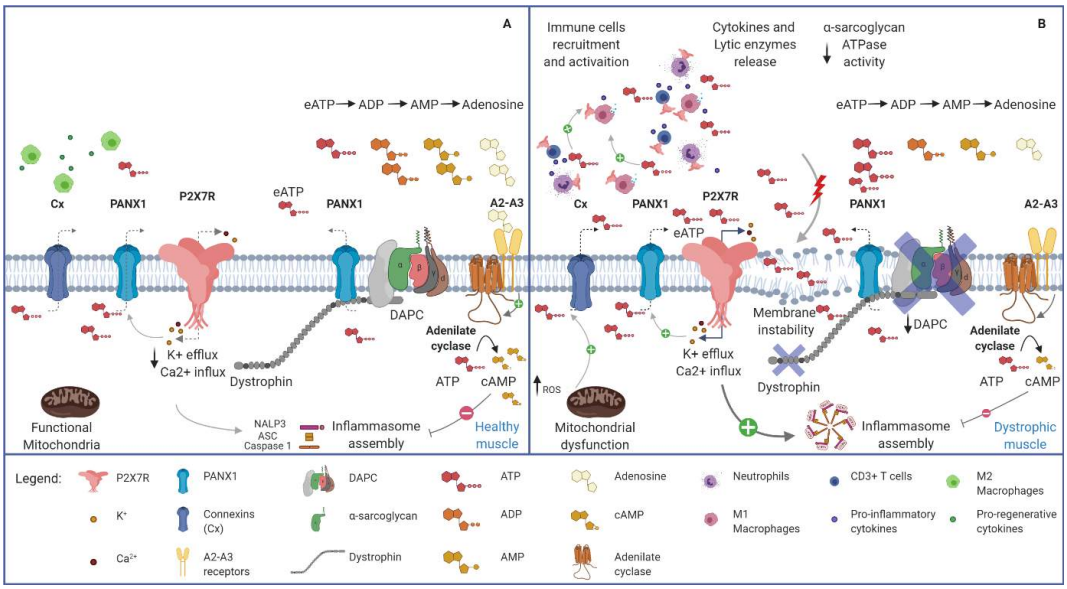

Figure 13. Purinergic signal in normal and dystrophic muscles. (A) Healthy skeletal muscle. Note the plasma membrane's integrity, and the physiological low concentration of eATP. (B) Dystrophic skeletal muscle. The membrane instability, due to DAPC alteration, induces chronic release of ATP in the extracellular space, and recalls pro-inflammatory immune cells (i.e., neutrophils, M1 macrophages and CD3+ Tcells). eATP, in turn, activates P2X7R receptors on muscular and immune cells, leading to pro-inflammatory citokines release via NLRP3 inflammasome activation. Adapted from [60].

Some of these topics have been reviewed in the following manustript:

Panicucci C, Raffaghello L, Bruzzone S, Baratto S, Principi E, Minetti C, Gazzerro E, Bruno C. **eATP/P2X7R Axis: An Orchestrated Pathway Triggering Inflammasome Activation in Muscle Diseases.** Int J Mol Sci. 2020 Aug 19;21(17):5963. doi: 10.3390/ijms21175963. PMID: 32825102; PMCID: PMC7504480 (see Appendix).

2. Natural history data and muscle biopsies analysis in a population of LGMDR3 patients

2.1 Objectives

Aim of this chapter was to deeply characterize the phenotype of 8 LGMDR3 patients currently in follow-up at our center, and to exploit a link between the clinical course and inflammation at muscle biopsy.

We considered the genotype, the age at onset, the clinical course, the muscle MRI pattern, and some histological features, i.e. the extent of inflammatory infiltrates, and the residual amount of α-SG measured by immunohistochemistry.

We correlated inflammatory infiltrates with the age at onset, the clinical course, and the muscle involvement at muscle MRI.

2.2 Materials and Methods

Clinical data collection

This study was designed as retrospective study, collecting clinical and genetic data from patients affected by LGMDR3, with a genetically confirmed diagnosis of α-sarcoglycanopathy.

The data were collected from clinical records to define disease onset and progression, muscle function status, and respiratory, cardiac and bone secondary complications.

The age at onset was defined as the age when the parents or the patient noticed the first symptoms. The age of loss of ambulation (LOA) was defined as the time when patients were not able to walk 10 meters independently.

At last examination, the best motor performance scored with a 4 point scale as follow: 3 (running), 2 (walking), 1 (sitting), 0 (laying).

Muscular function in ambulant patients was assessed by the North Star Ambulatory Assessment (NSAA), the timed-tests (time to climb 4 stairs, time to descend 4 stairs, time to rise from floor and time to run 10 meters) and the 6MWT. In not-ambulant patients, the Performance Upper Limb (PUL) was applied.

Respiratory function was evaluated by Forced Vital Capacity (FVC) and Forced Expiratory Volume in 1 second (FEV1) through Pulmonary Function Test (PFT).

Cardiac function was evaluated by ECG, echocardiography and Holter-ECG when appropriate.

Bone health was evaluated by dual-energy-x-ray absorptiometry (DXA) measurements (Lunar Prodigy, GE) of lumbar spine bone mineral density (LS BMD Z-score) and, total body less head bone mineral density (TB BMD Z-score). A pathologic bone mineral

density was defined when the BMD Z-score values were below -2.

Muscular MRI of the thighs was performed to assess the degree of fibroadipose substitution. MRI studies were performed using a 1.5 Tesla scanner according to standard protocols [67]. All the scans were analyzed by two blinded evaluators (C.P. and C.B.), applying a 5-point scale which evaluates the extent of fatty replacement of single muscles as previously reported [27], with scores ranging from 0 (normal signal) to 4 (complete fatty replacement). A cumulative score per patient (T1-MRI score) was calculated as the sum of the median score for the following muscles: vastus lateralis, vastus intermedius, vastus medialis, rectus femoris, sartorius, gracilis, adductor longus, adductor magnus, adductor minimus, adductor brevis, semi tendinosus, semi membranosus, biceps femori long head, biceps femori short head.

Muscle biopsy analysis in LGMDR3 patients

Muscle specimens' collection and preparation

Open muscle biopsies were performed under general anesthesia and processed according to standard protocols. In details, quadriceps muscle specimens were mounted on cork discs with a small amount of OCT mounting medium (Merck) at the base of the specimen and immerged for 20 seconds in isopentane cooled in liquid nitrogen to -160 °C, then stored in liquid nitrogen until processed.

Muscle sections were then cut in a cryostat at -23 to -25 °C and collected on poly-L-lysine (0.5 mg/mL) coated glass slides. Section thickness measured 8 um for histology, and 5 um for immunohistochemistry.

Histological and immunohistochemistry procedures and analysis

Histological Stains. Haematoxylin and eosin (H&E) stain was used to show the overall structure of the tissue in relation to the fibers, nuclei, fibrous and adipose tissue, the presence of inflammatory cells and vacuoles.

Acid phosphatase (AP) stain was used to detect the inflammatory infiltrate areas, exploiting the properties of AP-rich inflammatory cells producing an azo dye when coupled with a naphthol based buffer. The whole section was scanned at a 20X magnification by Axioplan Imager M2 microscope software AxioVs40 version 4.8.2.0 (Zeiss, Jena, Germany) and the positive signal was captured in a semi-automatic scheme using the Color Detection function of the IHC Toolbox developed for ImageJ (ImageJ 1.53k free software). For the Color Detection, the functions of semi-automatic color

selection and automatic statistical color detection model were combined together. Color selection was used to select and reserve the positive color pixels while the background color pixels were eliminated. Then, the area of the Color Detection Mask was calculated by a function of ImageJ and referred to the total area of the section, and later expressed as percentage of the total area of the section.

Immunofluorescence (IF) stains. The sarcoglycan complex expression was tested by IF labelling according to manufacturer instructions. Primary antibody: Monoclonal Antibody Alpha-Sarcoglycan (Adhalin) 3.7g/L (mouse-anti human, clone Ad1/20A6, Novocastra Leica Biosystems Newcastle Ltd, NCL-L-a-SARC, indiluited), Monoclonal Antibody Beta-Sarcoglycan 5g/L (mouse-anti human, clone βSarc1/5B1, Novocastra Leica Biosystems Newcastle Ltd, NCL-L-b-SARC, indiluited), Monoclonal Antibody Gamma-Sarcoglycan 4.3g/L (mouse -anti human, clone 35DAG/21B5, Novocastra Leica Biosystems Newcastle Ltd, NCL-L-g-SARC, indiluited), Monoclonal Antibody Delta Sarcoglycan 4.3g/L (mouse-anti human, clone δSarc3/12C1, Novocastra Leica Biosystems Newcastle Ltd, NCL-L-d-SARC, indiluited). Secondary antibody: Anti-mouse IgG, Biotinylated species-specific whole antibody (from sheep) Cytiva (GE Healthcare UK Limited, RPN1001V, 1/100), Streptavidin, Alexa Fluor™ 488 Conjugate 2mg/ml (Invitrogen Life Technology Corporation, S32354, 1/250).

Immunolabelled muscle specimens were blindly evaluated by two different operators (C.P. and P.B.) and the protein expression quantified by a 5-point scale, ranging from 0 to 5: 0 (no expression), 1 (severely reduced), 2 (moderately reduced), 3 (mild reduction), 4 (normal expression).

Statistical analysis

For descriptive statistics, continues variables are shown as median values and interquartile ranges (IQR), while nominal variables as relative and percentage frequencies. Kruskall Wallis, Mann Whitney test and Fisher's test were applied when appropriate. Correlations between variables were assessed by Spearman correlation test for non-parametric data. *p*-values < 0.05 was considered statistically significant. Graphs were performed with GraphPad8 (Graph-Pad Software, San Diego, CA, USA) or JAMOVI free software.

2.3 Results

Natural history data in our LGMDR3 cohort

Medical records of 8 patients affected by LGMDR3 were revised and summarized in **Table 1**.

ID	Sex	Allele 1 mutation	Allele 2 mutation	Age at onset (yrs)	Symptoms at onset	Age at cardiac involvement (yrs)	Cardiac features	Age at NIV support (yrs)
1	F	c. 329C>T p.Arg77Cys	c.1005C>A p.Cys335X	10,1	hyperckemia, exercise intolerance	NA	NA	NA
2	M	c.409G>A p.Glu1137Lys	c.850C>T p.Arg284Cys	16,4	hyperckemia, exercise intolerance	NA	NA	NA
3	F	c.308T>C p.Ile103Thr	c.850C>T p.Arg284Cys	22,2	hyperckemia, exercise intolerance	NA	NA	NA
4	F	c.329C>T p.Arg77Cys	IVS5:c.584+5G>A	4	proximal weakness	NA	NA	NA
5	M	c.409G>A p.Glu1137Lys	c.739G>A p.Val247Met	8,6	proximal weakness	NA	NA	NA
6	M	c.329C>T p.Arg77Cys	c.346A>C p.Thr116Pro	9,9	proximal weakness	NA	NA	NA
7	M	c.92T>C p.Leu31Pro	c.739G>A p.Val247Met	4	proximal weakness	14,8	Mild left ventricular dysfunction	NA
8	M	c.739G>A p.Val247Met	c.739G>A p.Val247Met	4	proximal weakness	18,7	Dilatative cardiomiopathy, WPW	17,2

Table 1. Genetic mutations, age at onset, respiratory and cardiological complications are summarized in the table.

Onset and diagnosis

Symptom's onset occurred at a median age at onset was 9,3 years (IQR 4.0-11.7). The most frequent symptom was proximal lower limb weakness, resulting in limitation in climbing stairs, that occurred in 5/8 of patients (62,5%). Three/8 patients (37,5%) were referred to our neuromuscular unit for hyperckemia and mild exercise intolerance.

Although a muscle biopsy was performed in all patients, the diagnoses was achieved by genetic test.

Last examination

Last evaluation was performed at a median age of 27.7 years (IQR 15.9-30.8). At last examination, the best performance was “running” for 3/8 (37,5%) subjects, “walking” for 2/8 (25%) and “sitting” for 3/8 patients (37,5%). Functional outcome measures performed at last examination are shown in **Table 2**. LOA occurred in 3/8 patients (37,5%) at a median age of 13 years (IQR 11.5-20.5).

ID	Sex	Age at last visit (yrs)	Best performance	6MWT (m)	NSAA (X/34)	FVC (%)	FEV1 (%)
1	F	10,5	running	417	34	34	93
2	M	39,2	running	614	34	103	104
3	F	26,5	running	496	34	110	117
4	F	13,8	walking	225	17	101	108
5	M	31,4	walking	220	12	95	83
6	M	30,6	sitting	NA	NA	69	71
7	M	16,7	sitting	NA	NA	79	87
8	M	29	sitting	NA	NA	8	9

Table 2. Age at last visit and the relative oucome measures are summarized are summarized in the table.

Muscle MRI study

Muscular MRI scans were performed in all patients at a median age of 20 years (IQR 8,5-26) to assess the muscular fibro adipose substitution of the tights (Figure 1).

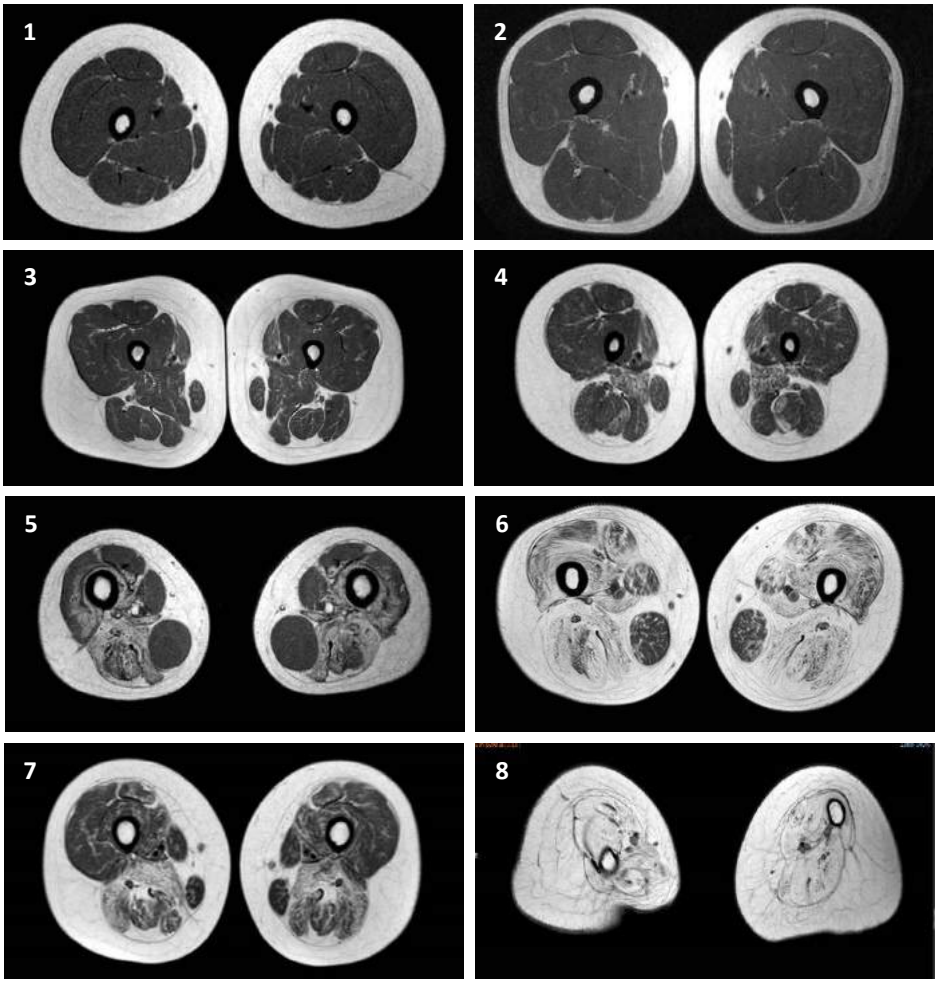

Figure 1. T1-weighted MRI sequences of the tights in our LGMDR3 patients, showing a variable degree of muscle substitution with fibro-adipose tissue.

Single and cumulative T1-MRI scores are shown in Table 3.

ID	sex	Age at MRI (yrs)	Ambulant (Y/N)	Side (R/L)	Vastus lateralis	Vastus Intermedius	Vastus Medialis	Rectus femoris	Sartorius	Gracilis	Adductor Longus	Adductor magnus	Adductor Minimus	Adductor Brevis	Semi Tendinosus	Semi Membranosus	Biceps Femori long head	Biceps femoris Short head	T1-MRI tigh score
1	F	8,5	Y	R	0	0	0	0	0	0	0	0	0	0	0	0	0	0	0
				L	0	0	0	0	0	0	0	0	0	0	0	0	0	0	
2	M	38	Y	R	0	0	0	0	0	0	0	0	0	0	0	0	0	0	0
				L	0	0	0	0	0	0	0	0	0	0	0	0	0	0	
3	F	17	Y	R	0	0	0	0	2	0	0	0	0	0	1	0	0	0	6
				L	0	0	0	0	2	0	0	0	0	0	1	0	0	0	
4	F	8,5	Y	R	0	0	0	0	2	0	0	3	0	0	2	0	1	0	16
				L	0	0	0	0	2	0	0	3	0	0	2	0	1	0	
5	M	28	Y	R	2	4	2	1	0	0	3	4	4	4	1	3	0	3	62
				L	2	4	2	1	0	0	3	4	4	4	1	3	0	3	
6	M	22	Y	R	3	3	3	3	3	1	2	4	4	4	4	4	4	3	90
				L	3	3	3	3	3	1	2	4	4	4	4	4	4	3	
7	M	7,8	N	R	2	3	3	3	1	0	3	4	4	4	3	3	2	4	78
				L	2	3	3	3	1	0	3	4	4	4	3	3	2	4	
8	M	25	N	R	4	4	4	4	4	4	4	4	4	4	4	4	4	4	112
				L	4	4	4	4	4	4	4	4	4	4	4	4	4	4	

Table 3. Sex, age at muscle MRI, singular T1 scores of all the tight muscle and total T1-MRI tig score are shown in the table.

We observed a marked variability of the T1-MRI tigh score (median=39; IQR 4,5-81). Patients 1 and 2 presented with an almost normal muscle MRI pattern, patient 3 showed only minor changes, patients 4 and 5 an intermediate MRI, while patients 6, 7, and 8 showed a severe muscle substitution, with almost all the tigh muscle involved. Overall the involvement was symmetrical. Adductor magnus, minimus and brevis were the most frequently and severely affected muscles, followed by vastus intermedius, biceps femoris shoer head and semimembranosus. Among the vasti muscles, vastus intermedius was the most severely involved, followed by vastus medialis and lateralis. Sartorius and gracilis were the most spared muscles. Patients 4, 5 and 6 were also included in a multi-center study for the evaluation of lower limb MRI pattern in sarcoglycanopathies (marked as patients ITA3_1, ITA3_3 and ITA3_6 respectively) [27].

Comorbidities

Non-invasive respiratory support was required in 1/8 patient (12,5%) from the age of 17.21 years.

Two/8 patients (25%) required cardiological interventions from a median age of 16.7 years. Patient 7 was started on bisoprololo at 14.8 years, for a mild left ventricular dysfunction; patient 8 was started on ACE inhibitors and beta-blockers at 18,7 years, and underwent a radiofrequency ablation for a Wolf Parkinson White syndrome at 21 years. At last cardiological examination, at the age of 29, patient 8 presented a severe dilatative cardiomyopathy with a Left Ventricular Ejection Fraction of 20%, requiring an implantable cardioverter-defibrillator.

Bone mineral density was below the normal ranges for age and sex in 2/8 patients (25%) (patients 3 and 8). They presented a low-trauma fracture at femur at the age of 11 and 25 years respectively. At the time of fracture, both patients presented pathologic values of the Total Body BMD Z-score and normal values of the Lumbar Spine BMD Z-score. Patient 3 underwent XII cycles of intravenous bisphosphonate with a stabilization of the BMD Z-score values, while patient 8 refused to be treated with bisphosphonate. None of them presented further fractures.

Genetic features

Genetic mutations are listed in Table 1. Two/8 (25%) patients were homozygous for a single variant. The most common mutation previously reported in a European cohort [13] were distributed as follow: c.229C>T, p.(Arg77Cys) was present at least in on allele in 1 patient (12,5%), c.850C>T, p.(Arg 284Cys) in 2 patients (25%), and c.739G>A, p.(Val247Met) in 4 patients (50%). Four/8 carried two missense mutations (50%), while 4/8 patients presented at least one deletion, or frameshift or nonsense mutation (50%).

Muscle biopsy

All patients underwent an open muscle biopsy (MB) of quadriceps muscle at a median age of 10 years (IQR 5-13), between the 1997 and the 2020. MB was performed as first diagnostic tool in 7/8 patients (87,5%), and in 1/8 case (12,5%) it served to assess the α-SG expression for a prognostic purpose.

α-SG residual expression highly varied between patients, ranging from patients with normal expression (patients 2 and 3), and patients with very low levels (patients 4, 6, 7, and 8) (median α-SG expression Arbitrary Unit (AU)= 1,5, IQR 0,75-3,25). The reduction

of the other component of the SG complex was also variable (Table 4).

ID	Age at MB (yrs)	CK at MB (UI/l)	α-SG (AU)	β-SG (AU)	γ-SG (AU)	δ-SG (AU)	SG-complex (AU)	AP (%)
1	10,2	229	2	3	3	3	11	0,003
2	19,5	237	4	4	4	4	16	0,006
3	11,9	585	4	4	4	4	16	0,009
4	0,8	2734	0	0	1	0	1	0,23
5	26,3	3013	3	3	3	3	12	0,07
6	9,9	1457	1	2	2	2	7	0,1
7	2,2	14271	1	1	1	2	5	0,6
8	6	NA	0	1	1	2	4	NA

Table 4. Age and serum CK levels at muscle biopsy (MB), protein expression of singular sarcoglycans, and % of acid phosphatase (AP) stain are shown in the table.

Inflammatory infiltrates analyzed by AP stain

At the time of the Acid Phosphatase study, only 7 out of 8 muscle specimens were available for analysis (muscle biopsy of patient 8 was not available). Representative images of the H&E stain, performed to assess the general architecture of the tissue, and Acid Phosphatase (AP) stain, used to define the inflammatory infiltrates, are shown in Figure 2 (H&E left column, AP right column).

We appreciated a great variability dystrophic pattern severity, as muscle abnormalities ranged from mild fiber diameter variability (subjects 1, 2, 5), and mild increased extracellular fibrosis (subjects 1, 3), to severe distruption of muscular architecture with muscle fiber necrosis, inflammatory cells infiltration and mild to severe fibro-adipose substitution (subjects 4,6,7).

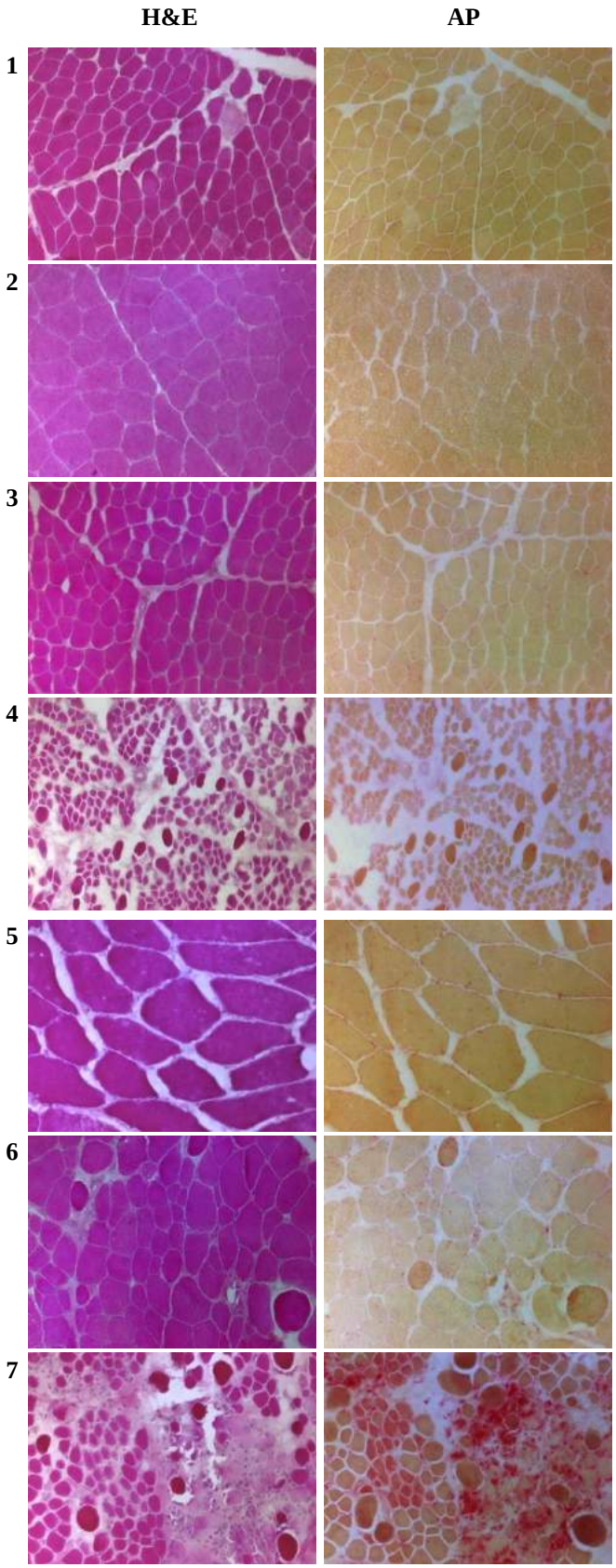

Figure 2. Representative images of H&E and AP stains in our cohort of LGMDR3 patients show a high variability in dystrophic pattern severity. Original magnification 20X.

AP stain was quantified with a semi-automatic approach, as explained in Material and Methods. The positive pink/red signal (Figure 3, left panel) was detected by the IHC Toolbox for ImageJ software and a Color Detection Mask was generated (Figure 3, middle panel) and the area reported as a percentage of the total section area (Table 4).

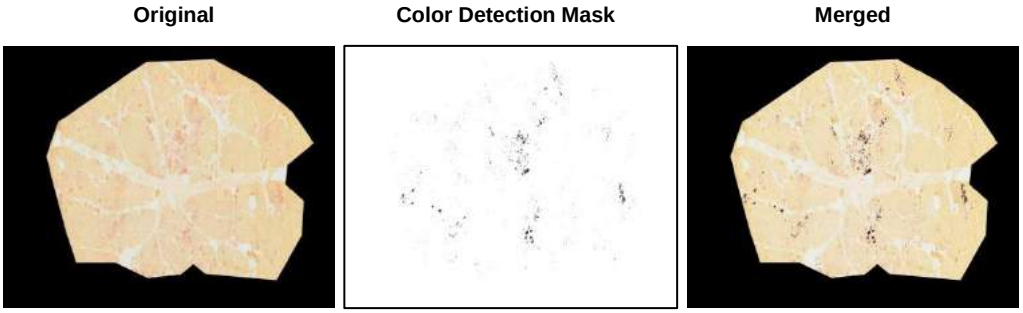

Figure 3. The original AP images (left panel) were quantified with a semi-automatic approach in Image J, that treansformed the AP pink/red signal in a grey-scale image (Color Detection Mask, middle panel).

The median % of the AP positive area measured 0.07 % of the total section area (IQR 0.007-0.16).

In a Spearman correlation analysis, the % of the AP positive area was inversely related to the age at onset (rho -0.82, $p<0.05$), and to the best performance at last visit (rho -0.87, $p<0.05$), whereas it was positively correlated with the CK value measured at the time of muscle biopsy (rho 0.86, $p<0.05$), and with the T1-MRI tigh score (rho 0.8, $p<0.05$) (Table 5). AP% was negatively related the sarcoglycan protein expression, β-SG or γ-SG or δ-SG or expression, while a trend, although not significant, was noted for α-SG and the whole SG complex (Table 5).

A positive correlation linked the residual α-SG expression and the age at onset (rho 0.8, $p<0.05$) and the best performance at last visit (rho 0.74, $p<0.05$) (Table 5).

ID		Age at onset (yrs)	α-SG (AU)	β-SG (AU)	γ-SG (AU)	δ-SG (AU)	SG-complex (AU)	AP (%)	CK at MB (UI/l)	T1-MRI score (AU)	Best performance at last visit (score 1-4)
Onset (yrs)	Spearman rho p-value	- -									
α-SG (AU)	Spearman rho p-value	**0,80** **0,016**	- -								
β-SG (AU)	Spearman rho p-value	**0,89** **0,03**	**0,96** **<0,001**	- -							
γ-SG (AU)	Spearman rho p-value	**0,93** **0,001**	**0,95** **0,001**	**0,98** **0,001**	- -						
δ-SG (AU)	Spearman rho p-value	**0,83** **0,001**	**0,95** **0,001**	**0,98** **0,001**	**0,94** **0,001**	- -					
SG-complex (AU)	Spearman rho p-value	**0,84** **0,009**	**0,98** **0,001**	**0,98** **0,001**	**0,97** **0,001**	**0,97** **0,001**	- -				
AP (%)	Spearman rho p-value	**-0,82** **0,034**	-0,71 0,074	**-0,8** **0,031**	**-0,83** **0,022**	**-0,77** **0,042**	-0,74 0,058	- -			
CK at MB (UI/l)	Spearman rho p-value	**-0,86** **0,024**	-0,56 0,187	-0,69 0,086	**-0,73** **0,006**	-0,64 0,12	-0,61 0,144	**-0,86** **0,027**	- -		
T1-MRI score (AU)	Spearman rho p-value	**-0,66** **0,073**	-0,66 0,072	-0,62 0,10	**-0,71** **0,049**	-0,63 0,091	-0,59 0,119	**-0,81** **0,02**	**0,775** **0,04**	- -	
Best performance at last visit (score 1-4)	Spearman rho p-value	**0,79** **0,19**	**0,74** **0,037**	**0,74** **0,037**	**0,817** **0,013**	**0,752** **0,031**	0,697 0,055	**-0,869** **0,011**	**-0,79** **0,033**	**-0,951** **0,001**	- -

Table 4. Correlation matrix summarizing the Spearman analysis. In bold are indicated the statistically significant results. In red, the most relevant results discussed in the test.

2.4 Discussion

We report on clinical, functional, radiological, genetic, and histological findings in 8 LGMDR3 patients.

In a previous multicenter study, we already demonstrated that the genetic background plays an important role as a prognostic tool for LGMDR3 patients and that c.850C4T, p.(Arg284Cys) and c.739G4A, p.(Val247Met) variants are often associated to higher protein expression at muscle biopsy [13]. Conversely, it is known that the missense mutations c.229C>T, p.(Arg284Cys) is associated with a very reduced protein expression, always <30%, leading to with a worse prognosis, and that harboring two null mutations is generally associated with total or severe loss of protein expression [13].

Indeed, we noticed that patients homozygous or compound heterozygous for the c.850C4T, p.(Arg284Cys) and c.739G4A, p.(Val247Met) variants, namely patients 1-2 and 3, presented with an age of onset later than 10 years and a mild clinical course. At last visit, two of them were in their second and third decade of life, all of them showed the best functional performance (running), a good respiratory function, no cardiac involvement and normal muscle MRI (median T1-MRI tigh score =0; IQR 3).

Patient 4, heterozygous for the c.229C>T, p.(Arg284Cys) variant, presented an early onset of symptoms (<10 years), and a more rapid progression of the disease. At last visit, 13.8 years, her best performance was “walking”, and the muscle MRI performed at the same age of patient 1, showed a more severe involvement of the thigh muscles (T1-MRI tigh score =16).

Patients 6, 7, and 8, harboring 1 or 2 null mutations, presented the most severe phenotypes (median T1-MRI tigh score =90; IQR 84-101). Patient 7 and 8 showed the most rapid disease progression, with onset at 4 years, loss of ambulation within the 10th year, and cardiac involvement. Muscle MRI showed the worst T1-MRI tigh scores, measured as 78 and 112 respectively.

Our muscle MRI data confirm previous results [27], i.e. i) a variability MRI severity, with some cases presenting with normal MRI or minor changes, and patients showing an over muscle fibro-adipose substitution, ii) a symmetrical involvement, iii) a predominance of posterior thigh muscle involvement, and iv) a sparing of sartorius and gracilis.

To the best of our knowledge, this is the first time that bone mineral density has been assessed in LGMDR3. We diagnosed a low mineral density in 2 patients (subjects 7 and 8) that led to long bone fragility fractures. It is established that muscle mass and force are

primary determinants of bone mineral density (BMD) in healthy children, therefore we suggest that LGMDR3 patients should be included in bone health monitoring program as per guidelines of Duchenne Muscular Dystrophy management, at least those LGMDR3 patients with an early age at onset and rapid disease course.

Muscle biopsy data showed a broad spectrum of abnormalities, ranging from cases with only mild myopathic changes, to cases with a severe dystrophic pattern encompassing muscle fiber necrosis, inflammatory infiltrates and fibrosis. These results are consistent with the general understanding that patients with severe clinical course usually have severe histological alterations [68]. Moreover, a statistically significant positive correlation between the residual muscular α-SG level and residual muscle motor function was observed, thus confirming that disease severity may be predicted by α-SG expression in LGMDR3, as previously reported [12].

Data on inflammation, measured by Acid Phosphatase, were also informative on clinical course. Indeed, our results indicated that the higher the amount of inflammation, the earlier is the age at onset and the worse the residual muscle motor function. More severe inflammatory infiltrates were also found in patients with higher CK levels at muscle biopsy and with higher degree of muscle substitution measure at muscle MRI. The role of inflammation in LGMDR3, and, in general, in sarcoglycanopathies, has been studied in a separate project, in part 3, and remain an interesting topic to be further studied, with some important clinical implications in term of defining a specific immunomodulatory regime for patients with major inflammatory features.

Despite muscle biopsies showed the potential to link with some crucial clinical information, it was not enough to reach a diagnosis. As already known [12, 17], patients with LGMDR3 show a variable reduction not only of α-SG expression, but also of the other component of the SG-complex, making difficult to predict the genotype from immunohistochemistry studies. Therefore, in the diagnostic-workout we suggest to firstly perform the genetic, considering a muscle biopsy as a second step, to obtain further prognostic information.

Part of these results were included in the following manuscript:

Alonso-Pérez J, González-Quereda L, Bello L, Guglieri M, Straub V, Gallano P, Semplicini C, Pegoraro E, Zangaro V, Nascimento A, Ortez C, Comi GP, Dam LT, De Visser M, van der Kooi AJ, Garrido C, Santos M, Schara U, Gangfuß A, Løkken N, Storgaard JH, Vissing J, Schoser B, Dekomien G, Udd B, Palmio J, D'Amico A, Politano L, Nigro V, Bruno C, Panicucci C, Sarkozy A, Abdel-Mannan O, Alonso-Jimenez A, Claeys KG, Gomez-Andrés D, Munell F, Costa-Comellas L, Haberlová J, Rohlenová M, Elke V, De Bleecker JL, Dominguez-González C, Tasca G, Weiss C, Deconinck N, Fernández-Torrón R, López de Munain A, Camacho-Salas A, Melegh B, Hadzsiev K, Leonardis L, Koritnik B, Garibaldi M, de Leon-Hernández JC, Malfatti E, Fraga-Bau A, Richard I, Illa I, Díaz-Manera J. **New genotype-phenotype correlations in a large European cohort of patients with sarcoglycanopathy.** Brain. 2020 Sep 1;143(9):2696-2708. doi: 10.1093/brain/awaa228. PMID: 32875335 (see Appendix).

3. Immunophenotype on LGMDR3 and LGMDR5 biopsies: a multi-center study

3.1 Objectives

Aim of this project was to characterize the immune cell infiltrates in muscle biopsies collected from a cohort of sarcoglycan-deficient patients afferent to several Italian Tertiary Neuromuscular Centers, with the goal to determine possible differences between α- and γ-sarcoglycanopathy (LGMDR3 and R5).

Immune cells invasion is a histological hallmark of diverse muscular dystrophies, but only few data are available on the relative contribute of inflammatory sub-type populations in the dystrophic process in sarcoglycanopathies.

3.2 Materials and Metods

Muscle specimens' collection and preparation

Muscle biopsies from 10 LGMDR3 alpha-sarcoglycan and 8 LGMDR5 gamma-sarcoglycan genetically confirmed patients were retrospectively collected from 6 Italian tertiary Neuromuscular Centers.

Quadriceps muscle biopsies were performed for diagnostic purposes. Families of patient gave their consent for research studies in muscle specimens. As positive controls, we analyzed muscle biopsies from 6 patient with DMD. Six muscle biopsies, from patients with not specific muscle weakness or myalgia and without dystrophic signs at pathological examination, served as negative controls.

Muscle specimens were processed as previously reported in part 2 (see "Muscle specimens' collection and preparation").

Other than H&E stain, sections were also stained for the following antibodies according to the manufacturer's instruction and developed in 3,3'-diaminobenzidine (DAB) substrate: CD45 (Clone 2B11, Invitrogen, Carlsbad, CA, USA), MHCI (Clone W6/32, Sigma, St. Louis, MO, USA), CD68 (Clone 514H12, Leica, Newcastle, UK), CD8 (Clone 4B11, Leica), and CD4 (Clone 4B12, Leica).

For each staining, muscle sections were scanned with Axioplan Imager M2 microscope software AxioVs40 version 4.8.2.0 (Zeiss, Jena, Germany). Non-overlapping images at × 10 magnification were snapped through the whole section to cover the entire muscle cross-sectional area. For CD45, CD68, CD8, and CD4 staining, the positive cells were blindly manually enumerated throughout the whole section and reported as density of positive cells to the unit of area (amount of cells/number of sections).

For MHC class I stain, the signal was quantified as previously reported [69]. MHCI

staining was considered as negative if only capillaries were stained, and positive when both capillaries and sarcolemma were positive for MHCI.

3.3 Results

LGMDR3 and R5 patients' information, including gender, gene mutations, histological parameters, and clinical features such as age, symptoms, and serum CK at onset, cardiac involvement, respiratory insufficiency, and MRI study are listed in Table 1.

Patient ID	Sex	Age at MB (y)	Allele 1 mutation	Allele 2 mutation	Fiber size variability	Central nucleation	Necrosis and inflammation	Fibrosis	Dystrophic score
LGMD R3.1	M	9,9	c. 329C>T p.Arg77Cys	c.1005C>A p.Cys335X	2	0	2	2	6
LGMD R3.2	F	4,0	c.409G>A p.Glu1137Lys	c.850C>T p.Arg284Cys	2	1	3	1	7
LGMD R3.3	F	7,4	c.308T>C p.Ile103Thr	c.850C>T p.Arg284Cys	1	1	1	1	4
LGMD R3.4	F	0,8	c.329C>T p.Arg77Cys	IVS5:c.584+5G>A	1	1	1	2	5
LGMD R3.5	M	26,3	c.409G>A p.Glu1137Lys	c.739G>A p.Val247Met	2	2	0	1	5
LGMD R3.6	M	49,6	c.329C>T p.Arg77Cys	c.346A>C p.Thr116Pro	2	1	0	1	4
LGMD R3.7	F	19,2	c.92T>C p.Leu31Pro	c.739G>A p.Val247Met	1	1	0	1	3
LGMD R3.8	F	9,1	c.739G>A p.Val247Met	c.739G>A p.Val247Met	1	0	1	1	3
LGMD R3.9	F	41,8	c.739G>A p.Val247Met	c.739G>A p.Val247Met	2	1	0	1	4
LGMD R3.10	F	25,2	c.92T>C p.Leu31Pro	c.850C>T p.Arg284Cys	2	0	0	1	3
LGMD R5.1	F	19,5	c.525delT p.Phe175Leufs*20	c.525delT p.Phe175Leufs*20	3	1	2	3	9
LGMD R5.2	F	15,6	c.525delT p.Phe175Leufs*20	c.525delT p.Phe175Leufs*20	3	1	0	2	6
LGMD R5.3	M	13,4	**IVS4:c.385+2T>C**	c.801_802delTC p.Pro268Argfs*24	2	1	1	1	5
LGMD R5.4	M	1,5	c.848G>A p.Cys283Tyr	c.848G>A p.Cys283Tyr	2	1	3	1	7
LGMD R5.5	F	2,2	c.342dupT p.Ala115Cysfs*41	c.525delT p.Phe175Leufs*20	1	1	2	3	7
LGMD R5.6	F	6,2	c.371G>A p.Gly124Asp	c.371G>A p.Gly124Asp	2	1	0	1	4
LGMD R5.7	F	6	c.89delG p.Gly30fs*20	c.307C>G p.Leu130Val	1	1	2	2	6
LGMD R5.8	M	3,5	deletion exon 7	deletion exon 7	2	0	3	2	7

Table 1. Genetic mutations, age at onset, and the dystrophic score are summarized in the table.

The H&E staining was performed to assess the overall architecture of the tissues (Figure 1 a-d). To quantify the common dystrophic features, a dystrophic score was assigned (Table 1). MHCI signal was absent in the negative controls and was up-regulated in all the dystrophic patients. Positive MHCI staining was localized both on the surface of inflammatory cells and on the sarcolemma of several myofibers (Figure 1 e-h).

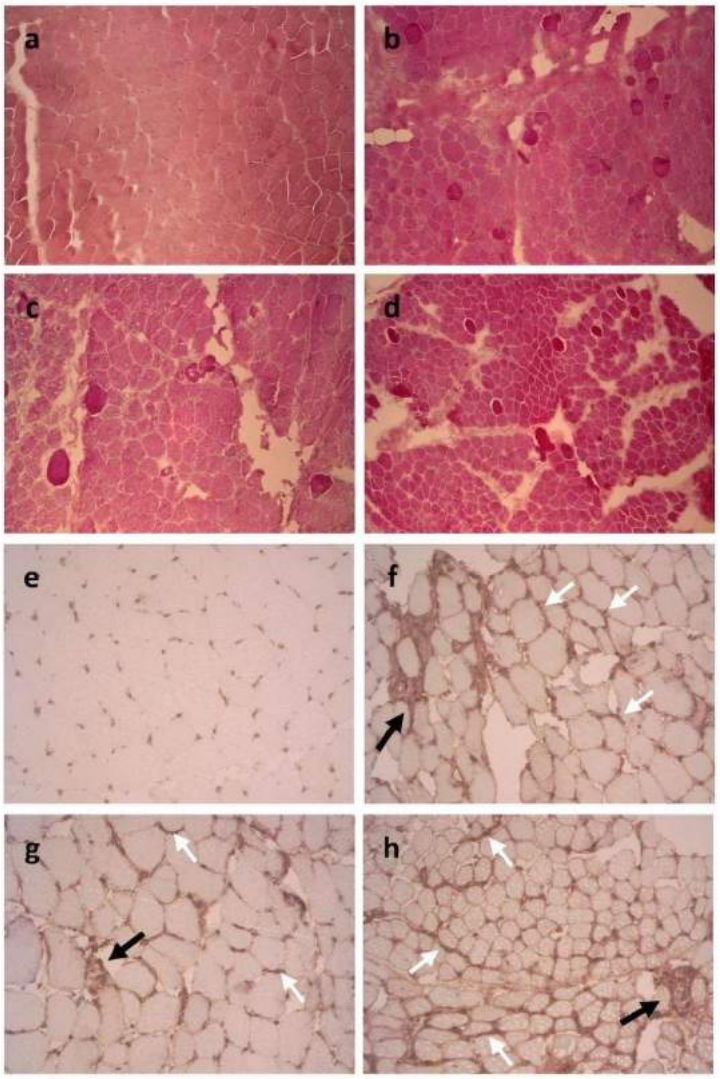

Figure 1. Dystrophic features and MHC class I molecules expression in DMD and LGMDR3-R5. Representative pictures of the H & E staining of negative controls (a), Duchenne muscular dystrophy (b), limbgirdle muscular dystrophy R3 (c), and limb-girdle muscular dystrophy R5 (d). Original magnification × 10. Representative pictures of the MHC class I (MHC I) molecules in negative controls (e), Duchenne muscular dystrophy (f), limb-girdle muscular dystrophy R3 (g), and limb-girdle muscular dystrophy R5 (h). Original magnification × 20. Black arrows show positive staining on the membrane of immune cells, and white arrows show positive staining along the plasma membrane of muscle cells.

To detect the infiltrating immune cells, muscle tissues were stained for CD45, a panleucocytes marker (Figure 2 a-d). $CD45^+$ cells were significantly higher in DMD and LGMDR3-R5 groups in comparison to the negative controls (Figure 2 e).

To characterize the inflammatory infiltrates, muscle samples were stained for markers of the innate and adaptive immune response. Specifically, for the innate immune cells, we checked CD68 (Figure 2 f-i), a surface marker for macrophages; and for the adaptive immunity, we analyzed the $CD8^+$ (Figure 2 m-p) and $CD4^+$ T cells (Figure 2 r-u). $CD68^+$ cells were significantly higher in DMD and LGMDR3-R5 groups in comparison to the negative controls (Figure 2 l). $CD8^+$ cells/area of tissue were significantly increased in the DMD compared to the negative controls and to the sarcoglycanopathies (Figure 2 q). The amount of $CD4^+$ T-cells was significantly higher in the DMD and LGMDR3-R5 than in the negative control group (Figure 2 v). No significant correlations were found between the dystrophic score and the age at muscle biopsy, although a trend showed the two parameters to be linked by an inverse correlation in sarcoglycanopathies (Figure 2 z). A significant inverse correlation was found between the age at muscle biopsy and the number of $CD45^+$ cells in the sarcoglycan group (Figure 2 z).

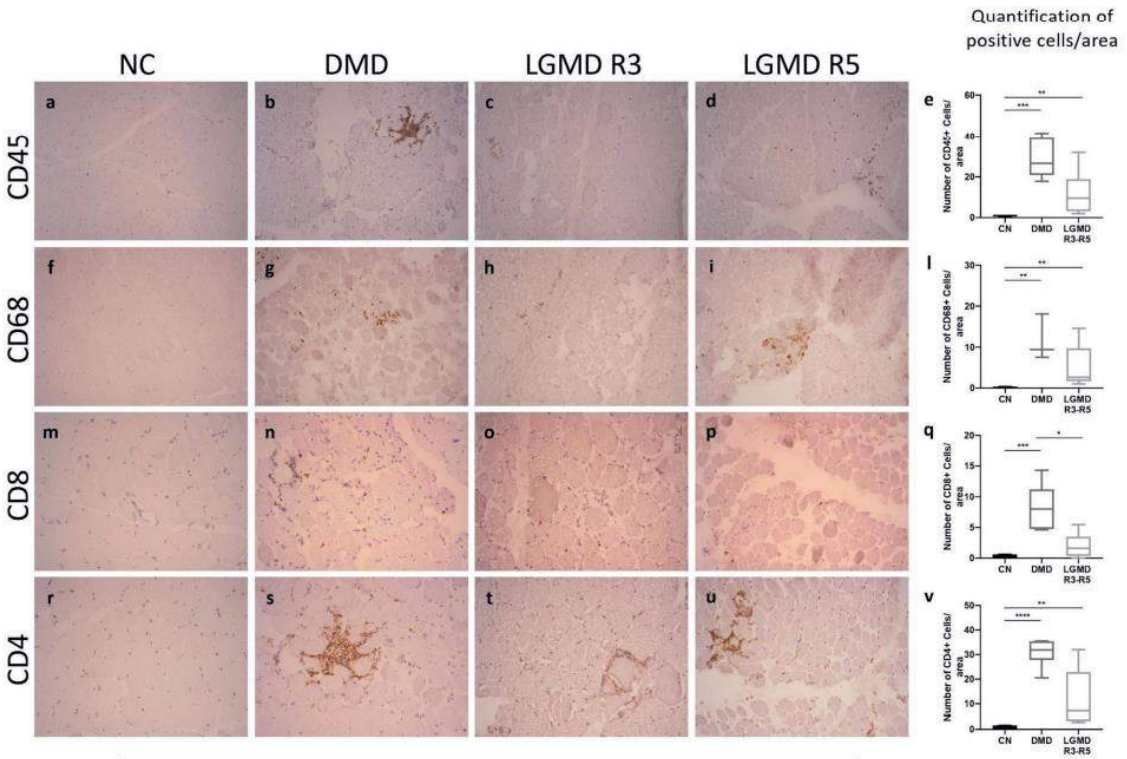

z

	DMD		LGMD R3-R5	
	Spearman r	p-value	Spearman r	p-value
DS vs Age at MB	-0.2	0.7	-0.5	0.07
DS vs CD45+cells	0.39	0.47	0.63	0.09
Age at MB vs CD45+ cells	0.5	0.45	-0.61	0.014

Figure 2. Immunophenotype of the muscle inflammatory infiltrates DMD and LGMDR3-R5. Representative pictures of the CD45 (a, b, c, d), CD68 (f, g, h, i), CD8 (m, n, o, p), and CD4 (r, s, t, u) staining. The muscle biopsies were taken from negative controls (a, f, m, r), Duchenne muscular dystrophy (b, g, n, s), limb-girdle muscular dystrophy R3 (c, h, o, t), and limb-girdle muscular dystrophy R5 (d, i, p, u). Original magnification × 20. Box plots represent the number of $CD45^+$ cells (e), $CD68^+$ cells (l), $CD8^+$ cells (q), and $CD4^+$ cells (v), showing the median, the 10th, and the 90th percentiles.

*p-value< 0.05, **p-value < 0.01, ***p-value < 0.001. z: The table shows the results of the Spearman correlation between the number of $CD45^+$ cells, the age at muscle biopsy, and the dystrophic score. DS = dystrophic score. The p-value was considered as statistically significant when < 0.05.

3.3 Discussion

In this multicenter study, we immunophenotyped the intra-muscular inflammatory infiltrates in muscle biopsies from LGMDR3 and R5 patients in parallel with samples from DMD patients, which we used as disease controls for their known inflammatory features.

We found that MHC class I pattern expression was similar throughout all the dystrophic samples. MHCI molecules are not constitutively expressed in skeletal muscle tissue under physiological conditions [70]. It is known that upon exposure to a high concentration of interferons IFN-α, -β, or -γ, myo cells markedly increase the transcription of MHCI that binds peptides generated mainly from the degradation of cytosolic proteins by the proteasome. So far, MHCI up-regulation has been considered a diagnostic marker of inflammatory myopathies [71-73], while its detection in muscular dystrophies is rather inconsistent [74-77]. In our samples, all dystrophic muscles expressed MHC class I molecules, specifically on the surface of inflammatory cells and on the sarcolemma of almost all muscle fibers. According to these results, MHCI abnormal expression, besides being a diagnostic marker of inflammatory myopathies, can be considered a sign of the inflammatory activation of dystrophic muscles, likely due to the direct involvement of the muscle cells in promoting the local immune response by antigen presentation.

Nevertheless, further studies are needed to systematically quantify the MHC class I expression in inflammatory myopathies and muscular dystrophies to identify possible differential involvement of the antigen-presenting system.

The CD45 staining provided a general view of the muscular immune infiltrates that were evident in LGMDR3-R5, although in both cases less evident than in DMD. In LGMDR3-R5, the density of $CD45^+$ cells inversely correlates with the age at muscle biopsy, mimicking what is already shown in DMD where inflammatory pathways predominate in the early stages, suggesting a stage-specific remodeling of human dystrophic muscle [78]. We immunophenotyped the $CD45^+$ cell infiltrates by checking macrophages, $CD8^+$, and $CD4^+$ T cell markers. All the disease groups showed a predominance of $CD4^+$ Tcells, less macrophages, and occasional $CD8^+$T cells as previously reported in DMD and dysferlinopathy [75, 76], and to our knowledge, this is the first immuno-characterization of cell infiltrates in LGMDR3 and R5. Dystrophic patients showed a significantly higher density of $CD45^+$, $CD68^+$, and $CD4^+$ cells compared to the negative controls, without statistically significant differences between DMD and sarcoglycanopathies. The only exception was represented by CD8+ effector T cells, which were significantly up-regulated in DMD compared to sarcoglycanopathies, suggesting that a different regulation of the

cell-mediated adaptive immunity might occur in the two groups. Nevertheless, no information about the activation state of the immune cells infiltrating the dystrophic muscles can be assumed from this paper.

Despite the difference in the density of $CD8^+$ T cells, overall, our data show that DMD and α- and γ-sarcoglycanopathies share a common immune response, involving both innate and adaptive response. We hypothesize that the instability and loss of the dystrophin-associated protein complex (DAPC) might be the trigger of the chronic inflammatory response. A possible correlation between the extension of the immune response and the representation of the DAPC on muscle membranes needs to be explored in further studies.

DMD therapeutic approach includes low doses of continuative oral steroids, as they proved to slow down disease progression [79], dampening the muscle inflammatory status [80]. Conversely, a placebo-controlled trial assessing the effects of steroids in sarcoglycan-related muscular dystrophies has never been proposed, although the efficacy of immunomodulatory treatments improved muscle repair and performance in α- and γ-sarcoglycan deficient mouse models [81, 82] and in 1 female patient affected by LGMD R3 [83]. Thus, sarcoglycan LGMDs might benefit from an immunomodulatory regimen.

In conclusion, we characterized the intramuscular immune infiltrates in patients with α- and γ-sarcoglycan gene deficiencies. However, we recognize some limitations in our study: the groups were not homogeneous by gender and age at muscle biopsy, given the limited number of patients, and due to the parceling of the muscular immune infiltrates analyzed.

Currently, clinical trials offer different approaches, including gene therapy, which is rapidly developing for many muscular dystrophies. In this scenario, the right immunosuppressant scheme could endorse the efficacy of disease-specific gene therapy by dampening the basal muscular inflammation, and our findings might be useful to fine-tune a disease-specific immunomodulatory regimen.

These results have been published in the following manuscript:

Panicucci C, Baratto S, Raffaghello L, Tonin P, D'Amico A, Tasca G, Traverso M, Fiorillo C, Minetti C, Previtali SC, Pegoraro E, Bruno C. **Muscle inflammatory pattern in alpha- and gamma-sarcoglycanopathies.** Clin Neuropathol. 2021 Nov-Dec;40(6):310-318. doi: 10.5414/NP301393. PMID: 34281632 (see Appendix).

4. In vivo study on a model of Sgca null mouse: the effect of anti-purinergic molecules on disease progression

4.1 Objectives

Aim of this research was to evaluate the effect on disease progression of pharmacological P2X7 receptor inhibition in a mouse model of LGMDR3.

Two different drug regimens were applied: the first, the oxidase ATP (oATP) was a broad purinergic inhibitor, the second, the A438079, consisted in a specific P2X7 receptor antagonist. Both treatments provided encouraging results, indicating that purinergic signal might be deleterious for disease progression in LGMDR3.

4.2 oATP study

4.2.1. Materials and methods

In vivo experiments

Sgca null mice were treated with oATP at 6 mmol/L or phosphate-buffered saline (PBS) alone daily for 4 weeks by i.p. injection and were sacrificed at the end of treatment by carbon dioxide inhalation. A group of age-matched wild-type (WT) C57Bl/6J male mice was used as internal control. The experiment was repeated

in two separate 4-week trials, which both included 5 to 7 mice in each experimental group. Thus, the results are indicative of at least 10 animals per group. The Sgca mice were randomly assigned to the experimental groups, and the testing of samples was performed blindly (S.A. and S.Bal.).

Blood samples were collected by intracardial puncture at the end of the fourth week of treatment and centrifuged for 10 minutes at 7000 x g. Immediately after centrifugation, the serum was isolated and stored at -20°C. Serum creatine kinase levels were measured using the creatine kinase N-acetyl cysteine quantitative system, according to manufacturer's instructions (BPC BioSED, Rome, Italy).

All animal experiments were performed in accordancewith the Swiss Federal Veterinary Office guidelines and authorized by the Animal Studies Committee of Cantonal Veterinary.

Four-Limb Hanging Test

At the beginning of the study and at the end of the second and fourth week of treatment,

the muscle strength of oATP-treated, PBS-treated Sgca, and WT control mice was scored through the four-limb hanging test. In this method, mice are subjected to a 180-second lasting hanging test, during which a falling score is recorded. In each of the two treatments, all the mice had to hang for three trials, and the average maximum hanging time of the three trials was measured (standard operating procedure, http://www.treat-nmd.eu/research/ preclinical/preclinical-efficacy-standards).

Reagents and Antibodies

oATP (Sigma-Aldrich, St. Louis, MO) was reconstituted at a final concentration of 100 mmol/L in PBS and stored at -80 àC; the reconstituted drug was thawed and diluted in PBS at 6 mmol/L immediately before use. Lipopolysaccharide (LPS; Sigma-Aldrich) was reconstituted at a final concentration of 1 mg/mL in Hanks' balanced salt solution and stored at -20 °C, ATP (Sigma-Aldrich) was reconstituted at 100 mmol/L (pH 7) in water with sodium hydroxide and stored at -20 °C, and benzoyl ATP (BzATP; Sigma-Aldrich) was reconstituted at 10 mmol/L in water and stored at -20°C.

The antibodies and dilutions used in the study include the following: mouse monoclonal antibody to collagen type I [1:500 for Western blot (WB) analysis] and rat monoclonal antibody to Ly6C [1:500 for immunohistochemistry (IHC)] from Abcam (Cambridge, UK); rat monoclonal antibody to CD45 (1:10 for IHC) from BD Pharmigen (San Jose, CA);mouse monoclonal antibody to activating signal cointegratore1 (ASC-1) (1:500 for WB analysis) and rabbit

polyclonal antibodies to glyceraldehyde phosphate dehydrogenase (1:500 for WB analysis) from Santa Cruz

Biotechnology (Dallas, TX); rabbit polyclonal antibody to CD3 (1:20 for IHC); rabbit polyclonal antibodies to P2X7 receptor (R; extracellular) and P2X4R (1:50 and 1:300, respectively, for immunofluorescence) from Alomone Labs (Jerusalem, Israel); rabbit polyclonal antibody to transforming growth factor (TGF)-b (1:1000 for WB analysis) from Cell Signaling Technology (Danvers, MA); mouse monoclonal antibody to CD39 (1:1000) from Abcam; mouse monoclonal antibody to a-SG (1:100 for WB analysis) from Novocastra (Newcastle upon Tyne, UK); mouse monoclonal antibody to b-dystroglycan (1:50 for WB

analysis) from Novocastra; mouse monoclonal antie caveolin-3 (1:10,000 for WB analysis) from BD Bioscience (Milan, Italy); mouse monoclonal antibody to myosin heavy chain (fast; 1:1000 for WB analysis) from Novocastra; rabbit anti-mouse IgG horseradish

peroxidaseeconjugated (1:700 for WB analysis) antibodies from Dako (Glostrup, Denmark); donkey anti-rabbit IgG horseradish peroxidaseeconjugated (1:5000 for WB analysis) antibodies from GE Health Care (Little Chalfont, UK); mouse monoclonal anti-rat k and l light chain horseradish peroxidaseeconjugated (1:100 for IHC) antibody from Sigma-Aldrich; rat monoclonal to FOXP3 (1:20 for IHC) from eBioscience (Waltham, MA); and goat anti-mouse AlexaFluor 488 and donkey anti-rat AlexaFluor 594 (1:750 for immunofluorescence) antibodies from Thermo Fisher Scientific (Waltham, MA). The EnVision Detection System Peroxidase/Diaminobenzidine, rabbit and mouse, was from Dako. The Annexin A5-FITC/7-AAD Kit was purchased from Beckman Coulter (Marseille, France).

Satellite Cell Isolation from Total Muscle

Satellite cells were isolated from WT and Sgca mice at passage 8 to passage 10. Forelimb, hind limb, and diaphragm muscles were dissected, mechanically cut, and enzymatically digested at 37°C under constant shaking with a solution containing collagenase I (100 mg/mL; Sigma-Aldrich), dispase (500 mg/mL; Gibco, Waltham, MA), and DNaseI (100 mg/mL; Roche, Basel, Switzerland) in PBS (Sigma-Aldrich). Undigested tissue was precipitated for 5 minutes, and the supernatant was centrifuged for 5 minutes at 1200 x g. The cell pellet was resuspended in Dulbecco's modified Eagle's medium plus 10% fetal bovine serum, 1% L-glutamine, 1% penicillin/streptomycin, and 1% gentamicin; then, it was preplated in 150-mm Petri uncoated dishes for 1 hour. After preplating, the nonadherent satellite celleenriched population was collected and plated in collagen-coated (collagen from calf skin; Sigma-Aldrich) 90-mm Petri dishes at a density of 30,000 cells per Petri dish. After a few days in proliferation, the myoblasts were eventually plated at high density in differentiation medium (Dulbecco's modified Eagle's medium, 10% donor horse serum, 1% L-glutamine, 1% penicillin/streptomycin, 1% gentamicin, and 2.5 ng/mL basic fibroblast growth factor).

Histologic Studies

Sections (7 mm thick) from gastrocnemii (GN) and anterior tibialis muscles isolated from PBS-treated mice, oATP-Sgca mice, and WT controls were cut on a cryostat and stained with standard hematoxylin and eosin and acid phosphatase for inflammatory reactions and Masson trichrome stain. Image analysis in terms of area fraction quantification, signal intensity, and object counting was performed using semiautomated measurement tools in

NIS-Elements AR software version 4.20.00 (Laboratory Imaging, s.r.o., Prague, Czech Republic). Central nucleation (expressed as percentage of the total nuclei in each section) was quantified in a blinded manner (S.A. and S.Bal.) in three sections for each muscle (n Z 10 mice for each experimental group, n Z 400 to 600 myofibers per single animal) with the Axioplan Imager M2 microscope software AxioVs40 version 4.8.2.0 (Zeiss, Oberkochen, Germany). Paraffin-embedded diaphragms isolated from PBS-treated oATP-Sgca and WT control mice were cut in cross section at the midbelly of the muscle (7 mm thick). After deparaffinization, the slides were stained with hematoxylin and eosin12 and Picrosirius red staining for collagen fibers.

Immunohistochemistry

Cryosections (5 mm thick) of GN and anterior tibialis muscles isolated from PBS-treated, oATP-Sgca, and WT control mice were fixed in acetone at -20°C for 10 minutes, washed three times in PBS, and then washed twice in 0.025% PBS/Triton. Sections were incubated in 8% bovine serum albumin in PBS (blocking solution) for 1 hour at room temperature. Then, sections were incubated with primary antibodies diluted in 1% bovine serum albumin in PBS solution overnight at 4°C. The next day, sections were washed two times with 0.025% Triton in PBS, incubated 15 minutes in 0.3% H2O2 in PBS, and subsequently incubated with an Envision secondary antibody for 1 hour. After being rinsed two times with PBS (5 minutes each), the sections were stained with a diaminobenzidine substrate solution (freshly made just before use), counterstained with hematoxylin, washed with deionized water, dehydrated through five changes of alcohol (70%, 90%, 95%, 100%, and 100%) for 1 minute each, cleared in two changes of xylene (3 minutes each), and mounted with a Vectashield mounting medium (Vector Laboratories, Burlingame, CA). Slides were observed under a Leica Diaplan microscope (Leica, Wetzlar, Germany). The number of positive cells was blindly counted (S.Bar. and S.A.) on the whole sections per mouse. The total area of the section was measured and expressed in arbitrary units.

For immunofluorescence, unfixed cryosections (5 mm thick) of GN and anterior tibialis muscles were incubated in common antibody diluent (BioGenex, San Ramon, CA) for 10 minutes and after with primary antibodies (CD45, P2X4, and P2X7 antibodies) overnight at 4°C. After three washes with PBS, sections were incubated with fluorescent secondary antibodies in common antibody diluent for 1 hour at room temperature in the dark. After being washed three times with PBS, sections were mounted with Vectashield mounting medium with DAPI (Vector Laboratories). Images were obtained using a Leica SPE

confocal microscope equipped with argon/He-Ne laser sources and an HCX PL APO CS 63.0 x 1.40 oil objective. During image acquisition, the 488 and 594 lasers were set at 20% energy, and the emission range was between 500 and 550 and between 650 and 700 nm for P2X 488 and CD45 594, respectively. The photomultiplier voltage gain was set to eliminate cell autofluorescence. Single-plane images were taken at the center of cell thickness.

Western Blot Analysis

Total protein lysates were isolated from PBS-treated mice, oATP-Sgca mice, and WT GN muscles, as previously described [62]. Equal amounts of protein (40 to 120 mg) were resolved in 8% to 15% SDS-PAGE gel and transferred onto polyvinylidene difluoride membranes (Immobilon PVDF, Billerica, MA). Membranes were blocked with 5% bovine serum albumin in PBS/0.1% Tween 20. Blots were then incubated overnight at 4°C with primary antibodies. Horseradish peroxidase anti-IgG was used to visualize bound primary antibodies with the chemiluminescence system (Bio-Rad Laboratories). Band intensities were evaluated by densitometry using the Alliance Mini HD9 AutoAutomatic system (Uvitec, Cambridge, UK).

Ecto-ATPase Activity

Satellite cells were seeded in 24-well plates (5.5 x 104 cells/ well) and cultured until they completely differentiated into mature myotubes. After removal of the culture medium, cells were washed once with 1 mL Hanks' balanced salt solution, and 0.35 mL Hanks' balanced salt solution containing 0.3 mmol/L ATP was added. At various times (0, 5, and 15 minutes), 100-l aliquots of the incubations were withdrawn and incubations were stopped by filtration with a multiscreen vacuum manifold using Immobilon-P membrane plates (Millipore, Bedford, MA). ATP degradation was determined by the phosphate high-performance liquid chromatography analysis, as previously described [84]. Cells were lysed, and protein content in each well was determined by Bradford assay.

Apoptosis

Satellite cells were seeded in 24-well plates (6 x 104 cells/ well) and cultured until they completely differentiated into mature myotubes. The cells were pretreated with LPS (1 mg/mL) for 4 hours and then incubated with 3 mmol/L ATP and 300 mmol/L BzATP for 16 hours. Then, myotubes were analyzed by flow cytometry, according to other studies that

have adopted the same technique [85-87]. Specifically, the cells were stained with the Annexin A5 FITC/7-AAD Kit, and apoptosis was evaluated by flow cytometry, according to the manufacturer's instructions. Sample analysis was performed using a Gallios cytometer (Beckman-Coulter) and Kaluza software version 1.1 (Beckman-Coulter).

Statistical Analysis

Most of the analyzed variables were not normally distributed, as confirmed by the Shapiro-Wilk test, and therefore differences of quantitative parameters between two groups of mice were analyzed by the U-Mann Whitney test for nonparametric data. $P < 0.05$ was considered statistically significant. Data are expressed as medians, first and third quartiles, as described in *Results* and figure legends. Statistica software version 9.1 (StatSoft Co, Tulsa, OK) was used for all of the statistical analyses. Graphs were generated with Graph Pad Prism software
version 6.0 (Graph Pad Software, San Diego, CA).

4.2.2. Results

Sgca Primary Myotubes Are Characterized by a Defect in Ecto-ATPase Activity and Undergo Apoptosis on ATP Treatment

Primary satellite cells were isolated from the forelimb, hind limb, and diaphragm muscles of passage 8 to passage 10 old Sgca and WT mice and cultured until they completely differentiated into mature myotubes. The absence of expression of a-SG was confirmed by Western blot analysis on total cellular extracts. Sgca-deficient cells displayed normal levels of caveolin-3 and myosin heavy chain, thus indicating the achievement of a functional muscle cell phenotype. The decrease observed in b-dystroglycan levels is in accordance with the disruption of the dystrophin-glycoprotein complex in a-sarcoglycanopathies (Figure 1A).

The ecto-ATPase activity was quantified by measuring ATP metabolism in mass spectrometry, in WT and Sgca cells switched to a basal medium containing ATP at 0.3 mmol/L. When compared with theWT, Sgca cells were characterized by decreased ecto-ATPase activity (Figure 1B), resulting in increased ATP levels in culture medium. Muscle cells express the ecto-ATPase CD39, which converts ATP to ADP. However, the increase in ATP levels observed in the Sgca group appeared to be specifically related to the absence of the a-SG ecto-ATPase activity because the protein levels of CD39 were not modified

between Sgca and WT muscle lysates (Figure 1C).

For the evaluation of apoptosis, the cells were pretreated with 1 mg/mL LPS for 4 hours, incubated with 3 mmol/L ATP and 300 mmol/L BzATP for 16 hours, and then stained with the Annexin A5 FITC/7-AAD Kit. The feasibility of a citofluorimetric assay in myotubes has been previously determined [85-87]. The number of apoptotic muscle cells was determined measuring the percentage of Annexin V^+/7- AAD^- and Annexin V^+/7-AAD^+ cells (early and late apoptosis, respectively). The pretreatment with LPS is supported by the observation that LPS caused a marked up-regulation of striatal P2X7 expression.18 ATP and, more potently, BzATP induced apoptosis, an effect that was further enhanced by a pretreatment with LPS (Figure 1D).

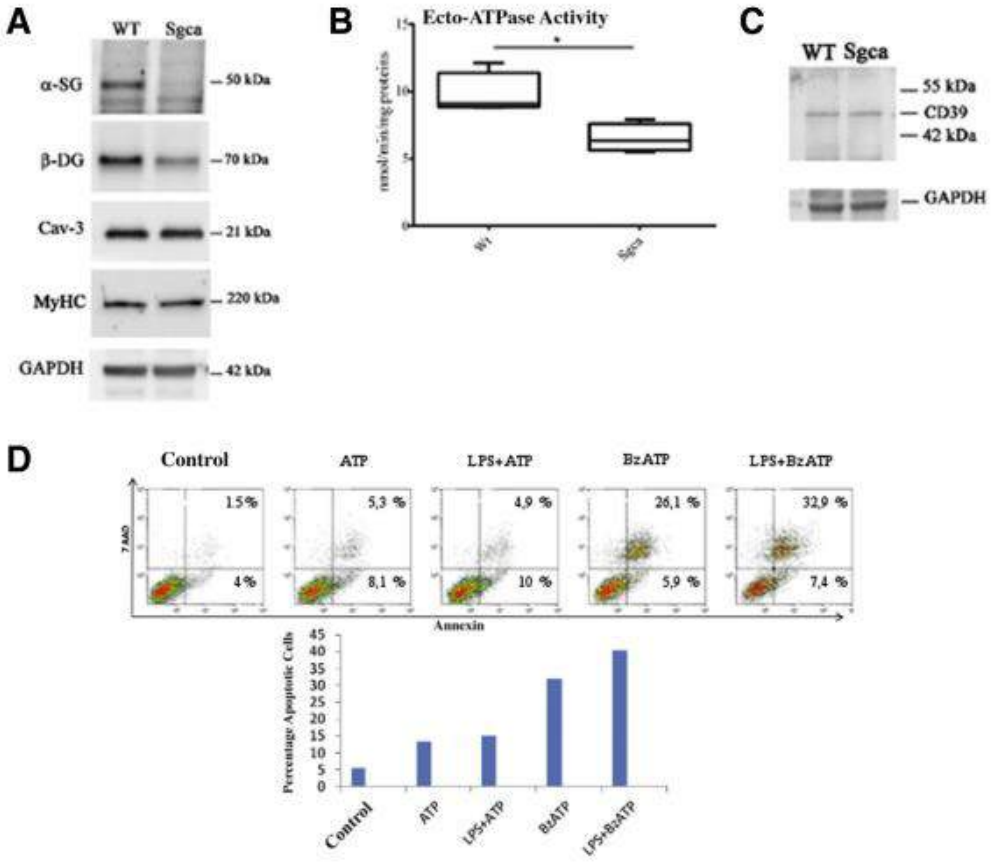

Figure 1. Sgca myoblasts display a decreased ecto-ATPase activity and undergo apoptosis on treatment with ATP or benzoyl ATP (BzATP).

(A) Total protein lysates, isolated from primary myotubes from Sgca and WT age-matched controls, were subjected to Western blot analysis. Membranes were probed with a mouse monoclonal antiea-SG, b-dystroglycan (b-DG), antiecaveolin-3 (Cav-3), and myosin heavy chain (MyHC) antibody. Glyceraldehyde-3-phosphate dehydrogenase (GAPDH) was used as a loading control. Representative images are shown. (B) Primary myotubes isolated from Sgca and WT mice were cultured in basal medium containing ATP at 0.3 mmol/L. At subsequent times (0, 5, and 15 minutes), 100-mL aliquots of

the incubations were withdrawn and ATP degradation was determined by the phosphate high-performance liquid chromatography analysis. (C) Total protein lysates, isolated from primary myotubes from Sgca and WT age-matched controls, were subjected to Western blot analysis. Membranes were probed with a mouse monoclonal anti-CD39 antibody. GAPDH was used as a loading control. Representative images are shown. (D) Primary myotubes isolated from Sgca mice were pretreated with 1 mg/mL lipopolysaccharide (LPS) for 4 hours and then incubated with 3 mmol/L ATP and 300 mmol/L BzATP for 16 hours. The cells were stained with the Annexin A5 FITC/7-AAD Kit, and apoptosis was evaluated by flow cytometry.

P2XR Is Expressed in Sgca Muscle Tissue

The pattern of expression of the P2XR was evaluated in muscle lysates from the GN of Sgca mice and age-matched WT controls. A specific up-regulation of P2X4R and P2X7R transcripts (sixfold and fourfold, respectively) was observed (Figure 2), whereas P2X2R transcript levels were not measurable (Figure 2).

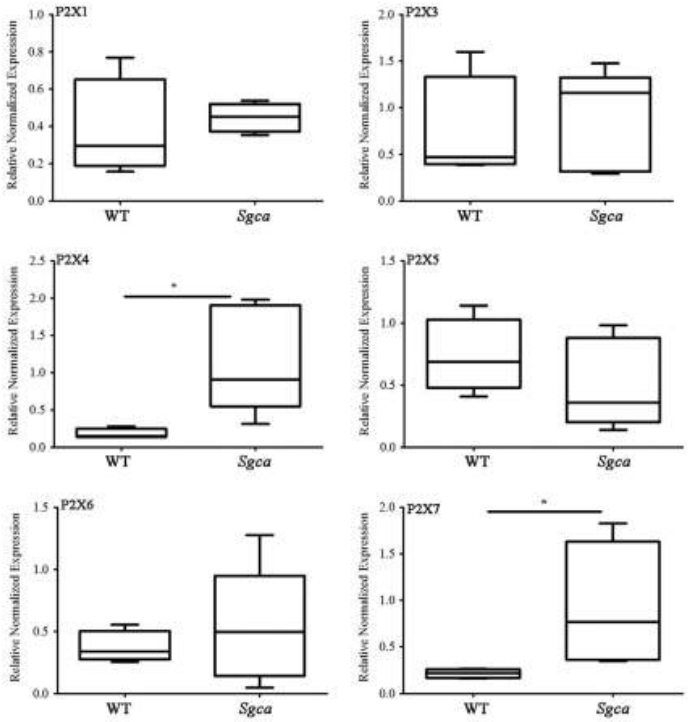

Figure 2. P2X4 and P2X7 purinergic receptors are significantly up-regulated in Sgca muscle tissue.

To determine whether P2X4R and P2XR7 were expressed in myofibers or in infiltrating inflammatory cells, a coimmunostaining was completed with the pan-granulocyte marker CD45 and P2X4 and P2X7R antibodies, respectively, in GN sections. P2X4R was hardly detectable on the muscle cell membrane in WT mice, and it was up-regulated and

colocalized with $CD45^+$ cells in the Sgca mutants (Figure 3A). P2X7R expression was weak in WT myofibers, whereas clear and specific P2X7R patches at the plasma membrane level were detected in Sgca muscle fibers, suggesting an induction and a higher functionality of the receptor because of its cell surface localization. This same feature has been previously shown in the monocytic subset of myeloid-derived suppressor cells isolated from tumor bearing mice (Figure 3B).

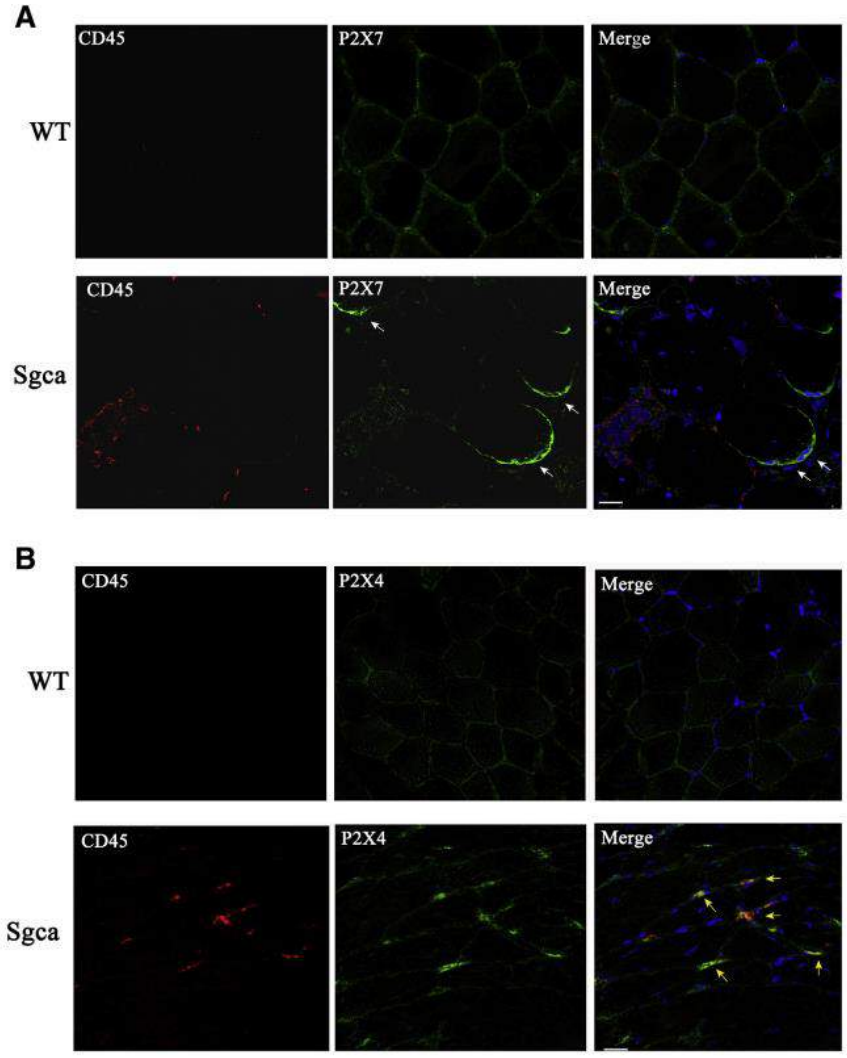

Figure 3. P2X7R is overexpressed in Sgca muscle cells, whereas P2X4R is mainly expressed in $CD45^+$ cells. (A) Frozen muscle tissue sections of gastrocnemii from Sgca and WT mice were immunostained with a monoclonal anti-CD45 antibody (red) and a monoclonal P2X7R antibody (red). (B) Frozen muscle tissue sections of GN from Sgca and WT mice were immunostained with anti-CD45 antibody (red) and a monoclonal P2X4R antibody (red). Representative images are shown. Scale bar 25 mm (A and B). Original magnification, 40X (A and B).

Targeting P2X Signaling in Vivo Improves Biochemical and Functional Parameters of Disease Progression in Sgca Mice

Given the representation of different P2XR in Sgca muscles, we aimed at initially achieving a pleiotropic antagonistic effect on eATP signaling cascade. Four-week-old Sgca mice were treated with oATP, a compound known to act on multiple P2X receptor molecules. oATP was administered via i.p. injections, at the dose of 6 mmol/L. Sgca mice injected with vehicle alone (PBS) and a group of age- and sex-matched WT C57Bl/6 mice served as controls. Mice were weighted at the beginning (baseline) of the treatment and then on a weekly basis. No significant difference was

detected between the various groups (data not shown). The evaluation of muscle strength was completed by the four-limb hanging test at the beginning of the treatment (time 0) and at the end of the second and fourth weeks of treatment. As expected from the literature, the untreated Sgca group displayed a progressive worsening of muscle strength along time, whereas the oATP-Sgca cohort maintained the scores measured at time 0 ($P < 0.05$ for oATP-treated mice versus PBS-treated mice after 4 weeks) (Figure 4A).

Serum creatine kinase concentrations, a marker of muscle cell degeneration, were evaluated at the end of the trial by cardiac puncture. Creatine kinase was markedly increased in PBS-Sgca mice when compared with the WT cohort, whereas the treatment with the P2X antagonist led to a 35% decrease of this effect (Figure 4B).

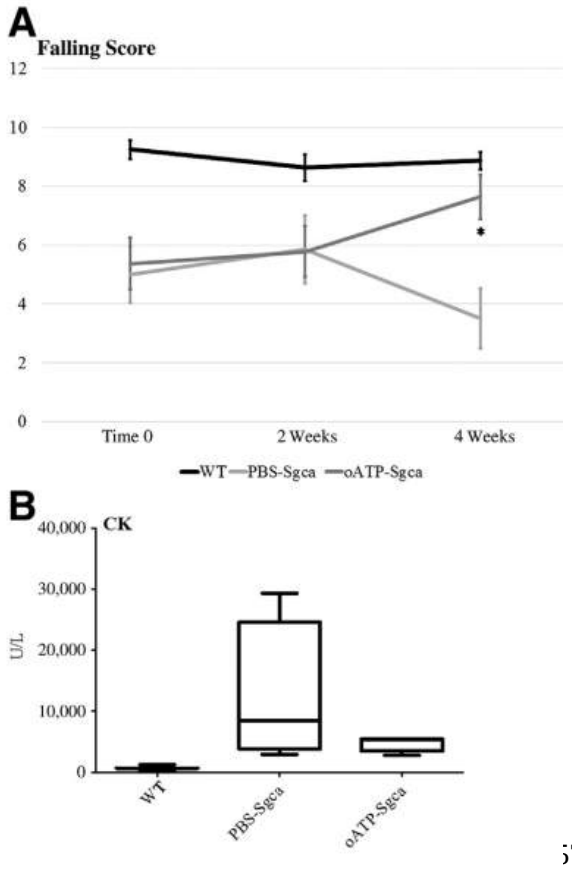

Figure 4. oATP improves muscle strength and ameliorates creatine kinase (CK) serum levels in Sgca mice. (A) Four-limb hanging test was performed on PBS-Sgca (light gray line), oATP-Sgca (dark gray line), and age-matched WT controls (black line). (B) Serum CK levels were evaluated at the end of the fourth week of treatment.

Data are expressed as Medians, first and third quartiles. Statistical analysis was performed using the U-test. n 10 animals for each experimental group (B). *$P < 0.05$ for oATP-treated mice versus PBS-treated mice.

Inhibition of P2X Signaling Ameliorates Morphologic Features and Reduces the Amplitude of the Innate and Adaptive Immune Responses in Sgca Mice

The fraction area and the intensity of the inflammatory reactions surrounding degenerative/necrotic muscle cells were evaluated in GN from PBS- and oATP-treated animals by acid phosphatase staining, which provides a red positive signal in activated macrophages and degenerative myofibers. These parameters were decreased in the oATP-treated group by 46% and 38%, respectively ($P < 0.01$ and $P < 0.05$, respectively) (Figure 5, A and B).

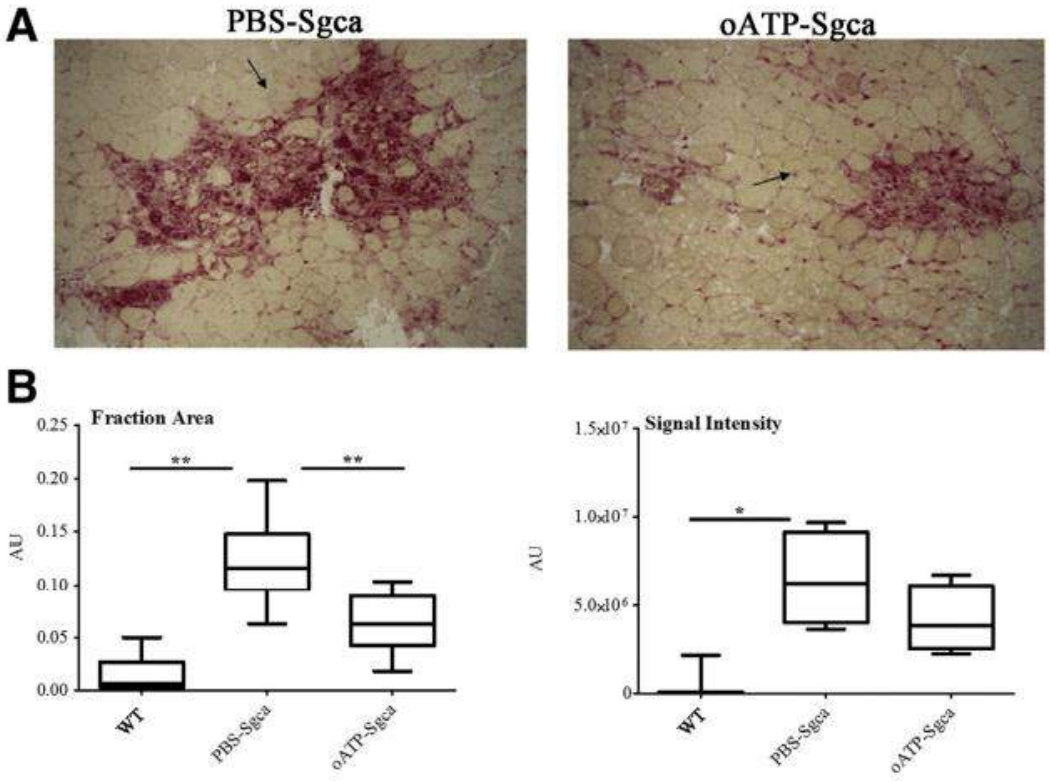

Figure 5. oATP improves the extension of reactive inflammatory infiltrates and morphologic features in Sgca mice. (A) Frozen muscle tissue sections of gastrocnemii (GN) from PBS-Sgca and oATP-Sgca mice were collected at the fourth week of treatment and stained with acid phosphatase. Black arrows indicate inflammatory infiltrates. Representative images are shown. (B) Graph of the analysis of the fraction areas and intensities of inflammatory infiltrates/total section area of muscles represented in A. Statistical analysis was performed using the U-test.

Muscle morphology was quantified in GN by standard hematoxylin and eosin staining. Central nucleation (percentage), a sign of dystrophic myopathic damage, was reduced by 14% in GN of oATP-treated animals. Moreover, muscle tissue from untreated Sgca mutants, when compared with WT mice, displayed an increase of myogenin transcripts, a muscle-specific transcription factor expressed by committed myoblasts in regeneration and typically up-regulated in the degenerative/regenerative cell cycles of active muscular dystrophies. This effect was blunted by 67% after oATP treatment, thus suggesting an inhibition of degenerative cellular events (data not shown).

Immunostaining and measurement of the $CD45^+$ and $Ly6C^+$ leukocytes infiltrating the muscle tissue revealed a positive signal for both markers in different sites of the inflammatory responses surrounding necrotic fibers. When quantified by automated microscopy on the total section area, the number of $CD45^+$ and $Ly6C^+$ cells in the total areas was inhibited by 45% and 25%, respectively, in oATP-treated mice (Figure 6, A and B). Accordingly, the protein levels of ASC-1, a coactivator of NF-kb, were undetectable in WT mice, markedly increased in Sgca muscle lysates, and significantly inhibited after P2X blockade (Figure 6C).

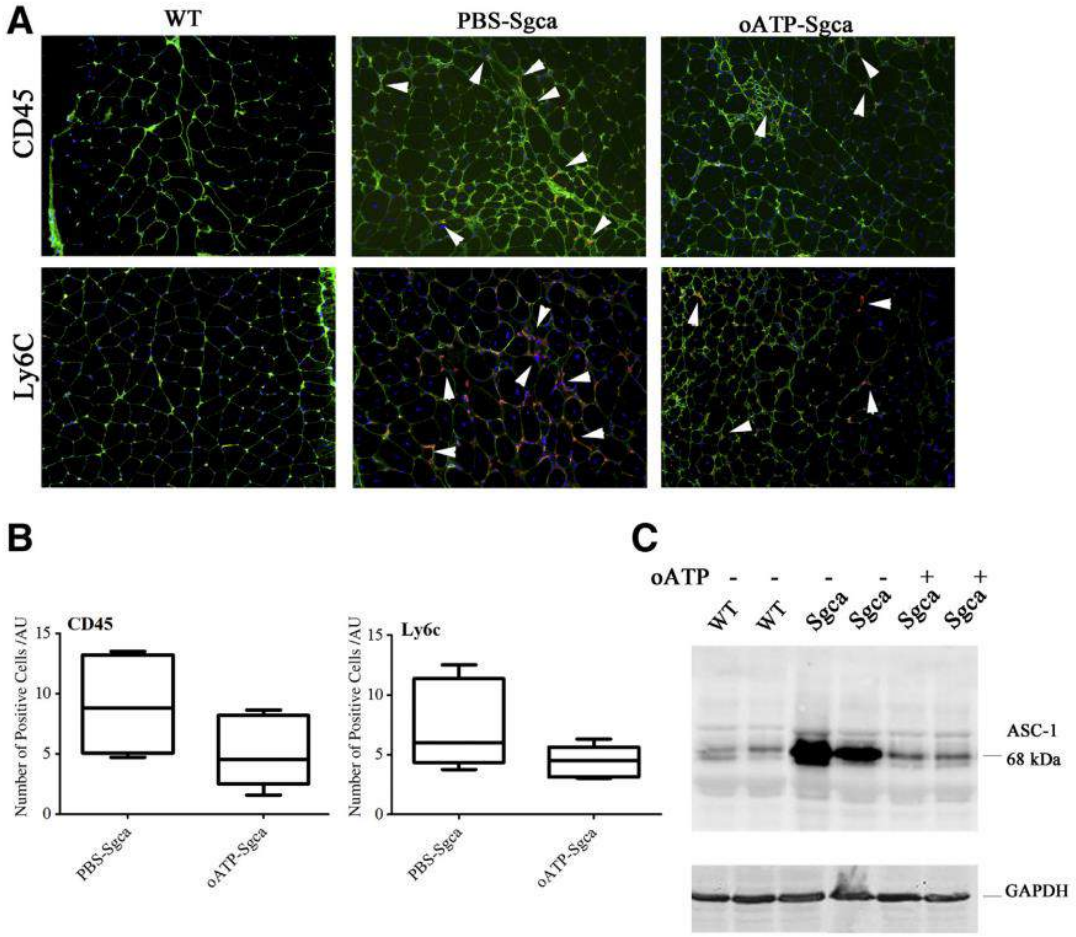

Figure 6. oATP induces a decrease of inflammatory cytokines and monocyte infiltration in muscles from Sgca mice. (A) Frozen muscle tissue sections of gastrocnemii (GN) from PBS-Sgca and oATP-Sgca mice were collected at the fourth week of treatment and immunostained with a monoclonal anti-CD45 antibody (red), monoclonal anti-Ly6C antibody (red), and monoclonal antiecaveolin-3 antibody (green). (B) Graph of the number of $CD45^+$, $Ly6C^+$ cells/arbitrary unit (AU) of total section area of muscles represented in A. Statistical analysis was performed using the U-test. (C) Total protein lysates,

were subjected to Western blot analysis. Membranes were probed with a mouse monoclonal antieactivating signal cointegratore1 (ASC-1) antibody. Representative images are shown. n 10 (A, PBS-Sgca and oATP-Sgca mice). Original magnification, 20X (A).

The immunostaining and measurement of the CD3 lymphocytes infiltrating the muscle tissue showed a CD3-positive signal in different sites of reactive inflammatory responses. When quantified by automated microscopy on the total section area, the fraction areas of CD3-positive signal were reduced by 52% in oATP-treated mice (data not shown). Despite the decrease in the total number of $CD3^+$ cells, $FOXP3^+$ cells were increased in muscle tissue of oATP-treated Sgca mutants by 34% (Figure 7, A and B). The mechanisms of how oATP affects innate and adaptive response in Sgca skeletal muscle were also investigated

by quantification of muscular IL-1b, IL-6, and IFN-g transcripts. When compared with the PBS cohort, these cytokines were reduced by 49%, 39%, and 44%, respectively, in the oATP group (Figure 7C).

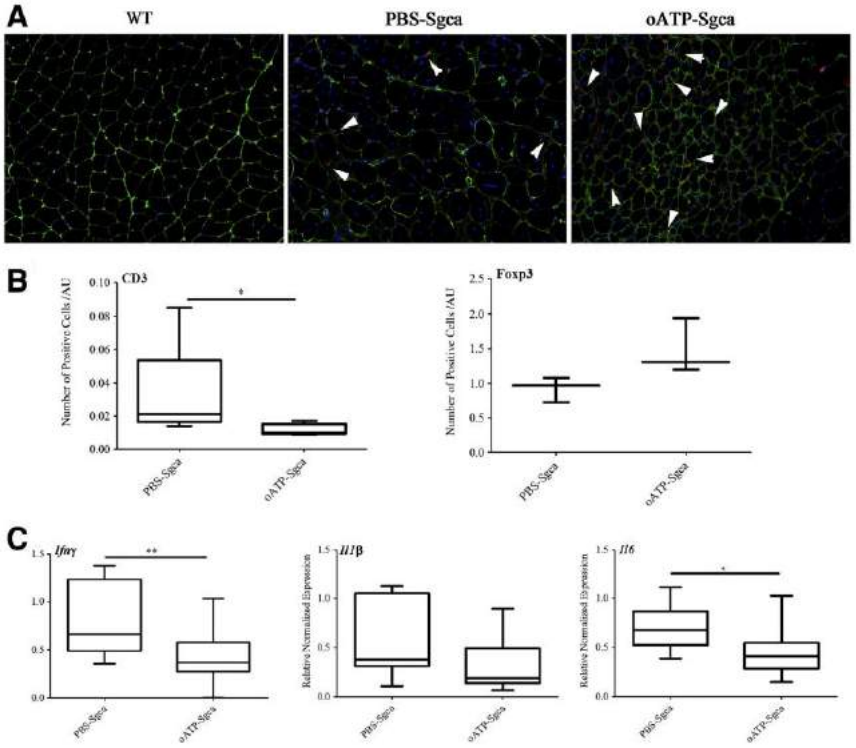

Figure 7. oATP decreases the total number of $CD3^+$ lymphocytes but increases the extension of forkhead box protein P3 $(Foxp3)^+$ positive cells in Sgca mice. (A) Frozen muscle tissue sections were collected at the fourth week of treatment and immunostained with a monoclonal anti-FOXP3 antibody. (B) Graph of the number of $CD3^+$ and $FOXP3^+$ cells/arbitrary unit (AU) of total section area of muscles represented in A. (C) Total RNA isolated from GN lysates from PBS-Sgca and oATP-Sgca mice was reverse transcribed. IL-1b, IL-6, and interferon (IFN)-g transcripts were quantified by real-time quantitative PCR.

Targeting P2X Signaling in Vivo Decreases Muscular Fibrotic Degeneration

In accordance with this anti-inflammatory image, P2X blockade led to a reduction of the transcription of fibrogenic factors, which ultimately stimulate endomysial fibrosis and connective replacement of muscle tissue. The effects of oATP on collagen type I and on TGF-b were tested at the protein levels. P2X antagonism prevented the up-regulation of collagen type I observed in the untreated cohort, and it led to a reduction of both dimeric (25 kDa) and monomeric (15 kDa) active TGF-b isoforms (Figure 8A). Accordingly,

histologic analyses by Masson trichrome staining on GN sections revealed that oATP treatment led to a 20% decrease of the fraction area (Figure 8, B and C).

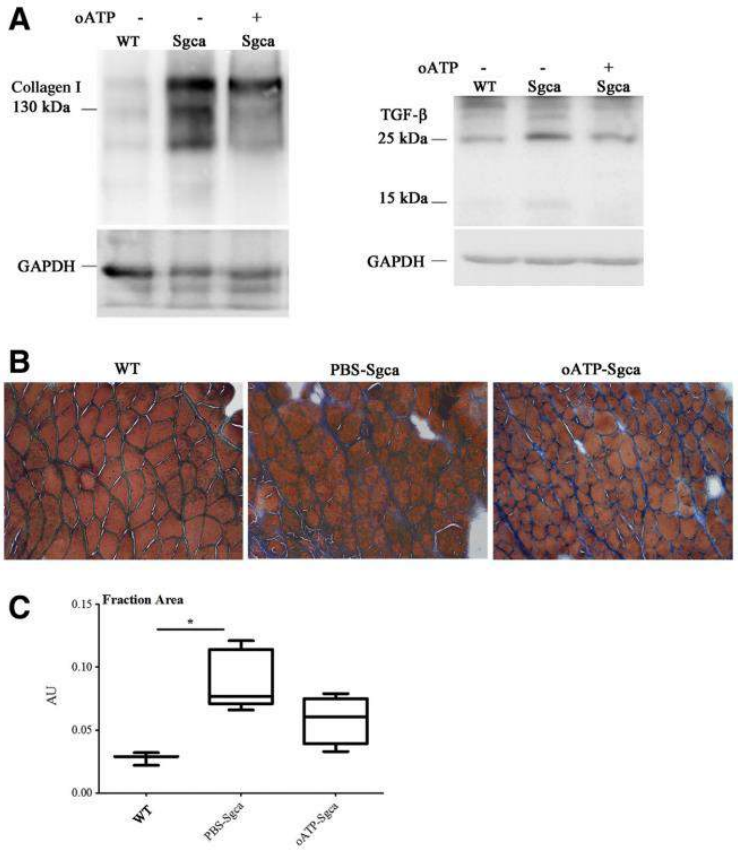

Figure 8. oATP induces a decrease of collagen profibrotic factors in muscles from Sgca mice. (A) Total protein lysates, were subjected to Western blot analysis. Membranes were probed with a rabbit polyclonal anti-collagen type I and a mouse monoclonal anti-transforming growth factor-b (TGF-b; the 25-kDa dimer and the 15-kDa monomer) antibody. Representative images are shown. (B) Frozen muscle tissue sections were stained with a standard Masson trichrome stain protocol. (C) Graph of the fraction areas of fibrotic blue positive signal/arbitrary unit (AU) of total section area of muscles represented in B.

4.2.3. Discussion

In sarcoglycanopathies, the mechanically weaker plasma membrane is easily damaged during muscle contraction, allowing release of intracellular antigens, infiltration of immune cells, and induction of profibrotic cytokines and growth factors [88]. Although different experimental models have shown how distinct anti-inflammatory approaches may enhance stem cell therapy in mice [89], the molecular mechanisms that trigger the immune-mediated damage in this disorder have not been described yet. Likewise, limited are the clinical studies and the clinical experience on anti-inflammatory strategies in human sarcoglycanopathies.

Conversely, in Duchenne muscular dystrophy, it has been extensively highlighted that the immune system exerts a dichotomous role because two types of inflammation that promote and repair muscle injury are activated in the muscle tissue [90-94]. Type 1 inflammation is characterized by increased expression of IFN-g and is counterregulated by type 2 cytokines, such as IL-4 and IL-13, and the Treg anti-inflammatory cytokine IL-10.

Herein, it was found that type 1 and type 2 inflammation are activated also in a-SG deficiency. When compared with WT animals, a-SG deficient muscle tissue displayed higher expression levels of proinflammatory cytokines, such as IL-1b, IFN-g, and IL-6, augmented content of the proinflammatory molecule ASC-1, and increased infiltration of CD45 leukocytes, macrophages (innate immunity), and $CD4^+$ lymphocytes (adaptive immunity). This process was counteracted by an increase in the number of $FOXP3^+$ $CD4^+$ Tregs, which also showed an activated phenotype, as confirmed by induced levels of the cytokine IL-10.

The potential role of the DAMP molecule eATP was next studied in the development of this tissue-specific immune-mediated damage, and it was shown, for the first time, that P2X-purinergic signaling is involved in this pathologic cascade.

Sgca mice were characterized by an enhanced expression of P2X4 and P2X7 receptors in muscle tissue, confirming that SG defects, as dystrophinopathies, result into a purinergic pathway overactivation. Although P2X4R was mainly up-regulated in $CD45^+$ inflammatory cells infiltrating the muscle, P2X7R was overexpressed on the plasma membrane of Sgca muscle fibers. Noteworthy, in dystrophic cells, the receptor molecules were found to be organized in specific patches, suggesting in the monocytic subset of myeloid-derived suppressor cells isolated from tumor-bearing mice [95].

An excess of ATP in the extracellular milieu can be counteracted by the action of the ecto-ATPases CD39 and CD73, which in subsequential order convert ATP to adenosine.

However, also, a-SG displays in its C-terminal domain an ecto-ATPase function, and its absence causes a more consistent accumulation of ATP in the culture medium of primary myotubes. In turn, as already shown in distinct cell systems, an excessive extracellular ATP stimulation is able to exert a direct toxic effect in muscle cells because it induces apoptosis [96, 97]. The molecular basis of the proapoptotic effect can be because of an effect on mitochondrial metabolism or the association with pannexin molecules and the formation of a cytolytic pore (ie, a large conductance channel).

According to these first observations, the pharmacologic inhibition of purinergic signaling via oATP led to an improvement of muscular function and structure, a reduction of the innate/adaptive immune response and fibrosis, and an increase in $FOXP3^{+}$ $CD4^{+}$ Treg muscle infiltration. In this scenario, it is likely that the oATP-mediated boosting of Treg muscle infiltration played a role in ameliorating the Sgca mice phenotype. It has been shown that skeletal muscle resident Treg, producing IL-10 and expressing Areg, controls the switch of type 1 to type 2 inflammation in injured muscle and acts directly on muscle satellite cells, improving muscle repair [98-100]. Noteworthy, myoblasts isolated from mdx mice showed an increased cytosolic $Ca2^{+}$ ion influx and IL-1b release when stimulated with BzATP [101], thus evoking an active role of skeletal muscle cells in the inflammatory mechanism through P2X-purinergic signaling. The assessment of Sgca and LGMDR3 primary myoblast behavior under eATP stimulation and the direct effect of P2XR inhibition on these cells will be evaluated in our future studies.

oATP was originally described as an irreversible P2X7R antagonist [102] but was shown later to also block other P2XRs, such as the P2X4 subtype [103], making this compound a good candidate for a first proof of principle of our hypothesis in Sgca mice, in which an up-regulation of both P2X7 and P2X4 receptors was found. oATP has also demonstrated promise as a treatment modality in several models of autoimmune diseases. Successful examples are experimental models of collagen-induced arthritis, autoimmune diabetes, allergic encephalitis, autoimmune colitis, and allograft rejection in cardiac and islet transplantation [103-109]. In these disorders, the compound works as a suppressor of the innate and adaptive immunity as well as an inductor of Treg expansion.

However, numerous other P2XR antagonists, more efficient and more specific, have been discovered in the past few years, especially anti-P2X7R [110-113]. CE-224,535 has been tested in clinical trials for rheumatoid arthritis in patients with an inadequate response to methotrexate. The drug was not efficacious, compared with placebo, but demonstrated an acceptable safety and tolerability profile (NCT00628095) [114, 115]. The purinergic P2X7

antagonist AZD9056 was shown to have the potential to improve symptoms in patients with moderate-to-severe Crohn disease combined with a beneficial risk profile. AZD9056 was well tolerated, and no serious adverse events were reported [116]. The molecule GSK1482160 has already been explored as a possible tool to detect neuroinflammation, and a phase I clinical study in humans is currently undergoing (NCT00849134) [117].

Currently, no therapies are available for LGMDR3 patients. Many studies in each of the four sarcoglycan deficiencies demonstrated that viral-mediated gene transfer, using adeno-associated vectors, can correct the pathologic signs of the disease in animal models [40, 118-124]. However, some previous a-SG gene transfer experiments revealed the occurrence of specific immune response, leading to generation of a-SG specific antibody, T-cell infiltration of treated muscles, and disappearance of the vector. In this respect, we suggest that P2X-purinergic signal antagonism, with its double anti-inflammatory effect (inhibition of innate/adaptive inflammatory response and enhancement of immune tolerance by Treg expansion), could be associated with gene transfer therapies for the treatment of LGMDR3 to obtain a more stable a-SG expression.

Moreover, this study is in agreement with recent lines of research, which emphasize the relevance of DAMPs in chronic degenerative disorders. Intriguingly, these sophisticated molecules are danger signals important not only for the inflammatory response but also for tissue repair because they can orchestrate tissue healing by acting on different receptors. Thus, better understanding of the consequences of DAMP signaling on muscle inflammation and on muscle regeneration is the key to promote tissue repair and healing

These results have been published in the following manuscript:

Gazzerro E, Baratto S, Assereto S, Baldassari S, Panicucci C, Raffaghello L, Scudieri P, De Battista D, Fiorillo C, Volpi S, Chaabane L, Malnati M, Messina G, Bruzzone S, Traggiai E, Grassi F, Minetti C, Bruno C. **The Danger Signal Extracellular ATP Is Involved in the Immunomediated Damage of α-Sarcoglycan-Deficient Muscular Dystrophy**. Am J Pathol. 2019 Feb;189(2):354-369. doi: 10.1016/j.ajpath.2018.10.008. Epub 2018 Nov 16. PMID: 30448410 (see Appendix).

4.3 A438079 study

4.3.1. Materials and Methods

In vivo experiments

C57BL/6 Wild Type (WT) and Sgca knockout mice (also termed Sgca-null) were bred in the animal facility at Policlinico San Martino, Genova. All mice were housed under standard specific pathogen–free conditions and allowed access to food and water ad libitum. All experimental protocols were approved by the Policlinico San Martino Animal Welfare Body and by the Italian Ministry of Health (Authorization n° 215-2018-PR). Sgca-null (here from referred as Sgca) mice were previously described [62]. Four week old male mice were randomly divided into two groups: one treated by i.p. injections with A438079 (Tocris Bioscience Bristol, UK) at 3 mg/Kg every other day for 24 weeks (Sgca A438079) and one treated with the same volume of phosphatase-buffered saline (PBS, Sigma Aldrich, St. Louis, MO) every other day for 24 weeks (Sgca Control: Sgca CTR). The dose of 3 mg/kg of A438079 proved to be well tolerated by wild type rats [125]. A438079 was reconstituted at a final concentration of 1 mg/mL in PBS and stored at -20°C; the reconstituted drug was thawed and immediately used at a final concentration of 3 mg/Kg. All animals were euthanized at the end of treatment by carbon dioxide inhalation and muscles were collected for histological and cytofluorimetric analysis. A group of age-matched WT C57Bl/6 male mice was used as internal control. All animals were weighed and followed for any sign of toxicity, including ruffled fur, numbness, vomiting, hyperactivity or loss of deambulation, and breathing depression once a week. Blood samples from Sgca CTR and Sgca A438079 mice were obtained by saphenous vein (90 µl), before treatment, 12 and 24 weeks after treatment. The samples were centrifuged at 3600 x g for 30 minutes and immediately after centrifugation, the serum was isolated and stored at – 80°C. Serum creatine kinase (CK) levels were measured using a clinical-standard automatic chemistry analyzer (BS-380 Mindray, Milan, Italy).

Functional tests, muscle specimens, pheripheral blood and spleen processing methods

Before treatment and at the end of the sixth, twelfth, eighteenth and twentyfourth week of treatment, the muscle strength of WT, Sgca CTR and Sgca A438079- mice was scored through the Four-Limb Hanging Test. Mice were subjected to a 180-second lasting hanging test, during which a falling score is recorded. The animals had to hang for three trials, and the average maximum hanging time of the three trials was measured (standard

operating procedure, https://treat-nmd.org/research-overview/preclinical-research/experimental-protocols-for-dmd-animal-models/ last accessed December, 2019).

Histological studies, imaging and analysis

Quadriceps isolated from WT, Sgca CTR and Sgca A438079 mice were cut on cryostat and 7 um thick sections were stained with standard Hematoxylin and Eosin (H&E) (reagents from Sigma Aldrich), acid phosphatase (reagents from Sigma Aldrich) to detect inflammatory reactions and Masson trichrome (reagents from Sigma Aldrich) to evaluate muscle fibrosis. Representative pictures were taken at 20X magnification. To quantify the extension of the inflammatory response and fibrotic area, images of stained sections were acquired using a Nikon Ti Eclipse microscope equipped with a 20X objective. Whole sections were imaged with an automated tile scan acquisition (usually over a 45 mm2-surface) by using the perfect focus system (PFS) to control the focal plane. Quantification of acid phosphatase and trichrome staining was performed using semi-automated measurement tools in NIS-Elements AR software version 4.20 and expressed in terms of fraction area (the ratio between total section area and the area of the stained objects that were detected by HSI thresholding mode).

Immunofluorescence

The Wheat Germ Agglutinin (WGA)/DAPI (WGA Alexa Fluor™ 488 Conjugate Invitrogen, Thermo Fisher Scientific, Waltham, USA; DAPI, Fluoromount-G® Southern Biotech, Birmingham, USA) staining was performed on quadricep 5 um thick sections, in order to calculate the Minimum Feret's Diameter and the percentage of centralized nuclei. Briefly, unfixed quadriceps sections were incubated with a blocking solution containing 0.2% TritonX-100 (Sigma Aldrich), 2% Bovine Serum Albumin (Sigma Aldrich), 5% Fetal Bovine Serum (GIBCO, Thermo Fisher Scientific), 2% Goat Serum (GIBCO) in PBS for 1 hour at room temperature (RT) and then with WGA Alexa Fluor 488 conjugated diluted 1:200 in Hank's Balanced Salt Solution (HBSS) (GIBCO) for 2 hours at RT. Finally, sections were mounted with Fluoromount G. Images were acquired by Axioplan Imager M2 miscroscope software AxioVs40 version 4.8.2.0 (Zeiss, Oberkochen, Germany) and manually overlapped using Adobe Photoshop CS6 to generate whole cross-section. Image analysis was performed using Fiji, ImageJ, open-source software (NIH, USA). A plugin (Muscle Morphometry) developed as described in [126] was used to quantify the muscle fiber diameter (minimal Feret’s diameter) and the percentage of centralized nuclei,

as described in TREAT-NMD-recommended protocol (https://treat-nmd.org/research-overview/preclinical-research/experimental-protocols-for-dmd-animal-models/).

Flow cytometry

Hematopoietic cells were collected from different districts, namely: peripheral blood (PB), spleen and limb muscles. Cells collected from PB were first incubated with 2 l/sample of TruStainFcXTM anti-mouse CD16/32 for 5 minutes in order to block Fc receptor and then with cocktails of antibodies specific for CD45, CD3, CD4, CD8, CD11b, CD11c, CD25, F4/80, Ly-6C, Ly-6G, Foxp3, for 30 minutes. The intracellular staining of transcription factor Foxp3 was performed using the Foxp3/Transcription factor staining buffer set (Thermo Fisher) as described by the manufacturer. After antibody incubation, samples were lysed (Becton Dickinson Pharm Lyse TM, San Josè, CA, USA), washed and resuspended in 300 ul of PBS (Sigma Aldrich). All the antibodies were purchased from Biolegend (San Diego, CA, USA).

Gastrocnemius, quadriceps, anterior tibialis excised from WT, Sgca CTR and Sgca A438079 mice were resuspended in RPMI 1640 base medium (Euro Clone, Milan, Italy), mechanically and enzimatically digested using Skeletal Muscle Dissociation Kit (Miltenyi Biotec, Bologna, Italy) and filtered through 100 and 70 μm mesh filters (BD Bioscience, San Jose, CA, USA). After filtration, cells were purified using gradient centrifugation by Percoll solution (GE Healthcare Bio-sciences, Uppsala, Sweden) and stained with Live/DeadTM Fixable Yellow Dead Cell Stain Kit (Invitrogen, Thermo Fisher Scientific) and the antibodies listed above. The spleen from WT, Sgca CTR and Sgca A438079 mice was mechanically digested, filtered through 100 and 70 μm mesh filters, counted and stained as described for PB and muscle.

All acquisitions were performed with a three laser LSR Fortessa X20 (Becton Dickinson) and obtained FSC files were analysed with Kaluza Software (version 2.1, Beckman Coulter).

Statistical analysis

Statistical parameters, including the exact value of n and statistical significance, are reported in the figures and their associated legends. Results were analyzed using an unpaired t Test or a one-way ANOVA where indicated, using GraphPad Prism 3.0 software (GraphPad Software, El Camino Real, San Diego, CA, USA). Asterisks indicate statistical significance (*, $p < 0.05$; **, $p < 0.01$; ***, $p < 0.001$, ****, $p < 0.0001$).

4.3.2. Results

P2X7 targeting by A438079 improves functional, biochemical and morphological parameters in Sgca mice.

To evaluate the therapeutic efficacy of a selective P2X7-targeting compound in an experimental model of α-sarcoglycanopathy, we treated four-week-old male Sgca mice with A438079, a specific antagonist of P2X7 [127]. The drug was administered to Sgca mice by i.p. injections at the dose of 3 mg/kg every other day for 24 weeks (Figure 1). Sgca mice injected with PBS (Sgca CTR) and WT mice served as controls.

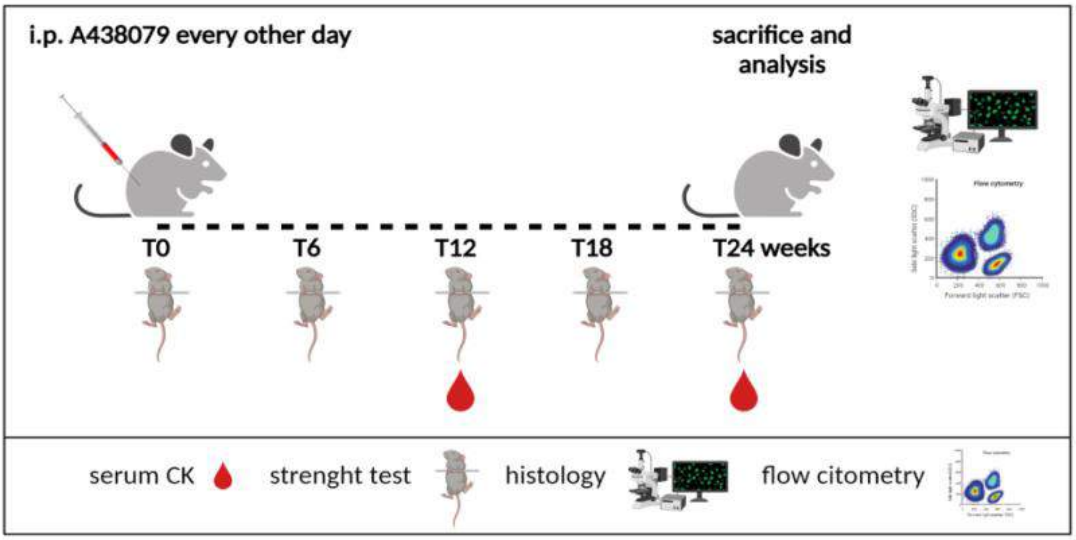

Figure 1. Experimental design**.** Four-week-old male Sgca mice were treated with PBS vehicle (Sgca CTR, n=12) and A438079 (Sgca A438079 n=8) that was administered intraperitoneally at the dose of 3 mg/Kg every other day for 24 weeks. Age-matched male C57BL/6 Wild Type (WT n=12) mice were used as negative control.

The animals were weighted and followed once a week for signs of toxicity until the sacrifice. As shown in Figure 2, the weight gain curve of Sgca mice treated with A438079 was not significantly different to that of Sgca CTR mice. In addition, no signs of toxicity, including ruffled fur, numbness, vomiting, hyperactivity or loss of ambulation and breathing depression, were observed (data not shown).

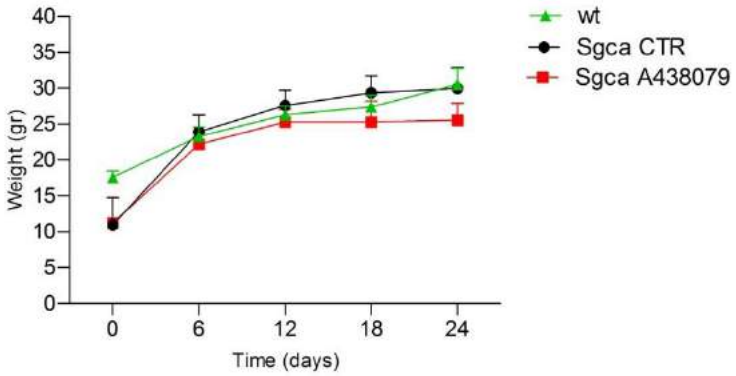

Figure 2. Weight of Sgca CTR (n=12) and Sgca A438079 (n=12) mice was recorded from 4 to 24 weeks. Weight was not significantly modified by A438079. Statistical analysis was performed by One-Way-ANOVA.

At the beginning (0 time), and after 6, 12, 18 and 24 weeks of treatment, animals were evaluated for muscle strength by the Four-Limb Hanging Test. Figure 3, panel a shows that Sgca CTR mice progressively lost muscle strength up to 18 weeks. At 24 weeks, they still showed significantly lower strength when compared to WT mice. The apparent slight recovery between 18 and 24 weeks was not significant. On the contrary, Sgca A438079 initially showed reduced functional performance, similarly to Sgca CTR mice, but after 6 weeks of treatment, muscle strength began to recover, almost reaching the performance of WT animals up to 24 weeks. The difference between Sgca CTR and Sgca A438079 mice at 12, 18 and 24 weeks was highly significant ($p<0.0001$ at 12 and 24 weeks, $p<0.001$ at 18 weeks). Accordingly, muscle strength in WT and Sgca A438079 mice was not significantly different at any time point. The efficacy of A438079 was confirmed by the analysis of serum levels of CK, a marker of muscle degeneration. As shown in Figure 3, panel b, CK serum levels of Sgca CTR mice measured >10 times more than the WT levels (mean value of WT mice: 406 UI/l, n=9; mean value of Sgca CTR mice: 5537 UI/l, n=12, $p<0.05$). Interestingly, A438079 treatment significantly reduced (by 76%) serum CK in Sgca mice after 12 weeks of treatment (mean value in Sgca A438079 mice: 1338 UI/l, n=8 vs Sgca

CTR mice p<0.05). After 24 weeks of treatment serum CK levels of Sgca CTR mice were 6,3 times higher than the WT levels and A438079 led to a serum CK decrease in the treated mice, although it did not reach statistical significance, likely due to increased variability of the measurements (mean value of WT mice: 829 UI/l, n=12; mean value of Sgca CTR mice: 5235 UI/l, n=10, p<0.05).

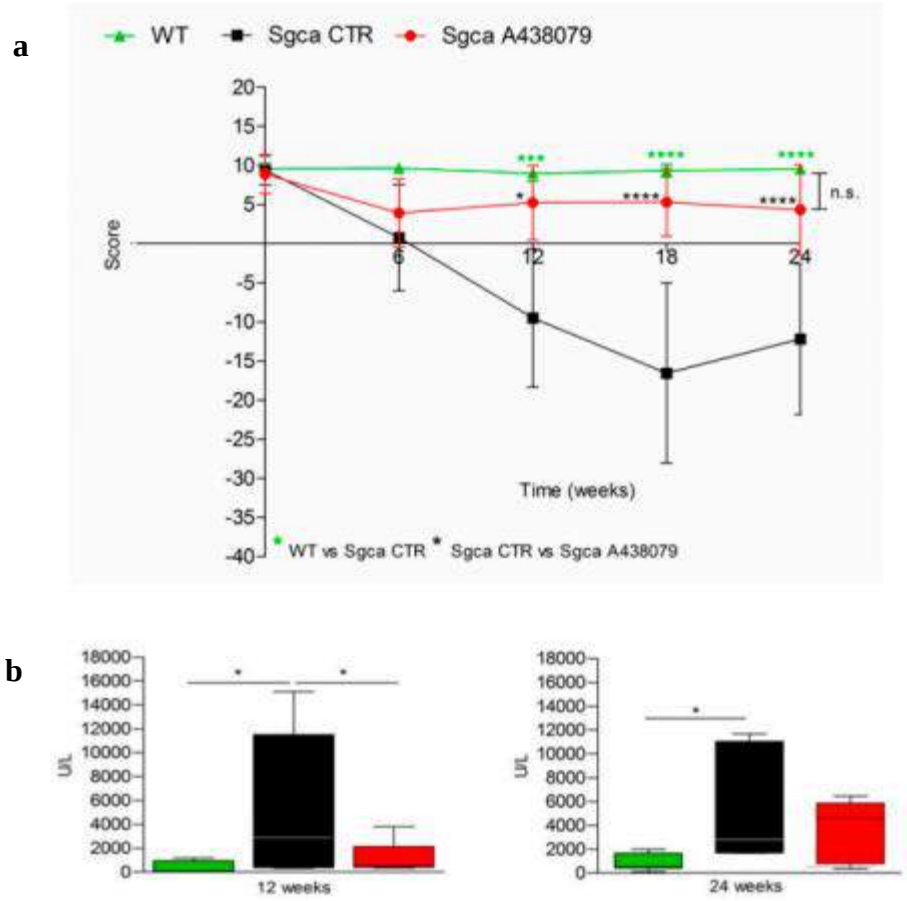

Figure 3 A438079 improves functional, biochemical parameters in Sgca mice.

Panel a: Four-Limb Hanging Test was performed before treatment and at the end of 6, 12, 18 and 24 weeks of treatment. Each value represents the mean ± SD of animals evaluated.

Panel b: serum creatine kinase (CK) levels were evaluated at the end of the twelfth and the twentyfourth week of treatment. Blood samples were obtained by retro orbital withdraw from WT, Sgca CTR and Sgca A438079 mice. Data are expressed as mean ± SD of animals evaluated.

Statistical analysis was performed by Two-tailed Unpaired t test. Asterisks indicate statistical significance (*, p < 0.05; **, p < 0.01; ***, p < 0.001, ****, p < 0.0001).

To investigate whether the improved functional performance of Sgca A438079 mice correlated with decreased inflammation and muscle degeneration, we performed histological analysis by H&E staining of quadriceps from WT, Sgca CTR and Sgca A438079 mice. Quadriceps from Sgca CTR mice presented areas of necrotic cells surrounded by reactive macrophage infiltration which were reduced upon A438079 treatment (Figure 4, panel a). According to the histological analysis (Figure 4, panel b), the percentage of centrally nucleated myofibers dramatically increased in quadriceps of Sgca mice in comparison to WT animals ($p<0.0001$) and was reduced by 12% in A438079-treated animals ($p<0.0001$) (Figure 4, panel c). As expected, the fiber size variability, calculated as coefficient variance Z of minimal Feret's diameter, was wider in Sgca compared to WT mice ($p<0.0001$) but was significantly down-modulated by A438079 treatment ($p<0.05$) (Figure 4, panel d).

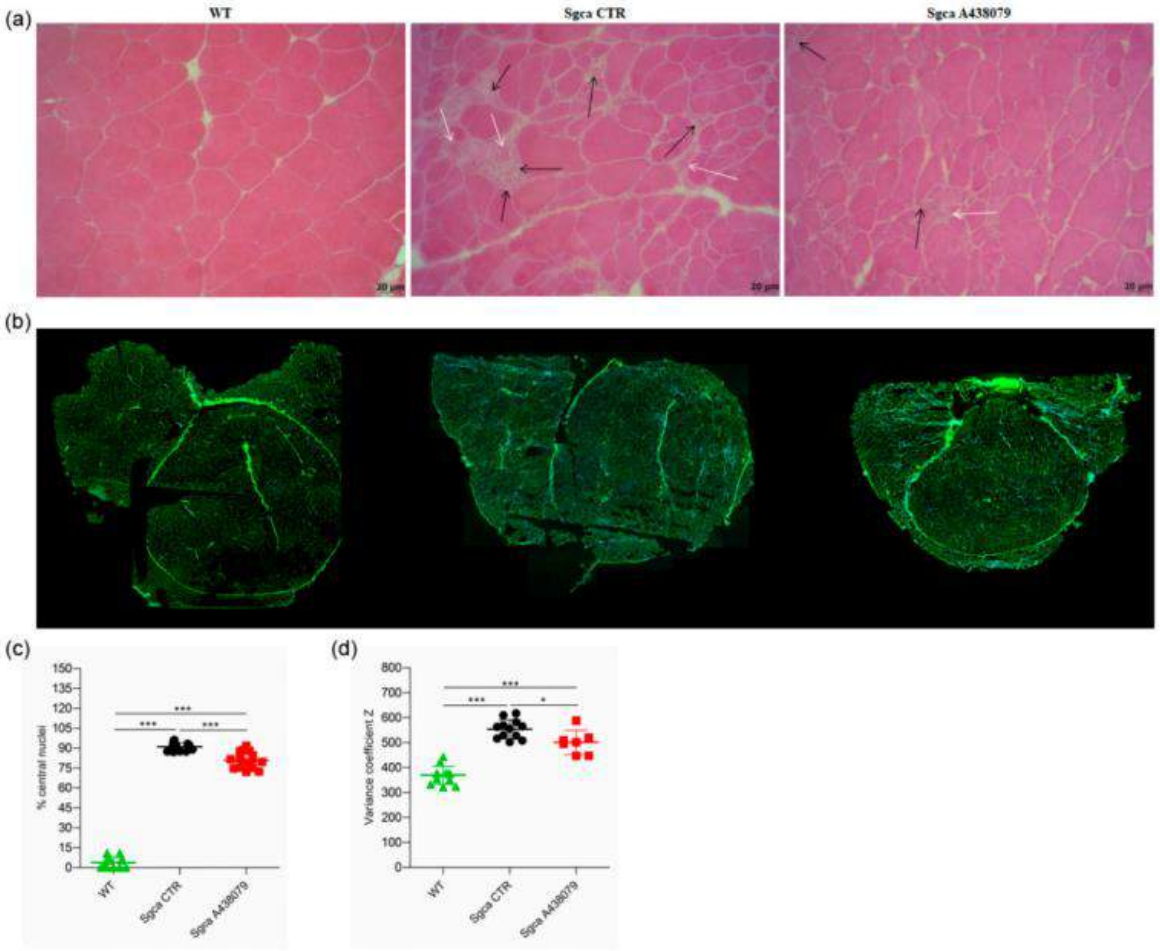

Figure 4. A438079 ameliorates the muscle morphology of Sgca mice. Panel a: frozen quadriceps tissue sections from WT, Sgca CTR and Sgca A438079 mice were collected at the end of the twenty-fourth week of treatment and stained with standard H&E technique. Black arrows indicate inflammatory infiltrates, white arrows indicate degenerating muscle fibers. Final magnification, 20X. Panel b: frozen quadriceps tissue sections from WT, Sgca CTR and Sgca A438079 mice were collected at the end of the 24th week of treatment and stained with Wheat Germ Agglutinin (WGA) and DAPI. Panel c: percentage of central nuclei was quantified in four consecutive fields for each muscle section stained with Wheat Germ Agglutinin (WGA) and DAPI and normalized for the fiber number of each field. Panel d: muscle fiber diameter variability from WT, Sgca CTR and Sgca A438079 mice was calculated in the whole area as variance coefficient Z of minimal Feret's diameter. Statistical analysis was performed by Two-tailed Unpaired t test. Asterisks indicate statistical significance (*, $p < 0.05$; **, $p < 0.01$; ***, $p < 0.001$, ****, $p < 0.0001$).

A438079 reduces muscular fibrosis and inflammation in Sgca mice

Fibrosis as characterized by replacement of muscle tissue with collagen deposits is the histopathological hallmark of end-stage muscular dystrophies including alfa-sarcoglycanopathy [126]. To establish whether A438079 might impact on collagen deposits, we performed a Masson trichrome staining on quadriceps of WT, Sgca CTR and Sgca A438079 mice and evaluated the fraction area of fibrotic reactions. As shown in Figure 5, panels a-b, Sgca CTR quadriceps accumulated abundant extracellular matrix deposits which were increased in comparison to WT mice (mean value of WT mice: 1.47, n=7; mean value of Sgca CTR mice: 2.92, n=11, $p<0.05$). A438079 treatment led to a 37% reduction of extracellular matrix deposition fraction area as compared to Sgca CTR mice (mean of Sgca A438079 mice: 1.85, n=7, $p<0.05$). No significant difference was observed between WT and Sgca A438079 animals.

To evaluate the anti-inflammatory effect of A438079, quadricep sections of WT, Sgca CTR and Sgca A438079 mice were stained with acid phosphatase, which provides a red positive signal in activated macrophages and degenerative myofibers. As shown in Figure 5, panels c-d, the acid phosphatase-positive area fraction of quadriceps from Sgca CTR mice was increased in comparison to that of WT mice (mean value of WT mice: 0.26, n=8; mean value of Sgca CTR mice: 1.47, n=12, $p<0.0001$). Interestingly, A438079 led to 52% reduction of inflammatory area fraction of Sgca mice (mean of Sgca A438079 mice: 0.70, n=8, $p<0.01$).

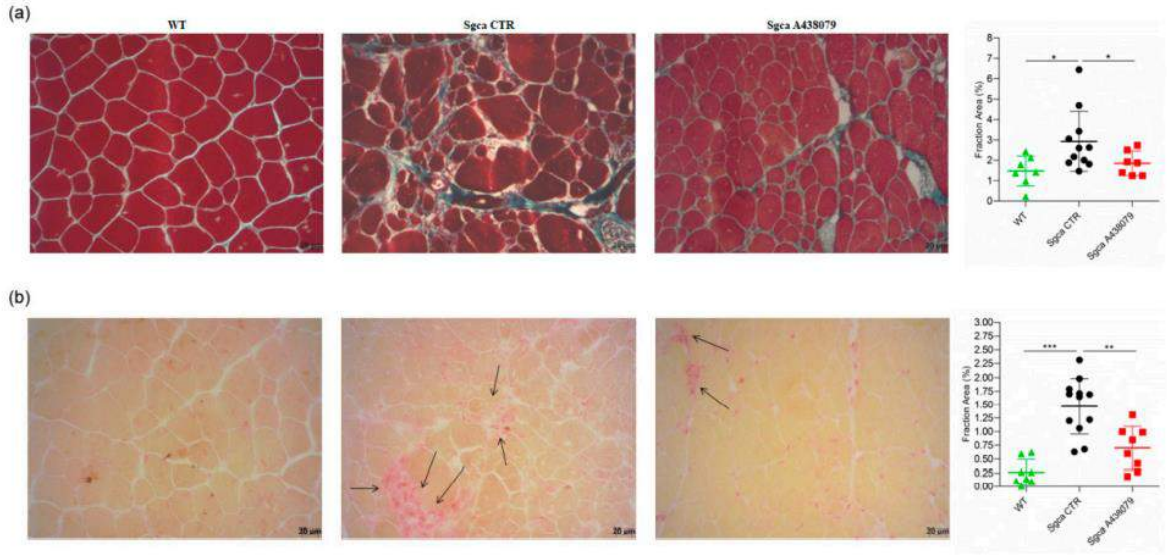

Figure 5. A438079 reduces muscle fibrosis and inflammatory infiltrates in Sgca mice. Panel a: frozen sections of quadriceps from WT (n=7), Sgca CTR (n=11) and Sgca A438079 (n=7) were collected after 24 weeks and stained with a standard Masson trichrome stain protocol. A representative image is shown. Final magnification, 20X.

Panel b: graph of the fraction areas of fibrotic green positive signal/fraction area (%) of total section area of muscles represented in A is shown. Data are expressed as mean ± SD.

Statistical analysis was performed by One-tailed Unpaired t test. Asterisks indicate statistical significance (*, $p < 0.05$; **, $p < 0.01$; ***, $p < 0.001$, ****, $p < 0.0001$).

Panel c:frozen sections of quadriceps from WT (n=8), Sgca CTR (n=12) and Sgca A438079 (n=8) were collected after 24 weeks and stained with a acid phosphatase technique. A representative image is shown. Black arrow indicate inflammatory infiltrates. Final magnification, 20X.

Panel d:graph of the fraction areas of inflammatory red positive signal/fraction area (%) of total section area of muscles represented in A is shown. Data are expressed as mean ± SD.

Statistical analysis was performed by Two-tailed Unpaired t test. Asterisks indicate statistical significance (*, $p < 0.05$; **, $p < 0.01$; ***, $p < 0.001$, ****, $p < 0.0001$).

A438079 reduces innate inflammatory cells and increases T regulatory lymphocytes in limb muscles of Sgca mice

To better characterize the phenotype of inflammatory muscle infiltrates, we performed a cytometric analysis of a pool of limb muscles including gastrocnemius, quadriceps and anterior tibialis, isolated from WT, Sgca CTR and Sgca A438079 mice. As expected, Figure 6, panel a, limb muscles of Sgca CTR mice were characterized by the presence of $CD45^+$ hematopoietic immune cells which, in contrast, were not detected in WT mice (WT vs Sgca CTR, $p<0.01$). A438079 treatment significantly reduced the percentage of $CD45^+$ cells infiltrating the limb muscles of Sgca mice (Sgca CTR vs Sgca A438079, $p<0.05$). The further characterization of $CD45^+$ cells was only performed for Sgca animals since the amount of $CD45^+$ cells was negligible in the muscle of WT mice. Sgca A438079 mice presented a significant reduction of muscle infiltrating innate inflammatory cells, including $Ly6G^+/CD11b^+$ neutrophils (Figure 6, panel b, Sgca CTR vs Sgca A438079, $p<0.05$), $Ly6G^-/CD11b^+/Ly6C^+$ activated monocytes (Figure 6, panel c, Sgca CTR vs Sgca A438079, $p<0.01$), $Ly6G^-/CD11b^+/F480^+$ macrophages (Figure 6, panel d, Sgca CTR vs Sgca A438079, $p<0.05$) and $Ly6G^-/CD11c^+/F480^-$dendritic cells (DC) (Figure 6, panel e, Sgca CTR vs Sgca A438079, $p<0.001$) in comparison to Sgca CTR animals. In contrast, the percentage of $CD3^+/CD4^+/CD25^+/Foxp3^+$ T Regulatory (T reg) was significantly increased in the muscles of A438079 Sgca mice in comparison to Sgca CTR mice (Figure 6 panel i, Sgca CTR vs Sgca A438079, $p<0.001$).

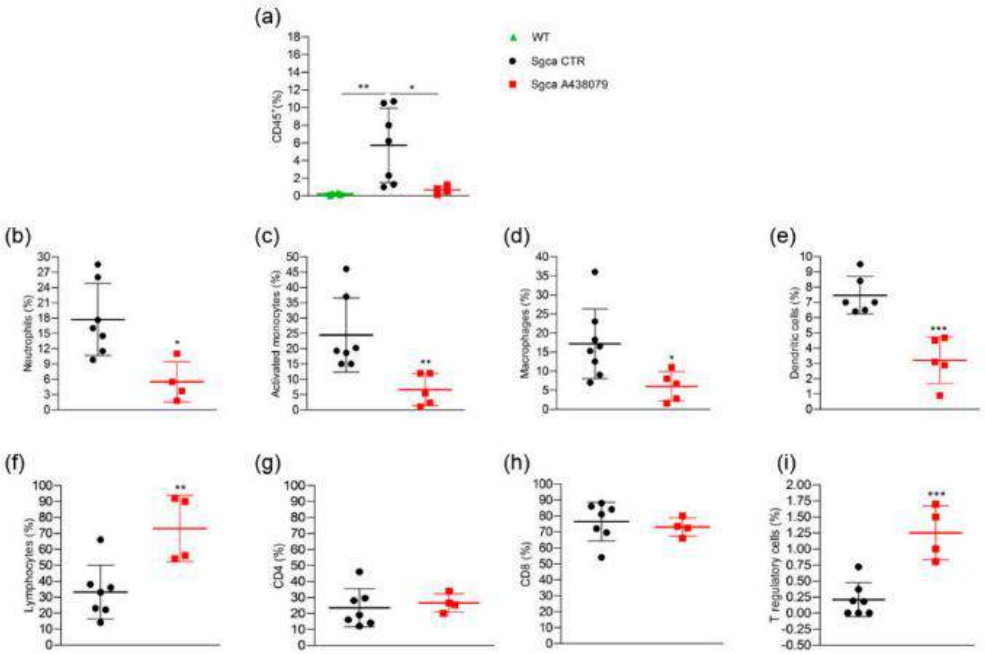

Figure 6. A438079 reduces innate inflammatory cells and increases T regulatory lymphocytes in limb muscles of Sgca mice. Flow cytometric analysis of immune cells isolated from a pool of gastrocnemius, quadriceps, anterior tibialis excised from WT (n=6), Sgca CTR (n=7) and Sgca A438079 (n=5) mice and stained with specific anti-surface markers mAbs are shown.

Panel a: percentage of CD45+ cells gated on alive cells. Panel b: percentage of $Ly6G^{+}/CD11b^{+}$neutrophils gated on $CD45^{+}$ alive cells. Panel c: percentage of $Ly6G^{-}/Ly6C^{+}/CD11b^{+}$ activated monocytes gated on $CD45^{+}$ alive cells. Panel d: percentage of $Ly6G^{-}/F480^{+}/CD11b^{+}$ macrophages gated on $CD45^{+}$ alive cells. Panel e: percentage of $Ly6G^{-}/F480^{-}/CD11c^{+}$ dendritic cells gated on $CD45^{+}$ alive cells. Panel f: percentage of CD3+ T cells gated on $CD45^{+}$ alive cells. Panel g: percentage of $CD3^{+}/CD4^{+}$ T cells gated on $CD45^{+}$ $CD3^{+}$ alive cells. Panel h: percentage of $CD3^{+}/CD8^{+}$ T cells gated on $CD45^{+}$ $CD3^{+}$ alive cells. Panel i: percentage of $CD3^{+}/CD4^{+}/CD25^{+}/Foxp3^{+}$ T cells gated on $CD3^{+}$ alive cells. Data are expressed as mean ± SD.

Statistical analysis was performed by Two-tailed Unpaired t test. Asterisks indicate statistical significance (*, $p < 0.05$; **, $p < 0.01$; ***, $p < 0.001$, ****, $p < 0.0001$).

Furthermore, the analysis of the PB immune cell populations of WT, Sgca CTR and Sgca A438079 mice showed that the dystrophic animals presented significantly higher percentages of DC and T lymphocytes compared to WT animals (Figure 7, panels c-d, WT vs Sgca CTR, $p<0.001$ for DC and $p<0.05$ for T lymphocytes). Within CD3+ T cells, treatment with A438079 significantly reduced the percentage of $CD8^+$ lymphocytes and T reg cells (Figure 7, panels f-g, Sgca CTR vs Sgca A438079, $p<0.001$ for CD8+ lymphocytes and $p<0.001$ for Treg).

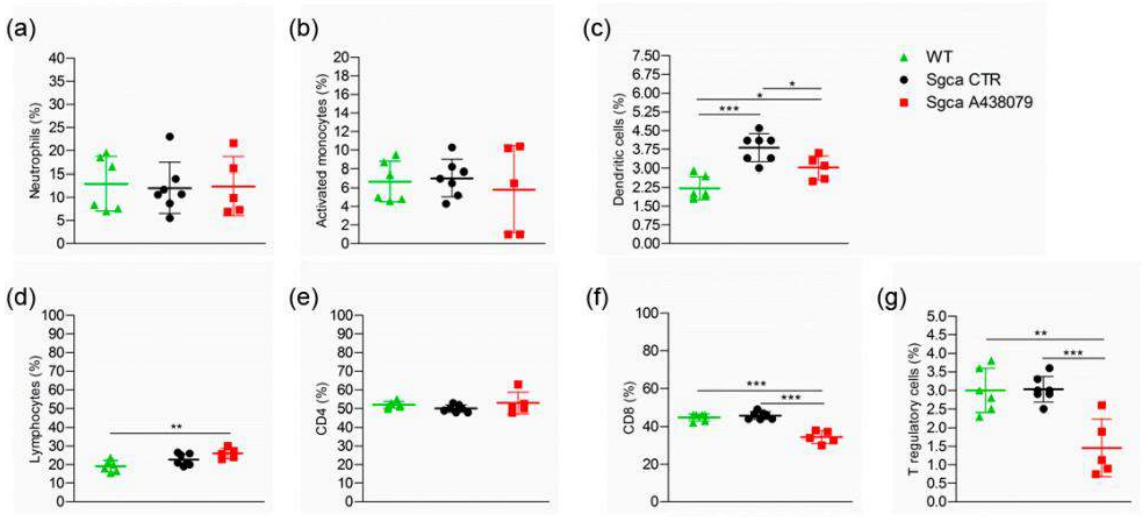

Figure 7. A438079 reduces peripheral cytotoxic and T regulatory cells in Sgca mice. Flow cytometric analysis of peripheral blood immune cells isolated from WT (n=6), Sgca CTR (n=9) and Sgca A438079 (n=6) mice and stained with specific anti-surface markers mAbs are shown.

Panel a: percentage of $Ly6G^+/CD11b^+$neutrophils gated on $CD45^+$ alive cells. Panel b: percentage of $Ly6G^-/Ly6C^+/CD11b^+$ activated monocytes gated on $CD45^+$ alive cells. Panel c: percentage of $Ly6G^-/F480^-/CD11c^+$ dendritic cells gated on $CD45^+$ alive cells. Panel d: percentage of $CD3^+$ T cells gated on $CD45^+$ alive cells. Panel e: percentage of $CD3^+$ /$CD4^+$ T cells gated on $CD45^+$ $CD3^+$ alive cells. Panel f: percentage of $CD3^+$ /$CD8^+$ T cells gated on $CD45^+$ $CD3^+$ alive cells. Panel g: Percentage of $CD3^+$ /$CD4^+$/$CD25^+$/$Foxp3^+$ T cells gated on $CD3^+$ alive cells. Statistical analysis was performed by Two-tailed Unpaired t test. Asterisks indicate statistical significance (*, $p < 0.05$; **, $p < 0.01$; ***, $p < 0.001$, ****, $p < 0.0001$).

No significant changes were observed in the spleen of WT, Sgca CTR and Sgca A438079 mice, with the only exception of CD3+ T lymphocytes, which were slightly increased in Sgca A43879 mice vs Sgca CTR (Sgca CTR vs Sgca A438079, $p<0.01$, data not shown).

4.3.3. Discussion

In the present study, we provide evidence that the pharmacological inhibition of P2X7 by the selective antagonist A438079 attenuated the dystrophic phenotype of Sgca-deficient mice by reducing fibrosis and inflammation and improved muscle performance.

P2X7 is an ATP receptor belonging to the ionotropic purinergic P2X subfamily, which is expressed on virtually all cell types of the immune system and regulates the innate and adaptive immune responses [127]. Alongside its expression on immune cells, P2X7 expression and function are up-regulated in the dystrophic muscle [61, 62, 128, 129]. In this context, we and other groups demonstrated that the genetic ablation of P2RX7 and its pharmacological inhibition by oATP, which is an irreversible, broad-spectrum P2X7 antagonist [130], produced significant improvements in key functional and molecular disease parameters in mdx mice [61, 62]. However, oATP can also interact with other P2X receptors including P2X4 [103, 131, 132], and appears to exert anti-inflammatory effects, modulating the immune response independently of P2X7 blockage [103, 130, 133]. Therefore, experiments using oATP cannot unambiguously establish a role in inflammatory diseases for a specific member of the P2X family. Noteworthy, neurotoxicity has been described for oATP, likely due to the low specificity of the drug [134].

In order to overcome the above-described limitations, and to define the therapeutic effect of P2X7 targeting approaches in α-sarcoglycan-deficient muscular dystrophy, we specifically inhibited P2X7 using the A438079 molecule, one of the most potent and selective antagonist that competitively blocks P2X7 receptor in vitro activation and produces anti-nociceptive effects in in vivo settings [135-137]. Beside nociception, A438079 has been already successfully used in in vivo models of hyperalgesia [138], epilepsy [139], Parkinson's disease [140], and Charcot-Marie-Tooth 1A disease [125].

Our results clearly show that, by targeting P2X7, A438079 ameliorated functional and morphological parameters in Sgca mice. In particular, A438079 improved muscle morphology by reducing the percentage of centralized nuclei and the coefficient variance Z of minimal Feret's diameter (Figure 2 panels C and D), which are typical signs of a dystrophic damage [141]. Furthermore, according to previous studies [61], a relevant therapeutic effect exerted by A438079 was the reduction of muscle fibrosis (Figure 3 panel A). P2X7 has been described to play a nodal role in triggering fibrosis through activation of multiple intracellular pathways that converge in inducing the collagen biosynthetic machinery in various organs [142]. As such, P2X7 blockade may interfere with the main pro-fibrotic pathways, thus possibly representing a target for the pharmacological

modulation of fibrotic processes.

The most evident beneficial effect of A438079 in Sgca animals was a significant modulation of muscle inflammation, a key feature of muscular dystrophies participating in the disease progression but also mediating muscle repair. The dichotomous role of inflammation has been extensively studied in Duchenne Muscular Dystrophy (DMD) where $CD4^+$ and $CD8^+$ T cells, macrophages, eosinophils and natural killer T cells infiltrated both human and mouse dystrophic muscle [49, 143]. In particular, proinflammatory monocytes $CD11b^+/Ly6G^-/Ly6c^+$ have been reported to be the first innate immune cells to be mobilized from the bone marrow into the circulation and recruited to the site of tissue injury [144], such as dystrophic muscles, where they differentiated into inflammatory macrophages [145, 146]. Different studies demonstrated that neutrophils actively participated in the exacerbation of muscular dystrophy and their specific depletion reduced muscular necrosis and inflammation in mdx mice [147-149]. Moreover, neutrophil-derived elastase impaired myoblast proliferation, survival and differentiation [150]. In line with this notion, we found that A438079 caused a significant reduction of innate immune cells including neutrophils, activated monocytes and dendritic cells infiltrating the limb muscles of Sgca mice.

The downregulation of innate immune response by P2X7 blockade was also observed in dystrophic mice (mdx and Sgca animals) treated with other P2X7 antagonists, i.e. oATP or Zidovudine (AZT) [62, 63]. However, the mechanism underlying the latter effect is still unclear. P2X7 antagonists could directly inhibit P2RX7 expressed by inflammatory innate immune cells infiltrating the dystrophic muscle. Alternatively, these agents might reduce inflammatory cell migration into the injured tissue. In favor of the first hypothesis, innate immune cells are known to express functional P2X7, which in turn triggers inflammasome activation [127, 151-153]. The second hypothesis is sustained by data showing P2X7-dependent release of chemotactic factors by macrophages. These factors, including CXCL2/macrophage inflammatory protein-2 (MIP-2), were involved in the recruitment of neutrophils into the injured tissue [154].

The immune phenotype of limb muscle from Sgca mice treated with A438079 also showed that the pharmacological treatment significantly increased $Foxp3^+$ Treg without affecting $CD4^+$ and $CD8^+$ T lymphocytes. These findings are consistent with previous studies where P2X7 blockade by oATP or P2X7 genetic ablation in dystrophic mice resulted in a significant increase of $Foxp3^+$ Treg [61, 62]. Treg have been described to play a dual beneficial role in dystrophic muscles. On one side they suppress type 1 inflammation by

secreting IL-10; on the other side, Treg may also have direct effects on muscle growth and regeneration through secretion of amphiregulin, an epidermal growth factor family member, whose receptors are expressed on muscle satellite cells that are critical for muscle regeneration [98, 155]. Interestingly, our results showed that A438079 exerted not only a local, but also a systemic anti-inflammatory effect by reducing circulating $CD8^+$ cytotoxic T lymphocytes in Sgca mice.

Currently, physical therapy and prevention of secondary cardiac, pulmonary, or othopedic complications are the only possible care interventions. Although a chronic inflammatory response is documented in muscle specimens from LGMDR3 patients, no trials assessing the effects of immunosuppressive therapies have never been proposed in alpha-sarcoglycan-deficiency. However, two unrelated LGMDR3 patients treated with steroids showed clinical improvement [83, 156, 157]. In light of these considerations, strategies aimed at reducing muscle inflammation, increasing the amount of Treg infiltrating an injured muscle and exerting a systemic anti-inflammatory effect, i.e. antagonists of P2X7, might represent a therapeutic approach for LGMDR3. Immunomodulatory regimens become even more relevant considered that new gene therapy or gene editing approaches are developing for alpha-sarcoglycanopathy [42, 158, 159], with gene therapy being in Phase I/II clinical trials for LGMDR3 patients (NCT01976091; NCT00494195). Since the successful of gene therapy in the muscle tissue has to challenge pre-existing status of chronic tissue inflammation typically identified in these diseases [42, 48, 158-160], our data suggest that P2X7 antagonism might represent a good strategy to dampen chronic inflammation, possibly leading to a better delivery of gene therapy.

To date P2X7 selective antagonists have already been tested in Phase I/II clinical trials for the treatment of Crohn disease, Rheumatoid arthritis, Basal cell carcinoma with an overall good tolerability and variable efficacy [161] and a new trial is currently ongoing assessing the effects of JNJ-54175446, a potent, brain-penetrant, selective P2X7 antagonist [162] in patients with Major Depressive Disorder (ClinicalTrials.gov Identifier: NCT04116606).

In conclusion, A438079 ameliorated the dystrophic phenotype of Sgca mice by reducing muscle fibrosis and inflammation and by improving functional muscle performance. In the current scenario of clinical trials including gene therapy, selective P2X7 antagonists could represent candidates for a combination therapy to endorse the efficacy of disease-specific gene therapy by dampening the basal muscular inflammation.

These results have been published in the following manuscript:

Raffaghello L, Principi E, Baratto S, Panicucci C, Pintus S, Antonini F, Del Zotto G, Benzi A, Bruzzone S, Scudieri P, Minetti C, Gazzerro E, Bruno C. **P2X7 Receptor Antagonist Reduces Fibrosis and Inflammation in a Mouse Model of Alpha-Sarcoglycan Muscular Dystrophy.** Pharmaceuticals (Basel). 2022 Jan 13;15(1):89. doi: 10.3390/ph15010089. PMID: 35056146; PMCID: PMC8777980 (see Appendix).

5. Conclusions

In this PhD thesis, focusing on a rare LGMD, the LGMDR3 due to alpha-sarcoglycan deficiency, we have analyzed for the first time the link between the disease course and the inflammation, providing new data on the role of the immune system in sarcolgycanopathies.

By confirming the variable clinical course and the genetic background, immunological processes emerge as crucial players of α-sarcoglycanopathy disease progression.

Considering the absence of specific drugs, a fine-tune immunomodulatory regimen should be proposed for LGMDR3 patients, at least for those with a high degree of inflammatory infiltrates at muscle biopsy. A limitation to this approach, is that muscle biopsy does not currently represent a fundamental step in the diagnostic process, therefore further researches are needed to identify circulating biomarkers reflecting the severity of immune system activation in these patients.

Moreover, with the imminent advent of gene-therapy for LGMDR3, the availability of immunosuppressant strategies aimed to dampen the basal immune-mediated damage, and favoring a better engraftment of the transgene, assumes even more importance.

In two *in vivo* treatments using P2X7 selective antagonisms, we demonstrated that P2X7 inhibitors were effective to counteract the progression of the dystrophic phenotype in Sgca-null mouse, by reducing the local inflammatory response. Thus, P2X7 antagonists could be suggested as good candidate to dampen muscle chronic inflammation in LGMDR3 and used in a combination therapy to endorse the efficacy of gene therapy.

6. References

1. Meryon E. On Granular and Fatty Degeneration of the Voluntary Muscles. Med Chir Trans. 1852;35:73-84.1.
2. Duchenne GB. Studies on pseudohypertrophic muscular paralysis or myosclerotic paralysis. Arch Neurol. 1968 Dec;19(6):629-36. doi: 10.1001/archneur.1968.00480060099015.
3. KLOEPFER HW, TALLEY C. Autosomal recessive inheritance of Duchennetype muscular dystrophy. Ann Hum Genet. 1958 Feb;22(2):138-43. doi: 10.1111/j.1469-1809.1957.tb01928.x.
4. Hoffman EP, Brown RH Jr, Kunkel LM. Dystrophin: the protein product of the Duchenne muscular dystrophy locus. Cell. 1987 Dec 24;51(6):919-28. doi: 10.1016/0092-8674(87)90579-4.
5. Roberds SL, Leturcq F, Allamand V, Piccolo F, Jeanpierre M, Anderson RD, Lim LE, Lee JC, Tomé FM, Romero NB, et al. Missense mutations in the adhalin gene linked to autosomal recessive muscular dystrophy. Cell. 1994 Aug 26;78(4):625-33. doi: 10.1016/0092-8674(94)90527-4.
6. Bönnemann CG, Modi R, Noguchi S, Mizuno Y, Yoshida M, Gussoni E, McNally EM, Duggan DJ, Angelini C, Hoffman EP. Beta-sarcoglycan (A3b) mutations cause autosomal recessive muscular dystrophy with loss of the sarcoglycan complex. Nat Genet. 1995 Nov;11(3):266-73. doi: 10.1038/ng1195-266. Erratum in: Nat Genet 1996 Jan;12(1):110.
7. Noguchi S, McNally EM, Ben Othmane K, Hagiwara Y, Mizuno Y, Yoshida M, Yamamoto H, Bönnemann CG, Gussoni E, Denton PH, Kyriakides T, Middleton L, Hentati F, Ben Hamida M, Nonaka I, Vance JM, Kunkel LM, Ozawa E. Mutations in the dystrophin-associated protein gamma-sarcoglycan in chromosome 13 muscular dystrophy. Science. 1995 Nov 3;270(5237):819-22. doi: 10.1126/science.270.5237.819.
8. Nigro V, de Sá Moreira E, Piluso G, Vainzof M, Belsito A, Politano L, Puca AA, Passos-Bueno MR, Zatz M. Autosomal recessive limb-girdle muscular dystrophy, LGMD2F, is caused by a mutation in the delta-sarcoglycan gene. Nat Genet. 1996 Oct;14(2):195-8. doi: 10.1038/ng1096-195.

9. Ghaoui R, Cooper ST, Lek M, Jones K, Corbett A, Reddel SW, et al. Use of whole-exome sequencing for diagnosis of limb-girdle muscular dystrophy: outcomes and lessons learned. JAMA Neurol 2015; 72: 1424–32.
10. Liu W, Pajusalu S, Lake NJ, Zhou G, Ioannidis N, Mittal P, et al. Estimating prevalence for limb-girdle muscular dystrophy based on public sequencing databases. Genet Med 2019; 21: 2512–20.
11. Winckler PB, da Silva AMS, Coimbra-Neto AR, Carvalho E, Cavalcanti E, Sobreira C, et al. Clinicogenetic lessons from 370 patients with autosomal recessive limb-girdle muscular dystrophy. Clin Genet 2019; 96: 341–53.
12. Xie Z, Hou Y, Yu M, Liu Y, Fan Y, Zhang W, Wang Z, Xiong H, Yuan Y. Clinical and genetic spectrum of sarcoglycanopathies in a large cohort of Chinese patients. Orphanet J Rare Dis. 2019 Feb 14;14(1):43. doi: 10.1186/s13023-019-1021-9.
13. Alonso-Pérez J, González-Quereda L, Bello L, Guglieri M, Straub V, Gallano P, Semplicini C, Pegoraro E, Zangaro V, Nascimento A, Ortez C, Comi GP, Dam LT, De Visser M, van der Kooi AJ, Garrido C, Santos M, Schara U, Gangfuß A, Løkken N, Storgaard JH, Vissing J, Schoser B, Dekomien G, Udd B, Palmio J, D'Amico A, Politano L, Nigro V, Bruno C, Panicucci C, Sarkozy A, Abdel-Mannan O, Alonso-Jimenez A, Claeys KG, Gomez-Andrés D, Munell F, Costa-Comellas L, Haberlová J, Rohlenová M, Elke V, De Bleecker JL, Dominguez-González C, Tasca G, Weiss C, Deconinck N, Fernández-Torrón R, López de Munain A, Camacho-Salas A, Melegh B, Hadzsiev K, Leonardis L, Koritnik B, Garibaldi M, de Leon-Hernández JC, Malfatti E, Fraga-Bau A, Richard I, Illa I, Díaz-Manera J. New genotype-phenotype correlations in a large European cohort of patients with sarcoglycanopathy. Brain. 2020 Sep 1;143(9):2696-2708. doi: 10.1093/brain/awaa228.
14. Alavi A, Esmaeili S, Nilipour Y, Nafissi S, Tonekaboni SH, Zamani G, et al. LGMD2E is the most common type of sarcoglycanopathies in the Iranian population. J Neurogenet. 2017;31(3):161–9.
15. Khadilkar SV, Singh RK, Hegde M, Urtizberea A, Love DR, Chong B. Spectrum of mutations in sarcoglycan genes in the Mumbai region of western India: high prevalence of 525del T. Neurol India. 2009;57(4):406–10.
16. Eymard B, Romero NB, Leturcq F, Piccolo F, Carrie´ A, Jeanpierre M, et al. Primary adhalinopathy (alpha-sarcoglycanopathy): clinical, pathologic, and genetic

correlation in 20 patients with autosomal recessive muscular dystrophy. Neurology 1997; 48: 1227–34

17. Angelini C, Fanin M, Freda MP, Duggan DJ, Siciliano G, Hoffman EP. The clinical spectrum of sarcoglycanopathies. Neurology 1999; 52: 176–9.
18. Nalini A, Gayathri N, Thaha F, Das S, Shylashree S. Sarcoglycanopathy Clinical and histochemical characteristics in 66 patients. Neurol India 2010; 58: 691–6.
19. Ferreira AFB, Carvalho MS, Resende MBD, Wakamatsu A, Reed UC, Marie S. Phenotypic and immunohistochemical characterization of sarcoglycanopathies. Clinics (Sao Paulo) 2011; 66: 1713–9.
20. Semplicini C, Vissing J, Dahlqvist JR, Stojkovic T, Bello L, Witting N, et al. Clinical and genetic spectrum in limb-girdle muscular dystrophy type 2E. Neurology 2015; 84: 1772–81.
21. Trabelsi M, Kavian N, Daoud F, Commere V, Deburgrave N, Beugnet C, et al. Revised spectrum of mutations in sarcoglycanopathies. Eur J Hum Genet. 2008;16(7):793–803.
22. Semplicini C, Vissing J, Dahlqvist JR, Stojkovic T, Bello L, Witting N, et al. Clinical and genetic spectrum in limb-girdle muscular dystrophy type 2E. Neurology. 2015;84(17):1772–81.
23. Tarnopolsky M, Hoffman E, Giri M, Shoffner J, Brady L. Alpha-sarcoglycanopathy presenting as exercise intolerance and rhabdomyolysis in two adults. Neuromuscul Disord 2015; 25: 952–4.
24. Krishnaiah B, Lee JJ, Wicklund MP, Kaur D. Young girl presenting with exercise-induced myoglobinuria. Muscle Nerve. 2016;54(1):161–4.
25. Kyriakides T, Angelini C, Vilchez J, Hilton-Jones D. European Federation of the Neurological Societies guidelines on the diagnostic approach to paucisymptomatic or asymptomatic hyperCKemia. Muscle Nerve 2020; 61: E14–E15.
26. Georganopoulou DG, Moisiadis VG, Malik FA, Mohajer A, Dashevsky TM, Wuu ST, Hu CK. A Journey with LGMD: From Protein Abnormalities to Patient Impact. Protein J. 2021 Aug;40(4):466-488.
27. Tasca G, Monforte M, Díaz-Manera J, Brisca G, Semplicini C, D'Amico A, Fattori F, Pichiecchio A, Berardinelli A, Maggi L, Maccagnano E, Løkken N, Marini-Bettolo C, Munell F, Sanchez A, Alshaikh N, Voermans NC, Dastgir J, Vlodavets D, Haberlová J, Magnano G, Walter MC, Quijano-Roy S, Carlier RY, van Engelen BGM, Vissing J, Straub V, Bönnemann CG, Mercuri E, Muntoni F, Pegoraro E,

Bertini E, Udd B, Ricci E, Bruno C. MRI in sarcoglycanopathies: a large international cohort study. J Neurol Neurosurg Psychiatry. 2018 Jan;89(1):72-77.

28. Ibraghimov-Beskrovnaya O, Ervasti JM, Leveille CJ, Slaughter CA, Sernett SW., and, Campbell KP. Primary structure of dystrophin-associated glycoproteins linking dystrophin to the extracellular matrix. Nature. 1992;355:696–702.
29. Wakayama Y, Inoue M, Kojima H, Murahashi M, Shibuya S, Jimi T, Hara H, Oniki H. Ultrastructural localization of alpha-, beta- and gamma-sarcoglycan and their mutual relation, and their relation to dystrophin, beta-dystroglycan and beta-spectrin in normal skeletal myofiber. Acta Neuropathol. 1999 Mar;97(3):288-96.
30. Roberds, S. L., Anderson, R. D., Ibraghimov-Beskrovnaya, O., Campbell, K. P. Primary structure and muscle-specific expression on the 50-kDa dystrophin-associated glycoprotein (adhalin). J. Biol. Chem. 1993; 268: 23739-23742.
31. Roberds, S. L., Leturcq, F., Allamand, V., Piccolo, F., Jeanpierre, M., Anderson, R. D., Lim, L. E., Lee, J. C., Tome, F. M. S., Romero, N. B., Fardeau, M., Beckmann, J. S., Kaplan, J.-C., Campbell, K. P. Missense mutations in the adhalin gene linked to autosomal recessive muscular dystrophy. Cell 1994;78: 625-633.
32. Kopanos C, Tsiolkas V, Kouris A, Chapple CE, Albarca Aguilera M, Meyer R, Massouras A. VarSome: the human genomic variant search engine. Bioinformatics. 2019 Jun 1;35(11):1978-1980.
33. Sandonà D, Betto R. Sarcoglycanopathies: molecular pathogenesis and therapeutic prospects. Expert Rev Mol Med. 2009 Sep 28;11:e28.
34. Ceravolo F, Messina S, Rodolico C, Strisciuglio P, Concolino D. Myoglobinuria as first clinical sign of a primary alpha-sarcoglycanopathy. Eur J Pediatr. 2014;173(2):239–42.
35. Duclos F, Straub V, Moore SA, Venzke DP, Hrstka RF, Crosbie RH, Durbeej M, Lebakken CS, Ettinger AJ, van der Meulen J, Holt KH, Lim LE, Sanes JR, Davidson BL, Faulkner JA, Williamson R, Campbell KP. Progressive muscular dystrophy in alpha-sarcoglycan-deficient mice. J Cell Biol. 1998 Sep 21;142(6):1461-71.
36. Pasteuning-Vuhman S, Putker K, Tanganyika-de Winter CL, Boertje-van der Meulen JW, van Vliet L, Overzier M, Plomp JJ, Aartsma-Rus A, van Putten M. Natural disease history of mouse models for limb girdle muscular dystrophy types 2D and 2F. PLoS One. 2017 Aug 10;12(8):e0182704.

37. Verhaart IEC, Putker K, van de Vijver D, Tanganyika-de Winter CL, Pasteuning-Vuhman S, Plomp JJ, Aartsma-Rus AM, van Putten M. Cross-sectional study into age-related pathology of mouse models for limb girdle muscular dystrophy types 2D and 2F. PLoS One. 2019 Aug 20;14(8):e0220665.
38. Vainzof M, Souza LS, Gurgel-Giannetti J, Zatz M. Sarcoglycanopathies: an update. Neuromuscul Disord. 2021 Oct;31(10):1021-1027.
39. Mendell JR, Rodino-Klapac LR, Rosales-Quintero X, Kota J, Coley BD, Galloway G, Craenen JM, Lewis S, Malik V, Shilling C, Byrne BJ, Conlon T, Campbell KJ, Bremer WG, Viollet L, Walker CM, Sahenk Z, Clark KR. Limb-girdle muscular dystrophy type 2D gene therapy restores alpha-sarcoglycan and associated proteins. Ann Neurol. 2009 Sep;66(3):290-7.
40. Mendell JR, Rodino-Klapac LR, Rosales XQ, Coley BD, Galloway G, Lewis S, Malik V, Shilling C, Byrne BJ, Conlon T, Campbell KJ, Bremer WG, Taylor LE, Flanigan KM, Gastier-Foster JM, Astbury C, Kota J, Sahenk Z, Walker CM, Clark KR. Sustained alpha-sarcoglycan gene expression after gene transfer in limb-girdle muscular dystrophy, type 2D. Ann Neurol. 2010 Nov;68(5):629-38.
41. Mendell JR, Chicoine LG, Al-Zaidy SA, Sahenk Z, Lehman K, Lowes L, Miller N, Alfano L, Galliers B, Lewis S, Murrey D, Peterson E, Griffin DA, Church K, Cheatham S, Cheatham J, Hogan MJ, Rodino-Klapac LR. Gene Delivery for Limb-Girdle Muscular Dystrophy Type 2D by Isolated Limb Infusion. Hum Gene Ther. 2019 Jul;30(7):794-801.
42. Griffin DA, Pozsgai ER, Heller KN, Potter RA, Peterson EL, Rodino-Klapac LR. Preclinical Systemic Delivery of Adeno-Associated α-Sarcoglycan Gene Transfer for Limb-Girdle Muscular Dystrophy. Hum Gene Ther. 2021 Apr;32(7-8):390-404.
43. Sandonà D, Betto R. Sarcoglycanopathies: molecular pathogenesis and therapeutic prospects. Expert Rev Mol Med. 2009 Sep 28;11:e28.
44. Bianchini E, Fanin M, Mamchaoui K, Betto R, Sandonà D. Unveiling the degradative route of the V247M α-sarcoglycan mutant responsible for LGMD-2D. Hum Mol Genet. 2014 Jul 15;23(14):3746-58.
45. Carotti M, Marsolier J, Soardi M, Bianchini E, Gomiero C, Fecchio C, Henriques SF, Betto R, Sacchetto R, Richard I, Sandonà D. Repairing folding-defective α-sarcoglycan mutants by CFTR correctors, a potential therapy for limb-girdle muscular dystrophy 2D. Hum Mol Genet. 2018 Mar 15;27(6):969-984.

46. Carotti M, Scano M, Fancello I, Richard I, Risato G, Bensalah M, Soardi M, Sandonà D. Combined Use of CFTR Correctors in LGMD2D Myotubes Improves Sarcoglycan Complex Recovery. Int J Mol Sci. 2020 Mar 6;21(5):1813.
47. Scano M, Benetollo A, Nogara L, Bondì M, Barba FD, Soardi M, Furlan S, Akyurek EE, Caccin P, Carotti M, Sacchetto R, Blaauw B, Sandonà D. CFTR corrector C17 is effective in muscular dystrophy, in vivo proof of concept in LGMDR3. Hum Mol Genet. 2021 Sep 9:ddab260.
48. Escobar H, Krause A, Keiper S, Kieshauer J, Müthel S, de Paredes MG, Metzler E, Kühn R, Heyd F, Spuler S. Base editing repairs an SGCA mutation in human primary muscle stem cells. JCI Insight. 2021 May 24;6(10):e145994.
49. Rosenberg AS, Puig M, Nagaraju K, Hoffman EP, Villalta SA, Rao VA, Wakefield LM, Woodcock J. Immune-mediated pathology in Duchenne muscular dystrophy. Sci Transl Med. 2015 Aug 5;7(299):299rv4.
50. Yang W, Hu P. Skeletal muscle regeneration is modulated by inflammation. J Orthop Translat. 2018 Feb 7;13:25-32.
51. Hyldahl RD, Nelson B, Xin L, Welling T, Groscost L, Hubal MJ, Chipkin S, Clarkson PM, Parcell AC. Extracellular matrix remodeling and its contribution to protective adaptation following lengthening contractions in human muscle. FASEB J. 2015 Jul;29(7):2894-904.
52. Tidball JG, Welc SS, Wehling-Henricks M. Immunobiology of Inherited Muscular Dystrophies. Compr Physiol. 2018 Sep 14;8(4):1313-1356.
53. Péladeau C, Sandhu JK. Aberrant NLRP3 Inflammasome Activation Ignites the Fire of Inflammation in Neuromuscular Diseases. Int J Mol Sci. 2021 Jun 4;22(11):6068. doi: 10.3390/ijms22116068.
54. Di Virgilio, F.; Sarti, A.C.; Grassi, F. Modulation of innate and adaptive immunity by P2X ion channels. Curr. Opin. Immunol. 2018,52, 51–59.
55. Munoz-Planillo, R.; Kuffa, P.; Martinez-Colon, G.; Smith, B.L.; Rajendiran, T.M.; Nunez, G. K(+) efflux is the common trigger of NLRP3 inflammasome activation by bacterial toxins and particulate matter. Immunity 2013, 38, 1142–1153.
56. MacKenzie, A.; Wilson, H.L.; Kiss-Toth, E.; Dower, S.K.; North, R.A.; Surprenant, A. Rapid secretion of interleukin-1beta by microvesicle shedding. Immunity 2001, 15, 825–835. Pharmaceuticals 2022, 15, 89 13 of 15

57. Karmakar, M.; Katsnelson, M.A.; Dubyak, G.R.; Pearlman, E. Neutrophil P2X7 receptors mediate NLRP3 inflammasome- dependent IL-1beta secretion in response to ATP. Nat. Commun. 2016, 7, 10555.
58. Yeung, D.; Zablocki, K.; Lien, C.F.; Jiang, T.; Arkle, S.; Brutkowski, W.; Brown, J.; Lochmuller, H.; Simon, J.; Barnard, E.A.; et al.Increased susceptibility to ATP via alteration of P2X receptor function in dystrophic mdx mouse muscle cells. FASEB J. 2006, 20,610–620.
59. Rawat, R.; Cohen, T.V.; Ampong, B.; Francia, D.; Henriques-Pons, A.; Hoffman, E.P.; Nagaraju, K. Inflammasome up-regulation and activation in dysferlin-deficient skeletal muscle. Am. J. Pathol. 2010, 176, 2891–2900.
60. Panicucci C, Raffaghello L, Bruzzone S, Baratto S, Principi E, Minetti C, Gazzerro E, Bruno C. eATP/P2X7R Axis: An Orchestrated Pathway Triggering Inflammasome Activation in Muscle Diseases. Int J Mol Sci. 2020 Aug 19;21(17):5963. doi: 10.3390/ijms21175963.
61. A, Young CN, Al-Khalidi R, Teti A, Kalinski P, Mohamad S, Floriot L, Henry T, Tozzi G, Jiang T, Wurtz O, Lefebvre A, Shugay M, Tong J, Vaudry D, Arkle S, doRego JC, Górecki DC. P2RX7 purinoceptor: a therapeutic target for ameliorating the symptoms of duchenne muscular dystrophy. PLoS Med. 2015 Oct 13;12(10):e1001888. doi: 10.1371/journal.pmed.1001888.
62. Gazzerro E, Baldassari S, Assereto S, Fruscione F, Pistorio A, Panicucci C, Volpi S, Perruzza L, Fiorillo C, Minetti C, Traggiai E, Grassi F, Bruno C. Enhancement of Muscle T Regulatory Cells and Improvement of Muscular Dystrophic Process in mdx Mice by Blockade of Extracellular ATP/P2X Axis. Am J Pathol. 2015 Dec;185(12):3349-60. doi: 10.1016/j.ajpath.2015.08.010. Epub 2015 Oct 24.
63. Al-Khalidi R, Panicucci C, Cox P, Chira N, Róg J, Young CNJ, McGeehan RE, Ambati K, Ambati J, Zabłocki K, Gazzerro E, Arkle S, Bruno C, Górecki DC. Zidovudine ameliorates pathology in the mouse model of Duchenne muscular dystrophy via P2RX7 purinoceptor antagonism. Acta Neuropathol Commun. 2018 Apr 11;6(1):27. doi: 10.1186/s40478-018-0530-4.
64. Yegutkin GG: Nucleotide- and nucleoside-converting ectoenzymes: important modulators of purinergic signalling cascade. Biochim Biophys Acta 2008, 1783:673-694
65. Betto R, Senter L, Ceoldo S, Tarricone E, Biral D, Salviati G: EctoATPase activity of alpha-sarcoglycan (adhalin). J Biol Chem 1999, 274:7907-7912.

66. Sandona D, Gastaldello S, Martinello T, Betto R: Characterization of the ATP-hydrolysing activity of alpha-sarcoglycan. Biochem J 2004, 381:105-112.
67. Tasca G, Ricci E, Monforte M, Laschena F, Ottaviani P, Rodolico C, Barca E, Silvestri G, Iannaccone E, Mirabella M, Broccolini A. Muscle imaging findings in GNE myopathy. J Neurol. 2012 Jul;259(7):1358-65. doi: 10.1007/s00415-011-6357-6. Epub 2012 Jan 10.
68. Cantero D, Hernandez-Lain A, Martinez JFG, Perez MR, Ruano Y, Lleixa C, et al. Milder forms of alpha- sarcoglicanopathies diagnosed in adulthood by NGS analysis. J Neurol Sci. 2018;394:63–7.
69. Jain A, Sharma MC, Sarkar C, Bhatia R, Singh S, Handa R. Major Histocompatibility Complex Class I and II detection as a diagnostic tool idiopathic inflammatory myopathies. Arch Pathol Lab Med. 2007,131:1070-6.
70. Villalta SA, Rao VA, Wakefield LM, Woodcock J. Immune-mediated pathology in Duchenne muscular dystrophy. Sci Transl Med. 2015; 7: 299rv4
71. van der Pas J, Hengstman GJD, ter Laak HJ, Borm GF, van Engelen BG. Diagnostic value of MHC class I staining in idiopathic inflammatory myopathies. J Neurol Neurosurg Psychiatry. 2004; 75: 136-139.
72. Dalakas MC, Hohlfeld R. Polymyositis and dermatomyositis. Lancet. 2003; 362: 971-982.
73. Jain A, Sharma MC, Sarkar C, Bhatia R, Singh S, Handa R. Major histocompatibility complex class I and II detection as a diagnostic tool in idiopathic inflammatory myopathies. Arch Pathol Lab Med.2007; 131: 1070-1076.
74. Pescatori M, Broccolini A, Minetti C, Bertini E, Bruno C, D'amico A, Bernardini C, Mirabella M, Silvestri G, Giglio V, Modoni A, Pedemonte M, Tasca G, Galluzzi G, Mercuri E, Tonali PA, Ricci E. Gene expression profiling in the early phases of DMD: a constant molecular signature characterizes DMD muscle from early postnatal life throughout disease progression. FASEB J. 2007; 21: 1210-1226.
75. Nagappa M, Nalini A, Narayanappa G. Major histocompatibility complex and inflammatory cell subtype expression in inflammatory myopathies and muscular dystrophies. Neurol India. 2013; 61: 614-621.
76. Yin X, Wang Q, Chen T, Niu J, Ban R, Liu J, Mao Y, Pu C. CD4+ cells, macrophages, MHC-I and C5b-9 involve the pathogenesis of dysferlinopathy. Int J Clin Exp Pathol. 2015, 8: 3069-3075.

77. Confalonieri P, Oliva L, Andreetta F, Lorenzoni R, Dassi P, Mariani E, Morandi L, Mora M, Cornelio F, Mantegazza R. Muscle inflammation and MHC class I up-regulation in muscular dystrophy with lack of dysferlin: an immunopathological study. J Neuroimmunol. 2003; 142: 130-136.
78. Chen YW, Nagaraju K, Bakay M, McIntyre O, Rawat R, Shi R, Hoffman EP. Early onset of inflammation and later involvement of TGFbeta in Duchenne muscular dystrophy. Neurology. 2005; 65: 826- 834
79. McDonald CM, Henricson EK, Abresch RT, Duong T, Joyce NC, Hu F, Clemens PR, Hoffman EP, Cnaan A, Gordish-Dressman H; CINRG Investigators. Long-term effects of glucocorticoids on function, quality of life, and survival in patients with Duchenne muscular dystrophy: a prospective cohort study. Lancet. 2018; 391: 451-461.
80. Kissel JT, Burrow KL, Rammohan KW, Mendell JR; CIDD Study Group. Mononuclear cell analysis of muscle biopsies in prednisone-treated and untreated Duchenne muscular dystrophy. Neurology. 1991; 41: 667-672.
81. Sciorati C, Buono R, Azzoni E, Casati S, Ciuffreda P, D'Angelo G, Cattaneo D, Brunelli S, Clementi E. Co-administration of ibuprofen and nitric oxide is an effective experimental therapy for muscular dystrophy, with immediate applicability to humans. Br J Pharmacol. 2010; 160: 1550-1560.
82. Quattrocelli M, Salamone IM, Page PG, Warner JL, Demonbreun AR, McNally EM. Intermittent glucocorticoid dosing improves muscle repair and function in mice with limb-girdle muscular dystrophy. Am J Pathol. 2017; 187: 2520-2535.
83. Angelini C, Fanin M, Menegazzo E, Freda MP, Duggan DJ, Hoffman EP. Homozygous alphasarcoglycan mutation in two siblings: one asymptomatic and one steroid-responsive mild limbgirdle muscular dystrophy patient. Muscle Nerve. 1998; 21: 769-775.
84. Grozio A, Sociali G, Sturla L, Caffa I, Soncini D, Salis A, Raffaelli N, De Flora A, Nencioni A, Bruzzone S: CD73 protein as a source of extracellular precursors for sustained NADþ biosynthesis in FK866-Ttreated tumor cells. J Biol Chem 2013, 288:25938e25949
85. Munoz J, Zhou Y, Jarrett HW: LG4-5 domains of laminin-211 binds alpha-dystroglycan to allow myotube attachment and prevent anoikis.J Cell Physiol 2010, 222:111

86. Muratore M, Srsen V, Waterfall M, Downes A, Pethig R: Biomarkerfree dielectrophoretic sorting of differentiating myoblast multipotent progenitor cells and their membrane analysis by Raman spectroscopy. Biomicrofluidics 2012, 6:034113
87. Pawlikowski B, Lee L, Zuo J, Kramer R: Analysis of human muscle stem cells reveals a differentiation-resistant progenitor cell population expressing Pax7 capable of self-renewal. Dev Dyn 2009, 238: 138e149
88. Kirschner J, Lochmuller H: Sarcoglycanopathies. Handb Clin Neurol 2011, 101:41e46.
89. Brunelli S, Sciorati C, D'Antona G, Innocenzi A, Covarello D, Galvez BG, Perrotta C, Monopoli A, Sanvito F, Bottinelli R, Ongini E, Cossu G, Clementi E: Nitric oxide release combined with nonsteroidal antiinflammatory activity prevents muscular dystrophy pathology and enhances stem cell therapy. Proc Natl Acad Sci U S A 2007, 104:264e269
90. De Paepe B, De Bleecker JL: Cytokines and chemokines as regulators of skeletal muscle inflammation: presenting the case of Duchenne muscular dystrophy. Mediators Inflamm 2013, 2013:540370
91. Saito K, Kobayashi D, Komatsu M, Yajima T, Yagihashi A, Ishikawa Y, Minami R, Watanabe N: A sensitive assay of tumor necrosis factor alpha in sera from Duchenne muscular dystrophy patients. Clin Chem 2000, 46:1703e1704
92. Evans NP, Misyak SA, Robertson JL, Bassaganya-Riera J, Grange RW: Immune-mediated mechanisms potentially regulate the disease time-course of Duchenne muscular dystrophy and provide targets for therapeutic intervention. PMR 2009, 1:755e768
93. De Pasquale L, D'Amico A, Verardo M, Petrini S, Bertini E, De Benedetti F: Increased muscle expression of interleukin-17 in Duchenne muscular dystrophy. Neurology 2012, 78:1309e1314
94. Rufo A, Del Fattore A, Capulli M, Carvello F, De Pasquale L, Ferrari S, Pierroz D, Morandi L, De Simone M, Rucci N, Bertini E, Bianchi ML, De Benedetti F, Teti A: Mechanisms inducing low bone density in Duchenne muscular dystrophy in mice and humans. J Bone Miner Res 2011, 26:1891e1903
95. Bianchi G, Vuerich M, Pellegatti P, Marimpietri D, Emionite L, Marigo I, Bronte V, Di Virgilio F, Pistoia V, Raffaghello L: ATP/P2X7 axis modulates myeloid-

derived suppressor cell functions in neuroblastoma microenvironment. Cell Death Dis 2014, 5: e1135

96. Orioli E, De Marchi E, Giuliani AL, Adinolfi E: P2X7 receptor orchestrates multiple signalling pathways triggering inflammation autophagy and metabolic/trophic responses. Curr Med Chem 2017, 24:2261e2275
97. Gulbransen BD, Bashashati M, Hirota SA, Gui X, Roberts JA, MacDonald JA, Muruve DA, McKay DM, Beck PL, Mawe GM, Thompson RJ, Sharkey KA: Activation of neuronal P2X7 receptor-pannexin1 mediates death of enteric neurons during colitis. Nat Med 2012, 18:600e604
98. Burzyn D, Kuswanto W, Kolodin D, Shadrach JL, Cerletti M, Jang Y, Sefik E, Tan TG, Wagers AJ, Benoist C, Mathis D: A special population of regulatory T cells potentiates muscle repair. Cell 2013, 155:1282e1295
99. Lei H, Schmidt-Bleek K, Dienelt A, Reinke P, Volk HD: Regulatory T cell-mediated anti-inflammatory effects promote successful tissue repair in both indirect and direct manners. Front Pharmacol 2015, 6:184 30.
100. Schiaffino S, Pereira MG, Ciciliot S, Rovere-Querini P: Regulatory T cells and skeletal muscle regeneration. FEBS J 2017, 284:517e524
101. Rawat R, Cohen TV, Ampong B, Francia D, Henriques-Pons A, Hoffman EP, Nagaraju K: Inflammasome up-regulation and activation in dysferlin-deficient skeletal muscle. Am J Pathol 2010, 176: 2891e2900
102. Murgia M, Hanau S, Pizzo P, Rippa M, Di Virgilio F, Oxidized ATP: An irreversible inhibitor of the macrophage purinergic P2Z receptor. J Biol Chem 1993, 268:8199e8203
103. Di Virgilio F: Novel data point to a broader mechanism of action of oxidized ATP: the P2X7 receptor is not the only target. Br J Pharmacol 2003, 140:441e443
104. Ardissone V, Radaelli E, Zaratin P, Ardizzone M, Ladel C, Gattorno M, Martini A, Grassi F, Traggiai E: Pharmacologic P2X purinergic receptor antagonism in the treatment of collagen-induced arthritis. Arthritis Rheum 2011, 63:3323e3332
105. Lang PA, Merkler D, Funkner P, Funkner P, Shaabani N, Meryk A, Krings C, Barthuber C, Recher M, Brück W, Häussinger D, Ohashi PS, Lang KS: Oxidized ATP inhibits T-cell-mediated autoimmunity. Eur J Immunol 2010, 40:2401e2408
106. Schenk U, Westendorf AM, Radaelli E, Casati A, Ferro M, Fumagalli M, Verderio C, Buer J, Scanziani E, Grassi F: Purinergic control of T cell activation by ATP released through pannexin-1 hemichannels. Sci Signal 2008, 1:ra6

107. Vergani A, Fotino C, D'Addio F, Tezza S, Podetta M, Gatti F, Chin M, Bassi R, Molano RD, Corradi D, Gatti R, Ferrero ME, Secchi A, Grassi F, Ricordi C, Sayegh MH, Maffi P, Pileggi A, Fiorina P: Effect of the purinergic inhibitor oxidized ATP in a model of islet allograft rejection. Diabetes 2013, 62:1665e1675

108. Kurashima Y, Amiya T, Nochi T, Fujisawa K, Haraguchi T, Iba H, Tsutsui H, Sato S, Nakajima S, Iijima H, Kubo M, Kunisawa J, Kiyono H: Extracellular ATP mediates mast cell-dependent intestinal inflammation through P2X7 purinoceptors. Nat Commun 2012, 3: 1034

109. Koo TY, Lee JG, Yan JJ, Jang J, Ju KD, Oh KH, Ahn C, Jang J: The P2X7 receptor antagonist, oxidized adenosine triphosphate, ameliorates renal ischemia-reperfusion injury by expansion of regulatory T cells. Kidney Int 2017, 92:415e431

110. Guile SD, Alcaraz L, Birkinshaw TN, Bowers KC, Ebden MR, Furber M, Stocks MJ: Antagonists of the P2X7 receptor: from lead identification to drug development. J Med Chem 2009, 52: 3123e3141

111. Subramanyam C, Duplantier AJ, Dombroski MA, Chang S-P, Gabel CA, Whitney-Pickett C, Perregaux DG, Labasi JM, Yoon K, Shepard RM: Discovery, synthesis and SAR of azinyl- and azolylbenzamides antagonists of the P2X 7 receptor. Bioorg Med Chem Lett 2011, 21:5475e5479

112. Lambertucci C, dal Ben D, Buccioni M, Marucci G, Thomas A, Volpini R: Medicinal chemistry of P2X receptors: agonists and orthosteric antagonists. Curr Med Chem 2015, 22:915e928

113. Caseley EA, Muench SP, Fishwick CW, Jiang LH: Structure-based identification and characterization of structurally novel human P2X7 receptor antagonists. Biochem Pharmacol 2016, 15:130e139

114. Keystone EC, Wang MM, Layton M, Hollis S, Mcinnes IB: Clinical evaluation of the efficacy of the P2X7 purinergic receptor antagonist AZD9056 on the signs and symptoms of rheumatoid arthritis in patients with active disease despite treatment with methotrexate or sulphasalazine. Ann Rheum Dis 2012, 71:1630e1635

115. Stock TC, Bloom BJ, Wei N, Ishaq S, Park W, Wang X, Gupta P, Mebus CA: Efficacy and safety of CE-224,535, an antagonist of P2X7 receptor, in treatment of patients with rheumatoid arthritis inadequately controlled by methotrexate. J Rheumatol 2012, 39: 720e727

116. Eser A, Colombel J-F, Rutgeerts P, Vermeire S, Vogelsang H, Braddock M, Persson T, Reinisch W: Safety and efficacy of an oral inhibitor of the purinergic

receptor P2X7 in adult patients with moderately to severely active Crohn's disease: a randomized placebo-controlled, double-blind, phase IIa study. Inflamm Bowel Dis 2015, 21:2247e2253

117. Han J, Liu H, Liu C, Jin H, Perlmutter JS, Egan TM, Tu Z: Pharmacologic characterizations of a P2X7 receptor-specific radioligand, [11C]GSK1482160 for neuroinflammatory response. Nucl Med Commun 2017, 38:372e382

118. Fougerousse F, Bartoli M, Poupiot J, Arandel L, Durand M, Guerchet N, Gicquel E, Danos O, Richard I: Phenotypic correction of alpha-sarcoglycan deficiency by intra-arterial injection of a muscle-specific serotype 1 rAAV vector. Mol Ther 2007, 15:53e61

119. Pacak CA, Conlon T, Mah CS, Byrne BJ: Relative persistence of AAV serotype 1 vector genomes in dystrophic muscle. Genet Vaccin Ther 2008, 6:14

120. Pacak CA, Walter GA, Gaidosh G, Bryant N, Lewis MA, Germain S, Mah CS, Campbell KP, Byrne BJ: Long-term skeletal muscle protection after gene transfer in a mouse model of LGMD-2D. Mol Ther 2007, 15:1775e1781

121. Cordier L, Hack AA, Scott MO, Barton-Davis ER, Gao G, Wilson JM, McNally EM, Sweeney HL: Rescue of skeletal muscles of gamma-sarcoglycan-deficient mice with adeno-associated virusmediated gene transfer. Mol Ther 2000, 1:119e129

122. Goehringer C, Rutschow D, Bauer R, Schinkel S, Weichenhan D, Bekeredjian R, Straub V, Kleinschmidt JA, Katus HA, Müller OJ: Prevention of cardiomyopathy in delta-sarcoglycan knockout mice after systemic transfer of targeted adeno-associated viral vectors. Cardiovasc Res 2009, 82:404e410

123. Li J, Dressman D, Tsao YP, Sakamoto A, Hoffman EP, Xiao X: rAAV vector-mediated sarcogylcan gene transfer in a hamster model for limb girdle muscular dystrophy. Gene Ther 1999, 6:74e82

124. Li J, Wang D, Qian S, Chen Z, Zhu T, Xiao X: Efficient and long-term intracardiac gene transfer in d-sarcoglycan-deficiency hamster by adeno-associated virus-2 vectors. Gene Ther 2003, 10:1807e1813

125. Sociali, G.; Visigalli, D.; Prukop, T.; Cervellini, I.; Mannino, E.; Venturi, C.; Bruzzone, S.; Sereda, M.W.; Schenone, A. Tolerability and efficacy study of P2X7 inhibition in experimental Charcot-Marie-Tooth type 1A (CMT1A) neuropathy. Neurobiol. Dis. 2016, 95, 145–157.

126. Pozsgai, E.R.; Griffin, D.A.; Heller, K.N.; Mendell, J.R.; Rodino-Klapac, L.R. β-Sarcoglycan gene transfer decreases fibrosis and restores force in LGMD2E mice. Gene Ther. 2016, 23, 57–66.

127. Di Virgilio, F.; Dal Ben, D.; Sarti, A.C.; Giuliani, A.L.; Falzoni, S. The P2X7 Receptor in Infection and Inflammation. Immunity 2017, 47, 15–31.

128. Young, C.N.; Sinadinos, A.; Lefebvre, A.; Chan, P.; Arkle, S.; Vaudry, D.; Gorecki, D.C. A novel mechanism of autophagic cell death in dystrophic muscle regulated by P2RX7 receptor large-pore formation and HSP90. Autophagy 2015, 11, 113–130.

129. Young, C.N.J.; Chira, N.; Rog, J.; Al-Khalidi, R.; Benard, M.; Galas, L.; Chan, P.; Vaudry, D.; Zablocki, K.; Gorecki, D.C. Sustained activation of P2X7 induces MMP-2-evoked cleavage and functional purinoceptor inhibition. J. Mol. Cell. Biol. 2017, 10, 229–242

130. Beigi, R.D.; Kertesy, S.B.; Aquilina, G.; Dubyak, G.R. Oxidized ATP (oATP) attenuates proinflammatory signaling via P2 receptor-independent mechanisms. Br. J. Pharmacol. 2003, 140, 507–519.

131. Savio, L.E.B.; de Andrade Mello, P.; da Silva, C.G.; Coutinho-Silva, R. The P2X7 Receptor in Inflammatory Diseases: Angel or Demon? Front. Pharmacol. 2016, 9, 52.

132. De Marchi, E.; Orioli, E.; Dal Ben, D.; Adinolfi, E. P2X7 Receptor as a Therapeutic Target. Adv. Protein Chem. Struct. Biol. 2016,104, 39–79.

133. Figliuolo, V.R.; Chaves, S.P.; Santoro, G.F.; Coutinho, C.M.; Meyer-Fernandes, J.R.; Rossi-Bergmann, B.; Coutinho-Silva, R.Periodate-oxidized ATP modulates macrophage functions during infection with Leishmania amazonensis. Cytom. A 2014, 85,588–600.

134. Craighead, M.W.; Middlehurst, K.M.; LeFeuvre, R.; Kimber, I.; Rothwell, N.J. Oxidised adenosine 50 -triphosphate, a P2X(7) antagonist, is toxic to rat cerebellar granule neurones in vitro. Neurosci. Lett. 2001, 311, 77–80.

135. Donnelly-Roberts, D.L.; Namovic, M.T.; Han, P.; Jarvis, M.F. Mammalian P2X7 receptor pharmacology: Comparison of recombinant mouse, rat and human P2X7 receptors. Br. J. Pharmacol. 2009, 157, 1203–1214.

136. Honore, P.; Donnelly-Roberts, D.; Namovic, M.T.; Hsieh, G.; Zhu, C.Z.; Mikusa, J.P.; Hernandez, G.; Zhong, C.; Gauvin, D.M.; Chandran, P.; et al. A-740003 [N-(1-{[(cyanoimino)(5-quinolinylamino)methyl]amino}-2,2-dimethylpropyl)-2-(3,4-

dimethoxyphenyl)acetamide], a novel and selective P2X7 receptor antagonist, dose-dependently reduces neuropathic pain in the rat. J. Pharmacol. Exp. Ther. 2006, 319, 1376–1385.

137. McGaraughty, S.; Chu, K.L.; Namovic, M.T.; Donnelly-Roberts, D.L.; Harris, R.R.; Zhang, X.F.; Shieh, C.C.; Wismer, C.T.; Zhu, C.Z.;Gauvin, D.M.; et al. P2X7-related modulation of pathological nociception in rats. Neuroscience 2007, 146, 1817–1828.

138. Teixeira, J.M.; Oliveira, M.C.; Parada, C.A.; Tambeli, C.H. Peripheral mechanisms underlying the essential role of P2X7 receptors in the development of inflammatory hyperalgesia. Eur. J. Pharmacol. 2010, 644, 55–60.

139. Jimenez-Pacheco, A.; Mesuret, G.; Sanz-Rodriguez, A.; Tanaka, K.; Mooney, C.; Conroy, R.; Miras-Portugal, M.T.; Diaz-Hernandez, M.; Henshall, D.C.; Engel, T. Increased neocortical expression of the P2X7 receptor after status epilepticus and anticonvulsant effect of P2X7 receptor antagonist A-438079. Epilepsia 2013, 54, 1551–1561.

140. Marcellino, D.; Suárez-Boomgaard, D.; Sánchez-Reina, M.D.; Aguirre, J.A.; Yoshitake, T.; Yoshitake, S.; Hagman, B.; Kehr, J.; Agnati, L.F.; Fuxe, K.; et al. On the role of P2X(7) receptors in dopamine nerve cell degeneration in a rat model of Parkinson's disease: Studies with the P2X(7) receptor antagonist A-438079. J. Neural Transm. 2010, 117, 681–687.

141. Folker, E.S.; Baylies, M.K. Nuclear positioning in muscle development and disease. Front. Physiol. 2013, 4, 363.

142. Gentile, D.; Natale, M.; Lazzerini, P.E.; Capecchi, P.L.; Laghi-Pasini, F. The role of P2X7 receptors in tissue fibrosis: A brief review. Purinergic Signal. 2015, 11, 435–440.

143. Villalta, S.A.; Rosenberg, A.S.; Bluestone, J.A. The immune system in Duchenne muscular dystrophy: Friend or foe. Rare Dis.2015, 3, e1010966.

144. Ingersoll, M.A.; Platt, A.M.; Potteaux, S.; Randolph, G.J. Monocyte trafficking in acute and chronic inflammation. Trends Immunol. 2011, 32, 470–477.

145. Mojumdar, K.; Liang, F.; Giordano, C.; Lemaire, C.; Danialou, G.; Okazaki, T.; Bourdon, J.; Rafei, M.; Galipeau, J.; Divangahi, M.;et al. Inflammatory monocytes promote progression of Duchenne muscular dystrophy and can be therapeutically targeted via CCR2. EMBO Mol. Med. 2014, 6, 1476–1492.

146. Villalta, S.A.; Nguyen, H.X.; Deng, B.; Gotoh, T.; Tidball, J.G. Shifts in macrophage phenotypes and macrophage competition for arginine metabolism affect the severity of muscle pathology in muscular dystrophy. Hum. Mol. Genet. 2009, 18, 482–496.

147. Kranig, S.A.; Tschada, R.; Braun, M.; Patry, C.; Poschl, J.; Frommhold, D.; Hudalla, H. Dystrophin deficiency promotes leukocyte recruitment in mdx mice. Pediatr. Res. 2019, 86, 188–194.

148. Hodgetts, S.; Radley, H.; Davies, M.; Grounds, M.D. Reduced necrosis of dystrophic muscle by depletion of host neutrophils, or blocking TNFalpha function with Etanercept in mdx mice. Neuromuscul. Disord. 2006, 16, 591–602.

149. Tulangekar, A.; Sztal, T.E. Inflammation in Duchenne Muscular Dystrophy-Exploring the Role of Neutrophils in Muscle Damage and Regeneration. Biomedicines 2021, 9, 1366.

150. Arecco, N.; Clarke, C.J.; Jones, F.K.; Simpson, D.M.; Mason, D.; Beynon, R.J.; Pisconti, A. Elastase levels and activity are increased in dystrophic muscle and impair myoblast cell survival, proliferation and differentiation. Sci. Rep. 2016, 6, 24708.

151. Karmakar, M.; Katsnelson, M.A.; Dubyak, G.R.; Pearlman, E. Neutrophil P2X7 receptors mediate NLRP3 inflammasome- dependent IL-1beta secretion in response to ATP. Nat. Commun. 2016, 7, 10555.

152. Pelegrin, P.; Barroso-Gutierrez, C.; Surprenant, A. P2X7 receptor differentially couples to distinct release pathways for IL-1beta in mouse macrophage. J. Immunol. 2008, 180, 7147–7157.

153. Pizzirani, C.; Ferrari, D.; Chiozzi, P.; Adinolfi, E.; Sandonà, D.; Savaglio, E.; Di Virgilio, F. Stimulation of P2 receptors causes release of IL-1beta-loaded microvesicles from human dendritic cells. Blood 2007, 109, 3856–3864.

154. Kawamura, H.; Kawamura, T.; Kanda, Y.; Kobayashi, T.; Abo, T. Extracellular ATP-stimulated macrophages produce macrophage inflammatory protein-2 which is important for neutrophil migration. Immunology 2012, 136, 448–458.

155. Villalta, S.A.; Rosenthal, W.; Martinez, L.; Kaur, A.; Sparwasser, T.; Tidball, J.G.; Margeta, M.; Spencer, M.J.; Bluestone, J.A. Regulatory T cells suppress muscle inflammation and injury in muscular dystrophy. Sci. Transl. Med. 2014, 6, 258ra142.

156. Quattrocelli, M.; Zelikovich, A.S.; Salamone, I.M.; Fischer, J.A.; McNally, E.M. Mechanisms and Clinical Applications of Glucocorticoid Steroids in Muscular Dystrophy. J. Neuromuscul. Dis. 2021, 8, 39–52.
157. Connolly, A.M.; Pestronk, A.; Mehta, S.; Al-Lozi, M. Primary alpha-sarcoglycan deficiency responsive to immunosuppression over three years. Muscle Nerve 1998, 21, 1549–1553.
158. Turan, S.; Farruggio, A.P.; Srifa, W.; Day, J.W.; Calos, M.P. Precise Correction of Disease Mutations in Induced Pluripotent Stem Cells Derived From Patients With Limb Girdle Muscular Dystrophy. Mol. Ther. J. Am. Soc. Gene Ther. 2016, 24, 685–696.
159. Pozsgai, E.; Griffin, D.; Potter, R.; Sahenk, Z.; Lehman, K.; Rodino-Klapac, L.R.; Mendell, J.R. Unmet needs and evolving treatment for limb girdle muscular dystrophies. Neurodegener. Dis. Manag. 2021, 11, 411–429.
160. Chu, M.L.; Moran, E. The Limb-Girdle Muscular Dystrophies: Is Treatment on the Horizon? Neurotherapeutics 2018, 15, 849–862
161. Shokoples, B.G.; Paradis, P.; Schiffrin, E.L. P2X7 Receptors: An Untapped Target for the Management of Cardiovascular Disease. Arterioscler. Thromb. Vasc. Biol. 2021, 41, 186–199.
162. Recourt, K.; van der Aart, J.; Jacobs, G.; de Kam, M.; Drevets, W.; van Nueten, L.; Kanhai, K.; Siebenga, P.; Zuiker, R.; Ravenstijn, P.; et al. Characterisation of the pharmacodynamic effects of the P2X7 receptor antagonist JNJ-54175446 using an oral dexamphetamine challenge model in healthy males in a randomised, double-blind, placebo-controlled, multiple ascending dose trial. J. Psychopharmacol. 2020, 34, 1030–1042.

7. Appendix

- Gazzerro E, Baratto S, Assereto S, Baldassari S, **Panicucci C**, Raffaghello L, Scudieri P, De Battista D, Fiorillo C, Volpi S, Chaabane L, Malnati M, Messina G, Bruzzone S, Traggiai E, Grassi F, Minetti C, Bruno C. The Danger Signal Extracellular ATP Is Involved in the Immunomediated Damage of α-Sarcoglycan-Deficient Muscular Dystrophy. Am J Pathol. 2019 Feb;189(2):354-369.

- **Panicucci C**, Raffaghello L, Bruzzone S, Baratto S, Principi E, Minetti C, Gazzerro E, Bruno C. eATP/P2X7R Axis: An Orchestrated Pathway Triggering Inflammasome Activation in Muscle Diseases. Int J Mol Sci. 2020 Aug 19;21(17):5963.

- Alonso-Pérez J, González-Quereda L, Bello L, Guglieri M, Straub V, Gallano P, Semplicini C, Pegoraro E, Zangaro V, Nascimento A, Ortez C, Comi GP, Dam LT, De Visser M, van der Kooi AJ, Garrido C, Santos M, Schara U, Gangfuß A, Løkken N, Storgaard JH, Vissing J, Schoser B, Dekomien G, Udd B, Palmio J, D'Amico A, Politano L, Nigro V, Bruno C, **Panicucci C**, Sarkozy A, Abdel-Mannan O, Alonso-Jimenez A, Claeys KG, Gomez-Andrés D, Munell F, Costa-Comellas L, Haberlová J, Rohlenová M, Elke V, De Bleecker JL, Dominguez-González C, Tasca G, Weiss C, Deconinck N, Fernández-Torrón R, López de Munain A, Camacho-Salas A, Melegh B, Hadzsiev K, Leonardis L, Koritnik B, Garibaldi M, de Leon-Hernández JC, Malfatti E, Fraga-Bau A, Richard I, Illa I, Díaz-Manera J. New genotype-phenotype correlations in a large European cohort of patients with sarcoglycanopathy. Brain. 2020 Sep 1;143(9):2696-2708.

- **Panicucci C**, Baratto S, Raffaghello L, Tonin P, D'Amico A, Tasca G, Traverso M, Fiorillo C, Minetti C, Previtali SC, Pegoraro E, Bruno C. Muscle inflammatory pattern in alpha- and gamma-sarcoglycanopathies. Clin Neuropathol. 2021 Nov-Dec;40(6):310-318.

- Raffaghello L, Principi E, Baratto S, **Panicucci C**, Pintus S, Antonini F, Del Zotto G, Benzi A, Bruzzone S, Scudieri P, Minetti C, Gazzerro E, Bruno C. P2X7 Receptor Antagonist Reduces Fibrosis and Inflammation in a Mouse Model of Alpha-Sarcoglycan Muscular Dystrophy. Pharmaceuticals (Basel). 2022 Jan 13;15(1):89.

The American Journal of Pathology, Vol. 189, No. 2, February 2019

ELSEVIER

The American Journal of PATHOLOGY

ajp.amjpathol.org

MUSCULOSKELETAL PATHOLOGY

The Danger Signal Extracellular ATP Is Involved in the Immunomediated Damage of α-Sarcoglycan—Deficient Muscular Dystrophy

Elisabetta Gazzerro,[*†] Serena Baratto,[‡] Stefania Assereto,[*] Simona Baldassari,[*] Chiara Panicucci,[‡] Lizzia Raffaghello,[‡§] Paolo Scudieri,[¶] Davide De Battista,[‖] Chiara Fiorillo,[*] Stefano Volpi,[**] Linda Chaabane,[‖] Mauro Malnati,[‖] Graziella Messina,[††] Santina Bruzzone,[‡‡] Elisabetta Traggiai,[§§] Fabio Grassi,[¶¶‖‖***] Carlo Minetti,[*] and Claudio Bruno[‡]

From the Pediatric Neurology and Muscle Disease Unit, the Center of Translational and Experimental Myology,‡ the Stem Cell Laboratory and Cell Therapy Center,§ and the Pediatria II Unit,** IRCCS Istituto Giannina Gaslini, Genova, Italy; the Charité Universität-Experimental and Clinical Research Center,† Berlin, Germany; the Telethon Institute of Genetics and Medicine,¶ Napoli, Italy; the Unit of Human Virology,‖ Division of Immunology, Transplantation and Infectious Disease, Ospedale San Raffaele, Milano, Italy; the Departments of Biosciences†† and Medical Biotechnologies and Translational Medicine,¶¶ University of Milan, Milan, Italy; the Department of Experimental Medicine,‡‡ University of Genova, Genova, Italy; the Novartis Institute for Research in Biomedicine,§§ Basel, Switzerland; the Institute for Research in Biomedicine,‖‖ Università della Svizzera Italiana, Bellinzona, Switzerland; and the Istituto Nazionale Genetica Molecolare "Romeo ed Enrica Invernizzi",*** Milan, Italy*

Accepted for publication October 16, 2018.

Address correspondence to Claudio Bruno, M.D., Ph.D., Center of Translational and Experimental Myology, Istituto Giannina Gaslini, Via G Gaslini, 5, Genova 16147, Italy; or Elisabetta Gazzerro, M.D., Charité Universität-Experimental and Clinical Research Center, Lindenberger Weg 80, Berlin 13125, Germany. E-mail: claudiobruno@gaslini.org or elisabetta.gazzerro@charite.de.

In muscular dystrophies, muscle membrane fragility results in a tissue-specific increase of danger-associated molecular pattern molecules (DAMPs) and infiltration of inflammatory cells. The DAMP extracellular ATP (eATP) released by dying myofibers steadily activates muscle and immune purinergic receptors exerting dual negative effects: a direct damage linked to altered intracellular calcium homeostasis in muscle cells and an indirect toxicity through the triggering of the immune response and inhibition of regulatory T cells. Accordingly, pharmacologic and genetic inhibition of eATP signaling improves the phenotype in models of chronic inflammatory diseases. In α-sarcoglycanopathy, eATP effects may be further amplified because α-sarcoglycan extracellular domain binds eATP and displays an ecto-ATPase activity, thus controlling eATP concentration at the cell surface and attenuating the magnitude and/or the duration of eATP-induced signals. Herein, we show that *in vivo* blockade of the eATP/P2X purinergic pathway by a broad-spectrum P2X receptor—antagonist delayed the progression of the dystrophic phenotype in α-sarcoglycan—null mice. eATP blockade dampened the muscular inflammatory response and enhanced the recruitment of forkhead box protein P3—positive immunosuppressive regulatory $CD4^+$ T cells. The improvement of the inflammatory features was associated with increased strength, reduced necrosis, and limited expression of profibrotic factors, suggesting that pharmacologic purinergic antagonism, altering the innate and adaptive immune component in muscle infiltrates, might provide a therapeutic approach to slow disease progression in α-sarcoglycanopathy. *(Am J Pathol 2019, 189: 354—369; https://doi.org/10.1016/j.ajpath.2018.10.008)*

Sarcoglycanopathies represent a subgroup of autosomal recessive limb-girdle muscular dystrophies (LGMDs) caused by mutations in one of the four sarcoglycan (SG) genes, which encode four transmembrane proteins (α-, β-, γ-, or δ-SG) organized in a tetrameric structure on the cell surface.[1]

The clinical phenotype of α-sarcoglycanopathy (LGMD2D; Online Mendelian Inheritance in Man number 608099) is heterogeneous.[2] Progressive degeneration of skeletal muscle leads to loss of ambulation, respiratory insufficiency, and often premature death in the early thirties.[3] The rapidity of disease progression and the age of onset are variable, ranging from severe forms with onset in

Supported by Telethon-Italy grant GEP12053 (C.B.) and Cinque per mille dell'IRPEF—Finanziamento della ricerca sanitaria, Finanziamento Ricerca Corrente, Ministero Salute (L.R.).

E.G., S.Bar., and S.A. contributed equally to this work.

Disclosures: None declared.

https://doi.org/10.1016/j.ajpath.2018.10.008

the first decade of life and rapid evolution, to milder forms with later onset and slower progression. Currently, no treatment is available for these patients.

Sarcoglycans and dystrophin are main components of the dystrophin-glycoprotein complex, the crucial structural linkage between the intracellular cytoskeleton and the extracellular matrix that provides stability to the sarcolemma and offers muscle fibers protection from muscle contraction–induced stress. In both sarcoglycanopathies and dystrophinopathies, dystrophin-glycoprotein complex disruption leads to a mechanically weaker muscle plasma membrane that is easily damaged during contraction, allowing release of intracellular molecules, which act as damage-associated molecular pattern molecules (DAMPs).[4] These self-molecules execute precise intracellular tasks in both innate and adaptive immunity, exerting disparate functions when released into the extracellular space. Among DAMPs, extracellular ATP (eATP) and its derivates are pleiotropic regulators of cell function.[5] In muscle, the primary function of ATP is energy transfer; however, after cell damage, it is quickly released in the extracellular space, where it acts as DAMP. Once in the extracellular space, eATP activates plasma-membrane nonselective ion channels purinergic P2X 1 to 7 receptors and P2Y 1, 2, 4, 6, and 11 to 14, guanine nucleotide binding protein-coupled receptors.[6,7] The role of eATP and P2X purinergic signal on *mdx* dystropathology has been recently well established. We have shown that blockade of eATP/P2X purinergic signaling by periodate-oxidase ATP (oATP) delayed the progression of the dystrophic phenotype, dampening the local inflammatory response in dystrophin-deficient *mdx* mice.[8] These results are in agreement with the phenotype displayed by *mdx*/P2X7 double-knockout mice, which showed a reduction of the inflammatory and fibrotic response in skeletal muscles and heart.[9]

We hypothesized that the role of eATP may be equally relevant in α-SG deficiency because this protein displays in its extracellular domain an ecto-ATPase activity, which allows conversion of ATP to the inactive form ADP.[10,11]

Herein, we provide the first set of evidences of a pathogenetic role of eATP in α-sarcoglycanopathy. Short-term pharmacologic inhibition of eATP signaling improved muscular function and morphology, inhibited the effector adaptive and the innate immune response, reduced the expression of profibrotic factors, and enhanced forkhead box protein P3–positive ($Foxp3^+$) $CD4^+$ T-regulatory cell muscle infiltration in α-sarcoglycan (*Sgca*) mice. It is thus feasible that α-SG deficiency can amplify the magnitude of eATP-induced signals, worsening the immunomediated damage in LGMD2D patients.

Materials and Methods

In Vivo Treatment with oATP

Sgca knockout mice [kindly donated by Prof. Giulio Cossu (University of Manchester, Manchester UK)] were treated with oATP at 6 mmol/L or phosphate-buffered saline (PBS) alone daily for 4 weeks by i.p. injection and were sacrificed at the end of treatment by carbon dioxide inhalation. A group of age-matched wild-type (WT) C57Bl/6J male mice was used as internal control. The experiment was repeated in two separate 4-week trials, which both included 5 to 7 mice in each experimental group. Thus, the results are indicative of at least 10 animals per group. The Sgca mice were randomly assigned to the experimental groups, and the testing of samples was performed blindly (S.A. and S.Bal.).

Blood samples were collected by intracardial puncture at the end of the fourth week of treatment and centrifuged for 10 minutes at 7000 × *g*. Immediately after centrifugation, the serum was isolated and stored at −20°C. Serum creatine kinase levels were measured using the creatine kinase–N-acetyl cysteine quantitative system, according to manufacturer's instructions (BPC BioSED, Rome, Italy).

All animal experiments were performed in accordance with the Swiss Federal Veterinary Office guidelines and authorized by the Animal Studies Committee of Cantonal Veterinary.

Four-Limb Hanging Test

At the beginning of the study and at the end of the second and fourth week of treatment, the muscle strength of oATP-treated, PBS-treated Sgca, and WT control mice was scored through the four-limb hanging test. In this method, mice are subjected to a 180-second lasting hanging test, during which a falling score is recorded. In each of the two treatments, all of the mice had to hang for three trials, and the average maximum hanging time of the three trials was measured (standard operating procedure, *http://www.treat-nmd.eu/research/preclinical/preclinical-efficacy-standards*, last accessed December 1, 2017).

Reagents and Antibodies

oATP (Sigma-Aldrich, St. Louis, MO) was reconstituted at a final concentration of 100 mmol/L in PBS and stored at −80°C; the reconstituted drug was thawed and diluted in PBS at 6 mmol/L immediately before use. Lipopolysaccharide (LPS; Sigma-Aldrich) was reconstituted at a final concentration of 1 mg/mL in Hanks' balanced salt solution and stored at −20°C, ATP (Sigma-Aldrich) was reconstituted at 100 mmol/L (pH 7) in water with sodium hydroxide and stored at −20°C, and benzoyl ATP (BzATP; Sigma-Aldrich) was reconstituted at 10 mmol/L in water and stored at −20°C.

The antibodies and dilutions used in the study include the following: mouse monoclonal antibody to collagen type I [1:500 for Western blot (WB) analysis] and rat monoclonal antibody to Ly6C [1:500 for immunohistochemistry (IHC)] from Abcam (Cambridge, UK); rat monoclonal antibody to CD45 (1:10 for IHC) from BD Pharmigen (San Jose, CA); mouse monoclonal antibody to activating signal

cointegrator−1 (ASC-1) (1:500 for WB analysis) and rabbit polyclonal antibodies to glyceraldehyde phosphate dehydrogenase (1:500 for WB analysis) from Santa Cruz Biotechnology (Dallas, TX); rabbit polyclonal antibody to CD3 (1:20 for IHC); rabbit polyclonal antibodies to P2X7 receptor (R; extracellular) and P2X4R (1:50 and 1:300, respectively, for immunofluorescence) from Alomone Labs (Jerusalem, Israel); rabbit polyclonal antibody to transforming growth factor (TGF)-β (1:1000 for WB analysis) from Cell Signaling Technology (Danvers, MA); mouse monoclonal antibody to CD39 (1:1000) from Abcam; mouse monoclonal antibody to α-SG (1:100 for WB analysis) from Novocastra (Newcastle upon Tyne, UK); mouse monoclonal antibody to β-dystroglycan (1:50 for WB analysis) from Novocastra; mouse monoclonal anti−caveolin-3 (1:10,000 for WB analysis) from BD Bioscience (Milan, Italy); mouse monoclonal antibody to myosin heavy chain (fast; 1:1000 for WB analysis) from Novocastra; rabbit anti-mouse IgG horseradish peroxidase−conjugated (1:700 for WB analysis) antibodies from Dako (Glostrup, Denmark); donkey anti-rabbit IgG horseradish peroxidase−conjugated (1:5000 for WB analysis) antibodies from GE Health Care (Little Chalfont, UK); mouse monoclonal anti-rat κ and λ light chain horseradish peroxidase−conjugated (1:100 for IHC) antibody from Sigma-Aldrich; rat monoclonal to FOXP3 (1:20 for IHC) from eBioscience (Waltham, MA); and goat anti-mouse AlexaFluor 488 and donkey anti-rat AlexaFluor 594 (1:750 for immunofluorescence) antibodies from Thermo Fisher Scientific (Waltham, MA). The EnVision Detection System Peroxidase/Diaminobenzidine, rabbit and mouse, was from Dako. The Annexin A5-FITC/7-AAD Kit was purchased from Beckman Coulter (Marseille, France).

Satellite Cell Isolation from Total Muscle

Satellite cells were isolated from WT and Sgca mice at passage 8 to passage 10. Forelimb, hind limb, and diaphragm muscles were dissected, mechanically cut, and enzymatically digested at 37°C under constant shaking with a solution containing collagenase I (100 μg/mL; Sigma-Aldrich), dispase (500 μg/mL; Gibco, Waltham, MA), and DNaseI (100 μg/mL; Roche, Basel, Switzerland) in PBS (Sigma-Aldrich). Undigested tissue was precipitated for 5 minutes, and the supernatant was centrifuged for 5 minutes at 1200 × *g*. The cell pellet was resuspended in Dulbecco's modified Eagle's medium plus 10% fetal bovine serum, 1% L-glutamine, 1% penicillin/streptomycin, and 1% gentamicin; then, it was preplated in 150-mm Petri uncoated dishes for 1 hour. After preplating, the nonadherent satellite cell−enriched population was collected and plated in collagen-coated (collagen from calf skin; Sigma-Aldrich) 90-mm Petri dishes at a density of 30,000 cells per Petri dish. After a few days in proliferation, the myoblasts were eventually plated at high density in differentiation medium (Dulbecco's modified Eagle's medium, 10% donor horse serum, 1% L-glutamine, 1% penicillin/streptomycin, 1% gentamicin, and 2.5 ng/mL basic fibroblast growth factor).

Histologic Studies

Sections (7 μm thick) from gastrocnemii (GN) and anterior tibialis muscles isolated from PBS-treated mice, oATP-Sgca mice, and WT controls were cut on a cryostat and stained with standard hematoxylin and eosin and acid phosphatase for inflammatory reactions and Masson trichrome stain.

Image analysis in terms of area fraction quantification, signal intensity, and object counting was performed using semi-automated measurement tools in NIS-Elements AR software version 4.20.00 (Laboratory Imaging, s.r.o., Prague, Czech Republic). Central nucleation (expressed as percentage of the total nuclei in each section) was quantified in a blinded manner (S.A. and S.Bal.) in three sections for each muscle ($n = 10$ mice for each experimental group, $n = 400$ to 600 myofibers per single animal) with the Axioplan Imager M2 microscope software AxioVs40 version 4.8.2.0 (Zeiss, Oberkochen, Germany). Paraffin-embedded diaphragms isolated from PBS-treated oATP-Sgca and WT control mice were cut in cross section at the midbelly of the muscle (7 μm thick). After deparaffinization, the slides were stained with hematoxylin and eosin[12] and Picrosirius red staining for collagen fibers.

Immunohistochemistry

Cryosections (5 μm thick) of GN and anterior tibialis muscles isolated from PBS-treated, oATP-Sgca, and WT control mice were fixed in acetone at −20°C for 10 minutes, washed three times in PBS, and then washed twice in 0.025% PBS/Triton. Sections were incubated in 8% bovine serum albumin in PBS (blocking solution) for 1 hour at room temperature. Then, sections were incubated with primary antibodies diluted in 1% bovine serum albumin in PBS solution overnight at 4°C. The next day, sections were washed two times with 0.025% Triton in PBS, incubated 15 minutes in 0.3% H_2O_2 in PBS, and subsequently incubated with an Envision secondary antibody for 1 hour. After being rinsed two times with PBS (5 minutes each), the sections were stained with a diaminobenzidine substrate solution (freshly made just before use), counterstained with hematoxylin, washed with deionized water, dehydrated through five changes of alcohol (70%, 90%, 95%, 100%, and 100%) for 1 minute each, cleared in two changes of xylene (3 minutes each), and mounted with a Vectashield mounting medium (Vector Laboratories, Burlingame, CA). Slides were observed under a Leica Diaplan microscope (Leica, Wetzlar, Germany). The number of positive cells was blindly counted (S.Bar. and S.A.) on the whole sections per mouse. The total area of the section was measured and expressed in arbitrary units.

For immunofluorescence, unfixed cryosections (5 μm thick) of GN and anterior tibialis muscles were incubated in common antibody diluent (BioGenex, San Ramon, CA) for

Table 1 List of Primers Used in This Study

Name	Accession number	Primer sequence
mPTPRC-F	NM_001111316.2	5′-ATCTATCCCGCCCAGAATGG-3′
mPTPRC-R	NM_001111316.2	5′-TGCTGTCTTCCTGGGCTTTA-3′
mADGRE-1-F	NM_010130.4	5′-CCCCAGTGTCCTTACAGAGTG-3′
mADGRE-1-R	NM_010130.4	5′-GTGCCCAGAGTGGATGTCT-3′
mEGR2-F	NM_010118	5′-GGACCCAGGTCTCATTCCTA-3′
mEGR2-R	NM_010118	5′-GAGTCCAGAGGACAGGGAAA-3′
mCD3e-F	NM_007648.4	5′-AAGCCTGTGACCCGAGGAAC-3′
mCD3e-R	NM_007648.4	5′-CTGGGTTGGGAACAGGTGGT-3′
mCD4-F	NM_013488.2	5′-GACAGTGTTCCTGGCTTGCG-3′
mCD4-R	NM_013488.2	5′-GCACCTGACACAGCAGAGGA-3′
mCD8a-F	NM_001081110.2	5′-ATGGCTTCATCCCACAACAAG-3′
mCD8a-R	NM_001081110.2	5′-CGTGTCCCTCATGGCAGAA-3′
mFOXP3-F	NM_001199347	5′-CAGTCAAAGAGCCCTCACAA-3′
mFOXP3-R	NM_001199347	5′-AAGGCAGGCTCTTCATGTTT-3′
mAREG-F	NM_009704	5′-AAGGAGGCTTCGACAAGAAA-3′
mAREG-R	NM_009704	5′-TTTACCCTGCATTGTCCTCA-3′
mIL10-F	NM_010548	5′-CCCAGAAATCAAGGAGCATT-3′
mIL10-R	NM_010548	5′-TCACTCTTCACCTGCTCCAC-3′
mMYOG-F	NM_031189	5′- AGTGAATGCAACTCCCACAG-3′
mMYOG-R	NM_031189	5′-CTGTCCACGATGGACGTAAG-3′
mSPP1-F	NM_001204201	5′-TGACGATGATGATGACGATG-3′
mSPP1-R	NM_001204201	5′-GGGACGATTGGAGTGAAAGT-3′
mIFNγ-F	NM_008337	5′-TCCTTTGGACCCTCTGACTT-3′
mIFNγ-R	NM_008337	5′-GTAACAGCCAGAAACAGCCA-3′
mIL6-F	NM_001314054	5′-CTGGAGCCCACCAAGAACGA-3′
mIL6-R	NM_001314054	5′-TGTGAAGTCTCCTCTCCGGACT-3′
mCTGF-F	NM_010217	5′-GAGTGTGCACTGCCAAAGAT-3′
mCTGF-R	NM_010217	5′-GGCAAGTGCATTGGTATTTG-3′
mTGFβ1-F	NM_011577	5′-CCCTATATTTGGAGCCTGGA-3′
mTGFβ1-R	NM_011577	5′-CTTGCGACCCACGTAGTAGA-3′
mGAPDH-F	NM_008084	5′-AACTTTGGCATTGTGGAAGG-3′
mGAPDH-R	NM_008084	5′-CCATCCACAGTCTTCTGGGT-3′
mPPIA-F	NM_008907	5′-TCCTGGCATCTTGTCCATGG-3′
mPPIA-R	NM_008907	5′-TTCAGTCTTGGCAGTGCAGA-3′
mRPL13a-F	NM_009438	5′-TCCGATAGTGCATCTTGGCC-3′
mRPL13a-R	NM_009438	5′-AAGTACCAGGCAGTGACAGC-3′

Accession numbers from *https://www.ncbi.nlm.nih.gov/pubmed/Nucleotide*.
F, forward; R, reverse.

10 minutes and after with primary antibodies (CD45, P2X4, and P2X7 antibodies) overnight at 4°C. After three washes with PBS, sections were incubated with fluorescent secondary antibodies in common antibody diluent for 1 hour at room temperature in the dark. After being washed three times with PBS, sections were mounted with Vectashield mounting medium with DAPI (Vector Laboratories). Images were obtained using a Leica SPE confocal microscope equipped with argon/He-Ne laser sources and an HCX PL APO CS 63.0 × 1.40 oil objective. During image acquisition, the 488 and 594 lasers were set at 20% energy, and the emission range was between 500 and 550 and between 650 and 700 nm for P2X 488 and CD45 594, respectively. The photomultiplier voltage gain was set to eliminate cell autofluorescence. Single-plane images were taken at the center of cell thickness.

Table 2 List of Primer/Probe Sets Used in This Study

Probe	Catalog number
mP2RX1	Mm00435460_m1
mP2RX2	Mm01202368_g1
mP2RX3	Mm00523699_m1
mP2RX4	Mm00501787_m1
mP2RX5	Mm00473677_m1
mP2RX6	Mm00440591_m1
mP2RX7	Mm00440578_m1
mIL1β	Mm00434228_m1
mGAPDH	4352932E
mACTA1	Mm00808218_g1

Real-Time Quantitative PCR

Total RNA was extracted from GN muscles (from 20 to 55 mg) isolated from PBS-treated mice, oATP-Sgca mice, and WT controls, according to the manufacturer's protocol

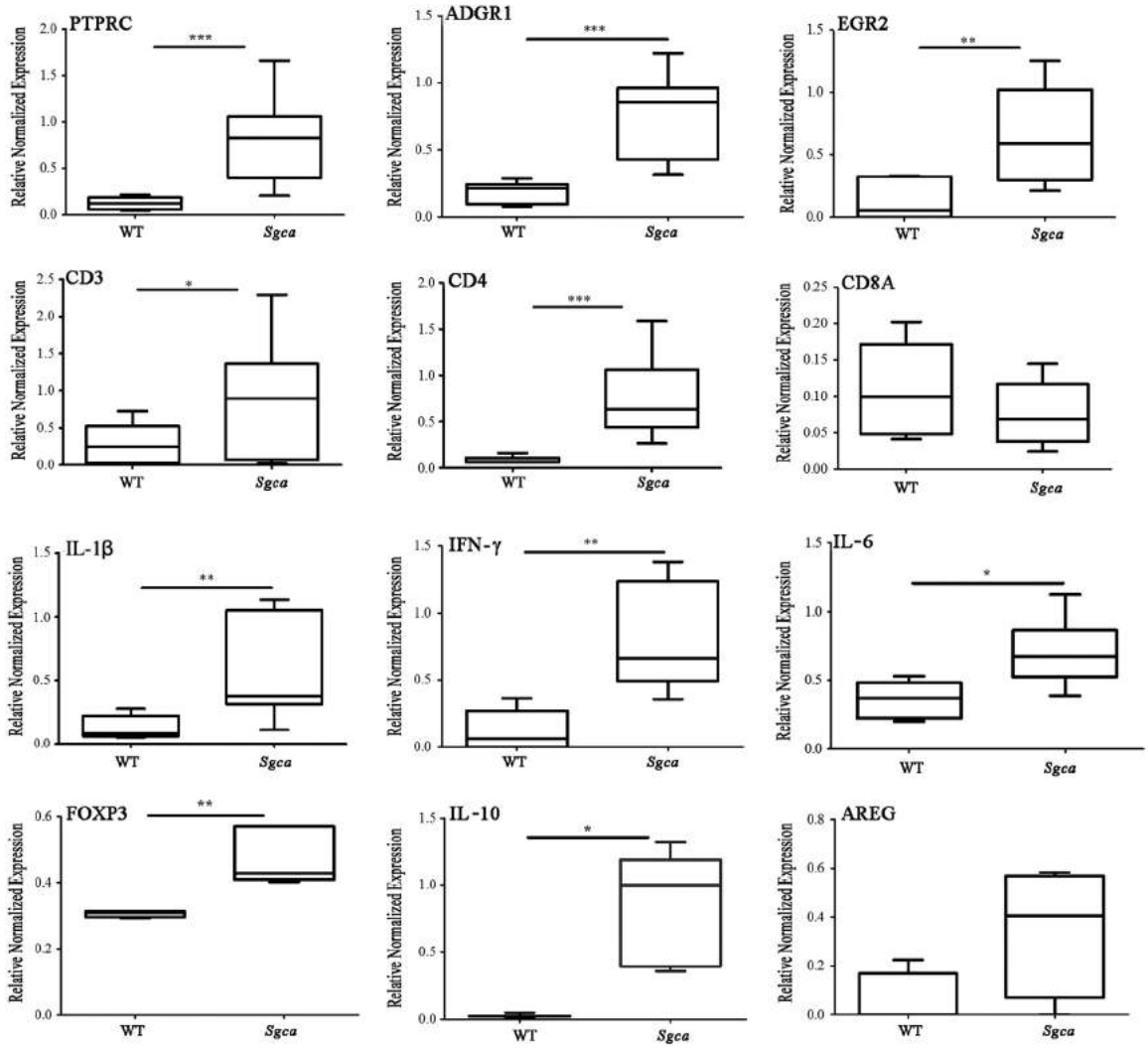

Figure 1 Inflammatory response and T-regulatory cell (Treg) activation in Sgca mice. Total RNA isolated from the gastrocnemii of 10 Sgca and 7 age- and sex-matched WT mice was reverse transcribed. The pattern of expression of molecular markers of innate [receptor-type tyrosine-protein phosphatase C (PTPRC), adhesion G-protein–coupled receptor E1 (ADGRE1), and early growth response protein 2 (EGR2)] and adaptive [CD3, CD4, and T-cell surface glycoprotein CD8 α chain (CD8A)] immunity, of Treg activation [forkhead box protein P3 (FOXP3), amphiregulin (AREG), and IL-10)], and of proinflammatory cytokines [interferon (IFN)-γ, IL-1β, and IL-6] was determined by real-time quantitative PCR. PPIA and RPL13A transcript levels were used as housekeeping genes. Data are expressed as medians ± first and third quartiles. PTPRC: WT = 0.11 (0.05 to 0.18), Sgca = 0.82 (0.39 to 1.05). ADGRE1: WT = 0.21 (0.09 to 0.24), Sgca = 0.85 (0.43 to 0.96). EGR2: WT = 0.05 (0.01 to 0.32), Sgca = 0.59 (0.29 to 1.02). CD3: WT = 0.25 (0.02 to 0.52), Sgca = 0.89 (0.06 to 1.36). CD4: WT = 0.06 (0.06 to 0.11), Sgca = 0.63 (0.44 to 1.05). CD8A: WT = 0.09 (0.04 to 0.17), Sgca = 0.06 (0.04 to 0.11). FOXP3: WT = 0.31 (0.30 to 0.31), Sgca = 0.43 (0.41 to 0.57). AREG: WT = 0.001 (0.001 to 0.17), Sgca = 0.40 (0.07 to 0.57). IL-10: WT = 0.02 (0.01 to 0.05), Sgca = 1.00 (0.39 to 1.18). IL-1β: WT = 0.02 (0.062 to 0.21), Sgca = 0.38 (0.31 to 1.05). IL-6: WT = 0.37 (0.22 to 0.489), Sgca = 0.67 (0.52 to 0.86). IFN-γ: WT = 0.06 (0.0 to 0.27), Sgca = 0.66 (0.49 to 1.24). Statistical analysis was performed using the *U*-test. $*P < 0.05$, $**P < 0.01$, and $***P < 0.001$.

(DNase treatment). Quality and quantity of RNA were analyzed using a NanoDrop spectrophotometer (NanoDrop Technologes, Inc., Wilmington, DE).

The cDNA was synthesized from 350 ng of total RNA with the iScript cDNA Synthesis Kit (Bio-Rad Laboratories, Hercules, CA). Each RNA sample was controlled for genomic DNA contamination without reverse transcriptase addition into a cDNA synthesis mixture. For receptor-type tyrosine-protein phosphatase C (CD45), adhesion G-protein–coupled receptor E1 (F4/80), early growth response protein 2, CD3 ε chain, CD4, CD8 α chain, interferon-γ (IFN-γ), IL-6, FOXP3, IL-10, amphiregulin, myogenin, osteopontin (secreted phosphorylated protein 1), connective tissue growth factor, and TGF-β1 transcript quantification, real-time quantitative PCR (qPCR) was performed in triplicate with the 2× Sso Fast EvaGreen Supermix in the CFX96 Real-Time PCR Detection System (Bio-Rad Laboratories). Specific primers for the mouse genes were designed through Beacon Designer software version 2.0 (Premier Biosoft International, Palo Alto, CA) and are listed in Table 1.

Briefly, the 15-μL PCR mixture contained diluted cDNA that corresponded to 8.75 ng of total RNA and 0.2 mmol/L of each primer. Relative expression levels were normalized using the comparative Ct (ΔΔCt) method with two

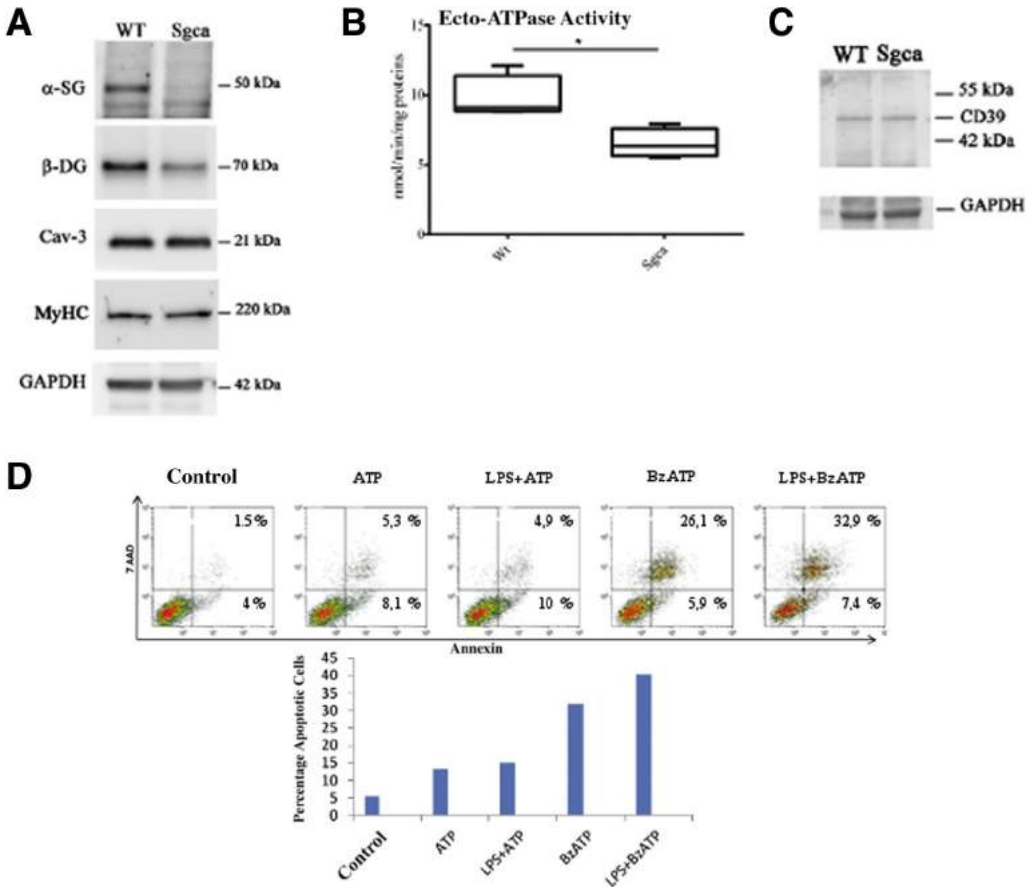

Figure 2 Sgca myoblasts display a decreased ecto-ATPase activity and undergo apoptosis on treatment with ATP or benzoyl ATP (BzATP). **A:** Total protein lysates, isolated from primary myotubes from Sgca and WT age-matched controls, were subjected to Western blot analysis. Membranes were probed with a mouse monoclonal anti—α-SG, β-dystroglycan (β-DG), anti—caveolin-3 (Cav-3), and myosin heavy chain (MyHC) antibody. Glyceraldehyde-3-phosphate dehydrogenase (GAPDH) was used as a loading control. Samples were run in triplicate. Representative images are shown. **B:** Primary myotubes isolated from Sgca and WT mice were cultured in basal medium containing ATP at 0.3 mmol/L. At subsequent times (0, 5, and 15 minutes), 100-μL aliquots of the incubations were withdrawn and ATP degradation was determined by the phosphate high-performance liquid chromatography analysis. **C:** Total protein lysates, isolated from primary myotubes from Sgca and WT age-matched controls, were subjected to Western blot analysis. Membranes were probed with a mouse monoclonal anti-CD39 antibody. GAPDH was used as a loading control. Samples were run in triplicate. Representative images are shown. **D:** Primary myotubes isolated from Sgca mice were pretreated with 1 μg/mL lipopolysaccharide (LPS) for 4 hours and then incubated with 3 mmol/L ATP and 300 μmol/L BzATP for 16 hours. The cells were stained with the Annexin A5 FITC/7-AAD Kit, and apoptosis was evaluated by flow cytometry. Data are expressed as medians ± first and third quartiles (**B**); statistical analysis was performed using the *U*-test. Data are expressed as percentage of apoptotic cells ($Annexin^{+}7\text{-}AAD^{-} + Annexin^{+}7\text{-}AAD^{+}$; **D**). One representative experiment of three performed is shown. $n = 4$ wells per genotype (**B**). $^{*}P < 0.05$.

housekeeping genes (peptidylprolyl isomerase A and ribosomal protein L 13a) by the Bio-Rad CFX Maestro software 1.0 version 4.0.2325.0418. For each specific primer set, the efficiency was >95% and a single product was seen on the melting curve analysis.

For mouse P2X receptors and IL-1β quantification, qPCR was performed in triplicate with the 2× Sso Fast Probes Supermix (Bio-Rad Laboratories) in a CFX96 Real-Time PCR Detection System. The 15-μL PCR mixture contained diluted cDNA that corresponded to 12.5 ng of total RNA, and premixed primer/probe sets were ordered from Applied Biosystems (Foster City, CA) (Table 2). Relative expression levels were normalized using the comparative Ct (ΔΔCt) method with the housekeeping gene *Gapdh* and actin-α 1 (*Acta1*, a muscle specific gene, NM_001272041.1), by the Bio-Rad CFX Maestro software.

Western Blot Analysis

Total protein lysates were isolated from PBS-treated mice, oATP-Sgca mice, and WT GN muscles, as previously described.[8] Equal amounts of protein (40 to 120 μg) were resolved in 8% to 15% SDS-PAGE gel and transferred onto polyvinylidene difluoride membranes (Immobilon PVDF, Billerica, MA). Membranes were blocked with 5% bovine serum albumin in PBS/0.1% Tween 20. Blots were then incubated overnight at 4°C with primary antibodies. Horseradish peroxidase anti-IgG was used to visualize bound primary antibodies with the chemiluminescence system (Bio-Rad Laboratories). Band intensities were evaluated by densitometry using the Alliance Mini HD9 AutoAutomatic system (Uvitec, Cambridge, UK).

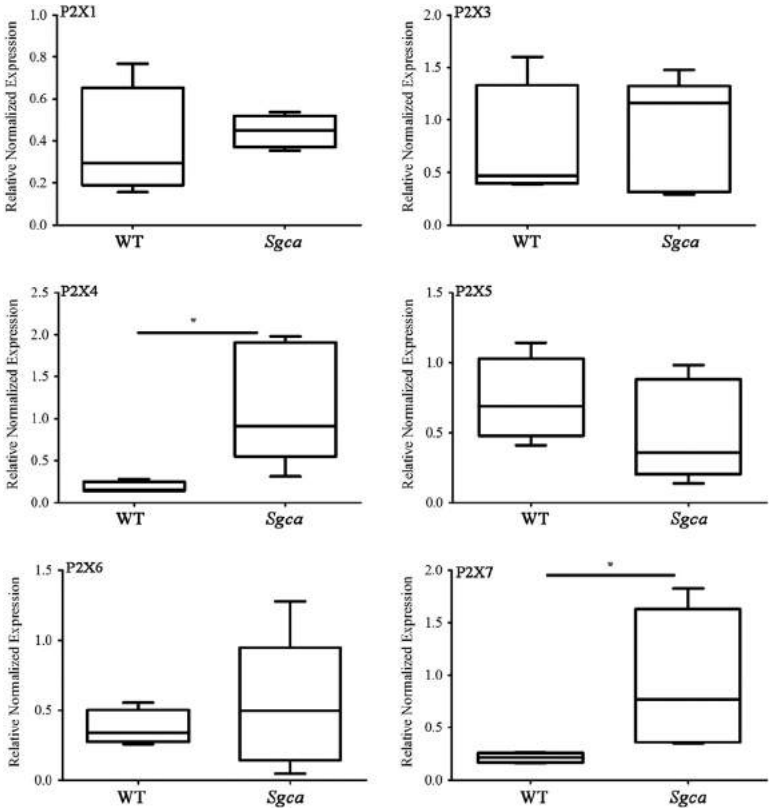

Figure 3 P2X4 and P2X7 purinergic receptors are significantly up-regulated in Sgca muscle tissue. Total RNA isolated from the gastrocnemii of 10 Sgca and 7 age- and sex-matched WT mice was reverse transcribed. The pattern of expression of P2X receptors (Rs) was determined by real-time quantitative PCR. P2X2R transcript levels were not measurable. P2X4R and P2X7R transcripts are significantly up-regulated in α-SG–deficient mice. *Gapdh* and *Acta1* were used as housekeeping genes. Data are expressed as medians ± first and third quartiles. P2X4: WT = 0.147 (0.140 to 0.249), Sgca = 0.907 (0.549 to 1.905). P2X7: WT = 0.217 (0.167 to 0.258), Sgca = 0.767 (0.362 to 1.630). Statistical analysis was performed using the *U*-test. $^*P < 0.05$.

Ecto-ATPase Activity

Satellite cells were seeded in 24-well plates (5.5×10^4 cells/well) and cultured until they completely differentiated into mature myotubes. After removal of the culture medium, cells were washed once with 1 mL Hanks' balanced salt solution, and 0.35 mL Hanks' balanced salt solution containing 0.3 mmol/L ATP was added. At various times (0, 5, and 15 minutes), 100-λ aliquots of the incubations were withdrawn and incubations were stopped by filtration with a multiscreen vacuum manifold using Immobilon-P membrane plates (Millipore, Bedford, MA). ATP degradation was determined by the phosphate high-performance liquid chromatography analysis, as previously described.[13] Cells were lysed, and protein content in each well was determined by Bradford assay.

Apoptosis

Satellite cells were seeded in 24-well plates (6×10^4 cells/well) and cultured until they completely differentiated into mature myotubes. The cells were pretreated with LPS (1 μg/mL) for 4 hours and then incubated with 3 mmol/L ATP and 300 μmol/L BzATP for 16 hours. Then, myotubes were analyzed by flow cytometry, according to other studies that have adopted the same technique.[14–16] Specifically, the cells were stained with the Annexin A5 FITC/7-AAD Kit, and apoptosis was evaluated by flow cytometry, according to the manufacturer's instructions. Sample analysis was performed using a Gallios cytometer (Beckman-Coulter) and Kaluza software version 1.1 (Beckman-Coulter).

Statistical Analysis

Most of the analyzed variables were not normally distributed, as confirmed by the Shapiro-Wilk test, and therefore differences of quantitative parameters between two groups of mice were analyzed by the *U*-Mann Whitney test for nonparametric data. $P < 0.05$ was considered statistically significant. Data are expressed as medians ± first and third quartiles, as described in *Results* and figure legends. Statistica software version 9.1 (StatSoft Co, Tulsa, OK) was used for all of the statistical analyses. Graphs were generated with Graph Pad Prism software version 6.0 (Graph Pad Software, San Diego, CA).

Results

Sgca Skeletal Muscle Displays an Increased Expression of Markers of Innate and Adaptive Immunity

To quantify the inflammatory response in muscles isolated from Sgca mice, the transcript levels of different immune cell markers and of distinct cytokines were analyzed, compared with muscles isolated from age-matched WT mice. α-SG–deficient muscle overexpressed leukocytes as well as macrophage surface proteins. Receptor-type tyrosine-protein phosphatase C (CD45), adhesion G-protein–coupled receptor E1 (F4/80), and early growth response protein 2

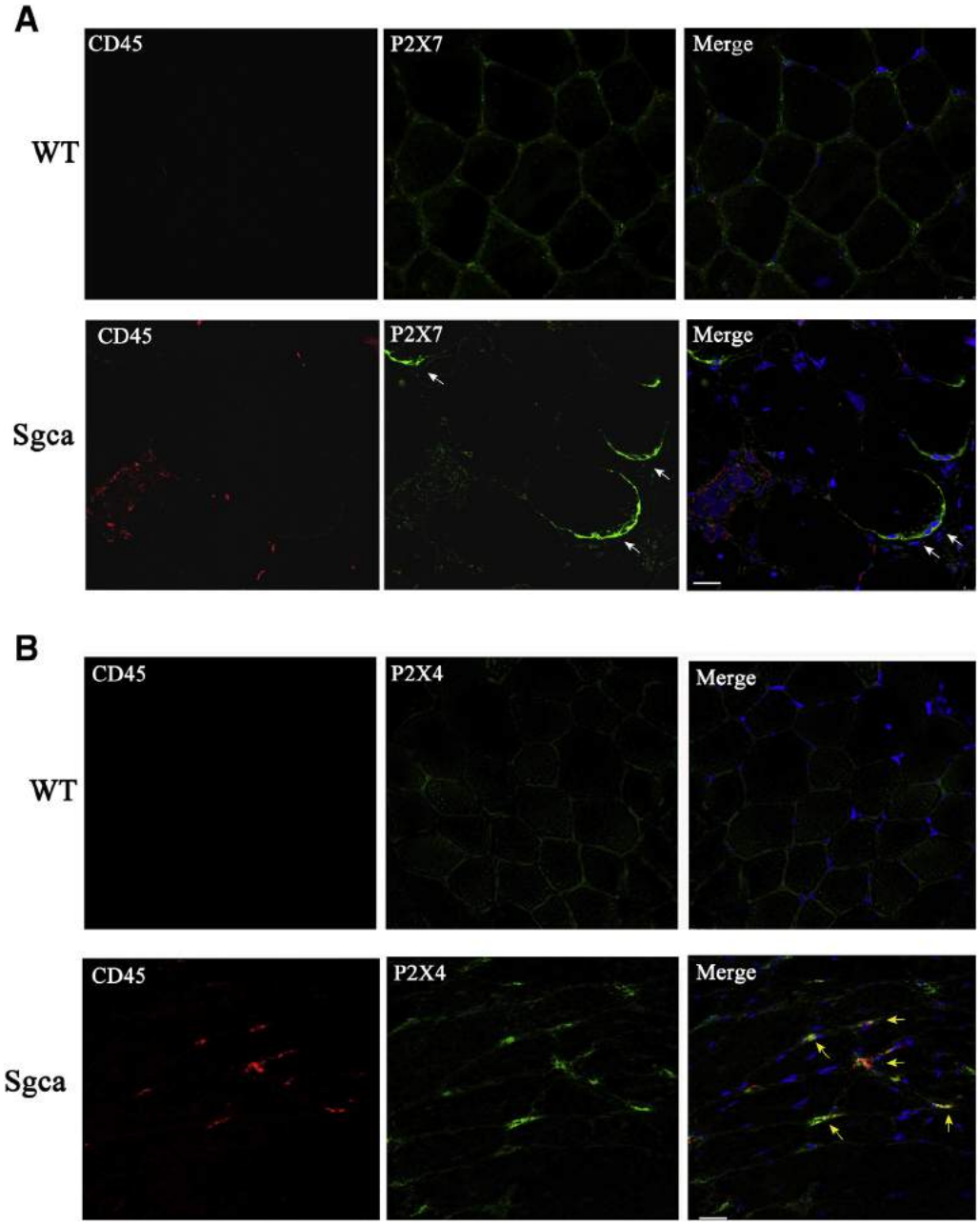

Figure 4 P2X7R is overexpressed in Sgca muscle cells, whereas P2X4R is mainly expressed in $CD45^+$ cells. **A:** Frozen muscle tissue sections of gastrocnemii (GN) from Sgca and WT mice were immunostained with a monoclonal anti-CD45 antibody (red) and a monoclonal P2X7R antibody (red). Representative images are shown. **White arrows** indicate examples of the positive cells for P2X7R. **B:** Frozen muscle tissue sections of GN from Sgca and WT mice were immunostained with a monoclonal anti-CD45 antibody (red) and a monoclonal P2X4R antibody (red). Representative images are shown. **Yellow arrows** indicate examples of the positive cells for P2X4R and CD45. $n = 4$ (**A** and **B**, Sgca and WT mice). Scale bar = 25 μm (**A** and **B**). Original magnification, ×40 (**A** and **B**).

were up-regulated by 7.5-, 4.1-, and 10-fold, respectively.[17] CD3 transcripts were increased by 3-fold, with a 10 fold-increase of the proportion of CD4-expressing lymphocytes, and a 30% reduction in *CD8A* mRNA levels. Moreover, CD4 induction was associated with a 1.8-fold up-regulation of FOXP3, a marker of $CD4^+$ T-regulatory (Treg) cells.

The recruitment of immune cells in the muscle of Sgca mice was confirmed by a 4.7-, 1.8-, and 11-fold induction of the proinflammatory cytokines IL-1β, IFN-γ, and IL-6, respectively, but also by a 50- and 3-fold induction of the Treg-specific anti-inflammatory cytokine IL-10 and of the Treg-secreted growth factor amphiregulin, respectively (Figure 1).

Sgca Primary Myotubes Are Characterized by a Defect in Ecto-ATPase Activity and Undergo Apoptosis on ATP Treatment

Primary satellite cells were isolated from the forelimb, hind limb, and diaphragm muscles of passage 8 to passage 10 old Sgca and WT mice and cultured until they completely

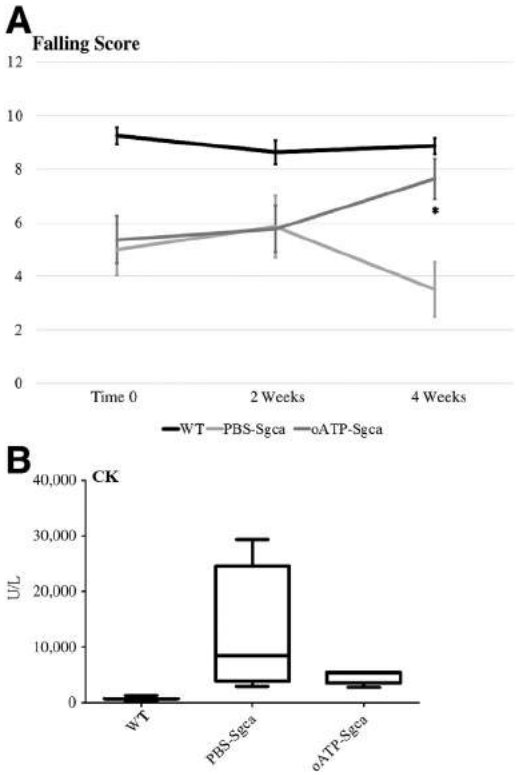

Figure 5 oATP improves muscle strength and ameliorates creatine kinase (CK) serum levels in Sgca mice. **A:** Four-limb hanging test was performed on PBS-Sgca (**light gray line**), oATP-Sgca (**dark gray line**), and age-matched WT controls (**black line**) at the beginning and at the end of the second and fourth week of treatment. **B:** Serum CK levels were evaluated at the end of the fourth week of treatment. Blood samples were obtained via cardiac puncture from PBS-Sgca, oATP-Sgca, and WT mice. Data are expressed as medians ± first and third quartiles. WT = 675 (130 to 1220), PBS-Sgca = 8460 (3835 to 24,635), oATP-Sgca = 5360 (3500 to 5440). Statistical analysis was performed using the *U*-test. Data are expressed as means ± SD (**A**). $n = 12$ animals (**A**); $n = 10$ animals for each experimental group (**B**). $^*P < 0.05$ for oATP-treated mice versus PBS-treated mice.

differentiated into mature myotubes. The absence of expression of α-SG was confirmed by Western blot analysis on total cellular extracts. Sgca-deficient cells displayed normal levels of caveolin-3 and myosin heavy chain, thus indicating the achievement of a functional muscle cell phenotype. The decrease observed in β-dystroglycan levels is in accordance with the disruption of the dystrophin-glycoprotein complex in α-sarcoglycanopathies (Figure 2A).

The ecto-ATPase activity was quantified by measuring ATP metabolism in mass spectrometry, in WT and Sgca cells switched to a basal medium containing ATP at 0.3 mmol/L. When compared with the WT, Sgca cells were characterized by decreased ecto-ATPase activity (Figure 2B), resulting in increased ATP levels in culture medium. Muscle cells express the ecto-ATPase CD39, which converts ATP to ADP. However, the increase in ATP levels observed in the Sgca group appeared to be specifically related to the absence of the α-SG ecto-ATPase activity because the protein levels of CD39 were not modified between Sgca and WT muscle lysates (Figure 2C).

For the evaluation of apoptosis, the cells were pretreated with 1 μg/mL LPS for 4 hours, incubated with 3 mmol/L ATP and 300 μmol/L BzATP for 16 hours, and then stained with the Annexin A5 FITC/7-AAD Kit. The feasibility of a citofluorimetric assay in myotubes has been previously determined.[14–16] The number of apoptotic muscle cells was determined measuring the percentage of Annexin V^+/7-AAD^- and Annexin V^+/7-AAD^+ cells (early and late apoptosis, respectively). The pretreatment with LPS is supported by the observation that LPS caused a marked up-regulation of striatal P2X7 expression.[18] ATP and, more potently, BzATP induced apoptosis, an effect that was further enhanced by a pretreatment with LPS (Figure 2D).

P2XR Is Expressed in Sgca Muscle Tissue

The pattern of expression of the P2XR was evaluated in muscle lysates from the GN of Sgca mice and age-matched WT controls. A specific up-regulation of P2X4R and P2X7R transcripts (sixfold and fourfold, respectively) was observed (Figure 3), whereas P2X2R transcript levels were not measurable (Figure 3). To determine whether P2X4R and P2XR7 were expressed in myofibers or in infiltrating inflammatory cells, a coimmunostaining was completed with the pan-granulocyte marker C45 and P2X4 and P2X7R antibodies, respectively, in GN sections.

P2X4R was hardly detectable on the muscle cell membrane in WT mice, and it was up-regulated and colocalized with CD45-positive cells in the Sgca mutants (Figure 4A). P2X7R expression was weak in WT myofibers, whereas clear and specific P2X7R patches at the plasma membrane level were detected in Sgca muscle fibers, suggesting an induction and a higher functionality of the receptor because of its cell surface localization. This same feature has been previously shown in the monocytic subset of myeloid-derived suppressor cells isolated from tumor-bearing mice[19] (Figure 4B).

Targeting P2X Signaling *in Vivo* Improves Biochemical and Functional Parameters of Disease Progression in Sgca Mice

Given the representation of different P2XR in Sgca muscles, we aimed at initially achieving a pleiotropic antagonistic effect on eATP signaling cascade. Four-week–old Sgca mice were treated with oATP, a compound known to act on multiple P2X receptor molecules. oATP was administered via i.p. injections, at the dose of 6 mmol/L. Sgca mice injected with vehicle alone (PBS) and a group of age- and sex-matched WT C57Bl/6 mice served as controls. Mice were weighted at the beginning (baseline) of the treatment and then on a weekly basis. No significant difference was detected between the various groups (data not shown). The evaluation of muscle strength was completed by the four-limb hanging test at the beginning of the treatment (time 0) and at the end of the second and fourth weeks of treatment.

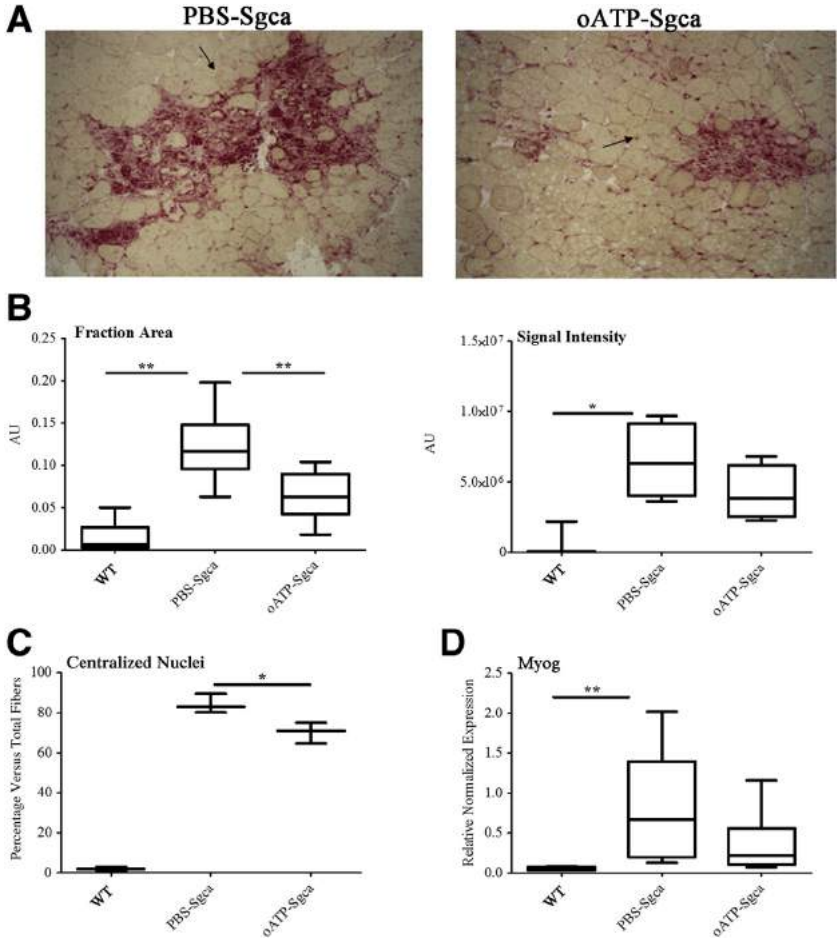

Figure 6 oATP improves the extension of reactive inflammatory infiltrates and morphologic features in Sgca mice. **A:** Frozen muscle tissue sections of gastrocnemii (GN) from PBS-Sgca and oATP-Sgca mice were collected at the fourth week of treatment and stained with acid phosphatase. **Black arrows** indicate inflammatory infiltrates. Representative images are shown. **B:** Graph of the analysis of the fraction areas and intensities of inflammatory infiltrates/total section area of muscles represented in **A**. Data are expressed as medians ± first and third quartiles. Area: WT = 0.006 (0.002 to 0.0267), PBS-Sgca = 0.117 (0.09 to 0.14), oATP-Sgca = 0.063 (0.04 to 0.09). Signal intensity: WT = 71,886 (12,400 to 217,000), PBS-Sgca = 6.30×10^6 (4.01×10^6 to 9.12×10^6), oATP-Sgca = 3.85×10^6 (2.53×10^6 to 6.13×10^6). Statistical analysis was performed using the *U*-test. **C:** The number of central nuclei was quantified in 600 fibers of three consecutive fields for each muscle section stained with hematoxylin and eosin. Data are expressed as medians ± first and third quartiles. WT = 2.00 (1.00 to 3.00), PBS-Sgca = 82.91 (80.18 to 89.34), oATP-Sgca = 70.89 (64.76 to 75.01). Statistical analysis was performed using the *U*-test. **D:** Total RNA isolated from GN lysates from PBS-Sgca, oATP-Sgca, and WT age-matched controls was reverse transcribed. Myogenin transcripts (Myog) were quantified by real-time quantitative PCR. *Ppia* and *Rpl13a* served as housekeeping genes. Data are expressed as medians ± first and third quartiles. WT = 0.054 (0.037 to 0.076), PBS-Sgca = 0.669 (0.19-1.39), oATP-Sgca = 0.217 (0.10 to 0.55). Statistical analysis was performed using the *U*-test. $n = 10$ (**A**, PBS-Sgca and oATP-Sgca mice, **C**, mice for each experimental group, and **D**, PBS-Sgca, oATP-Sgca, and WT mice). $^*P < 0.05$, $^{**}P < 0.01$. Original magnification, ×10 (**A**). AU, arbitrary unit.

As expected from the literature, the untreated Sgca group displayed a progressive worsening of muscle strength along time, whereas the oATP-Sgca cohort maintained the scores measured at time 0 ($P < 0.05$ for oATP-treated mice versus PBS-treated mice after 4 weeks) (Figure 5A).

Serum creatine kinase concentrations, a marker of muscle cell degeneration, were evaluated at the end of the trial by cardiac puncture. Creatine kinase was markedly increased in PBS-Sgca mice when compared with the WT cohort, whereas the treatment with the P2X antagonist led to a 35% decrease of this effect (Figure 5B).

Inhibition of P2X Signaling Ameliorates Morphologic Features and Reduces the Amplitude of the Innate and Adaptive Immune Responses in Sgca Mice

The fraction area and the intensity of the inflammatory reactions surrounding degenerative/necrotic muscle cells were evaluated in GN from PBS- and oATP-treated animals by acid phosphatase staining, which provides a red positive signal in activated macrophages and degenerative myofibers. These parameters were decreased in the oATP-treated group by 46% and 38%, respectively ($P < 0.01$ and $P < 0.05$, respectively) (Figure 6, A and B).

Muscle morphology was quantified in GN by standard hematoxylin and eosin staining. Central nucleation (percentage), a sign of dystrophic myopathic damage, was reduced by 14% in GN of oATP-treated animals (Figure 6C). Moreover, muscle tissue from untreated Sgca mutants, when compared with WT mice, displayed an increase of myogenin transcripts, a muscle-specific transcription factor expressed by committed myoblasts in regeneration and typically up-regulated in the degenerative/regenerative cell cycles of active muscular dystrophies. This effect was blunted by 67% after oATP treatment, thus suggesting an inhibition of degenerative cellular events (Figure 6D).

In diaphragms, P2X antagonism resulted in a 71% and 11% decrease in the areas and number of the inflammatory reactions surrounding the muscle cells in necrosis, respectively (hematoxylin and eosin staining). The beneficial effect of purinergic antagonism was associated also with a 16% reduction of centralized nuclei ($P<0.05$) (Supplemental Figure S1).

Immunostaining and measurement of the $CD45^+$ and $Ly6C^+$ leukocytes infiltrating the muscle tissue revealed a positive signal for both markers in different sites of the inflammatory responses surrounding necrotic fibers. When quantified by automated microscopy on the total section area, the number of $CD45^+$ and $Ly6C^+$ cells in the total

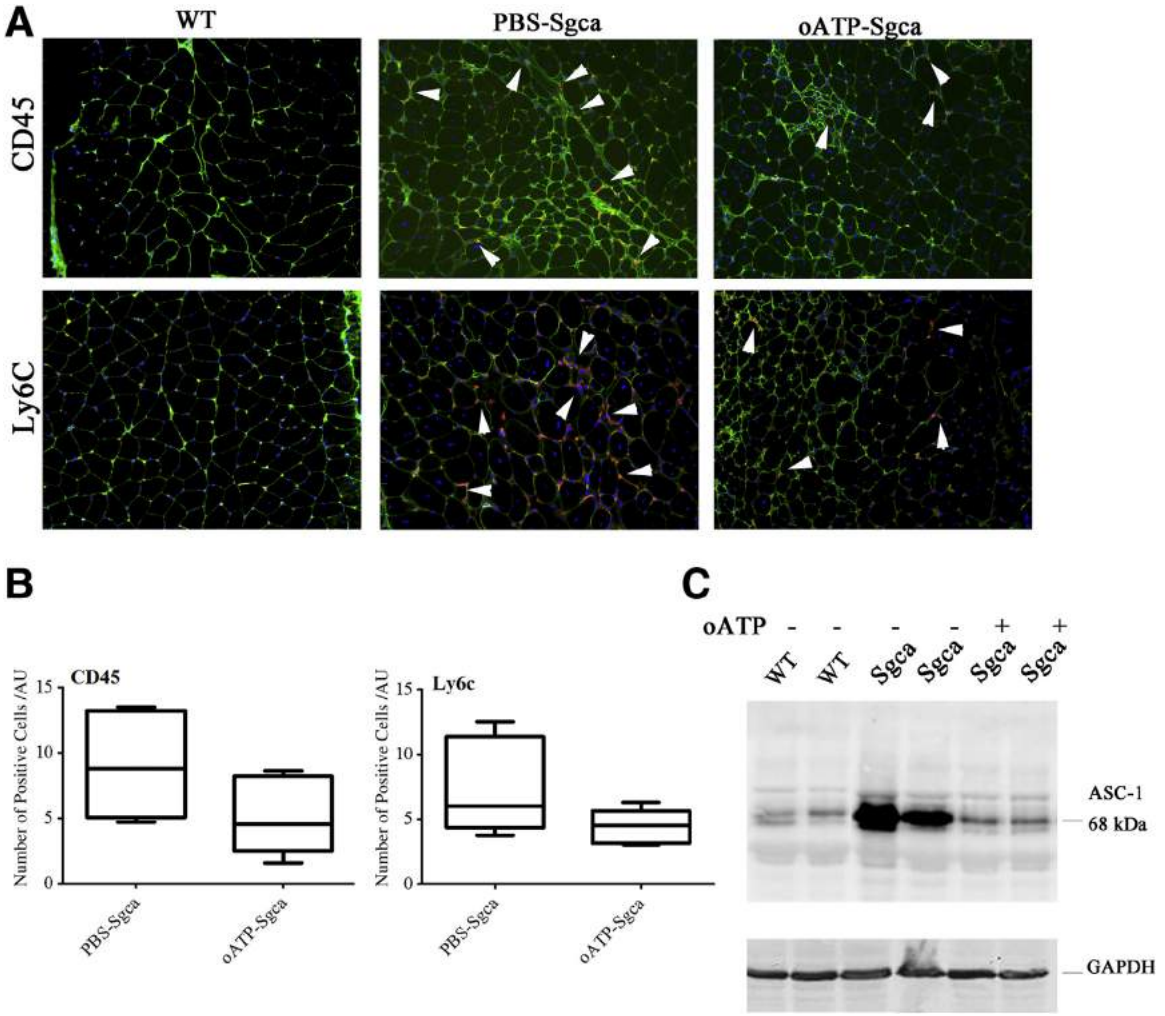

Figure 7 oATP induces a decrease of inflammatory cytokines and monocyte infiltration in muscles from Sgca mice. **A:** Frozen muscle tissue sections of gastrocnemii (GN) from PBS-Sgca and oATP-Sgca mice were collected at the fourth week of treatment and immunostained with a monoclonal anti-CD45 antibody (red), monoclonal anti-Ly6C antibody (red), and monoclonal anti—caveolin-3 antibody (green). Representative images are shown. **White arrowheads** indicate examples of the positive cells for CD45 and Ly6C markers. **B:** Graph of the number of $CD45^+$, $Ly6C^+$ cells/arbitrary unit (AU) of total section area of muscles represented in **A**. Data are expressed as medians ± first and third quartiles. CD45: PBS-Sgca = 8.80 (5.06 to 13.22), oATP-Sgca = 4.54 (2.51 to 8.18). Ly6C: PBS-Sgca = 6.02 (4.35 to 11.36), oATP-Sgca = 4.51 (3.14 to 5.64). Statistical analysis was performed using the *U*-test. **C:** Total protein lysates, isolated from GN of oATP-treated Sgca ($oATP^+$), untreated Sgca ($oATP^-$), and WT age-matched controls, were subjected to Western blot analysis. Membranes were probed with a mouse monoclonal anti—activating signal cointegrator—1 (ASC-1) antibody. Samples were run in triplicate. Representative images are shown. $n = 10$ (**A**, PBS-Sgca and oATP-Sgca mice). Original magnification, ×20 (**A**). GAPDH, glyceraldehyde-3-phosphate dehydrogenase.

areas was inhibited by 45% and 25%, respectively, in oATP-treated mice (Figure 7, A and B).

Accordingly, the protein levels of ASC-1, a coactivator of NF-κβ, were undetectable in WT mice, markedly increased in Sgca muscle lysates, and significantly inhibited after P2X blockade (Figure 7C).

The immunostaining and measurement of the CD3 lymphocytes infiltrating the muscle tissue showed a CD3-positive signal in different sites of reactive inflammatory responses. When quantified by automated microscopy on the total section area, the fraction areas of CD3-positive signal were reduced by 52% in oATP-treated mice (data not shown).

Despite the decrease in the total number of CD3-positive cells, $FOXP3^+$ cells were increased in muscle tissue of oATP-treated Sgca mutants by 34% (Figure 8, A and B).

The mechanisms of how oATP affects innate and adaptive response in Sgca skeletal muscle were also investigated by quantification of muscular IL-1β, IL-6, and IFN-γ transcripts. When compared with the PBS cohort, these cytokines were reduced by 49%, 39%, and 44%, respectively, in the oATP group (Figure 8C).

Targeting P2X Signaling *in Vivo* Decreases Muscular Fibrotic Degeneration, Reducing the Transcription of Muscle Profibrotic Factors in Sgca Mice

In accordance with this anti-inflammatory image, P2X blockade led to a reduction of the transcription of fibrogenic factors, which ultimately stimulate endomysial fibrosis and connective replacement of muscle tissue. The transcripts of

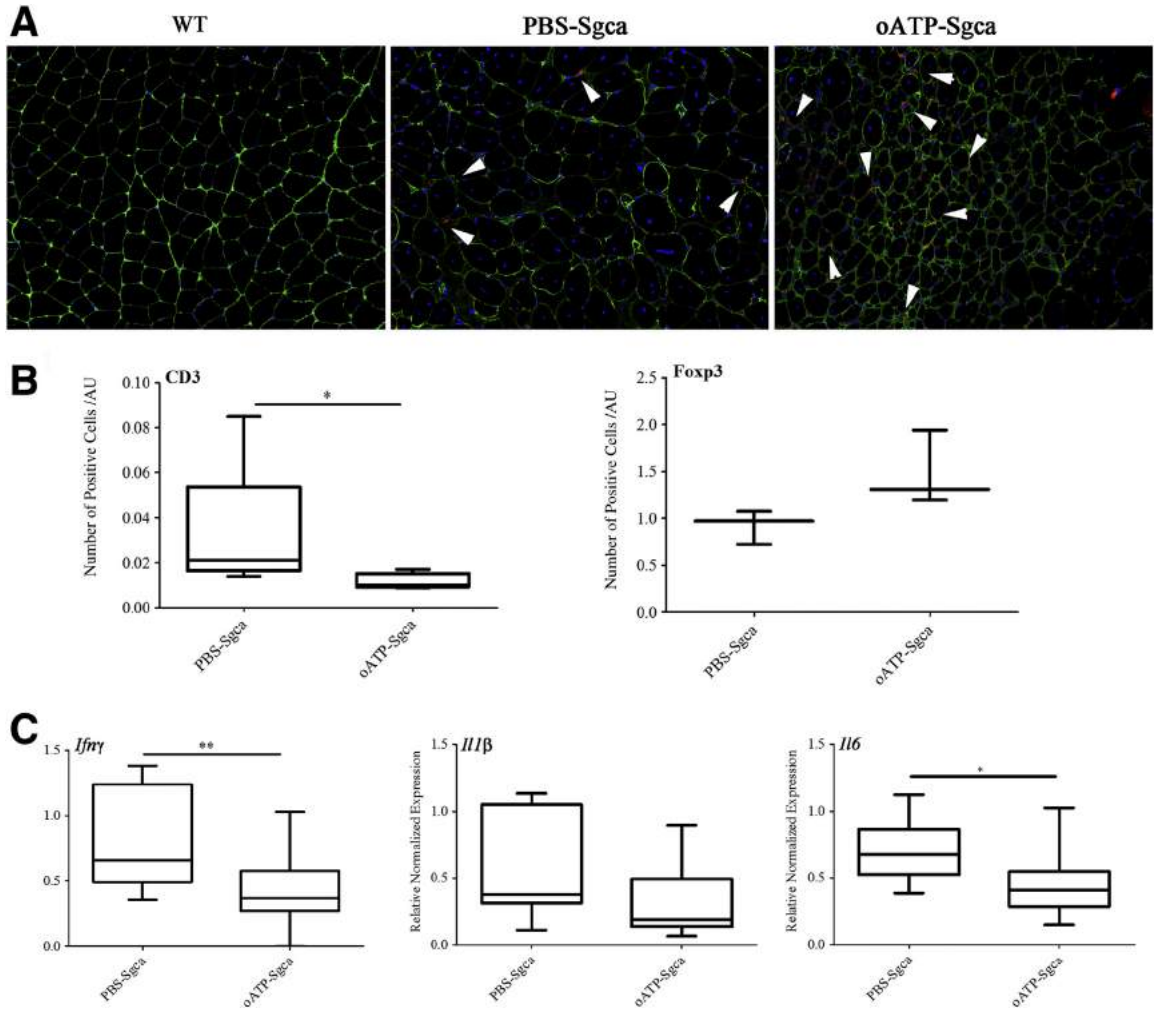

Figure 8 oATP decreases the total number of $CD3^+$ lymphocytes but increases the extension of forkhead box protein P3 (Foxp3)—positive cells in Sgca mice. **A:** Frozen muscle tissue sections of gastrocnemii (GN) from PBS-Sgca and oATP-Sgca mice were collected at the fourth week of treatment and immunostained with a monoclonal anti-FOXP3 antibody. **White arrowheads** indicate $FOXP3^+$ cells. Representative images are shown. **B.** Graph of the number of $CD3^+$ and $FOXP3^+$ cells/arbitrary unit (AU) of total section area of muscles represented in **A**. Data are expressed as medians ± first and third quartilesPBS-Sgca = 0.971 (0.72 to 1.07), oATP-Sgca = 1.308 (1.19 to 1.94). Statistical analysis was performed using the *U*-test. **C:** Total RNA isolated from GN lysates from PBS-Sgca and oATP-Sgca mice was reverse transcribed. IL-1β, IL-6, and interferon (IFN)-γ transcripts were quantified by real-time quantitative PCR. *Ppia* and *Rpl13a* served as housekeeping genes. Data are expressed as medians ± first and third quartilesIL-1β: PBS-Sgca = 0.378 (0.311 to 1.04), oATP-Sgca = 0.190 (0.13 to 0.49). IL-6: PBS-Sgca = 0.674 (0.52 to 0.86); oATP-Sgca = 0.409 (0.28 to 0.54). IFN-γ: PBS-Sgca = 0.660 (0.49 to 1.23), oATP-Sgca = 0.367 (0.27 to 0.57). Statistical analysis was performed using the *U*-test. $n = 10$ (**A** and **C**, PBS-Sgca and oATP-Sgca mice). $^*P < 0.05$, $^{**}P < 0.01$. Original magnification, ×20 (**A**).

osteopontin (secreted phosphorylated protein 1), connective tissue growth factor, and TGF-β1 were quantified in total muscle lysates isolated from the GN of WT, PBS-treated, and oATP-treated Sgca mice and displayed a 79%, 45%, and 77% reduction in the presence of eATP blockade, respectively (Figure 9).

The effects of oATP on collagen type I and on TGF-β were also confirmed at the protein levels. P2X antagonism prevented the up-regulation of collagen type I observed in the untreated cohort, and it led to a reduction of both dimeric (25 kDa) and monomeric (15 kDa) active TGF-β isoforms (Figure 10A).

Accordingly, histologic analyses by Masson trichrome staining on GN sections revealed that oATP treatment led to a 20% decrease of the fraction area (Figure 10, B and C). Staining with Picrosirius red in diaphragms corroborated a 40% and 43% decrease of the fraction area and the intensity of fibrotic tissue in the oATP-treated group, respectively (Supplemental Figure S2).

Discussion

In sarcoglycanopathies, the mechanically weaker plasma membrane is easily damaged during muscle contraction, allowing release of intracellular antigens, infiltration of immune cells, and induction of profibrotic cytokines and growth factors.[3] Although different experimental models

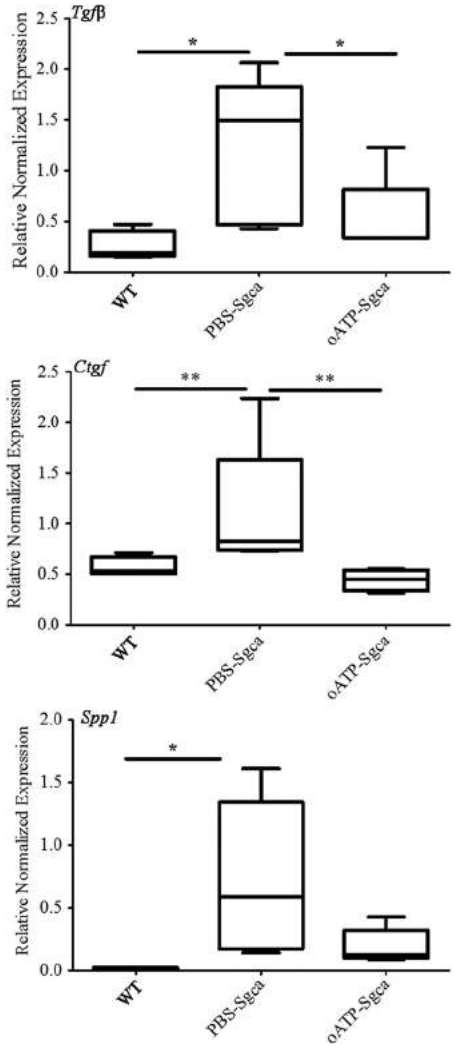

Figure 9 oATP induces a decrease of profibrotic factors in muscles from Sgca mice. Total RNA isolated from gastrocnemii lysates from PBS-Sgca, oATP-Sgca, and WT age-matched controls was reverse transcribed. Secreted phosphorylated protein 1 (SPP1), connective tissue growth factor (CTGF), and transforming growth factor-β (TGF-β) transcripts were quantified by real-time quantitative PCR. *Ppia* and *Rpl13a* served as housekeeping genes. Data are expressed as medians ± first and third quartiles. SPP1: WT = 0.015 (0.01 to 0.02); PBS-Sgca = 0.591 (0.16 to 1.34), oATP-Sgca = 0.123 (0.11 to 0.32). CTGF: WT = 0.532 (0.51 to 0.71), PBS-Sgca = 0.822 (0.74 to 1.62), oATP-Sgca = 0.452 (0.33 to 0.53). TGF-β: WT = 0.187 (0.15 to 0.40), PBS-Sgca = 1.491 (0.36 to 1.82), oATP-Sgca = 0.339 (0.34 to 0.81). Statistical analysis was performed using the *U*-test. $n = 10$ (PBS-Sgca and oATP-Sgca mice); $n = 5$ (WT age-matched controls). $^{*}P < 0.05$, $^{**}P < 0.01$.

have shown how distinct anti-inflammatory approaches may enhance stem cell therapy in mice,[20] the molecular mechanisms that trigger the immune-mediated damage in this disorder have not been described yet. Likewise, limited are the clinical studies and the clinical experience on anti-inflammatory strategies in human sarcoglycanopathies.

Conversely, in Duchenne muscular dystrophy, it has been extensively highlighted that the immune system exerts a dichotomous role because two types of inflammation that promote and repair muscle injury are activated in the muscle tissue.[21–25] Type 1 inflammation is characterized by increased expression of IFN-γ and is counterregulated by type 2 cytokines, such as IL-4 and IL-13, and the Treg anti-inflammatory cytokine IL-10.

Herein, it was found that type 1 and type 2 inflammation are activated also in α-SG deficiency. When compared with WT animals, α-SG–deficient muscle tissue displayed higher expression levels of proinflammatory cytokines, such as IL-1β, IFN-γ, and IL-6, augmented content of the proinflammatory molecule ASC-1, and increased infiltration of CD45 leukocytes, macrophages (innate immunity), and $CD4^+$ lymphocytes (adaptive immunity). This process was counteracted by an increase in the number of $FOXP3^+$ $CD4^+$ Tregs, which also showed an activated phenotype, as confirmed by induced levels of the cytokine IL-10.

The potential role of the DAMP molecule eATP was next studied in the development of this tissue-specific immune-mediated damage, and it was shown, for the first time, that P2X-purinergic signaling is involved in this pathologic cascade.

Sgca mice were characterized by an enhanced expression of P2X4 and P2X7 receptors in muscle tissue, confirming that SG defects, as dystrophinopathies, result into a purinergic pathway overactivation. Although P2X4R was mainly up-regulated in $CD45^+$ inflammatory cells infiltrating the muscle, P2X7R was overexpressed on the plasma membrane of Sgca muscle fibers. Noteworthy, in dystrophic cells, the receptor molecules were found to be organized in specific patches, suggesting in the monocytic subset of myeloid-derived suppressor cells isolated from tumor-bearing mice.[19]

An excess of ATP in the extracellular milieu can be counteracted by the action of the ecto-ATPases CD39 and CD73, which in subsequential order convert ATP to adenosine. However, also, α-SG displays in its C-terminal domain an ecto-ATPase function, and its absence causes a more consistent accumulation of ATP in the culture medium of primary myotubes. In turn, as already shown in distinct cell systems, an excessive extracellular ATP stimulation is able to exert a direct toxic effect in muscle cells because it induces apoptosis.[26,27] The molecular basis of the proapoptotic effect can be because of an effect on mitochondrial metabolism or the association with pannexin molecules and the formation of a cytolytic pore (ie, a large conductance channel).

According to these first observations, the pharmacologic inhibition of purinergic signaling via oATP led to an improvement of muscular function and structure, a reduction of the innate/adaptive immune response and fibrosis, and an increase in $FOXP3^+$ $CD4^+$ Treg muscle infiltration. In this scenario, it is likely that the oATP-mediated boosting of Treg muscle infiltration played a role in ameliorating the Sgca mice phenotype. It has been shown that skeletal muscle resident Treg, producing IL-10 and expressing Areg, controls the switch of type 1 to type 2 inflammation in injured muscle and acts directly on muscle satellite cells, improving muscle repair.[28–30] Noteworthy, myoblasts

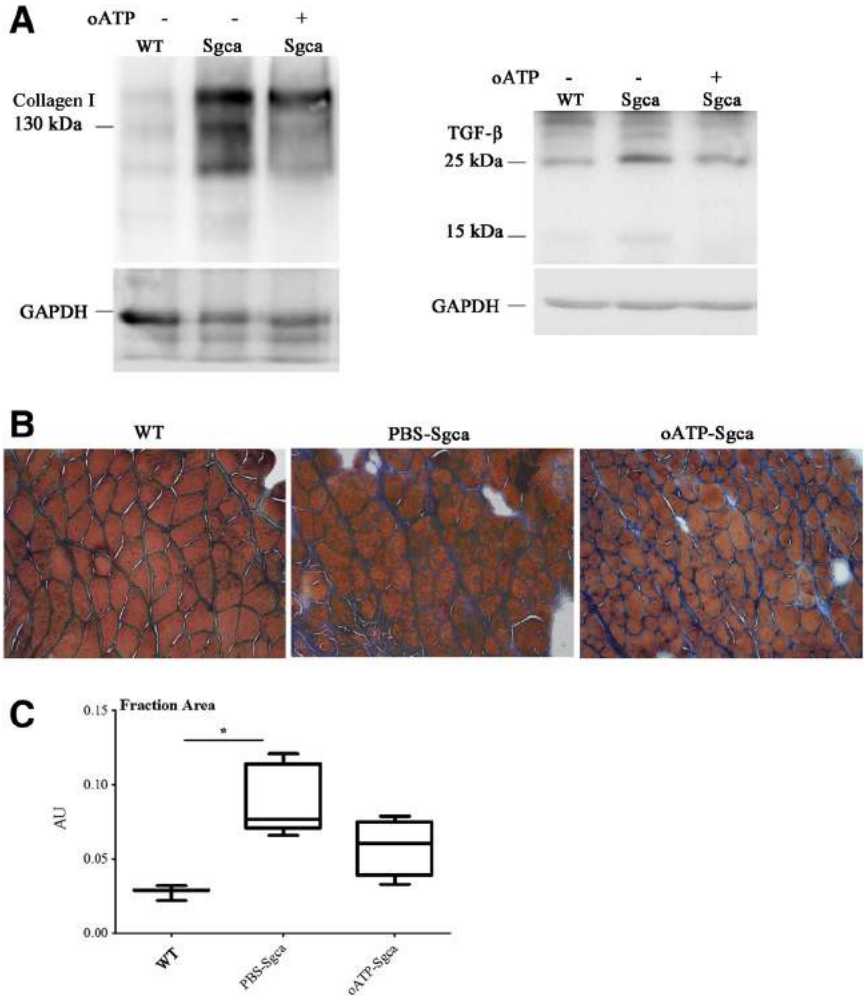

Figure 10 oATP induces a decrease of collagen profibrotic factors in muscles from Sgca mice. **A:** Total protein lysates, isolated from gastrocnemii (GN) of PBS-Sgca, oATP-Sgca, and WT age-matched controls, were subjected to Western blot analysis. Membranes were probed with a rabbit polyclonal anti-collagen type I and a mouse monoclonal anti—transforming growth factor-β (TGF-β; the 25-kDa dimer and the 15-kDa monomer) antibody. Representative images are shown. **B:** Frozen muscle tissue sections of GN from PBS-Sgca, oATP-Sgca, and WT age-matched controls were collected at the fourth week of treatment and stained with a standard Masson trichrome stain protocol. Representative images are shown. **C:** Graph of the fraction areas of fibrotic blue positive signal/arbitrary unit (AU) of total section area of muscles represented in **B**. Data are expressed as medians ± first and third quartiles. WT = 0.029 (0.026-0-031), PBS-Sgca = 0.077 (0.076 to 0.107), oATP-Sgca = 0.061 (0.052 to 0.067). Statistical analysis was performed using the *U*-test. $n = 6$ (**A**, PBS-Sgca, oATP-Sgca, and WT mice); $n = 5$ (**B**, PBS-Sgca, oATP-Sgca, and WT mice). $^*P < 0.05$ for WT versus Sgca. Original magnification, ×10 (**B**). GAPDH, glyceraldehyde-3-phosphate dehydrogenase.

isolated from *mdx* mice showed an increased cytosolic Ca^{2+} ion influx and IL-1β release when stimulated with BzATP,[31] thus evoking an active role of skeletal muscle cells in the inflammatory mechanism through P2X-purinergic signaling. The assessment of Sgca and LGMD2D primary myoblast behavior under eATP stimulation and the direct effect of P2XR inhibition on these cells will be evaluated in our future studies.

oATP was originally described as an irreversible P2X7R antagonist[32] but was shown later to also block other P2XRs, such as the P2X4 subtype,[33] making this compound a good candidate for a first proof of principle of our hypothesis in Sgca mice, in which an up-regulation of both P2X7 and P2X4 receptors was found. oATP has also demonstrated promise as a treatment modality in several models of autoimmune diseases. Successful examples are experimental models of collagen-induced arthritis, autoimmune diabetes, allergic encephalitis, autoimmune colitis, and allograft rejection in cardiac and islet transplantation.[33–39] In these disorders, the compound works as a suppressor of the innate and adaptive immunity as well as an inductor of Treg expansion.

However, numerous other P2XR antagonists, more efficient and more specific, have been discovered in the past few years, especially anti-P2X7R.[40–43] CE-224,535 has been tested in clinical trials for rheumatoid arthritis in patients with an inadequate response to methotrexate. The drug was not efficacious, compared with placebo, but demonstrated an acceptable safety and tolerability profile (NCT00628095).[44,45] The purinergic P2X7 antagonist AZD9056 was shown to have the potential to improve symptoms in patients with moderate-to-severe Crohn disease combined with a beneficial risk profile. AZD9056 was well tolerated, and no serious adverse events were reported.[46] The molecule GSK1482160 has already been explored as a possible tool to detect neuroinflammation, and a phase I clinical study in humans is currently undergoing (NCT00849134).[47]

Currently, no therapies are available for LGMD2D patients. Many studies in each of the four sarcoglycan deficiencies demonstrated that viral-mediated gene transfer, using adeno-associated vectors, can correct the pathologic signs of the disease in animal models.[48–56] However, some previous α-SG gene transfer experiments revealed the

occurrence of specific immune response, leading to generation of α-SG–specific antibody, T-cell infiltration of treated muscles, and disappearance of the vector. In this respect, we suggest that P2X-purinergic signal antagonism, with its double anti-inflammatory effect (inhibition of innate/adaptive inflammatory response and enhancement of immune tolerance by Treg expansion), could be associated with gene transfer therapies for the treatment of LGMD2D to obtain a more stable α-SG expression.

Moreover, this study is in agreement with recent lines of research, which emphasize the relevance of DAMPs in chronic degenerative disorders. Intriguingly, these sophisticated molecules are danger signals important not only for the inflammatory response but also for tissue repair because they can orchestrate tissue healing by acting on different receptors. Thus, better understanding of the consequences of DAMP signaling on muscle inflammation and on muscle regeneration is the key to promote tissue repair and healing.

Acknowledgment

We thank Prof. Giulio Cossu for donating Sgca mice.

Supplemental Data

Supplemental material for this article can be found at *https://doi.org/10.1016/j.ajpath.2018.10.008*.

References

1. Vainzof M, Passos-Bueno MR, Pavanello RC, Marie SK, Oliveira AS, Zatz M: Sarcoglycanopathies are responsible for 68% of severe autosomal recessive limb-girdle muscular dystrophy in the Brazilian population. J Neurol Sci 1999, 164:44–49
2. Angelini C, Fanin M, Freda MP, Duggan DJ, Siciliano G, Hoffman EP: The clinical spectrum of sarcoglycanopathies. Neurology 1999, 52:176–179
3. Kirschner J, Lochmuller H: Sarcoglycanopathies. Handb Clin Neurol 2011, 101:41–46
4. Rubartelli A, Lotze MT: Inside, outside, upside down: damage–associated molecular–pattern molecules (DAMPs) and redox. Trends Immunol 2007, 28:429–436
5. Bours MJ, Swennen EL, Di Virgilio F, Cronstein BN, Dagnelie PC: Adenosine 5'–triphosphate and adenosine as endogenous signaling molecules in immunity and inflammation. Pharmacol Ther 2006, 112: 358–404
6. Willart MA, Lambrecht BN: The danger within: endogenous danger signals, atopy and asthma. Clin Exp Allergy 2009, 39:12–19
7. Khakh BS, North RA: P2X receptors as cell-surface ATP sensors in health and disease. Nature 2006, 442:527–532
8. Gazzerro E, Baldassari S, Assereto S, Fruscione F, Pistorio A, Panicucci C, Volpi S, Perruzza L, Fiorillo C, Minetti C, Traggiai E, Grassi F, Bruno C: Enhancement of muscle T regulatory cells and improvement of muscular dystrophic process in mdx mice by blockade of extracellular ATP/P2X axis. Am J Pathol 2015, 185: 3349–3360
9. Sinadinos A, Young CN, Al-Khalidi R, Teti A, Kalinski P, Mohamad S, Floriot L, Henry T, Tozzi G, Jiang T, Wurtz O, Lefebvre A, Shugay M, Tong J, Vaudry D, Arkle S, doRego JC, Górecki DC: P2RX7 purinoceptor: a therapeutic target for ameliorating the symptoms of Duchenne muscular dystrophy. PLoS Med 2015, 12:e1001888
10. Betto R, Senter L, Ceoldo S, Tarricone E, Biral D, Salviati G: Ecto-ATPase activity of alpha-sarcoglycan (adhalin). J Biol Chem 1999, 274:7907–7912
11. Sandonà D, Gastaldello S, Martinello T, Betto R: Characterization of the ATP-hydrolyzing activity of alpha-sarcoglycan. Biochem J 2004, 381:105–112
12. Gazzerro E, Assereto S, Bonetto A, Sotgia F, Scarfì S, Pistorio A, Bonuccelli G, Cilli M, Bruno C, Zara F, Lisanti MP, Minetti C: Therapeutic potential of proteasome inhibition in Duchenne and Becker muscular dystrophies. Am J Pathol 2010, 176:1863–1877
13. Grozio A, Sociali G, Sturla L, Caffa I, Soncini D, Salis A, Raffaelli N, De Flora A, Nencioni A, Bruzzone S: CD73 protein as a source of extracellular precursors for sustained NAD+ biosynthesis in FK866-treated tumor cells. J Biol Chem 2013, 288:25938–25949
14. Munoz J, Zhou Y, Jarrett HW: LG4-5 domains of laminin-211 binds alpha-dystroglycan to allow myotube attachment and prevent anoikis. J Cell Physiol 2010, 222:111
15. Muratore M, Srsen V, Waterfall M, Downes A, Pethig R: Biomarker-free dielectrophoretic sorting of differentiating myoblast multipotent progenitor cells and their membrane analysis by Raman spectroscopy. Biomicrofluidics 2012, 6:034113
16. Pawlikowski B, Lee L, Zuo J, Kramer R: Analysis of human muscle stem cells reveals a differentiation-resistant progenitor cell population expressing Pax7 capable of self-renewal. Dev Dyn 2009, 238: 138–149
17. Jablonski KA, Amici SA, Webb LM, Ruiz-Rosado JdD, Popovich PG, Partida-Sanchez S, Guerau-de-Arellano M: Novel markers to delineate murine M1 and M2 macrophages. PLoS One 2015, 10:e0145342
18. Choi HB, Ryu JK, Kim SU, McLarnon JG: Modulation of the purinergic P2X7 receptor attenuates lipopolysaccharide-mediated microglial activation and neuronal damage in inflamed brain. J Neurosci 2007, 27:4957–4968
19. Bianchi G, Vuerich M, Pellegatti P, Marimpietri D, Emionite L, Marigo I, Bronte V, Di Virgilio F, Pistoia V, Raffaghello L: ATP/P2X7 axis modulates myeloid-derived suppressor cell functions in neuroblastoma microenvironment. Cell Death Dis 2014, 5: e1135
20. Brunelli S, Sciorati C, D'Antona G, Innocenzi A, Covarello D, Galvez BG, Perrotta C, Monopoli A, Sanvito F, Bottinelli R, Ongini E, Cossu G, Clementi E: Nitric oxide release combined with nonsteroidal antiinflammatory activity prevents muscular dystrophy pathology and enhances stem cell therapy. Proc Natl Acad Sci U S A 2007, 104:264–269
21. De Paepe B, De Bleecker JL: Cytokines and chemokines as regulators of skeletal muscle inflammation: presenting the case of Duchenne muscular dystrophy. Mediators Inflamm 2013, 2013:540370
22. Saito K, Kobayashi D, Komatsu M, Yajima T, Yagihashi A, Ishikawa Y, Minami R, Watanabe N: A sensitive assay of tumor necrosis factor alpha in sera from Duchenne muscular dystrophy patients. Clin Chem 2000, 46:1703–1704
23. Evans NP, Misyak SA, Robertson JL, Bassaganya-Riera J, Grange RW: Immune-mediated mechanisms potentially regulate the disease time-course of Duchenne muscular dystrophy and provide targets for therapeutic intervention. PMR 2009, 1:755–768
24. De Pasquale L, D'Amico A, Verardo M, Petrini S, Bertini E, De Benedetti F: Increased muscle expression of interleukin-17 in Duchenne muscular dystrophy. Neurology 2012, 78:1309–1314
25. Rufo A, Del Fattore A, Capulli M, Carvello F, De Pasquale L, Ferrari S, Pierroz D, Morandi L, De Simone M, Rucci N, Bertini E, Bianchi ML, De Benedetti F, Teti A: Mechanisms inducing low bone density in Duchenne muscular dystrophy in mice and humans. J Bone Miner Res 2011, 26:1891–1903
26. Orioli E, De Marchi E, Giuliani AL, Adinolfi E: P2X7 receptor orchestrates multiple signalling pathways triggering inflammation,

autophagy and metabolic/trophic responses. Curr Med Chem 2017, 24:2261–2275
27. Gulbransen BD, Bashashati M, Hirota SA, Gui X, Roberts JA, MacDonald JA, Muruve DA, McKay DM, Beck PL, Mawe GM, Thompson RJ, Sharkey KA: Activation of neuronal P2X7 receptor-pannexin1 mediates death of enteric neurons during colitis. Nat Med 2012, 18:600–604
28. Burzyn D, Kuswanto W, Kolodin D, Shadrach JL, Cerletti M, Jang Y, Sefik E, Tan TG, Wagers AJ, Benoist C, Mathis D: A special population of regulatory T cells potentiates muscle repair. Cell 2013, 155: 1282–1295
29. Lei H, Schmidt-Bleek K, Dienelt A, Reinke P, Volk HD: Regulatory T cell-mediated anti-inflammatory effects promote successful tissue repair in both indirect and direct manners. Front Pharmacol 2015, 6:184
30. Schiaffino S, Pereira MG, Ciciliot S, Rovere-Querini P: Regulatory T cells and skeletal muscle regeneration. FEBS J 2017, 284:517–524
31. Rawat R, Cohen TV, Ampong B, Francia D, Henriques-Pons A, Hoffman EP, Nagaraju K: Inflammasome up-regulation and activation in dysferlin-deficient skeletal muscle. Am J Pathol 2010, 176: 2891–2900
32. Murgia M, Hanau S, Pizzo P, Rippa M, Di Virgilio F, Oxidized ATP: An irreversible inhibitor of the macrophage purinergic P2Z receptor. J Biol Chem 1993, 268:8199–8203
33. Di Virgilio F: Novel data point to a broader mechanism of action of oxidized ATP: the P2X7 receptor is not the only target. Br J Pharmacol 2003, 140:441–443
34. Ardissone V, Radaelli E, Zaratin P, Ardizzone M, Ladel C, Gattorno M, Martini A, Grassi F, Traggiai E: Pharmacologic P2X purinergic receptor antagonism in the treatment of collagen-induced arthritis. Arthritis Rheum 2011, 63:3323–3332
35. Lang PA, Merkler D, Funkner P, Funkner P, Shaabani N, Meryk A, Krings C, Barthuber C, Recher M, Brück W, Häussinger D, Ohashi PS, Lang KS: Oxidized ATP inhibits T-cell-mediated autoimmunity. Eur J Immunol 2010, 40:2401–2408
36. Schenk U, Westendorf AM, Radaelli E, Casati A, Ferro M, Fumagalli M, Verderio C, Buer J, Scanziani E, Grassi F: Purinergic control of T cell activation by ATP released through pannexin–1 hemichannels. Sci Signal 2008, 1:ra6
37. Vergani A, Fotino C, D'Addio F, Tezza S, Podetta M, Gatti F, Chin M, Bassi R, Molano RD, Corradi D, Gatti R, Ferrero ME, Secchi A, Grassi F, Ricordi C, Sayegh MH, Maffi P, Pileggi A, Fiorina P: Effect of the purinergic inhibitor oxidized ATP in a model of islet allograft rejection. Diabetes 2013, 62:1665–1675
38. Kurashima Y, Amiya T, Nochi T, Fujisawa K, Haraguchi T, Iba H, Tsutsui H, Sato S, Nakajima S, Iijima H, Kubo M, Kunisawa J, Kiyono H: Extracellular ATP mediates mast cell-dependent intestinal inflammation through P2X7 purinoceptors. Nat Commun 2012, 3: 1034
39. Koo TY, Lee JG, Yan JJ, Jang J, Ju KD, Oh KH, Ahn C, Jang J: The P2X7 receptor antagonist, oxidized adenosine triphosphate, ameliorates renal ischemia-reperfusion injury by expansion of regulatory T cells. Kidney Int 2017, 92:415–431
40. Guile SD, Alcaraz L, Birkinshaw TN, Bowers KC, Ebden MR, Furber M, Stocks MJ: Antagonists of the P2X7 receptor: from lead identification to drug development. J Med Chem 2009, 52: 3123–3141
41. Subramanyam C, Duplantier AJ, Dombroski MA, Chang S-P, Gabel CA, Whitney-Pickett C, Perregaux DG, Labasi JM, Yoon K, Shepard RM: Discovery, synthesis and SAR of azinyl- and azolylbenzamides antagonists of the P2X 7 receptor. Bioorg Med Chem Lett 2011, 21:5475–5479
42. Lambertucci C, dal Ben D, Buccioni M, Marucci G, Thomas A, Volpini R: Medicinal chemistry of P2X receptors: agonists and orthosteric antagonists. Curr Med Chem 2015, 22:915–928
43. Caseley EA, Muench SP, Fishwick CW, Jiang LH: Structure-based identification and characterization of structurally novel human P2X7 receptor antagonists. Biochem Pharmacol 2016, 15:130–139
44. Keystone EC, Wang MM, Layton M, Hollis S, Mcinnes IB: Clinical evaluation of the efficacy of the P2X7 purinergic receptor antagonist AZD9056 on the signs and symptoms of rheumatoid arthritis in patients with active disease despite treatment with methotrexate or sulphasalazine. Ann Rheum Dis 2012, 71:1630–1635
45. Stock TC, Bloom BJ, Wei N, Ishaq S, Park W, Wang X, Gupta P, Mebus CA: Efficacy and safety of CE-224,535, an antagonist of P2X7 receptor, in treatment of patients with rheumatoid arthritis inadequately controlled by methotrexate. J Rheumatol 2012, 39: 720–727
46. Eser A, Colombel J-F, Rutgeerts P, Vermeire S, Vogelsang H, Braddock M, Persson T, Reinisch W: Safety and efficacy of an oral inhibitor of the purinergic receptor P2X7 in adult patients with moderately to severely active Crohn's disease: a randomized placebo-controlled, double-blind, phase IIa study. Inflamm Bowel Dis 2015, 21:2247–2253
47. Han J, Liu H, Liu C, Jin H, Perlmutter JS, Egan TM, Tu Z: Pharmacologic characterizations of a P2X7 receptor-specific radioligand, [11C]GSK1482160 for neuroinflammatory response. Nucl Med Commun 2017, 38:372–382
48. Fougerousse F, Bartoli M, Poupiot J, Arandel L, Durand M, Guerchet N, Gicquel E, Danos O, Richard I: Phenotypic correction of alpha-sarcoglycan deficiency by intra-arterial injection of a muscle-specific serotype 1 rAAV vector. Mol Ther 2007, 15:53–61
49. Pacak CA, Conlon T, Mah CS, Byrne BJ: Relative persistence of AAV serotype 1 vector genomes in dystrophic muscle. Genet Vaccin Ther 2008, 6:14
50. Pacak CA, Walter GA, Gaidosh G, Bryant N, Lewis MA, Germain S, Mah CS, Campbell KP, Byrne BJ: Long-term skeletal muscle protection after gene transfer in a mouse model of LGMD-2D. Mol Ther 2007, 15:1775–1781
51. Rodino-Klapac LR, Lee JS, Mulligan RC, Clark KR, Mendell JR: Lack of toxicity of alpha-sarcoglycan overexpression supports clinical gene transfer trial in LGMD2D. Neurology 2008, 71:240–247
52. Cordier L, Hack AA, Scott MO, Barton-Davis ER, Gao G, Wilson JM, McNally EM, Sweeney HL: Rescue of skeletal muscles of gamma-sarcoglycan-deficient mice with adeno-associated virus-mediated gene transfer. Mol Ther 2000, 1:119–129
53. Goehringer C, Rutschow D, Bauer R, Schinkel S, Weichenhan D, Bekeredjian R, Straub V, Kleinschmidt JA, Katus HA, Müller OJ: Prevention of cardiomyopathy in delta-sarcoglycan knockout mice after systemic transfer of targeted adeno-associated viral vectors. Cardiovasc Res 2009, 82:404–410
54. Li J, Dressman D, Tsao YP, Sakamoto A, Hoffman EP, Xiao X: rAAV vector-mediated sarcogylcan gene transfer in a hamster model for limb girdle muscular dystrophy. Gene Ther 1999, 6:74–82
55. Li J, Wang D, Qian S, Chen Z, Zhu T, Xiao X: Efficient and long-term intracardiac gene transfer in δ-sarcoglycan-deficiency hamster by adeno-associated virus-2 vectors. Gene Ther 2003, 10:1807–1813
56. Mendell JR, Rodino-Klapac LR, Rosales XQ, Coley BD, Galloway G, Lewis S, Malik V, Shilling C, Byrne BJ, Conlon T, Campbell KJ, Bremer WG, Taylor LE, Flanigan KM, Gastier-Foster JM, Astbury C, Kota J, Sahenk Z, Walker CM, Clark KR: Sustained alpha-sarcoglycan gene expression after gene transfer in limb-girdle muscular dystrophy, type 2D. Ann. Neurol 2010, 68:629–638

International Journal of
Molecular Sciences

MDPI

Review

eATP/P2X7R Axis: An Orchestrated Pathway Triggering Inflammasome Activation in Muscle Diseases

Chiara Panicucci [1], Lizzia Raffaghello [1], Santina Bruzzone [2], Serena Baratto [1], Elisa Principi [1], Carlo Minetti [3], Elisabetta Gazzerro [4,*] and Claudio Bruno [1,*]

1 Center of Translational and Experimental Myology, IRCCS Istituto Giannina Gaslini, 16147 Genova, Italy; chiarapanicucci@gaslini.org (C.P.); lizziaraffaghello@gaslini.org (L.R.); sere.baratto@gmail.com (S.B.); elisaprincipi83@hotmail.it (E.P.)
2 Department of Experimental Medicine, University of Genova, 16126 Genova, Italy; santina.bruzzone@unige.it
3 Pediatric Neurology Unit, IRCCS Istituto Giannina Gaslini, and University of Genova, 16147 Genova, Italy; minettic@unige.it
4 Unit of Muscle Research, Experimental and Clinical Research Center Charité Universitätsmedizin and Max Delbrück Research Center, 13125 Berlin, Germany
* Correspondence: elisabetta.gazzerro@charite.de (E.G.); claudio2246@gmail.com (C.B.); Tel.: +39-010-5636-2756 (C.B.)

Received: 8 July 2020; Accepted: 17 August 2020; Published: 19 August 2020

Abstract: In muscle ATP is primarily known for its function as an energy source and as a mediator of the "excitation-transcription" process, which guarantees muscle plasticity in response to environmental stimuli. When quickly released in massive concentrations in the extracellular space as in presence of muscle membrane damage, ATP acts as a damage-associated molecular pattern molecule (DAMP). In experimental murine models of muscular dystrophies characterized by membrane instability, blockade of eATP/P2X7 receptor (R) purinergic signaling delayed the progression of the dystrophic phenotype dampening the local inflammatory response and inducing Foxp3$^+$ T Regulatory lymphocytes. These discoveries highlighted the relevance of ATP as a harbinger of immune-tissue damage in muscular genetic diseases. Given the interactions between the immune system and muscle regeneration, the comprehension of ATP/purinerigic pathway articulated organization in muscle cells has become of extreme interest. This review explores ATP release, metabolism, feedback control and cross-talk with members of muscle inflammasome in the context of muscular dystrophies.

Keywords: eATP; P2X7R; inflammasome; muscular dystrophies; Duchenne Muscular Dystrophy; Sarcoglycanopathies

1. Introduction

In muscle cells, intracellular adenosine triphosphate (ATP) is the most abundant energy molecule participating in various signaling pathways (i.e., substrate in kinase-mediated signal transduction, synthesis of cyclic (c)AMP, nucleotides and DNA, etc.). However, ATP is also released in the extracellular space, where it acts as a signaling molecule with paracrine/autocrine effects. It can act as a find me signal from apoptotic cells, where it helps phagocytes to find and safely clear apoptotic cells [1] or as a damage-associated molecular patterns (DAMPs) when it is massively dispersed in the extracellular space in several cell stress—and cell death-inducing conditions, such as mechanical stress, cytotoxic agents, hypoxia or plasma membrane damage [2–4]. In this scenario, extracellular ATP (eATP) activates P2 receptors, which include P2XRs and P2YRs, respectively ionotropic and metabotropic

receptors. Currently, seven P2XRs have been cloned in mammals (P2XR1-7) [5]. Their activation leads to intracellular modification of cations, such as K^+, Na^+ and Ca^{2+} [6].

Among the P2XRs, P2X7R responds to high concentration of eATP (>100 μM) [5]. P2X7R is composed by the assembly of three sub-units (homo-trimer) [5]. Each subunit is composed of 595 aminoacids and is formed by a bulky extracellular loop, two transmembrane domains, a short intracellular N-terminus (26 aminoacids) and an extended intracellular C-terminus [7]. In addition to be a non-selective cation channel, P2X7R induces the formation of a plasma membrane pore, permeable to large molecules [8,9] and whose formation can be followed by measurements of the uptake of fluorescent dyes up to 900 kDa, such as ethidium bromide and YO-PRO1 [10–12]. The P2X7R's ability to form the membrane large pore is intrinsic to the receptor itself; however, it has been debated whether P2X7R requires pannexins, annexins or connexins in order to create the pore [13–15]. Pore formation occurs upon eATP sustained stimulation and induces cell death via a range of several pathways (e.g., aponecrosis, autosis and autophagy) [9,16,17]. Experimental evidence indicates that, upon ATP stimulation, the opening of P2X7R non-selective cation channel occurs within milliseconds, whereas the formation of a large pore takes place within seconds [18,19].

P2X7R activation results in a plethora of additional downstream effects, including cell proliferation and differentiation [20–22], release of pro-inflammatory mediators [23] and activation of metabolic pathways such as the PI3K/Akt/GSK-3 which has been associated with oncogene regulation [24,25] and tumor progression towards malignancy [26,27]. Most of these effects are due to the P2X7R-mediated Ca^{2+} influx or K^+ efflux and are mediated by the C-terminus tail, which is involved in the proper positioning of the receptor in signaling complexes and in the preservation of an efficient channel function [28,29].

P2XR7 was first described in lymphocytes and macrophages [30,31] and later identified in all immune cell types belonging to both the innate and the adaptive immunity where its role has been extensively elucidated [32–34]. Nevertheless, P2X7R has also been detected in non-hematopoietic cells, which can cooperate with the immune cells and contribute to the amplification of the inflammatory processes triggered by eATP [34].

The signal triggered by P2X7R is modulated by the activity of ecto-ATPase enzymatic activities, such as ecto-nucleoside triphosphate diphosphohydrolases (ENTPDases) and ecto-5′-nucleotidase (5′-NT) [4]. More specifically, eATP is hydrolyzed to ADP and AMP, mainly by CD39, an ENTDPase. Subsequently, CD73, a 5′-NT, hydrolyzes AMP to adenosine, which, in turn activates receptors of the P1 ADORA receptor family, represented by four subfamilies (A1, A2A, A2B, and A3) [4]. Stimulation of P1 receptors exerts mostly immunosuppressive and anti-inflammatory effects, contributing to dampen the inflammatory response induced by P2X7R activation [35]. Adenosine deaminase (ADA) regulates adenosine levels by deaminating this nucleoside intoinosine.

Hence, P2X7R-mediated signal activity varies according to the tissue availability of eATP, the receptor density on the cell membrane surface, the co-factors expressed in the specific tissue and the efficiency of hydrolyzing enzymes, which switch off the purinergic signal. Moreover, in the same cellular system, the role for P2X7R may profoundly vary according to the proliferative stage, the functional differentiation phase and the occurrence of pathological derangements.

We will focus on the role of the eATP/P2X7R axis in skeletal muscle cells and muscular tissue in physiological and pathological conditions. Furthermore, we will represent the purinergic signal in muscle as a fine tuned signaling, which activates the inflammasome pathway and requires the orchestrated regulation of different players such as the connexin and pannexin channels, the adenosine receptors and the toll-like receptors (TLRs).

2. P2X7R in Skeletal Muscle Cells and Muscular Tissue at Steady State and Under Pathological Conditions

P2X7R activation in muscle cells shows a dichotomic effect: at physiological low eATP concentrations P2X7R tonic activation is crucial for myoblasts proliferation and differentiation. Under

pathological conditions, with increased eATP release and pro-inflammatory state, P2X7R signaling activates cell inflammatory pathways and accelerates cell death.

2.1. P2X7R Signaling in Muscle Cells

P2X7R was first detected in C2C12 cell line, an immortalized mouse myoblast cell line [36], in which the purinergic signal is developmentally regulated. Mature myotubes present higher ATP release, P2 receptor surface expression and activity, as well as ATP-hydrolyzing enzyme expression when compared to undifferentiated myoblasts [37]. Among P2XRs, P2X7R protein expression is low in quiescent myoblasts, it increases in proliferating myoblasts and is highly represented in myotubes. In myoblasts, P2X7R stimulates proliferation, which is enhanced by Benzoil ATP (BzATP), an agonist of P2X7R, and inhibited by oxidized ATP (oATP), an antagonist of P2X7R. P2X7R blockade, via oATP, prevents myotubes formation, suggesting a role in full myoblast differentiation [38], although the specific molecular mechanisms still need to be clarified.

P2X7R's role in muscle regeneration is controversial. Muscle regeneration and growth are regulated by the muscle stem cells, named satellite cells (SCs), which express the Pax7 transcriptional factor and support the muscle homeostasis through their capacity to activate and to start differentiation and self-renewal. The latter processes are driven by the transcriptional factor MyoD, which regulates the transition of SCs from the state of quiescence toward the activation [39–41]. In the *mdx*/P2X7R$^{-/-}$ mice, a double knock-out lacking P2X7R and the dystrophin protein (*mdx*, a spontaneous mouse model of Duchenne Muscular Dystrophy), P2XR7 gene inactivation led to enhanced expression of Myogenin compared to the *mdx* mice [42]. However, P2X7R indirect inhibitory effects on inflammation with the consequent reduction of myofiber degeneration/regeneration cycles hinders the dissection of P2X7R direct action on muscle progenitors in in vivo experiments with dystrophic models. Although the role of P2X7R in muscle regeneration has been evaluated in different neuromuscular disorders, this aspect has been not fully characterized in normal muscle after an acute injury.

The ability to dampen the P2X7R signal is also differently modulated during muscle cell development. Ecto-nucleotidase activity is low in myoblasts and progressively increases during differentiation [37]. Skeletal muscle also presents with a tissue specific ENTPDase, the α-sarcoglycan, expressed in fully differentiated myoblasts, which hydrolyzes only ATP and accounts for the 25% of the total ecto-nucleotidase activity in myoblasts [43]. Contrarily to other ENTPDases [44,45], α-sarcoglycan shows low affinity for ATP (in the mM range) [43], making its role crucial in muscular diseases such as muscular dystrophies characterized by an increased availability of eATP.

2.2. P2X7R Triggers the Inflammasome Signaling in Dystrophic Muscle Cells

Primary myoblasts isolated from *mdx* mice show a significantly increase of P2X7R both at the transcript and the protein levels compared to wild types (wt) [46]. Indeed, P2X7R expression is up-regulated by the increased concentration of eATP itself and by exposure to a chronic inflammatory milieu [47]. Accordingly, *mdx* myoblasts demonstrate an enhanced P2X7R-dependent calcium influx and a sustained extracellular signal-regulated kinases 1/2 (ERK1/2) phosphorylation [46,48], which is involved in Reactive Oxygen Species (ROS) production via NADPH oxidases (NOXs) phosphorylation [49,50].

Adinolfi et al. reviewed the P2X7R-driven intracellular inflammatory pathways which range from the leucine-rich repeat (LRR)-containing protein 3 (NLRP3)-inflammasome activation, to the ERK/MAPK kinases and phospholipase A2 phosphorylation and NF-kB transcription factor induction [51]. Muscle cells express the inflammasome platform including NLRP3, a member of the Nucleotide-binding domain (NBD) and leucine-rich repeat (LRR)-containing proteins (NLRs) which contains a pyrin domain 3, the adaptor protein apoptosis-associated speck-like protein containing a caspase recruitment domain (ASC), and the cysteine protease pro-caspase-1. The latter cleaves the cytokines pro-IL-1β and pro-IL-18 into their active forms, facilitating the infiltration of immune cells to damaged or infected tissues and inducing the IL-18 mediated interferon-gamma (IFN-γ) production [52–54]. An in vitro

challenge with P2X7R agonists of primary skeletal muscle cells isolated from dysferlin-deficient and *mdx* mice was used to simulate the pathological condition occurring in muscular dystrophies [55]. Both myoblasts and myotubes from dysferlin-deficient and *mdx* mice showed a higher basal expression of P2XR, and treatment with Lipopolysaccharides/BzATP (LPS/BzATP) increased the levels of ASC, pro-caspase-1 and pro-IL1b in comparison to wt cells [55]. As a consequence of NLRP3 activation, IL-1β inhibits muscle regeneration and conversely its blocking with recombinant IL-1 receptor antagonist (Kineret®) leads to a marked improvement of in vitro muscle differentiation and in vivo amelioration of muscle strength [56,57]. Thus, skeletal muscle cells are equipped with a functional inflammasome pathway and actively participate to the inflammatory response upon P2X7R stimulation. A two-signal model has been suggested for NLRP3 inflammasome turn-on. The priming signal (first step) is provided by TLRs, upon DAMPs or pathogen associated molecular patterns (PAMPs) stimulation. Among DAMPs, the molecules which can trigger TLRs activation are the high-mobility group box 1 (HMGB1), the heat shock proteins (HSPs), as well as extracellular matrix degradation products (hyaluronan, heparan sulphate and biglycan) generated as a result of proteolytic enzymes derived from dying cells [58]. Particular interest has been focused on HMGB1, a nuclear protein that acts as a DNA chaperone in the nucleus and as a signal of tissue damage (DAMP) when extracellularly released, thus contributing to inflammation [59].

TLRs have raised particular attention as potential contributors to muscular dystrophies pathogenesis. As such, TLR2 and TLR4 expression has been reported in myoblasts isolated from wt (C57BL/6J) and dysferlin deficient mice (SJL/J) [55] and *mdx* mice have shown increased HMGB1 together with increased TLR4 sensitivity [60,61].

The first step induces an intracellular downstream signaling leading to NF-kB nuclear translocation with the subsequent upregulation of pro-IL-1β and pro-IL-18 transcripts, together with an increase in NLRP3 expression to a functional level [62]. All TLRs but TLR3, require the Myddosome adaptor protein to initiate the downstream intracellular signaling. The Myddosome complex is an oligomeric signaling platform, consisting of the Myeloid differentiation primary response 88 (MyD88) and IL-1 receptor associated kinases 1 and 4 (IRAK1-4) which recruits the TNFR-associated factor (TRAF) 6 to induce NF-kB nuclear translocation [63,64].

The triggering signal (second step) leads to the NLRP3 inflammasome assembly and is provided by a multitude of stimuli, ranging from K^+ efflux, ROS generation, mitochondrial and lysosomal damage [62]. Despite the heterogeneity of stimuli listed above, the quick drop of intracellular K^+ concentration, caused by opening of plasma membrane channels (P2X7R included) and responsible of the assembly of the fully active NLRP3 complex (NLRP3-ASC-NEK7-Caspase-1), is considered the most common event for inflammasome triggering [65–67] (Figure 1).

As shown in other cell types [9,16], also myoblasts are susceptible to the detrimental effect of the P2X7R-dependent large pore formation. Indeed, a sustained exposure of *mdx* primary myoblasts to BzATP induces the formation of a large non-selective membrane pore which leads to an increased cell death rate mediated by the heat shock proteins HSP90 and HSPA2 [17].

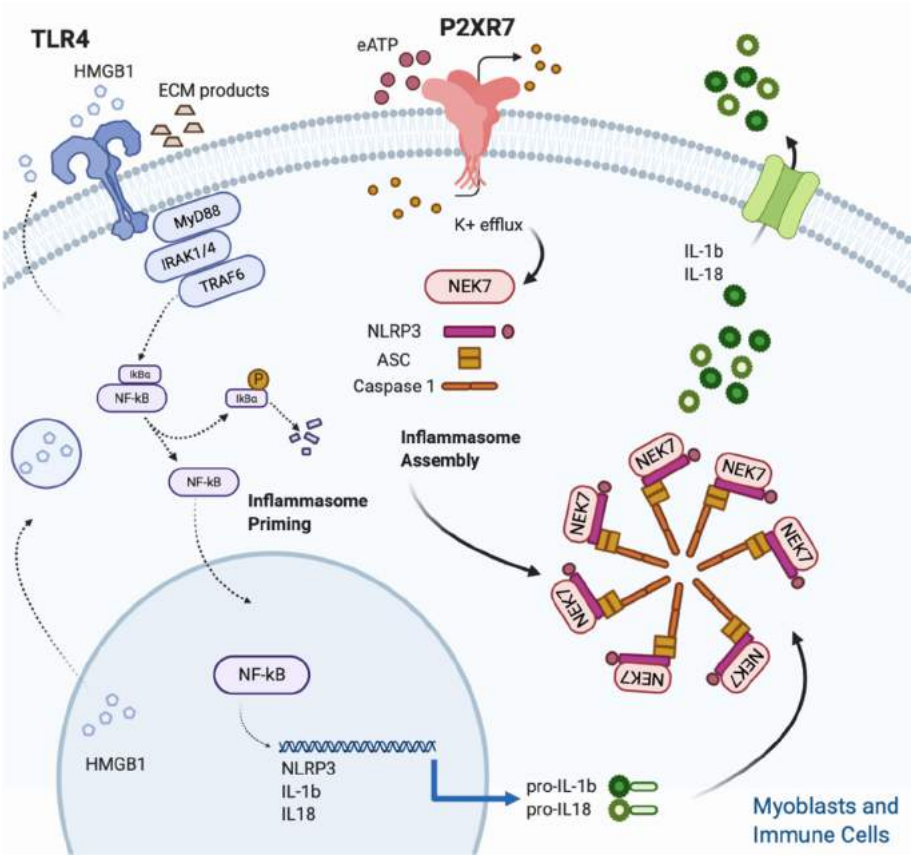

Figure 1. Figure 1. NLRP3 inflammasome activation in skeletal muscle. Skeletal muscle cells are equipped with a functional inflammasome pathway and actively participate to the inflammatory response upon P2X7R stimulation. A two signals model is proposed for NLRP3 inflammasome activation. The Inflammasome priming (first step) is triggered by TLR 4 which in turn is activated upon binding with its cognate ligands such as extracellular matrix degradation (ECM) products and high mobility group Box 1 (HMGB1). HMGB1 is a nuclear protein that acts as a DNA chaperone in the nucleus and as a signal of tissue damage when extracellularly released. Ligand binding and conformational change that occur in the receptor lead to the recruitment of the adaptor protein MyD88, which in turn recruits IRAK4, IRAK1 and IRAK2. IRAK kinases then phosphorylate and activate the protein TRAF6, resulting in IκBα degradation and NF-κB diffusion into the cell nucleus. The nucleus of NFκB activates the transcription of NLRP3, IL-1β and IL-18. The inflammasome assembly (second step) is triggered by the eATP/P2XR7/K^+ efflux. In particular, intracellular K^+ efflux, caused by opening of plasma membrane channels (P2X7R included), induces the assembly of the fully active NLRP3 complex (NLRP3-ASC-NEK7-Caspase-1). Finally, caspase-1, cleaves the pro-IL1β and pro IL-18 into their mature forms.

2.3. P2X7R in Dystrophic Skeletal Muscle

Despite the genetic and epidemiologic heterogeneity, several muscular dystrophies share inflammatory features at the muscle biopsy [68–70] (Figure 2). The plasma membrane of dystrophic muscular cells shows fragility due to defects on different structural proteins, like dystrophin or sarcoglycans. This induces a chronic release of ATP together with other DAMPs in the extracellular space, thus setting a pro-inflammatory milieu which recruits immune cells within the muscle tissue [71,72]. Specifically, pro-inflammatory M1 macrophages that express the inducible nitric oxide synthase (iNOS) and are specialized in free radicals production, dominate the initial inflammatory response in dystrophic muscle [72]. Although macrophages are the most prevalent inflammatory cell type at early stages, other myeloid cells invade the dystrophic tissue and cooperate with the M1 releasing pro-inflammatory cytokines and chemokines, thus recalling further immune cells, included the

adaptive T lymphocytes [72,73]. As such, once triggered, muscle inflammation maintains itself through autocrine/paracrine mechanisms and is involved in the progressive muscle cell death, connective replacement and exhaustion of satellite cell regeneration. In normal muscle, after acute injury, regeneration is promoted by the replacement of M1 with M2 anti-inflammatory macrophages (M2) which express CD163 and support muscle regeneration and repair [72]. Contrarily, in dystrophic muscle, M2 macrophage activation is suppressed by type 1 inflammatory response characterized by increased M1 macrophages, $CD4^+$ T helper 1 (Th1), $CD8^+$ T cells, natural killer (NK) and $CD4^+$ Th17 lymphocytes [74–77]. In this scenario, given the persistent leakage of DAMPs in the extracellular space, the high expression of P2X7R on the surface of infiltrating immune cells and the active contribution of myoblasts and myotubes to inflammasome activation, the eATP/P2X7R axis represents a possible therapeutic target to ameliorate the dystrophic process. This hypothesis is endorsed by the evidence that P2X7R expression is up-regulated in skeletal muscle tissue isolated from *mdx* mice [46,48] and in muscle biopsies from patients affected by Duchenne muscular dystrophy (DMD) [78].

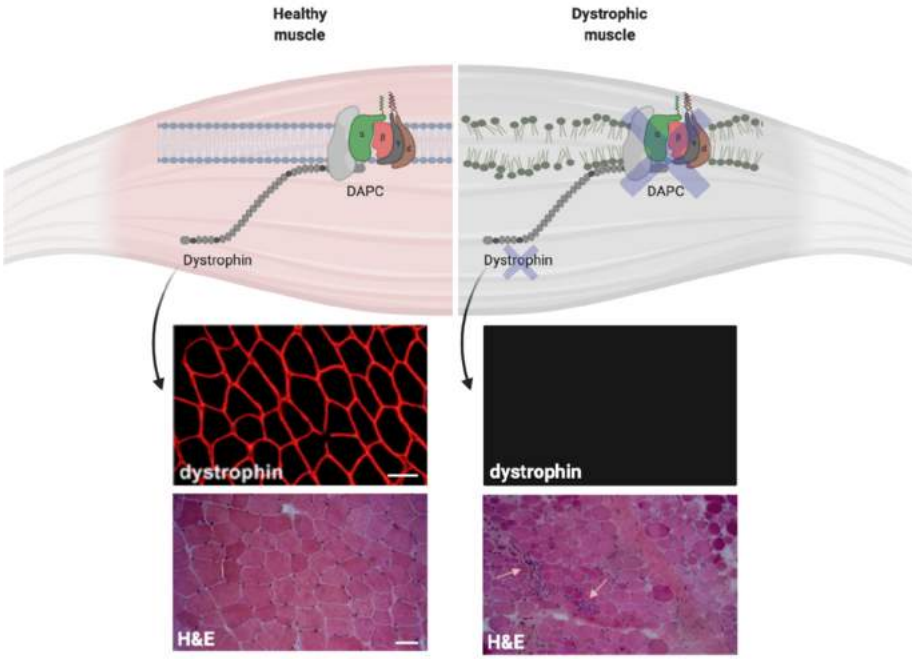

Figure 2. Dystrophin expression influences the plasma membrane stability in muscle cells. Dystrophin expression on the plasma membrane of normal and dystrophic cells. The immunofluorescence stainings for dystrophin show normal dystrophin signal in muscle biopsy collected from healthy control (top left) and the absence of dystrophin in muscle biopsy from Duchenne muscular dystrophy (DMD) patient (top right). The hematoxylin and eosin (H&E) staining show normal muscle architecture in healthy control (bottom left) and tissue architecture disruption in DMD muscle biopsy (bottom right). Small arrows show immune infiltrates within the dystrophic tissue. Scale bars = 50 μm.

The action of eATP/P2X7R in accelerating muscle cell death in muscular dystrophy is realized through direct and indirect mechanisms. Activation of an abnormal influx of Ca^{2+} leading to myofiber apoptotic events, induction of NLRP3 inflammasome and formation of membrane pores in muscle cells imbricate with an indirect tissue damage from cells of the innate and adaptive immunity infiltrating the tissue (Figure 3). Indeed, P2X7R participates in a feed-forward loop, which contributes to productive T-cell activation [79,80], while P2XR7 blockade determines the functional polarization of naive $CD4^+$ cells to adaptive T Regulatory (Tregs) on T-cell receptor stimulation [81,82].

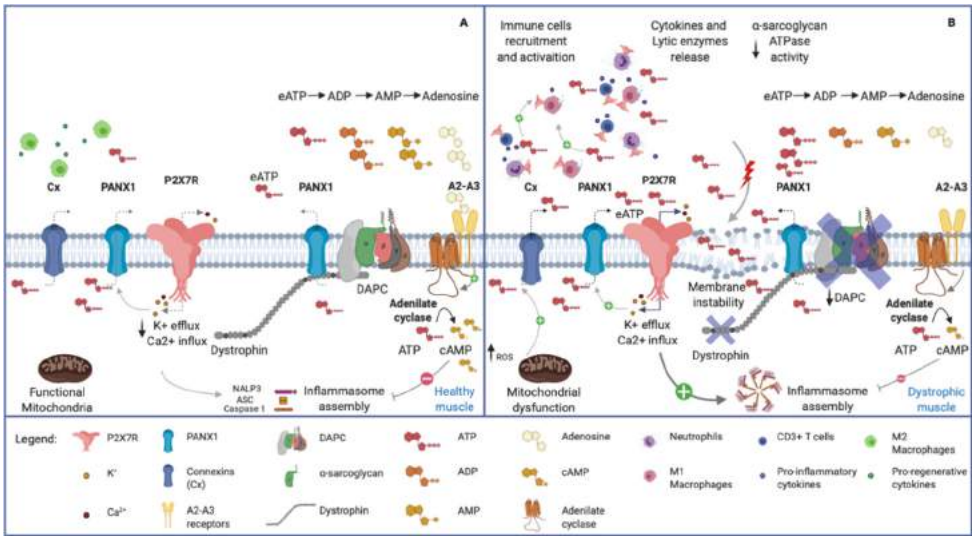

Figure 3. Purinergic signal in normal and dystrophic muscles. (**A**) Healthy skeletal muscle. Note the plasma membrane's integrity, the normal expression of Dystrophin Associated Protein Complex (DAPC) and the physiological low concentration of eATP. (**B**) Dystrophic skeletal muscle. The membrane instability, due to DAPC alteration, induces chronic release of ATP in the extracellular space, and recalls pro-inflammatory immune cells (i.e., neutrophils, M1 macrophages and $CD3^+$ Tcells). eATP, in turn, activates P2X7R receptors on muscular and immune cells, leading to pro-inflammatory citokines release via NLRP3 inflammasome activation. Connexin and Pannexin hemichannels contribute to the release of ATP, being activated respectively by increased ROS production and P2X7R-mediated K^+ efflux. The high eATP concentration in dystrophic tissue is influenced by the reduced ectoATPase activity mediated by the α-sarcoglycan. Adenosine, acting via A2–A3 receptors, stimulates adenilate cyclase which produces cAMP. The latter compound activates the phosphorylation of NLRP3 reducing its oligomerization and increasing its ubiquitination to be degraded in autophagosomes.

The first in vivo evidence of a beneficial effect of P2X7R inhibition in muscular dystrophies was provided in the mdx model with the broad-spectrum P2X7R antagonist Coomassie Brilliant Blue (CBB) [46]. The treatment determined a significant decrease in the number of revertant fibers in treated mice, indicating a reduced number of degeneration–regeneration cycles. Nevertheless, the hind limb grip strength was significantly reduced in wild-type rats treated with CBB or high doses of a different P2X7 antagonist, compared to vehicle-treated rats, suggesting that in case of future (pre)-clinical trials with P2X7 antagonists, the dose will have to be carefully defined [83].

Similarly, we showed that a short pharmacological in vivo treatment with oATP, a not selective antagonist of P2X7R, improves *mdx* muscular function [78]. The functional beneficial effect exerted by pharmacological P2X7R blockade is associated with a decrease of the pro-inflammatory IL-6 concentration, as well as with a shaping of the T cell composition, with selective increase of the Tregs population. Moreover, Gorecki et al. highlighted a dampening of the *mdx* associated immune response upon in vivo administration of Zidovudine [84], a mainstay of the anti-HIV infection which was shown to exert an anti-purinergic activity [85]. Likewise, P2X7R genetic ablation in *mdx* mice (double knockout *mdx*/$P2X7^{-/-}$ mouse model) showed an overall reduction of muscle inflammatory signature, associated to a decrease of infiltrating leukocytes, and increase in Tregs cell recruitment in muscle [42].

A novel activation of the purinergic pathway was also found in α-sarcoglycan deficient mice (Sgca) [86], the mouse model of α-sarcoglycan-related limb-girdle muscular dystrophy R3 (LGMDR3). Besides being a crucial component of the plasma membrane, α-sarcoglycan retains an ecto-ATPase activity, making the eATP/P2X7R axis activation relevant in the pathogenesis of this muscular dystrophy [43,87]. All together, these results indicate the eATP/P2X7R axis as a promising therapeutic target to dampen the immune response characteristic of muscular dystrophies due to defects in the dystrophin/sarcoglycan complex. The shift of the T-cell pool toward an immunosuppressive phenotype,

via purinergic antagonism, is of particular interest since Tregs acutely and chronically infiltrate injured muscle tissue [75,76], exerting a double protective activity. Tregs modulate the myeloid population from a pro- to an anti-inflammatory phenotype and actively promote muscle repair, directly acting on satellite cells, via Areg secretion [75].

P2X7R genetic ablation or pharmacological inhibition exerts not only an anti-inflammatory activity but also an anti-fibrotic effect [42] with a decreased concentration of fibrotic mediators such as Transforming Growth Factor (TGF)-β and connective tissue growth factor (CTGF) [78]. Interestingly, P2X7R ablation also ameliorates the cardiac pathology, improves brain performance [42] and bone osteoporotic phenotype [88].

3. Other Regulators of P2X7R Signaling

The presence of eATP in the extracellular space depends on a balance between ATP release and ATP-degradation by ecto-enzymes. ATP release occurs through both nonspecific and specific mechanisms. The former as consequence of plasma membrane disruption or cell death, and the latter mediated by different mechanisms, including vesicle and microvesicle exocytosis and transporters/channels, mainly connexin and pannexin hemichannels or the P2X7R itself [4]. In the context of muscular dystrophy, both the mechanisms including the plasma membrane instability, pannexin, connexin and P2X7R work together in controlling the release of ATP.

Each connexin hemichannel consists of six protein subunits, and each subunit is characterized by four transmembrane domains, connected by two extracellular loops and one intracellular loop, with cytoplasmic carboxyl and amine terminals. Connexins are classified according to the molecular weight (MW) of their subunits, with connexin 43 being the more abundant and involved in many processes. A gap junction is formed by two hemichannels exposed by adjacent cells: through gap juctions, different molecules are exchanged between cells. Instead, a single hemichannel can mediate the release in the extracellular environment of molecules with a MW below 1–2 kDa, including transmitters, as for instance ATP and nicotinamide adenine dinucleotide (NAD). Connexin hemichannels opening can occur at both physiological and pathological conditions and is regulated by different factors, including Ca^{2+} concentration, pH, oxidative stress and mechanical stimulation [4,89,90]. Although connexins and pannexins do not share sequence homology, they possess a similar structure (N and C terminal domain in the cytosol, four transmembrane domain and extra- and intra-cellular loops). The pannexin family in humans is composed of pannexin-1,-2 and -3. Pannexins are only present as hexamerich emichannels, and, as connexin hemichannel, they mediate the extracellular release of small molecules, including nucleotides. Pannexin channels opening is mediated by different conditions, i.e., cleavage of the C-terminal tail by caspases, intracellular Ca^{2+} concentration, plasma membrane depolarization, activation of the P2X7R, redox potential changes, and mechanical stress [4,91]. In the following paragraphs we will review the role of pannexins and connexins in skeletal muscle, and the possibility of targeting these channels in muscle diseases. In addition, we will discuss a novel feedback loop inactivating P2X7R, i.e., the upregulation of MMP2 expression.

3.1. Pannexins

Pannexin hemichannels were reported to mediate ATP release upon electrical stimulation [92,93], mechanical stress, and elevated extracellular potassium ion concentration [94]. Pannexin (PANX) 1 and 3 are expressed by myoblasts and SCs and are involved in the regulation of myoblast proliferation, differentiation and skeletal muscle development [92,95,96]. PANX1 levels are dramatically induced during myoblast differentiation, whereas PANX3 is mainly expressed in differentiated human skeletal muscle tissue, and its over-expression inhibits myoblast proliferation and induces their differentiation [95,96].

In adult muscle tissue, the PANX1-mediated ATP release after electrical stimulation was shown to potentiate skeletal muscle contraction [97,98] and, as part of a multiprotein complex with the voltage sensor dihydropyridine receptor and Cav1.1, to regulate gene expression, including slow-type Troponin

gene [99]. In addition, PANX1 regulates the oxidative state during exercise [100]. PANX3 has also been demonstrated to mediate eATP release [101], likely being involved in contraction and metabolism [96].

In *mdx* mice PANX1 and PANX3 levels are dysregulated, even though in different ways depending on the muscle type [96]. ThePANX3 role in DMD is still to be fully characterized: it has been suggested that PANX3-mediated ATP release may contribute to attraction of monocytes, which may enhance muscle inflammation [94].

Overall, pannexins are important to regulate myoblasts proliferation, differentiation and commitment. Electrical stimulation of myotubes, by causing ATP release, regulates gene expression and muscle plasticity. Furthermore, and importantly to this review, pannexins are critical in enhancing the purinergic signaling to potentiate muscle contraction [102]; in muscular dystrophies, the purinergic signaling seems to be over-activated by the pannexin-mediated eATP release, upon mechanical stress and high concentration of extracellular K^+. Accordingly, PANX1 and P2X7R were found to functionally and physically interact [103–105], thus enabling Pannexins to sense the P2X7R mediated K^+ efflux and to release ATP with a positive feedback loop primed by P2X7R activation.

3.2. Connexins

The role of connexins (Cxs), particularly of Cx43, in different cardiomyopathies, including DMD-associated cardiomyopathies, is well established. Less is known regarding the role of Cx43 and other connexins in skeletal muscle [106].

Some members of the connexin family, i.e., Cx39, Cx43 and Cx45, are expressed, along with pannexins, by murine myoblasts and are involved in the regulation of cell proliferation and differentiation [92,107]. In myofibers, connexin expression is down-regulated, and their re-expression occurs during healing processes of injured muscle [107].

Muscle biopsies obtained from patients affected by dysferlinopathy are characterized by expression of Cx40.1 (the Cx hortolog of Cx39 in humans), Cx43 and Cx45. Connexins were expressed by myotubes in a functional form, as demonstrated by uptake assays, together with P2X7R and the Ca^{2+} channel TRPV2. These three channels are likely responsible for a dysregulation in Ca^{2+} homeostasis [108]. Similarly, also myofibers from DMD patients and from *mdx* mice express Cx40.1/Cx39, Cx43 and Cx45 and form functional hemichannels, likely representing key elements in the pathogenesis of the disease [109].

The main isoforms shown to determine ATP release are Cx43, Cx37, Cx26 and Cx36 [110]. Cx43 activation is triggered by changes in the intracellular calcium concentration, cell membrane depolarization, ROS and nitric oxide (NO) [111]. Moreover, in monocytes and macrophages, it has been reported a role of TLR 2-4 in Cx43 activation [111,112]. All these trigger factors have been reported in dystrophic mouse models, making likely an involvement of these channels in ATP release in muscular dystrophies.

Recently, Nouet and coll. confirmed that Cx43 is over expressed in DMD skeletal muscle, by the use of a mouse *mdx*/wt chimera, a mouse model of DMD manifesting female carriers. Interestingly, in their study, they unveil that Cx43 is not expressed by wt or dystrophinopathic muscle fibers but rather by infiltrating $F4/80^+$ mononuclear cells. Cx43 gene inactivation improved histological features of muscular dystrophy in *mdx*/chimera mice suggesting that the development of anti-Cx43 therapies could be beneficial to ameliorate inflammation in DMD [106].

3.3. eATP/P2X7R Turning off Mechanisms in Skeletal Muscle

No studies reported the role of the ectoenzymes CD39 and CD73, hydrolyzing extracellular nucleotides, in regulating P2X7R opening in skeletal muscle. Nevertheless, as previously reported, skeletal muscle presents with a tissue specific ENTPDase, the α-sarcoglycan, which carries on the 25% of the total ecto-nucleotidase activity in myoblasts [43].

A novel feedback loop inactivating P2X7R and involving the matrix metalloproteinases (MMPs) has been proposed in muscular cells as in different cell types [113,114]. MMPs are a family of zinc-dependent

endopeptidases that are involved in the degradation of various proteins in the extracellular matrix (ECM) [115] and recently, the P2X7R has been unveiled as a MMP2 target [114]. In presence of chronic P2X7R stimulation, MMP-2 activity is up-regulated in skeletal muscle and MMP-2 takes part in an autocrine P2X7R negative feedback signaling. Indeed, high eATP concentration leads to P2X7R large pore formation, which triggers MMP-2 translocation from the cytosol into the extracellular space. The released MMP-2, in turn, exerts its proteolytic function, inactivating the P2X7R [114,116].

3.4. Adenosine and ADORA Receptors

Adenosine, the nucleoside derived primarily from the extracellular hydrolysis of adenine nucleotides, is a potent regulator of inflammation and mediates the transition from inflammation to healing, negatively feedbacking eATP effects. Adenosine is active on inflammatory cells (monocytes, macrophages and T cells) by engaging one or more cell-surface receptors. The adenosine receptors belong to the category of purinergic P1-receptors, which have been classified into different subtypes (A1, A2A, A2B, A3) [4]. The cellular effects are mediated by G-proteins. A1 and A3 adenosine receptors exert an inhibitory action on adenylyl cyclase via Gi-proteins, while A2A and A2B receptors stimulate the enzyme by virtue of the Gs-protein. A1 and A2A are high affinity receptors with activity in the low to mid-nanomolar range whereas A2B has a substantially lower affinity and it is triggered by high and rapid eATP accumulation and conversion to adenosine [117]. Adenosine-A2A binding turns-on a wide range of anti-inflammatory pathways among which inhibition of NF-kB signaling and NLRP3 inflammasome, ultimately inducing the switch from M1 to modified M2 macrophage phenotype [118,119]. The role of A2B is not completely clear and the results of current research seem ambiguous. While some studies indicate that Th17 differentiation is stimulated by increasing IL-6 production in dendritic cells upon A2B triggering [120], others sustain that A2B, when stimulated, promotes T cell differentiation in Tregs [121]. Similarly, the A3 receptor function varies from a pro-to an anti-inflammatory and anti-fibrotic effect in different cell types [122,123]. The adenosine A2A and A2B, but not the A1 receptors were found to be present in human skeletal muscle cell membrane and cytosol. The adenosine A1, A2A and A2B receptors were also observed in smooth muscle cells as well as in the endothelial cells [124]. The main intracellular pathway allocated downstream of adenosine A2 receptors in muscular cells is the cAMP/PKA cascade. Stimulation of the adenosine A2 receptors will lead to activation of adenylyl cyclase and the production of cAMP, causing activation of the cAMP-dependent protein kinase (PKA) which in turn may phosphorylate an array of different proteins, e.g., transcription factors such as the cAMP response element binding protein (CREB), thus leading to changes in gene transcription [125].

In cardiac and skeletal muscle adenosine is involved in both the regulation of blood flow [126] and in the synergistic effect of contraction and insulin stimulated glucose uptake [127].

Injured murine skeletal muscle is characterized by increased expression of A2B and A3; however, different cell types including macrophages infiltrating the site of injury express adenosine receptors and a complete study dissecting the involvement of the different cells has not been performed yet [124].

A recent study showed that increased number of systemic CD8/CD26 T cells correlated with muscle strength in DMD patients. The binding of ADA to T cells and the conversion of adenosine to inosine was increased in subject with high CD8/CD26 cells [128], suggesting that prevention of adenosine accumulation may protect muscle from immune damage. However, adenosine/inosine role in muscular dystrophies has not been investigated yet.

4. Prospects, Challenges and Future Directions

In muscular dystrophies, the close coupling between stages of inflammation and stages of muscle regeneration is encouraging preclinical approaches that explore whether manipulating inflammation can promote muscle growth and regeneration and can be used in conjunction with gene therapies to ensure efficacy. In this context, eATP and purinergic signaling seem to be ideal harbingers of tissue damage in muscular dystrophies. They activate both innate and adaptive immune responses and inhibit

Treg immunosuppressive feedback mechanisms. eATP also exerts a direct toxic effect on muscle cells through P2X receptors. Therefore, the inhibition of purinoreceptors represents a translational potential as a therapeutic strategy for muscular dystrophies. Moreover, due to the fact that the inflammatory response in DMD and sarcoglycanopathies may abrogate the efficacy of gene replacement therapies, therapeutic approaches subduing the immune response, can be used in conjunction with gene therapies to ensure efficacy. However, anti-inflammatory approaches should be considered with extreme caution since inflammation not only causes detrimental effects in muscular tissue but can also support muscle regeneration, as demonstrated in experimental models [129,130]. So far, different P2X7R antagonists have been tested in clinical trials for chronic inflammatory disorders in the past few years (Supplemental Table S1). Although characterized by satisfactory safety and tolerability profile, they were not effective at the designed outcomes. New emerging compounds targeting P2XR7 with high specificity and efficacy were produced [131,132]. Noteworthy, before proposing new P2XR7 antagonists for muscle diseases, the analysis of in vivo P2X7R conditional gene inactivation in muscle cells versus innate/adaptive immune cells can provide relevant and novel inputs. Moreover, targeting other components of the inflammatory machinery such as IL-1β and NLRP3 inflammasome have to be considered. In this regard, IL-1 receptor antagonist has been shown to improve motor functional outcomes in *mdx* mice, although dosage and timing optimization is needed before application in dystrophic patients [57]. In addition it has to be considered that IL-1β production can be mediated by other inflammasomes rather than NLRP3 or by inflammasome-independent pathways; thus inhibitors aimed at IL-1β can result in unintentional immunosuppressive effects. In the past decade, many small molecule inhibitors for NLRP3 inflammasome have been reported and some of them have shown remarkable therapeutic potential, i.e., MCC950, Tranilast and OLT1177 [133]. However, there are no evidences of efficacy of the latter compounds in experimental models of muscular dystrophies.

As in other biological systems, the eATP/purinergic pathway is finely modulated also in muscle cells, which are adequately fitted with molecules regulating ATP release, metabolism, feedback control and signal activation. Challenging is the development of additional preclinical studies aimed to evaluate the relevance and potential therapeutic effectiveness of other ATP receptors, of the ATP channels, Pannexins and Connexins and of adenosine receptors in dystrophic or inflammatory muscle diseases.

Supplementary Materials: The following are available online at http://www.mdpi.com/1422-0067/21/17/5963/s1. Supplemental Table S1: anti-P2X7R drugs in clinical trials. List of the available anti-P2X7R drugs which have been proposed in clinical trials.

Author Contributions: Conceptualization, C.P and E.G.; writing, original draft preparation, C.P., L.R., E.G.; review and editing, S.B. (Santina Bruzzone), E.P., E.G. and C.B.; visualization, S.B. (Serena Baratto), E.P. and E.G.; funding acquisition, E.G. and C.B.; supervision, C.M., E.G. and C.B. All authors have read and agreed to the published version of the manuscript.

Funding: This research was supported by Telethon-Italy grant GGP17192, and by Italian Ministry of Health (RF 2016-02364503).

Conflicts of Interest: The authors declare no conflict of interest.

References

1. Park, S.Y.; Kim, I.S. Engulfment signals and the phagocytic machinery for apoptotic cell clearance. *Exp. Mol. Med.* **2017**, *49*, e331. [CrossRef] [PubMed]
2. Forrester, T.; Williams, C.A. Release of adenosine triphosphate from isolated adult heart cells in response to hypoxia. *J. Physiol.* **1977**, *268*, 371–390. [CrossRef] [PubMed]
3. Kroemer, G.; Galluzzi, L.; Kepp, O.; Zitvogel, L. Immunogenic cell death in cancer therapy. *Annu. Rev. Immunol.* **2013**, *31*, 51–72. [CrossRef] [PubMed]
4. Giuliani, A.L.; Sarti, A.C.; Di Virgilio, F. Extracellular nucleotides and nucleosides as signalling molecules. *Immunol. Lett.* **2018**, *205*, 16–24. [CrossRef] [PubMed]
5. North, R.A. Molecular physiology of P2X receptors. *Physiol. Rev.* **2002**, *82*, 1013–1067. [CrossRef]
6. North, R.A. P2X receptors. *Philos. Trans. R. Soc. Lond B Biol. Sci.* **2016**, *371*, 1700. [CrossRef]

7. Karasawa, A.; Kawate, T. Structural basis for subtype-specific inhibition of the P2X7 receptor. *Elife* **2016**, *5*. [CrossRef]
8. Harkat, M.; Peverini, L.; Cerdan, A.H.; Dunning, K.; Beudez, J.; Martz, A.; Calimet, N.; Specht, A.; Cecchini, M.; Chataigneau, T.; et al. On the permeation of large organic cations through the pore of ATP-gated P2X receptors. *Proc. Natl. Acad Sci. USA* **2017**, *114*, E3786–E3795. [CrossRef]
9. Browne, L.E.; North, R.A. P2X receptor intermediate activation states have altered nucleotide selectivity. *J. Neurosci.* **2013**, *33*, 14801–14808. [CrossRef]
10. Karasawa, A.; Michalski, K.; Mikhelzon, P.; Kawate, T. The P2X7 receptor forms a dye-permeable pore independent of its intracellular domain but dependent on membrane lipid composition. *Elife* **2017**, *6*. [CrossRef]
11. Kaczmarek-Hajek, K.; Zhang, J.; Kopp, R.; Grosche, A.; Rissiek, B.; Saul, A.; Bruzzone, S.; Engel, T.; Jooss, T.; Krautloher, A.; et al. Re-evaluation of neuronal P2X7 expression using novel mouse models and a P2X7-specific nanobody. *Elife* **2018**, *7*. [CrossRef] [PubMed]
12. Bruzzone, S.; Basile, G.; Chothi, M.P.; Nobbio, L.; Usai, C.; Jacchetti, E.; Schenone, A.; Guse, A.H.; Di Virgilio, F.; De Flora, A.; et al. Diadenosine homodinucleotide products of ADP-ribosyl cyclases behave as modulators of the purinergic receptor P2X7. *J. Biol. Chem.* **2010**, *285*, 21165–21174. [CrossRef] [PubMed]
13. Pelegrin, P.; Surprenant, A. Pannexin-1 couples to maitotoxin- and nigericin-induced interleukin-1beta release through a dye uptake-independent pathway. *J. Biol. Chem.* **2007**, *282*, 2386–2394. [CrossRef] [PubMed]
14. Baroja-Mazo, A.; Barbera-Cremades, M.; Pelegrin, P. The participation of plasma membrane hemichannels to purinergic signaling. *Biochim. Biophys. Acta* **2013**, *1828*, 79–93. [CrossRef]
15. Di Virgilio, F.; Schmalzing, G.; Markwardt, F. The Elusive P2X7 Macropore. *Trends Cell Biol.* **2018**, *28*, 392–404. [CrossRef]
16. Surprenant, A.; Rassendren, F.; Kawashima, E.; North, R.A.; Buell, G. The cytolytic P2Z receptor for extracellular ATP identified as a P2X receptor (P2X7). *Science* **1996**, *272*, 735–738. [CrossRef]
17. Young, C.N.; Sinadinos, A.; Lefebvre, A.; Chan, P.; Arkle, S.; Vaudry, D.; Gorecki, D.C. A novel mechanism of autophagic cell death in dystrophic muscle regulated by P2RX7 receptor large-pore formation and HSP90. *Autophagy* **2015**, *11*, 113–130. [CrossRef]
18. Burnstock, G.; Knight, G.E. The potential of P2X7 receptors as a therapeutic target, including inflammation and tumour progression. *Purinergic Signal.* **2018**, *14*, 1–18. [CrossRef]
19. Volonte, C.; Apolloni, S.; Skaper, S.D.; Burnstock, G. P2X7 receptors: Channels, pores and more. *CNS Neurol. Disord. Drug Targets* **2012**, *11*, 705–721. [CrossRef]
20. Monif, M.; Burnstock, G.; Williams, D.A. Microglia: Proliferation and activation driven by the P2X7 receptor. *Int. J. Biochem. Cell Biol.* **2010**, *42*, 1753–1756. [CrossRef]
21. Massicot, F.; Hache, G.; David, L.; Chen, D.; Leuxe, C.; Garnier-Legrand, L.; Rat, P.; Laprevote, O.; Coudore, F. P2X7 Cell death receptor activation and mitochondrial impairment in oxaliplatin-induced apoptosis and neuronal injury: Cellular mechanisms and in vivo approach. *PLoS ONE* **2013**, *8*, e66830. [CrossRef]
22. Nobbio, L.; Sturla, L.; Fiorese, F.; Usai, C.; Basile, G.; Moreschi, I.; Benvenuto, F.; Zocchi, E.; De Flora, A.; Schenone, A.; et al. P2X7-mediated increased intracellular calcium causes functional derangement in Schwann cells from rats with CMT1A neuropathy. *J. Biol. Chem.* **2009**, *284*, 23146–23158. [CrossRef] [PubMed]
23. Rissiek, B.; Haag, F.; Boyer, O.; Koch-Nolte, F.; Adriouch, S. P2X7 on mouse T cells: One channel, many functions. *Front. Immunol.* **2015**, *6*, 204. [CrossRef]
24. Amoroso, F.; Capece, M.; Rotondo, A.; Cangelosi, D.; Ferracin, M.; Franceschini, A.; Raffaghello, L.; Pistoia, V.; Varesio, L.; Adinolfi, E. The P2X7 receptor is a key modulator of the PI3K/GSK3beta/VEGF signaling network: Evidence in experimental neuroblastoma. *Oncogene* **2015**, *34*, 5240–5251. [CrossRef] [PubMed]
25. Orioli, E.; De Marchi, E.; Giuliani, A.L.; Adinolfi, E. P2X7 receptor orchestrates multiple signalling pathways triggering inflammation, autophagy and metabolic/trophic responses. *Curr. Med. Chem.* **2017**, *24*, 2261–2275. [CrossRef] [PubMed]
26. Qiu, Y.; Li, W.H.; Zhang, H.Q.; Liu, Y.; Tian, X.X.; Fang, W.G. P2X7 mediates ATP-driven invasiveness in prostate cancer cells. *PLoS ONE* **2014**, *9*, e114371. [CrossRef] [PubMed]
27. Xia, J.; Yu, X.; Tang, L.; Li, G.; He, T. P2X7 receptor stimulates breast cancer cell invasion and migration via the AKT pathway. *Oncol. Rep.* **2015**, *34*, 103–110. [CrossRef]
28. Murrell-Lagnado, R.D. Regulation of P2X purinergic receptor signaling by cholesterol. *Curr. Top. Membr.* **2017**, *80*, 211–232.

29. Kim, J.E.; Kim, D.S.; Jin Ryu, H.; Il Kim, W.; Kim, M.J.; Won Kim, D.; Young Choi, S.; Kang, T.C. The effect of P2X7 receptor activation on nuclear factor-kappaB phosphorylation induced by status epilepticus in the rat hippocampus. *Hippocampus* **2013**, *23*, 500–514. [CrossRef]
30. Cockcroft, S.; Gomperts, B.D. ATP induces nucleotide permeability in rat mast cells. *Nature* **1979**, *279*, 541–542. [CrossRef]
31. Di Virgilio, F.; Bronte, V.; Collavo, D.; Zanovello, P. Responses of mouse lymphocytes to extracellular adenosine 5′-triphosphate (ATP). Lymphocytes with cytotoxic activity are resistant to the permeabilizing effects of ATP. *J. Immunol.* **1989**, *143*, 1955–1960. [PubMed]
32. Di Virgilio, F.; Sarti, A.C.; Grassi, F. Modulation of innate and adaptive immunity by P2X ion channels. *Curr. Opin. Immunol.* **2018**, *52*, 51–59. [CrossRef] [PubMed]
33. Bianchi, G.; Vuerich, M.; Pellegatti, P.; Marimpietri, D.; Emionite, L.; Marigo, I.; Bronte, V.; Di Virgilio, F.; Pistoia, V.; Raffaghello, L. ATP/P2X7 axis modulates myeloid-derived suppressor cell functions in neuroblastoma microenvironment. *Cell Death Dis.* **2014**, *5*, e1135. [CrossRef] [PubMed]
34. Di Virgilio, F.; Dal Ben, D.; Sarti, A.C.; Giuliani, A.L.; Falzoni, S. The P2X7 Receptor in Infection and Inflammation. *Immunity* **2017**, *47*, 15–31. [CrossRef] [PubMed]
35. Antonioli, L.; Fornai, M.; Blandizzi, C.; Pacher, P.; Hasko, G. Adenosine signaling and the immune system: When a lot could be too much. *Immunol. Lett.* **2018**, *205*, 9–15. [CrossRef]
36. Banachewicz, W.; Suplat, D.; Krzeminski, P.; Pomorski, P.; Baranska, J. P2 nucleotide receptors on C2C12 satellite cells. *Purinergic Signal.* **2005**, *1*, 249–257. [CrossRef]
37. Martinello, T.; Baldoin, M.C.; Morbiato, L.; Paganin, M.; Tarricone, E.; Schiavo, G.; Bianchini, E.; Sandona, D.; Betto, R. Extracellular ATP signaling during differentiation of C2C12 skeletal muscle cells: Role in proliferation. *Mol. Cell Biochem.* **2011**, *351*, 183–196. [CrossRef]
38. Araya, R.; Riquelme, M.A.; Brandan, E.; Saez, J.C. The formation of skeletal muscle myotubes requires functional membrane receptors activated by extracellular ATP. *Brain Res. Brain Res. Rev.* **2004**, *47*, 174–188. [CrossRef]
39. Almada, A.E.; Wagers, A.J. Molecular circuitry of stem cell fate in skeletal muscle regeneration, ageing and disease. *Nat. Rev. Mol. Cell Biol.* **2016**, *17*, 267–279. [CrossRef]
40. Zammit, P.S.; Golding, J.P.; Nagata, Y.; Hudon, V.; Partridge, T.A.; Beauchamp, J.R. Muscle satellite cells adopt divergent fates: A mechanism for self-renewal? *J. Cell Biol.* **2004**, *166*, 347–357. [CrossRef]
41. Yin, H.; Price, F.; Rudnicki, M.A. Satellite cells and the muscle stem cell niche. *Physiol. Rev.* **2013**, *93*, 23–67. [CrossRef]
42. Sinadinos, A.; Young, C.N.; Al-Khalidi, R.; Teti, A.; Kalinski, P.; Mohamad, S.; Floriot, L.; Henry, T.; Tozzi, G.; Jiang, T.; et al. P2RX7 purinoceptor: A therapeutic target for ameliorating the symptoms of duchenne muscular dystrophy. *PLoS Med.* **2015**, *12*, e1001888. [CrossRef] [PubMed]
43. Sandona, D.; Gastaldello, S.; Martinello, T.; Betto, R. Characterization of the ATP-hydrolysing activity of alpha-sarcoglycan. *Biochem. J.* **2004**, *381*, 105–112. [CrossRef]
44. Zimmermann, H. Extracellular metabolism of ATP and other nucleotides. *Naunyn Schmiedebergs Arch. Pharmacol.* **2000**, *362*, 299–309. [CrossRef] [PubMed]
45. Bollen, M.; Gijsbers, R.; Ceulemans, H.; Stalmans, W.; Stefan, C. Nucleotide pyrophosphatases/phosphodiesterases on the move. *Crit. Rev. Biochem. Mol. Biol.* **2000**, *35*, 393–432. [CrossRef] [PubMed]
46. Young, C.N.; Brutkowski, W.; Lien, C.F.; Arkle, S.; Lochmuller, H.; Zablocki, K.; Gorecki, D.C. P2X7 purinoceptor alterations in dystrophic mdx mouse muscles: Relationship to pathology and potential target for treatment. *J. Cell Mol. Med.* **2012**, *16*, 1026–1037. [CrossRef] [PubMed]
47. Khakh, B.S.; North, R.A. P2X receptors as cell-surface ATP sensors in health and disease. *Nature* **2006**, *442*, 527–532. [CrossRef]
48. Yeung, D.; Zablocki, K.; Lien, C.F.; Jiang, T.; Arkle, S.; Brutkowski, W.; Brown, J.; Lochmuller, H.; Simon, J.; Barnard, E.A.; et al. Increased susceptibility to ATP via alteration of P2X receptor function in dystrophic mdx mouse muscle cells. *FASEB J.* **2006**, *20*, 610–620. [CrossRef]
49. Guerra, A.N.; Gavala, M.L.; Chung, H.S.; Bertics, P.J. Nucleotide receptor signalling and the generation of reactive oxygen species. *Purinergic Signal.* **2007**, *3*, 39–51. [CrossRef]
50. Haslund-Vinding, J.; McBean, G.; Jaquet, V.; Vilhardt, F. NADPH oxidases in oxidant production by microglia: Activating receptors, pharmacology and association with disease. *Br. J. Pharmacol.* **2017**, *174*, 1733–1749. [CrossRef]

51. Adinolfi, E.; Giuliani, A.L.; De Marchi, E.; Pegoraro, A.; Orioli, E.; Di Virgilio, F. The P2X7 receptor: A main player in inflammation. *Biochem. Pharmacol.* **2018**, *151*, 234–244. [CrossRef] [PubMed]
52. Martinon, F.; Burns, K.; Tschopp, J. The inflammasome: A molecular platform triggering activation of inflammatory caspases and processing of proIL-beta. *Mol. Cell* **2002**, *10*, 417–426. [CrossRef]
53. Dinarello, C.A. Immunological and inflammatory functions of the interleukin-1 family. *Annu. Rev. Immunol.* **2009**, *27*, 519–550. [CrossRef]
54. Bryant, C.; Fitzgerald, K.A. Molecular mechanisms involved in inflammasome activation. *Trends Cell Biol.* **2009**, *19*, 455–464. [CrossRef] [PubMed]
55. Rawat, R.; Cohen, T.V.; Ampong, B.; Francia, D.; Henriques-Pons, A.; Hoffman, E.P.; Nagaraju, K. Inflammasome up-regulation and activation in dysferlin-deficient skeletal muscle. *Am. J. Pathol.* **2010**, *176*, 2891–2900. [CrossRef] [PubMed]
56. Cohen, T.V.; Many, G.M.; Fleming, B.D.; Gnocchi, V.F.; Ghimbovschi, S.; Mosser, D.M.; Hoffman, E.P.; Partridge, T.A. Upregulated IL-1beta in dysferlin-deficient muscle attenuates regeneration by blunting the response to pro-inflammatory macrophages. *Skelet. Muscle* **2015**, *5*, 24. [CrossRef]
57. Benny Klimek, M.E.; Sali, A.; Rayavarapu, S.; Van der Meulen, J.H.; Nagaraju, K. Effect of the IL-1 receptor antagonist kineret(r) on disease phenotype in mdx mice. *PLoS ONE* **2016**, *11*, e0155944. [CrossRef]
58. Babelova, A.; Moreth, K.; Tsalastra-Greul, W.; Zeng-Brouwers, J.; Eickelberg, O.; Young, M.F.; Bruckner, P.; Pfeilschifter, J.; Schaefer, R.M.; Grone, H.J.; et al. Biglycan, a danger signal that activates the NLRP3 inflammasome via toll-like and P2X receptors. *J. Biol. Chem.* **2009**, *284*, 24035–24048. [CrossRef]
59. Scaffidi, P.; Misteli, T.; Bianchi, M.E. Release of chromatin protein HMGB1 by necrotic cells triggers inflammation. *Nature* **2002**, *418*, 191–195. [CrossRef]
60. De Mori, R.; Straino, S.; Di Carlo, A.; Mangoni, A.; Pompilio, G.; Palumbo, R.; Bianchi, M.E.; Capogrossi, M.C.; Germani, A. Multiple effects of high mobility group box protein 1 in skeletal muscle regeneration. *Arter. Thromb. Vasc. Biol.* **2007**, *27*, 2377–2383. [CrossRef]
61. Sagheddu, R.; Chiappalupi, S.; Salvadori, L.; Riuzzi, F.; Donato, R.; Sorci, G. Targeting RAGE as a potential therapeutic approach to Duchenne muscular dystrophy. *Hum. Mol. Genet.* **2018**, *27*, 3734–3746. [CrossRef] [PubMed]
62. Kelley, N.; Jeltema, D.; Duan, Y.; He, Y. The NLRP3 inflammasome: An overview of mechanisms of activation and regulation. *Int. J. Mol. Sci.* **2019**, *20*, 3328. [CrossRef]
63. De Nardo, D. Toll-like receptors: Activation, signalling and transcriptional modulation. *Cytokine* **2015**, *74*, 181–189. [CrossRef] [PubMed]
64. Shi, H.; Wang, Y.; Li, X.; Zhan, X.; Tang, M.; Fina, M.; Su, L.; Pratt, D.; Bu, C.H.; Hildebrand, S.; et al. NLRP3 activation and mitosis are mutually exclusive events coordinated by NEK7, a new inflammasome component. *Nat. Immunol.* **2016**, *17*, 250–258. [CrossRef] [PubMed]
65. Munoz-Planillo, R.; Kuffa, P.; Martinez-Colon, G.; Smith, B.L.; Rajendiran, T.M.; Nunez, G. K(+) efflux is the common trigger of NLRP3 inflammasome activation by bacterial toxins and particulate matter. *Immunity* **2013**, *38*, 1142–1153. [CrossRef] [PubMed]
66. Christgen, S.; Place, D.E.; Kanneganti, T.D. Toward targeting inflammasomes: Insights into their regulation and activation. *Cell Res.* **2020**, *30*, 315–327. [CrossRef]
67. He, Y.; Zeng, M.Y.; Yang, D.; Motro, B.; Nunez, G. NEK7 is an essential mediator of NLRP3 activation downstream of potassium efflux. *Nature* **2016**, *530*, 354–357. [CrossRef]
68. Mercuri, E.; Bonnemann, C.G.; Muntoni, F. Muscular dystrophies. *Lancet* **2019**, *394*, 2025–2038. [CrossRef]
69. Birnkrant, D.J.; Bushby, K.; Bann, C.M.; Apkon, S.D.; Blackwell, A.; Colvin, M.K.; Cripe, L.; Herron, A.R.; Kennedy, A.; Kinnett, K.; et al. Diagnosis and management of Duchenne muscular dystrophy, part 3: Primary care, emergency management, psychosocial care, and transitions of care across the lifespan. *Lancet Neurol.* **2018**, *17*, 445–455. [CrossRef]
70. Kirschner, J.; Lochmuller, H. Sarcoglycanopathies. *Handb. Clin. Neurol.* **2011**, *101*, 41–46.
71. Petrilli, V.; Dostert, C.; Muruve, D.A.; Tschopp, J. The inflammasome: A danger sensing complex triggering innate immunity. *Curr. Opin. Immunol.* **2007**, *19*, 615–622. [CrossRef] [PubMed]
72. Tidball, J.G.; Welc, S.S.; Wehling-Henricks, M. Immunobiology of inherited muscular dystrophies. *Compr. Physiol.* **2018**, *8*, 1313–1356. [PubMed]
73. Wehling, M.; Spencer, M.J.; Tidball, J.G. A nitric oxide synthase transgene ameliorates muscular dystrophy in mdx mice. *J. Cell Biol.* **2001**, *155*, 123–131. [CrossRef] [PubMed]

74. Tidball, J.G.; Villalta, S.A. Regulatory interactions between muscle and the immune system during muscle regeneration. *Am. J. Physiol. Regul. Integr. Comp. Physiol.* **2010**, *298*, R1173–R1187. [CrossRef] [PubMed]
75. Burzyn, D.; Kuswanto, W.; Kolodin, D.; Shadrach, J.L.; Cerletti, M.; Jang, Y.; Sefik, E.; Tan, T.G.; Wagers, A.J.; Benoist, C.; et al. A special population of regulatory T cells potentiates muscle repair. *Cell* **2013**, *155*, 1282–1295. [CrossRef]
76. Villalta, S.A.; Rosenthal, W.; Martinez, L.; Kaur, A.; Sparwasser, T.; Tidball, J.G.; Margeta, M.; Spencer, M.J.; Bluestone, J.A. Regulatory T cells suppress muscle inflammation and injury in muscular dystrophy. *Sci. Transl. Med.* **2014**, *6*, 258ra142. [CrossRef]
77. Villalta, S.A.; Deng, B.; Rinaldi, C.; Wehling-Henricks, M.; Tidball, J.G. IFN-gamma promotes muscle damage in the mdx mouse model of Duchenne muscular dystrophy by suppressing M2 macrophage activation and inhibiting muscle cell proliferation. *J. Immunol.* **2011**, *187*, 5419–5428. [CrossRef]
78. Gazzerro, E.; Baldassari, S.; Assereto, S.; Fruscione, F.; Pistorio, A.; Panicucci, C.; Volpi, S.; Perruzza, L.; Fiorillo, C.; Minetti, C.; et al. Enhancement of muscle T regulatory cells and improvement of muscular dystrophic process in mdx mice by blockade of extracellular ATP/P2X axis. *Am. J. Pathol.* **2015**, *185*, 3349–3360. [CrossRef]
79. Ardissone, V.; Radaelli, E.; Zaratin, P.; Ardizzone, M.; Ladel, C.; Gattorno, M.; Martini, A.; Grassi, F.; Traggiai, E. Pharmacologic P2X purinergic receptor antagonism in the treatment of collagen-induced arthritis. *Arthritis Rheum.* **2011**, *63*, 3323–3332. [CrossRef]
80. Vergani, A.; Fotino, C.; D'Addio, F.; Tezza, S.; Podetta, M.; Gatti, F.; Chin, M.; Bassi, R.; Molano, R.D.; Corradi, D.; et al. Effect of the purinergic inhibitor oxidized ATP in a model of islet allograft rejection. *Diabetes* **2013**, *62*, 1665–1675. [CrossRef]
81. Schenk, U.; Frascoli, M.; Proietti, M.; Geffers, R.; Traggiai, E.; Buer, J.; Ricordi, C.; Westendorf, A.M.; Grassi, F. ATP inhibits the generation and function of regulatory T cells through the activation of purinergic P2X receptors. *Sci. Signal.* **2011**, *4*, ra12. [CrossRef] [PubMed]
82. Frascoli, M.; Marcandalli, J.; Schenk, U.; Grassi, F. Purinergic P2X7 receptor drives T cell lineage choice and shapes peripheral gammadelta cells. *J. Immunol.* **2012**, *189*, 174–180. [CrossRef] [PubMed]
83. Sociali, G.; Visigalli, D.; Prukop, T.; Cervellini, I.; Mannino, E.; Venturi, C.; Bruzzone, S.; Sereda, M.W.; Schenone, A. Tolerability and efficacy study of P2X7 inhibition in experimental Charcot-Marie-Tooth type 1A (CMT1A) neuropathy. *Neurobiol. Dis.* **2016**, *95*, 145–157. [CrossRef] [PubMed]
84. Al-Khalidi, R.; Panicucci, C.; Cox, P.; Chira, N.; Rog, J.; Young, C.N.J.; McGeehan, R.E.; Ambati, K.; Ambati, J.; Zablocki, K.; et al. Zidovudine ameliorates pathology in the mouse model of Duchenne muscular dystrophy via P2RX7 purinoceptor antagonism. *Acta Neuropathol. Commun.* **2018**, *6*, 27. [CrossRef]
85. Fowler, B.J.; Gelfand, B.D.; Kim, Y.; Kerur, N.; Tarallo, V.; Hirano, Y.; Amarnath, S.; Fowler, D.H.; Radwan, M.; Young, M.T.; et al. Nucleoside reverse transcriptase inhibitors possess intrinsic anti-inflammatory activity. *Science* **2014**, *346*, 1000–1003. [CrossRef]
86. Gazzerro, E.; Baratto, S.; Assereto, S.; Baldassari, S.; Panicucci, C.; Raffaghello, L.; Scudieri, P.; De Battista, D.; Fiorillo, C.; Volpi, S.; et al. The danger signal extracellular ATP is involved in the immunomediated damage of alpha-sarcoglycan-deficient muscular dystrophy. *Am. J. Pathol.* **2019**, *189*, 354–369. [CrossRef]
87. Betto, R.; Senter, L.; Ceoldo, S.; Tarricone, E.; Biral, D.; Salviati, G. Ecto-ATPase activity of alpha-sarcoglycan (adhalin). *J. Biol. Chem.* **1999**, *274*, 7907–7912. [CrossRef]
88. Mohamad, N.S.; Sinadinos, A.; Gorecki, D.C.; Zioupos, P.; Tong, J. Impact of P2RX7 ablation on the morphological, mechanical and tissue properties of bones in a murine model of duchenne muscular dystrophy. *J. Biomech.* **2016**, *49*, 3444–3451. [CrossRef]
89. Saez, J.C.; Berthoud, V.M.; Branes, M.C.; Martinez, A.D.; Beyer, E.C. Plasma membrane channels formed by connexins: Their regulation and functions. *Physiol. Rev.* **2003**, *83*, 1359–1400. [CrossRef]
90. Bruzzone, S.; Guida, L.; Zocchi, E.; Franco, L.; De Flora, A. Connexin 43 hemi channels mediate Ca2+-regulated transmembrane NAD+ fluxes in intact cells. *FASEB J.* **2001**, *15*, 10–12. [CrossRef]
91. Navis, K.E.; Fan, C.Y.; Trang, T.; Thompson, R.J.; Derksen, D.J. Pannexin 1 channels as a therapeutic target: Structure, inhibition, and outlook. *ACS Chem. Neurosci.* **2020**, *11*, 2163–2172. [CrossRef] [PubMed]
92. Cea, L.A.; Riquelme, M.A.; Cisterna, B.A.; Puebla, C.; Vega, J.L.; Rovegno, M.; Saez, J.C. Connexin- and pannexin-based channels in normal skeletal muscles and their possible role in muscle atrophy. *J. Membr. Biol.* **2012**, *245*, 423–436. [CrossRef] [PubMed]

93. Osorio-Fuentealba, C.; Contreras-Ferrat, A.E.; Altamirano, F.; Espinosa, A.; Li, Q.; Niu, W.; Lavandero, S.; Klip, A.; Jaimovich, E. Electrical stimuli release ATP to increase GLUT4 translocation and glucose uptake via PI3Kgamma-Akt-AS160 in skeletal muscle cells. *Diabetes* **2013**, *62*, 1519–1526. [CrossRef]
94. Linden, J.; Koch-Nolte, F.; Dahl, G. Purine release, metabolism, and signaling in the inflammatory response. *Annu. Rev. Immunol.* **2019**, *37*, 325–347. [CrossRef] [PubMed]
95. Langlois, S.; Xiang, X.; Young, K.; Cowan, B.J.; Penuela, S.; Cowan, K.N. Pannexin 1 and pannexin 3 channels regulate skeletal muscle myoblast proliferation and differentiation. *J. Biol. Chem.* **2014**, *289*, 30717–30731. [CrossRef] [PubMed]
96. Pham, T.L.; St-Pierre, M.E.; Ravel-Chapuis, A.; Parks, T.E.C.; Langlois, S.; Penuela, S.; Jasmin, B.J.; Cowan, K.N. Expression of Pannexin 1 and Pannexin 3 during skeletal muscle development, regeneration, and Duchenne muscular dystrophy. *J. Cell Physiol.* **2018**, *233*, 7057–7070. [CrossRef] [PubMed]
97. Cea, L.A.; Riquelme, M.A.; Vargas, A.A.; Urrutia, C.; Saez, J.C. Pannexin 1 channels in skeletal muscles. *Front. Physiol.* **2014**, *5*, 139. [CrossRef]
98. Riquelme, M.A.; Cea, L.A.; Vega, J.L.; Boric, M.P.; Monyer, H.; Bennett, M.V.; Frank, M.; Willecke, K.; Saez, J.C. The ATP required for potentiation of skeletal muscle contraction is released via pannexin hemichannels. *Neuropharmacology* **2013**, *75*, 594–603. [CrossRef]
99. Jorquera, G.; Altamirano, F.; Contreras-Ferrat, A.; Almarza, G.; Buvinic, S.; Jacquemond, V.; Jaimovich, E.; Casas, M. Cav1.1 controls frequency-dependent events regulating adult skeletal muscle plasticity. *J. Cell Sci.* **2013**, *126*, 1189–1198. [CrossRef]
100. Pillon, N.J.; Li, Y.E.; Fink, L.N.; Brozinick, J.T.; Nikolayev, A.; Kuo, M.S.; Bilan, P.J.; Klip, A. Nucleotides released from palmitate-challenged muscle cells through pannexin-3 attract monocytes. *Diabetes* **2014**, *63*, 3815–3826. [CrossRef]
101. Diaz-Vegas, A.; Campos, C.A.; Contreras-Ferrat, A.; Casas, M.; Buvinic, S.; Jaimovich, E.; Espinosa, A. ROS production via P2Y1-PKC-NOX2 is triggered by extracellular atp after electrical stimulation of skeletal muscle cells. *PLoS ONE* **2015**, *10*, e0129882. [CrossRef] [PubMed]
102. Plotkin, L.I.; Davis, H.M.; Cisterna, B.A.; Saez, J.C. Connexins and pannexins in bone and skeletal muscle. *Curr. Osteoporos. Rep.* **2017**, *15*, 326–334. [CrossRef] [PubMed]
103. Bao, L.; Locovei, S.; Dahl, G. Pannexin membrane channels are mechanosensitive conduits for ATP. *FEBS Lett.* **2004**, *572*, 65–68. [CrossRef] [PubMed]
104. Pelegrin, P.; Surprenant, A. Pannexin-1 mediates large pore formation and interleukin-1beta release by the ATP-gated P2X7 receptor. *EMBO J.* **2006**, *25*, 5071–5082. [CrossRef] [PubMed]
105. Locovei, S.; Scemes, E.; Qiu, F.; Spray, D.C.; Dahl, G. Pannexin1 is part of the pore forming unit of the P2X (7) receptor death complex. *FEBS Lett.* **2007**, *581*, 483–488. [CrossRef]
106. Nouet, J.; Himelman, E.; Lahey, K.C.; Zhao, Q.; Fraidenraich, D. Connexin-43 reduction prevents muscle defects in a mouse model of manifesting Duchenne muscular dystrophy female carriers. *Sci. Rep.* **2020**, *10*, 5683. [CrossRef]
107. Araya, R.; Eckardt, D.; Riquelme, M.A.; Willecke, K.; Saez, J.C. Presence and importance of connexin43 during myogenesis. *Cell Commun. Adhes.* **2003**, *10*, 451–456. [CrossRef]
108. Cea, L.A.; Bevilacqua, J.A.; Arriagada, C.; Cardenas, A.M.; Bigot, A.; Mouly, V.; Saez, J.C.; Caviedes, P. The absence of dysferlin induces the expression of functional connexin-based hemichannels in human myotubes. *BMC Cell Biol.* **2016**, *17* (Suppl. 1), 15. [CrossRef]
109. Cea, L.A.; Puebla, C.; Cisterna, B.A.; Escamilla, R.; Vargas, A.A.; Frank, M.; Martinez-Montero, P.; Prior, C.; Molano, J.; Esteban-Rodriguez, I.; et al. Fast skeletal myofibers of mdx mouse, model of Duchenne muscular dystrophy, express connexin hemichannels that lead to apoptosis. *Cell Mol. Life Sci.* **2016**, *73*, 2583–2599. [CrossRef]
110. Wang, N.; De Bock, M.; Decrock, E.; Bol, M.; Gadicherla, A.; Vinken, M.; Rogiers, V.; Bukauskas, F.F.; Bultynck, G.; Leybaert, L. Paracrine signaling through plasma membrane hemichannels. *Biochim. Biophys. Acta* **2013**, *1828*, 35–50. [CrossRef]
111. Wang, X.; Qin, W.; Xu, X.; Xiong, Y.; Zhang, Y.; Zhang, H.; Sun, B. Endotoxin-induced autocrine ATP signaling inhibits neutrophil chemotaxis through enhancing myosin light chain phosphorylation. *Proc. Natl. Acad. Sci. USA* **2017**, *114*, 4483–4488. [CrossRef] [PubMed]

112. Eltzschig, H.K.; Eckle, T.; Mager, A.; Kuper, N.; Karcher, C.; Weissmuller, T.; Boengler, K.; Schulz, R.; Robson, S.C.; Colgan, S.P. ATP release from activated neutrophils occurs via connexin 43 and modulates adenosine-dependent endothelial cell function. *Circ. Res.* **2006**, *99*, 1100–1108. [CrossRef] [PubMed]
113. Gu, B.J.; Wiley, J.S. Rapid ATP-induced release of matrix metalloproteinase 9 is mediated by the P2X7 receptor. *Blood* **2006**, *107*, 4946–4953. [CrossRef] [PubMed]
114. Young, C.N.J.; Chira, N.; Rog, J.; Al-Khalidi, R.; Benard, M.; Galas, L.; Chan, P.; Vaudry, D.; Zablocki, K.; Gorecki, D.C. Sustained activation of P2X7 induces MMP-2-evoked cleavage and functional purinoceptor inhibition. *J. Mol. Cell Biol.* **2018**, *10*, 229–242. [CrossRef] [PubMed]
115. Cui, N.; Hu, M.; Khalil, R.A. Biochemical and biological attributes of matrix metalloproteinases. *Prog. Mol. Biol. Transl. Sci.* **2017**, *147*, 1–73.
116. Young, C.N.J.; Gorecki, D.C. P2RX7 purinoceptor as a therapeutic target-the second coming? *Front. Chem.* **2018**, *6*, 248. [CrossRef]
117. Bours, M.J.; Swennen, E.L.; Di Virgilio, F.; Cronstein, B.N.; Dagnelie, P.C. Adenosine 5′-triphosphate and adenosine as endogenous signaling molecules in immunity and inflammation. *Pharmacol. Ther.* **2006**, *112*, 358–404. [CrossRef]
118. De Torre-Minguela, C.; Mesa Del Castillo, P.; Pelegrin, P. The NLRP3 and pyrin inflammasomes: Implications in the pathophysiology of autoinflammatory diseases. *Front. Immunol.* **2017**, *8*, 43. [CrossRef]
119. Csoka, B.; Selmeczy, Z.; Koscso, B.; Nemeth, Z.H.; Pacher, P.; Murray, P.J.; Kepka-Lenhart, D.; Morris, S.M., Jr.; Gause, W.C.; Leibovich, S.J.; et al. Adenosine promotes alternative macrophage activation via A2A and A2B receptors. *FASEB J.* **2012**, *26*, 376–386. [CrossRef]
120. Wilson, J.M.; Ross, W.G.; Agbai, O.N.; Frazier, R.; Figler, R.A.; Rieger, J.; Linden, J.; Ernst, P.B. The A2B adenosine receptor impairs the maturation and immunogenicity of dendritic cells. *J. Immunol.* **2009**, *182*, 4616–4623. [CrossRef]
121. Ehrentraut, H.; Westrich, J.A.; Eltzschig, H.K.; Clambey, E.T. Adora2b adenosine receptor engagement enhances regulatory T cell abundance during endotoxin-induced pulmonary inflammation. *PLoS ONE* **2012**, *7*, e32416. [CrossRef] [PubMed]
122. Da Silva, J.L.G.; Passos, D.F.; Bernardes, V.M.; Leal, D.B.R. ATP and adenosine: Role in the immunopathogenesis of rheumatoid arthritis. *Immunol. Lett.* **2019**, *214*, 55–64. [CrossRef] [PubMed]
123. Garrido, W.; Jara, C.; Torres, A.; Suarez, R.; Cappelli, C.; Oyarzun, C.; Quezada, C.; San Martin, R. Blockade of the adenosine A3 receptor attenuates caspase 1 activation in renal tubule epithelial cells and decreases interleukins IL-1beta and IL-18 in diabetic rats. *Int. J. Mol. Sci.* **2019**, *20*, 4531. [CrossRef]
124. Lynge, J.; Hellsten, Y. Distribution of adenosine A1, A2A and A2B receptors in human skeletal muscle. *Acta Physiol. Scand.* **2000**, *169*, 283–290. [CrossRef] [PubMed]
125. Lynge, J.; Schulte, G.; Nordsborg, N.; Fredholm, B.B.; Hellsten, Y. Adenosine A 2B receptors modulate cAMP levels and induce CREB but not ERK1/2 and p38 phosphorylation in rat skeletal muscle cells. *Biochem. Biophys. Res. Commun.* **2003**, *307*, 180–187. [CrossRef]
126. Dobson, J.G., Jr.; Rubio, R.; Berne, R.M. Role of adenine nucleotides, adenosine, and inorganic phosphate in the regulation of skeletal muscle blood flow. *Circ. Res.* **1971**, *29*, 375–384. [CrossRef]
127. Vergauwen, L.; Hespel, P.; Richter, E.A. Adenosine receptors mediate synergistic stimulation of glucose uptake and transport by insulin and by contractions in rat skeletal muscle. *J. Clin. Investig.* **1994**, *93*, 974–981. [CrossRef]
128. Soslow, J.H.; Markham, L.W.; Burnette, W.B.; Galindo, C.L.; Feoktistov, I.; Raucci, F.J., Jr.; Damon, B.M.; Sawyer, D.B.; Ryzhov, S. Increased number of circulating CD8/CD26 T cells in the blood of duchenne muscular dystrophy patients is associated with augmented binding of adenosine deaminase and higher muscular strength scores. *Front. Pharmacol.* **2017**, *8*, 914. [CrossRef]
129. Latroche, C.; Weiss-Gayet, M.; Muller, L.; Gitiaux, C.; Leblanc, P.; Liot, S.; Ben-Larbi, S.; Abou-Khalil, R.; Verger, N.; Bardot, P.; et al. Coupling between myogenesis and angiogenesis during skeletal muscle regeneration is stimulated by restorative macrophages. *Stem Cell Rep.* **2017**, *9*, 2018–2033. [CrossRef]
130. Dort, J.; Fabre, P.; Molina, T.; Dumont, N.A. Macrophages are key regulators of stem cells during skeletal muscle regeneration and diseases. *Stem Cells Int.* **2019**, *2019*, 4761427. [CrossRef]
131. Koch-Nolte, F.; Eichhoff, A.; Pinto-Espinoza, C.; Schwarz, N.; Schafer, T.; Menzel, S.; Haag, F.; Demeules, M.; Gonde, H.; Adriouch, S. Novel biologics targeting the P2X7 ion channel. *Curr. Opin. Pharmacol.* **2019**, *47*, 110–118. [CrossRef] [PubMed]

132. Danquah, W.; Meyer-Schwesinger, C.; Rissiek, B.; Pinto, C.; Serracant-Prat, A.; Amadi, M.; Iacenda, D.; Knop, J.H.; Hammel, A.; Bergmann, P.; et al. Nanobodies that block gating of the P2X7 ion channel ameliorate inflammation. *Sci. Transl. Med.* **2016**, *8*, 366ra162. [CrossRef] [PubMed]
133. Zahid, A.; Li, B.; Kombe, A.J.K.; Jin, T.; Tao, J. Pharmacological inhibitors of the NLRP3 inflammasome. *Front. Immunol.* **2019**, *10*, 2538. [CrossRef] [PubMed]

doi:10.1093/brain/awaa228 BRAIN 2020: 143; 2696–2708 | 2696

BRAIN
A JOURNAL OF NEUROLOGY

New genotype-phenotype correlations in a large European cohort of patients with sarcoglycanopathy

Jorge Alonso-Pérez,[1] Lidia González-Quereda,[2,3] Luca Bello,[4] Michela Guglieri,[5] Volker Straub,[5] Pia Gallano,[2,3] Claudio Semplicini,[4] Elena Pegoraro,[4] Vittoria Zangaro,[4] Andrés Nascimento,[6] Carlos Ortez,[6] Giacomo Pietro Comi,[7] Leroy ten Dam,[8] Marianne De Visser,[8] A.J. van der Kooi,[8] Cristina Garrido,[9] Manuela Santos,[9] Ulrike Schara,[10] Andrea Gangfuß,[10] Nicoline Løkken,[11] Jesper Helbo Storgaard,[11] John Vissing,[11] Benedikt Schoser,[12] Gabriele Dekomien,[13] Bjarne Udd,[14] Johanna Palmio,[14] Adele D'Amico,[15] Luisa Politano,[16] Vincenzo Nigro,[17] Claudio Bruno,[18] Chiara Panicucci,[18] Anna Sarkozy,[19] Omar Abdel-Mannan,[19] Alicia Alonso-Jimenez,[20] Kristl G. Claeys,[21,22] David Gomez-Andrés,[23] Francina Munell,[23] Laura Costa-Comellas,[23] Jana Haberlová,[24] Marie Rohlenová,[24] De Vos Elke,[25] Jan L. De Bleecker,[25] Cristina Dominguez-González,[4,26] Giorgio Tasca,[27] Claudia Weiss,[28] Nicolas Deconinck,[29] Roberto Fernández-Torrón,[30] Adolfo López de Munain,[30] Ana Camacho-Salas,[31] Béla Melegh,[32] Kinga Hadzsiev,[32] Lea Leonardis,[33] Blaz Koritnik,[33] Matteo Garibaldi,[34] Juan Carlos de Leon-Hernández,[35] Edoardo Malfatti,[36] Arturo Fraga-Bau,[37] Isabelle Richard,[38] Isabel Illa[1,4] and Jordi Díaz-Manera[1,2,5]

Sarcoglycanopathies comprise four subtypes of autosomal recessive limb-girdle muscular dystrophies (LGMDR3, LGMDR4, LGMDR5 and LGMDR6) that are caused, respectively, by mutations in the *SGCA*, *SGCB*, *SGCG* and *SGCD* genes. In 2016, several clinicians involved in the diagnosis, management and care of patients with LGMDR3–6 created a European Sarcoglycanopathy Consortium. The aim of the present study was to determine the clinical and genetic spectrum of a large cohort of patients with sarcoglycanopathy in Europe. This was an observational retrospective study. A total of 33 neuromuscular centres from 13 different European countries collected data of the genetically confirmed patients with sarcoglycanopathy followed-up at their centres. Demographic, genetic and clinical data were collected for this study. Data from 439 patients from 13 different countries were collected. Forty-three patients were not included in the analysis because of insufficient clinical information available. A total of 159 patients had a confirmed diagnosis of LGMDR3, 73 of LGMDR4, 157 of LGMDR5 and seven of LGMDR6. Patients with LGMDR3 had a later onset and slower progression of the disease. Cardiac involvement was most frequent in LGMDR4. Sixty per cent of LGMDR3 patients carried one of the following mutations, either in a homozygous or heterozygous state: c.229C>T, c.739G>A or c.850C>T. Similarly, the most common mutations in LMGDR5 patients were c.525delT or c.848G>A. In LGMDR4 patients the most frequent mutation was c.341C>T. We identified onset of symptoms before 10 years of age and residual protein expression lower than 30% as independent risk factors for losing ambulation before 18 years of age, in LGMDR3, LGMDR4 and LGMDR5 patients. This study reports clinical, genetic and protein data of a large European cohort of patients with sarcoglycanopathy. Improving our knowledge about these extremely rare autosomal recessive forms of LGMD was helped by a collaborative effort of neuromuscular centres across Europe. Our study provides important data on the genotype-phenotype correlation that is relevant for the design of natural history studies and upcoming interventional trials in sarcoglycanopathies.

Received March 15, 2020. Revised May 25, 2020. Accepted May 27, 2020. Advance access publication 1 September 2020

1 Neuromuscular Diseases Unit, Department of Neurology, Hospital de la Santa Creu i Sant Pau, Universitat Autònoma de Barcelona, Barcelona, Spain
2 U705 CIBERER, Genetics Department, Hospital de la Santa Creu i Sant Pau, Universitat Autònoma de Barcelona, Spain
3 Centro de Investigación Biomédica en Red en Enfermedades Raras (CIBERER), Spain
4 Department of Neuroscience, University of Padova, Padova, Italy
5 John Walton Muscular Dystrophy Research Centre, Newcastle University and Newcastle Hospitals NHS Foundation Trust, Newcastle Upon Tyne, UK
6 Neuromuscular Disorder Unit, Hospital Sant Joan de Deu, Barcelona, Spain
7 Fondazione IRCCS Ca' Granda Ospedale Maggiore Policlinico, Dino Ferrari Centre, University of Milan, Milan, Italy
8 Department of Neurology, Amsterdam UMC, University of Amsterdam, Amsterdam Neuroscience, Amsterdam, The Netherlands
9 Neuropediatric Department, Centro Hospitalar do Porto, Porto, Portugal
10 Neuromuscular Centre for Children and Adolescents, Department of Paediatric Neurology, University Hospital Essen, Essen, Germany
11 Copenhagen Neuromuscular Center, Department of Neurology, Rigshospitalet and University of Copenhagen, Copenhagen, Denmark
12 Friedrich-Baur-Institute, Department of Neurology Klinikum München Ludwig-Maximilians-University Munich, Munich, Germany
13 Department of Human Genetics, Ruhr-University Bochum, Germany
14 Neuromuscular Research Center, University of Tampere and Tampere University Hospital, Tampere, Finland
15 Unit of Neuromuscular and Neurodegenerative Diseases, Department of Neurosciences, Bambino Gesù Children's Hospital, Rome, Italy
16 Cardiomiology and Medical Genetics, Department of Experimental Medicine, University of Campania, Naples, Italy
17 Department of Precision Medicine - University of Campania, Naples, Italy
18 Center of Translational and Experimental Myology, IRCCS Istituto Giannina Gaslini, Genova, Italy
19 Dubowitz Neuromuscular Centre, MRC Centre for Neuromuscular Diseases, UCL Great Ormond Street Institute of Child Health, London, UK
20 Neuromuscular Reference Center, Department of Neurology, Antwerp University Hospital, Antwerp, Belgium
21 Department of Neurology, University Hospitals Leuven, KU Leuven, Leuven, Belgium
22 Laboratory for Muscle Diseases and Neuropathies, Department of Neurosciences, KU Leuven, Leuven, Belgium
23 Paediatric Neuromuscular disorders Unit, Pediatric Neurology, Vall d'Hebron University Hospital and Vall d'Hebron Institute of Research (VHIR), Barcelona, Spain
24 Department of Child Neurology, Charles University, 2nd Medical School, University Hospital Motol, Prague, Czech Republic
25 Department of Neurology, Ghent University and University Hospital Ghent, Ghent, Belgium
26 Neuromuscular Unit, Department of Neurology, Hospital Universitario 12 de Octubre, Instituto de Investigación imas12, Madrid, Spain
27 UOC Neurologia, Fondazione Policlinico Universitario A. Gemelli IRCCS, Roma, Italy
28 Department of Neuropediatrics, Charité - Universitätsmedizin Berlin, Berlin, Germany
29 Department of Neurology, Queen Fabiola Children's University Hospital (HUDERF), Free University of Brussels, Brussels, Belgium
30 Neurosciences, BioDonostia Health Research Institute, Hospital Donostia, San Sebastián, Spain
31 Division of Child Neurology, Hospital Universitario 12 de Octubre, Universidad Complutense de Madrid, Madrid, Spain
32 Department of Medical Genetics, and Szentagothai Research Center, University of Pécs, School of Medicine, Pécs, Hungary
33 Institute of Clinical Neurophysiology, University Medical Centre, Department of Neurology, Faculty of Medicine, University of Ljubljana, Ljubljana, Slovenia
34 Neuromuscular and Rare Disease Center, Department of Neurosciences, Mental Health and Sensory Organs (NESMOS), SAPIENZA Università di Roma, Rome, Italy
35 Department of Neurology, Hospital Universitario Nuestra Señora de la Candelaria, Tenerife, Spain
36 Department of Neurology, Raymond-Poincaré teaching hospital, centre de référence des maladies neuromusculaires Nord/Est/Ile-de-France, AP-HP, Garches, France
37 Department of Neurology, Álvaro Cunqueiro Hospital, Vigo, Spain
38 Integrare (UMR_S951), Inserm, Généthon, Univ Evry, Université Paris-Saclay, 91002, Evry, France

Correspondence to: Prof. Jordi Díaz-Manera
The John Walton Muscular Dystrophy Research Centre
University of Newcastle
Newcastle Upon Tyne, UK
E-mail: Jordi.Diaz-Manera@newcastle.ac.uk

Keywords: limb girdle muscular dystrophies; sarcoglycan; registries; treatment; cohort

Abbreviation: LGMD = limb girdle muscular dystrophy

Introduction

Limb girdle muscular dystrophy (LGMD) is a genetically inherited condition that primarily affects skeletal muscle leading to progressive, predominantly proximal muscle weakness at presentation caused by a loss of muscle fibres (Straub *et al.*, 2017). Mutations in 32 genes have been reported to cause different types of LGMD, with the sarcoglycanopathies being one of the most frequent forms (Vainzof *et al.*, 1999; Straub *et al.*, 2017; Winckler *et al.*, 2019). There are four different sarcoglycan genes associated with autosomal recessive LGMD (LGMDR3–6; LGMD2D–F): *SGCA*, *SGCB*, *SGCD* and *SGCG* encoding for the alpha-, beta-, delta- and gamma-sarcoglycan proteins respectively. Two other sarcoglycan genes, *SGCE* and *SGCZ* have not been associated with any muscular condition so far. Sarcoglycans are transmembrane glycoproteins that form a tetrameric complex across the cell membrane of skeletal and cardiac muscle fibres (Ervasti *et al.*, 1990; Chan *et al.*, 1998; Tarakci and Berger, 2016). They play an important role in maintaining muscle membrane integrity during cycles of contraction and relaxation through association with the dystroglycan complex, which links the subsarcolemmal protein dystrophin to the basement membrane (Ozawa *et al.*, 2005; Tarakci and Berger, 2016). Mutations in any of the four sarcoglycan genes disrupt the whole complex, leading to the loss of muscle membrane integrity (Duclos *et al.*, 1998; Lim and Campbell, 1998).

The sarcoglycan genes were identified in the 1990s, and since then several studies have reported the clinical features of small cohorts of patients (Eymard *et al.*, 1997; Angelini *et al.*, 1999; Nalini *et al.*, 2010; Ferreira *et al.*, 2011; Semplicini *et al.*, 2015; Winckler *et al.*, 2019; Xie *et al.*, 2019). Most patients develop progressive proximal muscle weakness during the first decade of life, although other rarer phenotypes, such as asymptomatic hyperCKemia or exercise intolerance, have also been reported (Trabelsi *et al.*, 2008; Tarnopolsky *et al.*, 2015; Kyriakides *et al.*, 2020). In general, sarcoglycanopathies are severe disorders characterized by loss of ambulation during adolescence or in early adulthood, though milder cases, in which patients are still ambulant at 50 or 60 years of age, have been described (Gonzalez-Quereda *et al.*, 2018; Oliveira Santos *et al.*, 2020). Cardiac and respiratory muscle involvement is frequently part of the clinical picture (Melacini *et al.*, 1999; Politano *et al.*, 2001; Sveen *et al.*, 2008). Several studies have tried to establish a correlation between genetic findings and phenotypes. It has been suggested that mutations leading to the absence of protein expression cause a severe phenotype characterized by early loss of ambulation, but it is not entirely clear if partial loss of expression is associated with milder phenotypes (Guglieri *et al.*, 2008; Semplicini *et al.*, 2015). Moreover, even if there are certain clinical similarities between the different types of sarcoglycanopathies, their relative frequency and the natural history of the individual subtypes is not fully understood.

To answer these questions, we collected demographic, genetic, clinical and muscle protein data from a large cohort of patients with mutations in the sarcoglycan genes followed at neuromuscular centres across Europe. Our aims were to describe the main clinical and genetic features of the disease subtypes, investigate potential correlations between genotype and phenotype, and identify factors influencing the progression of the disease.

Materials and methods

Study design

This study was designed as an observational retrospective study collecting clinical and genetic data from patients with confirmed pathogenic mutations in the sarcoglycan genes (*SGCA*, *SGCB*, *SGCD* or *SGCG*). The data were collected from clinical assessments during patient clinical care visits. A total of 33 centres from 16 different countries provided data from their patients.

Patient cohort

The inclusion criteria for the study were: (i) genetically confirmed diagnosis of sarcoglycanopathy by identification of two heterozygous or one homozygous pathogenic mutation in one of the sarcoglycan genes; and (ii) sufficient data available in the clinical records to answer questions about disease onset and progression, presence or absence of cardiac and respiratory involvement and muscle function status at last clinical assessment. To analyse all the collected data, patients were categorized according to the mutated gene in four groups, LGMDR3, R4, R5 and R6, and then further stratified by presence or absence of symptoms.

Data sources

All participating centres completed a survey for each patient followed and evaluated at the centre. The survey collected demographic, clinical and genetic data and muscle biopsy information if performed.

Clinical features at first visit and during disease progression were collected from medical records. The age of disease onset was defined as the age at which the first symptoms were noticed by the patients or parents. The following data were collected to analyse disease progression: age at which patients were not able to run, age at which patients were not able to get up from a chair without support, age at which patients were not able to climb up stairs without using the handrail and age at which patients began using any walking aids, such as canes, sticks or walkers. The age of loss of ambulation was defined as the time when patients were not able to walk short distances (such a crossing a room) and needed a wheelchair both at home or when out. Cardiac involvement was defined by a left ventricular ejection fraction lower than 50% or fractional shortening lower than 25%, the existence of morphological abnormalities in the ventricular walls evaluated by echocardiography or the existence of cardiac conduction defects (Ponikowski *et al.*, 2016; Lipshultz *et al.*, 2019). The need for ventilatory support was also recorded as well as the age at which it was started.

We collected the following data on the muscle biopsies: which muscle was biopsied, age at which the muscle biopsy was performed, main characteristics observed in the haematoxylin-eosin staining including the presence of internal

nuclei, existence of necrotic fibres, inflammatory infiltrates, fibrosis or fat replacement. We also collected data on the remaining protein expression analysed by western blot and stratified this quantification into: no protein expression (<1%), <30% protein expression, 30–60% protein expression and >60% protein expression compared to controls. Western blots were performed in all hospitals at the time the muscle biopsy was performed for diagnosis.

Mutations in the *SCGA*, *SCGB*, *SCGG* or *SCGD* genes were collected and centrally reviewed by experienced geneticists from Hospital Santa Creu I Sant Pau (L.G-Q and P.G.) to predict pathogenicity. We considered nonsense, frameshift and canonical splice site mutations as incompatible with full-length protein production as these mutations are predicted to cause a disruption of the reading frame or a considerable shortening of the transcript resulting in aberrant degradation. Missense variants and mutations that maintained the reading frame were considered as compatible with protein production. Deep intronic mutations were also considered as compatible with protein production, as mutations affecting splicing, located outside canonical splice sites, usually produces a certain amount of wild-type transcript.

To reduce the selection bias, patients with more than 30% of missing data were excluded from the study.

Statistical analysis

Quantitative variables were analysed using the Kolmogorov-Smirnov test, to verify the normal distribution. Comparison between the different subgroups of patients was performed using the ANOVA test for quantitative variables and the chi-squared test for categorical variables. To identify which level of protein expression, quantified using western blot, predicted with highest sensitivity and specificity loss of ambulation before 18 years of age, we generated a receiver operating characteristic curve (ROC). Area under the curve (AUC) and the optimal cut-off point (also known as Youden's index) are provided. We used a Cox proportional hazard regression model for the analysis of time to wheelchair. To select which variables were associated with loss of ambulation before 18 years old, we performed a two-step analysis. First, we performed a univariate analysis using the chi-squared test for categorical variables and the Student's *t*-test for quantitative variables. Those variables that showed a significantly different distribution among groups (considering in this case $P < 0.1$) were included in a multivariable logistic regression modelling and backward eliminated until reaching significance. A ROC curve was generated to test the predictive power of the final model and AUC is also provided. P was considered significant if <0.05. Statistics analysis was performed by J.D-M. and J.A-P. using SPSS software version 20 from IBM.

Data availability

The data that support the findings of this study are available from the corresponding author, upon reasonable request.

Results

Patient cohort

A total of 439 patients were collected (Fig. 1, STARD diagram). Forty-three patients were not included in the analysis because of insufficient genetic or clinical data. We

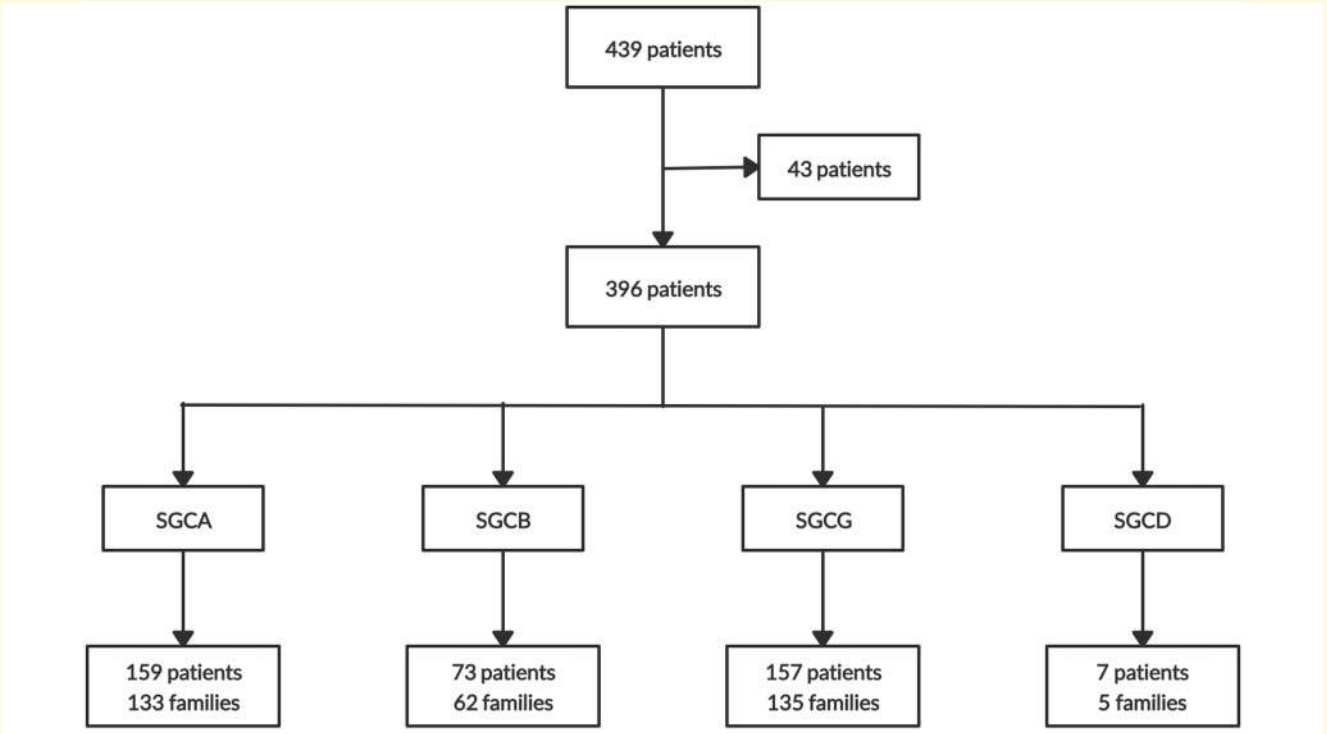

Figure 1 STARD diagram showing the flow of patients throughout the study.

included 396 patients from 329 different families in the analysis. We divided the cohort in four different subgroups depending on the mutated gene (Fig. 1): 159 patients were classified as LGMDR3 (alpha patients), 73 as LGMDR4 (beta patients), 157 patients as LGMDR5 (gamma patients), and seven as LGMDR6 (delta patients). Delta patients were excluded from the general comparisons between groups due to the low number of patients.

Patients data were collected from 33 hospitals in 13 European countries including: Spain, Portugal, Italy, The Netherlands, UK, Finland, Czech Republic, Hungary, Slovenia, France, Germany, Denmark and Belgium. We did not identify significant differences in the geographic distribution of subgroups across the 33 recruiting sites. However, beta patients were more prevalent in northern countries, such as The Netherlands, UK and Denmark, while gamma patients were more prevalent in southern countries, such as Spain, Italy and Portugal (Supplementary Fig. 1B and C). Most of the patients had Caucasian origin (91.9% alpha, 84.5% beta, 45% gamma and 57.1% delta patients). In the case of gamma patients, 27.7% had a Roma and 17.8% a Maghreb background.

There were not significant differences in gender in any of the subgroups studied (ANOVA, $P = 0.69$). Thirty-seven per cent of alpha, 28.8% of beta, 43.3% of gamma and 57.1% of delta patients had relatives affected by the disease. Consanguinity was reported in 15.5%, 25%, 49.2% and 85.7% of cases, respectively (Table 1).

Symptoms and muscle function status

Ninety-six per cent of the patients were symptomatic at the time of inclusion in the study (Table 1). Non-symptomatic patients were diagnosed either because they were relatives of patients with the disease or because they had asymptomatic hyperCKemia. Age at symptoms onset varied between the different subtypes: alpha patients experienced first symptoms later (mean: 10.2; range: 1–45 years) than beta (5.8; 1–22

Table 1 Clinical and demographic features for each type of sarcoglicanopathy

	Alpha patients (LGMDR3)	Beta patients (LGMDR4)	Gamma patients (LGMDR5)
Patients, *n*	159	73	157
Sex, male/female (Unk)	70/75 (14)	36/37	77/80
Families, *n*	133	62	135
Affected related, *n* (%)	60 (37.7)	21 (28.8)	68 (43.3)
Symptomatic, *n* (%)	148 (93.1)	73 (100)	152 (96.8)
Age onset, average ± SD [range]	10.2 ± 9 [1–45]	5.8 ± 4.1 [1–22]	5.8 ± 3.4 [1–20]
Diagnostic delay, average ± SD [range]	14.1 ± 13.9 [–2–53]	14.3 ± 13.4 [1–50]	9.2 ± 11.6 [–5–50]
Age at last evaluation, average ± SD [range]	28.9 ± 17.8 [2–74]	28.3 ± 15.9 [8–66]	19.9 ± 13 [2–61]
Evolution of the disease, years, average ± SD [range]	19.1 ± 13.6 [0–54]	21.5 ± 14.2 [4–60]	14.7 ± 11.6 [0–50]
Symptom onset, *n* (%)	*n* = 102 (46 Unk)	*n* = 46 (27 Unk)	*n* = 107 (45 Unk)
Proximal LL weakness	45 (44.1)	25 (54.3)	53 (49.5)
Proximal UL weakness	30 (20.3)	9 (19.6)	15 (14)
HyperCKemia	27 (18.2)	13 (28.3)	28 (26.2)
Symptoms, *n* (%); average ± SD [range]	*n* = 87 (61 Unk)	*n* = 35 (28 Unk)	*n* = 103 (49 Unk)
Tiptoe gait	20 (22.9); 7.4 ± 5.4 [3–25]	23 (65.7); 8.9 ± 5.9 [2–25]	38 (36.9); 5.7 ± 3 [1–11]
Calf hypertrophy	50 (57.5); 12.4 ± 11.5 [3–51]	21 (60); 6.1 ± 2.6 [2–12]	66 (64.1); 6.4 ± 3.7 [2–16]
Scoliosis	29 (33.3); 16 ± 7.5 [6–35]	17 (48.6); 17.6 ± 13.6 [7–37]	43 (39.8); 14.7 ± 8 [7–31]
Scapular winging	39 (44.8); 20.5 ± 12.2 [6–51]	18 (51.4); 14.9 ± 13 [4–43]	41 (39.8); 12.5 ± 7.3 [2–30]
Motor function, *n* (%); average age ± SD [range]	*n* = 129 (19 Unk)	*n* = 65 (8 Unk)	*n* = 135 (17 Unk)
Running	15 (11.7); 13.1 ± 4.6 [5–19]	2 (3.2); 16 ± 2.8 [14–18]	10 (7.7); 8.4 ± 8.7 [2–9]
Walk without aids	30 (23.4); 29.7 ± 18.5 [4–63]	7 (10.9); 19.3 ± 11.6 [8–34]	25 (19.2); 12.2 ± 8.7 [4–48]
WCB	72 (56.3); 18.6 ± 11.9 [6–62]	50 (78.1); 16.7 ± 9.5 [5–45]	87 (66.9); 14.6 ± 7 [8–42]
Cardiac involvement, *n* (%); average age ± SD (range)	14 (10.4); 34.1 ± 14.4 [11–55]	30 (41.1); 25.8 ± 13.1 [12–54]	32 (22.5); 21.1 ± 11.2[5–48]
Heart rhythm abnormalities, *n* (%)	10 (71.4)	4 (13.3)	6 (18.8)
Dilated cardiomyopathy, *n* (%)	1 (7.1)	19 (63.3)	19 (59.4)
Unknow type of cardiac involvement, *n* (%)	3 (21.4)	7 (23.3)	7 (21.8)
Respiratory support, *n* (%); average age ± SD [range]			
Non-invasive ventilation	40 (27); 29 ± 11 [12–58]	21 (28.8); 29.8 ± 9.2 [12–44]	35 (23.6); 28.7 ± 11.4 [8–58]
Invasive ventilation	1 (0.7); 51	3 (3.9); 47,7 ± 8.3 [41–57]	2 (1.4); 37
Death, *n* (%)	3 (1.9)	2 (2.7)	4 (2.6)

LL = lower limbs; UL = upper limbs; Unk = unknown; WCB = wheelchair-bound.

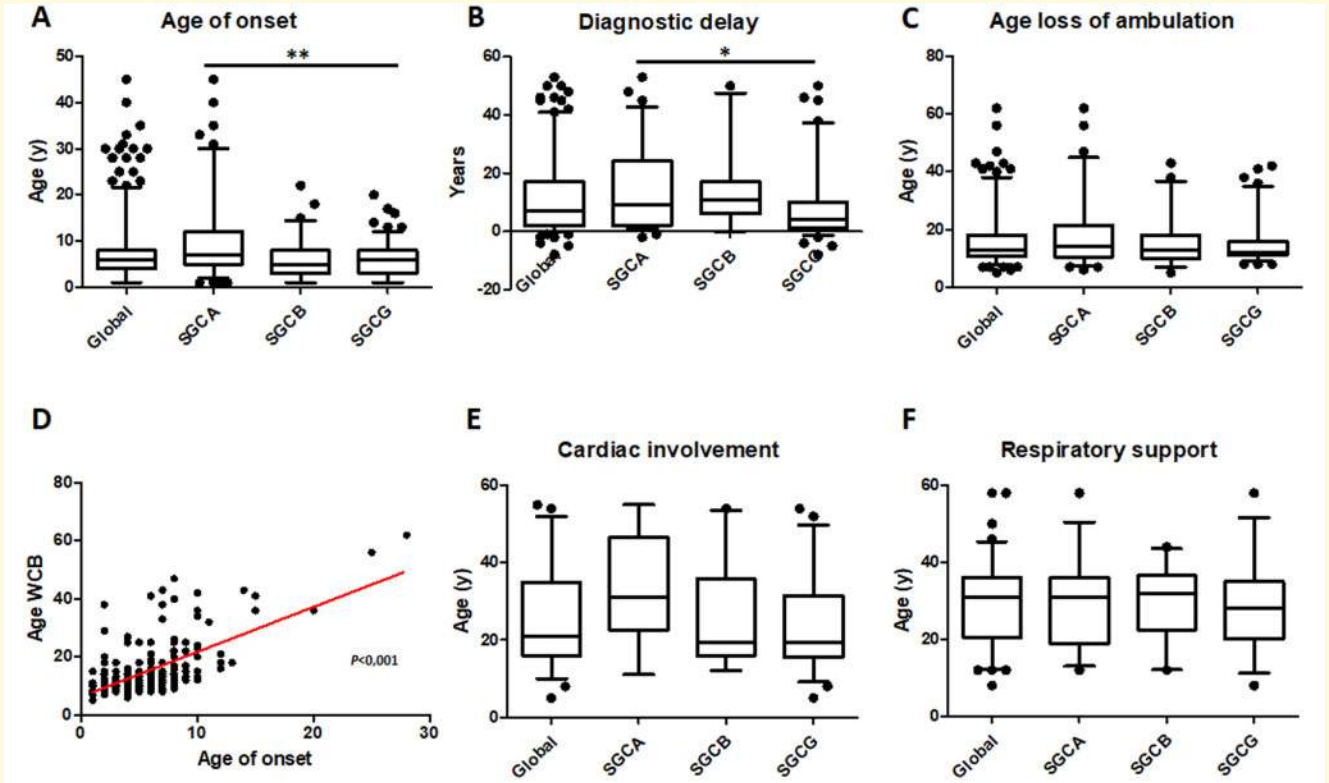

Figure 2 Demographic and clinical data of patients with sarcoglycanopathy. (**A**) Age of onset of the global cohort, the alpha, beta and gamma patients are shown. (**B**) Diagnostic delay measured as time in years from onset of symptoms to a genetic confirmatory diagnosis for the global cohort, alpha, beta and gamma patients. (**C**) Age of loss of ambulation for the global cohort, alpha (*SCGA*), beta (*SCGB*) and gamma (*SCGG*) patients. (**D**) Correlation between age of onset of symptoms and age of loss of ambulation. Pearson test was performed showing a statistically significant correlation ($P < 0.001$) with a correlation coefficient of 0.61. (**E**) Age at which cardiac involvement was detected for the global cohort, alpha (*SCGA*), beta (*SCGB*) and gamma (*SCGG*) patients. (**F**) Age at which ventilatory support was required for the global cohort, alpha (*SCGA*), beta (*SCGB*) and gamma (*SCGG*) patients. The box plot includes the 25th–75th percentile, the mid lines indicate the median, bars are the 5th–95th percentiles. Dots represent outlier patients who were standard deviation outliers. ANOVA test, $^{*}P < 0.05$, $^{**}P < 0.01$. WCB = wheelchair-bound; y = years.

years) and gamma (5.8; 1–20 years) patients (ANOVA test, $P < 0.001$), while there was no difference in the age of onset between beta and gamma patients (Table 1 and Fig. 2A). Mean age at symptoms onset in delta patients was 8.5 years (range 1–30). Delay in diagnosis, defined as the time from onset of symptoms to the genetic confirmation of the disease varied from one subtype to the other, but it was significantly shorter in gamma patients compared to alpha and beta patients (ANOVA test, $P = 0.004$) (Table 1 and Fig. 2B). The most frequent symptom at onset in all subgroups was proximal lower limb weakness. However, ~25% of all patients were diagnosed because of the presence of asymptomatic hyperCKemia, muscle pain or because they were relatives of already diagnosed patients (Table 1). At the time of the survey, 4% of all patients were considered non-symptomatic, as these patients did not have any symptom of muscle weakness and clinical examination was normal. Supplementary Table 1 describes their clinical data. In summary, there were 11 alpha, 0 beta and 5 gamma patients considered non-symptomatic. Mean age at last visit was 14.6 years old (range: 2–38) for the alpha and 11 years (range: 3–24) for the gamma. Clinical examination was normal, and these patients did not have cardiac or respiratory involvement.

At the time of the survey, 23.4% of all alpha patients were able to walk without aids while 56.3% were wheelchair-bound. Only 10.9% of beta patients were able to walk without aids while 78.1% of them were wheelchair-bound. In the case of gamma patients, 19.2% were able to walk without aids and 66.9% were wheelchair-bound (Table 1). Only two of the seven delta patients had lost ambulation at the time of the survey (mean age of loss of ambulation was 12 years). There were not significant differences in the age at loss of ambulation between subgroups (ANOVA, $P = 0.053$), but we identified a non-significant trend for an earlier loss of ambulation in beta and gamma patients compared to alpha patients (Fig. 2C). We identified a significant correlation between the age of onset of symptoms and the age at loss of ambulation (Pearson correlation, $P < 0.001$, $r = 0.61$) (Fig. 2D). Interestingly, there were significant differences in the age at loss of ambulation when patients were classified as age of onset of symptoms before and after

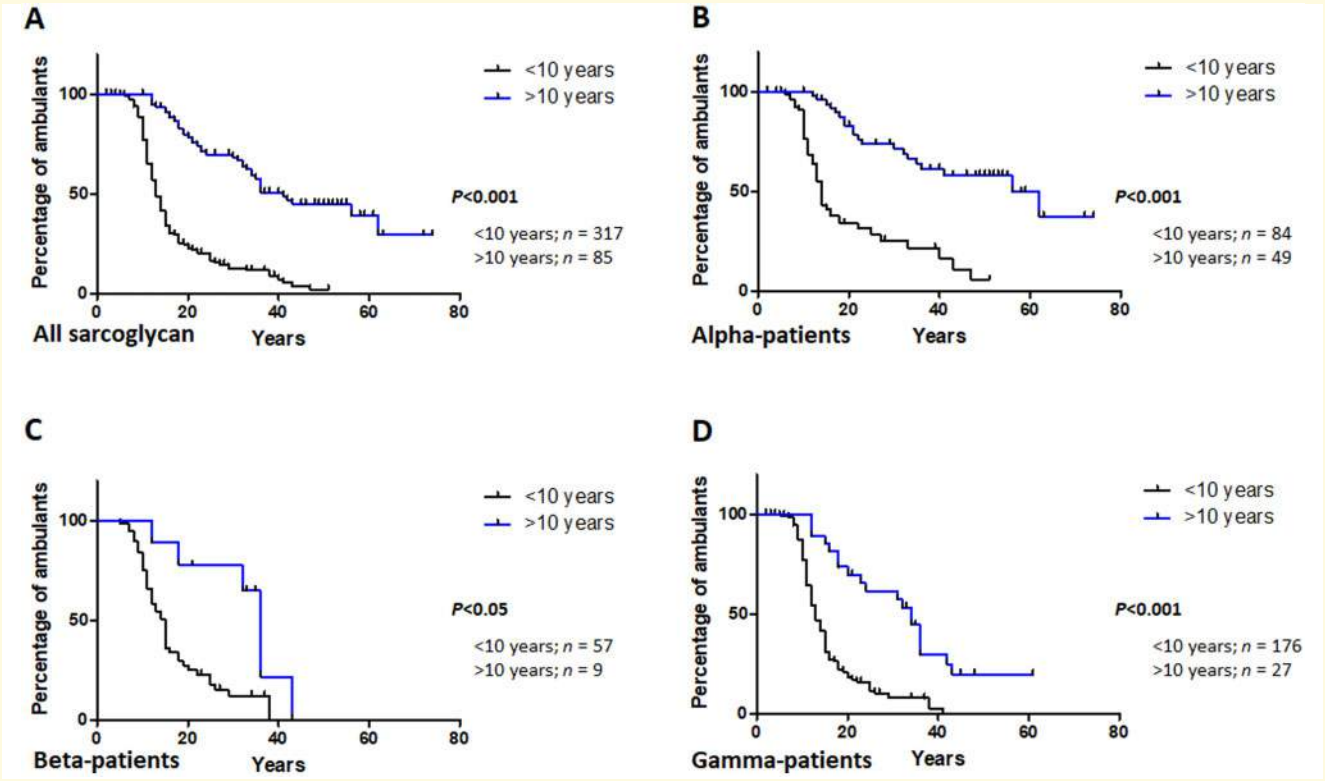

Figure 3 Influence of age of onset of symptoms on the time to wheelchair. Kaplan-Meier estimates age in age at wheelchair based in the age of the patients for all sarcoglycan patients (**A**), alpha patients (**B**), beta patients (**C**) and gamma patients (**D**). Patients were stratified into two groups: onset of symptoms before 10 years of age and onset of symptoms after 10 years of age. SGC = sarcoglycan; SGCA = alpha patients; SGCB = beta patients; SGCG = gamma patients.

10 years old (Mantel-Cox test, $P < 0{,}001$) both when the analysis was performed with all sarcoglycan patients and when it was performed in each subgroup (Fig. 3). Furthermore, we observed that the patients who began with muscle weakness after 18 years of age ($n = 20$) did not lose ambulation during the follow-up assessments (Supplementary Fig. 2).

Cardiac and respiratory involvement

The frequency and type of cardiac involvement varied between subgroups and are described in Table 1. Nineteen per cent of all patients had cardiac involvement as defined in the 'Materials and methods' section. There were significant differences in the frequency of cardiac involvement (ANOVA test, $P = 0.001$) between the subgroups, with beta patients showing more frequent cardiac involvement than alpha or gamma patients, but no differences in the age at which cardiac involvement was identified (ANOVA test, $P = 0.34$) (Fig. 2E). However, we identified a statistically significant correlation between the duration of the disease, measured as the time from the onset of symptoms, and the presence of cardiac involvement both in beta and gamma patients.

Up to 25% of all patients required ventilatory support, with the treatment recommended at a mean age of 29.1 years (range 8–58). Between the different subgroups we neither identified differences in the frequency of patients requiring ventilatory support (ANOVA test, $P = 0.64$) nor in the age at which it was recommended (ANOVA test, $P = 0.93$) (Fig. 2F). However, patients requiring ventilatory support had a significant longer duration of the disease. We specifically analysed the potential influence of scoliosis in the need of ventilatory support: 69.1% of patients requiring ventilation had scoliosis, while only 31.9% that did not require ventilation support had scoliosis. These differences were statistically significant (chi-square, $P < 0.001$). Additionally, we observed a non-significant trend of starting the ventilation earlier for patients with scoliosis compared to those patients without scoliosis (Student t-test, $P = 0.085$).

We did not identify differences in the age at onset, age at loss of ambulation or the remaining sarcoglycan expression between patients with or without cardiomyopathy and those with or without ventilatory support.

Genetic studies

A total of 131 different pathogenic variants were identified in the four sarcoglycan genes (Fig. 4). Interestingly, in each

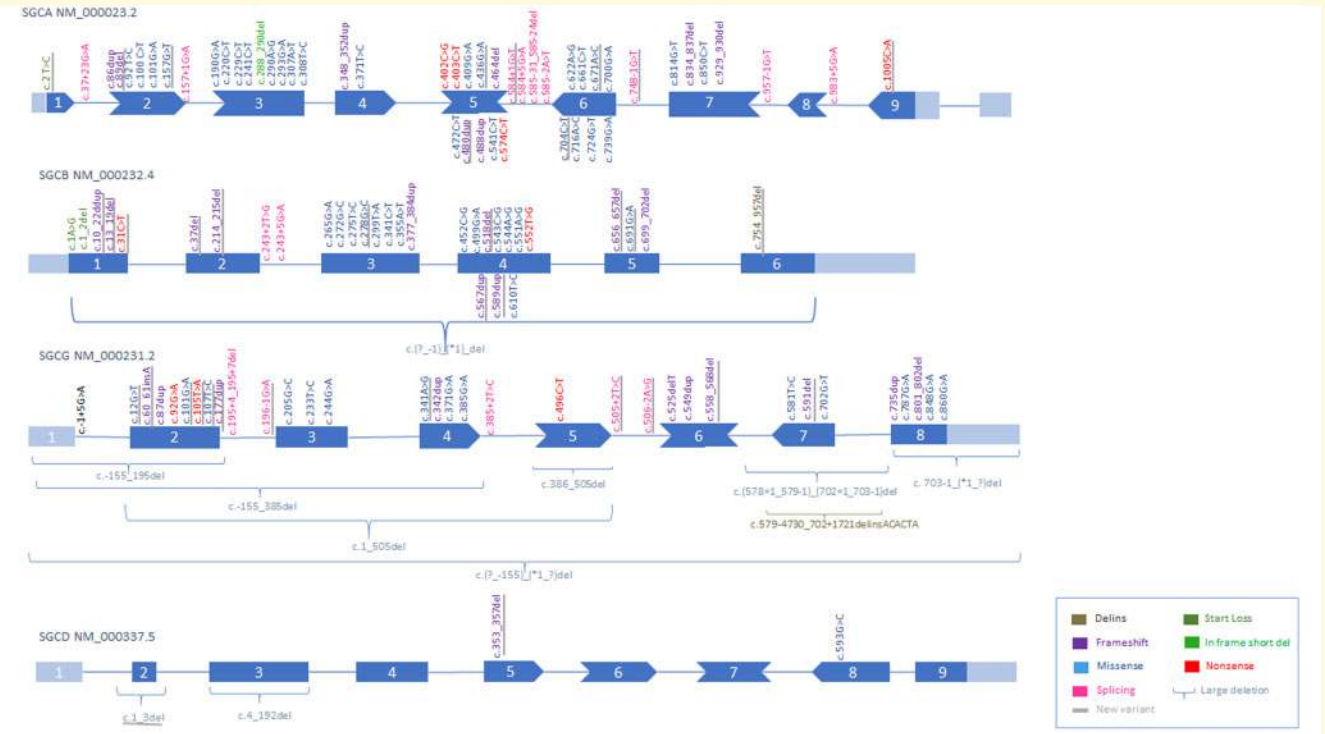

Figure 4 Distribution of the pathogenic variants found in our cohort of patients among the different sarcoglycan genes. The graph shows the distribution of the pathogenic variants identified in the patients that participated in the study. New variants not previously described are underlined. *Bottom right*: legend describes the type of mutation. Delins = deletion or insertion.

gene two or three mutations were more prevalent than the others. Moreover, mutations were mainly concentrated in two or three exons of the genes.

Alpha patients

Eighty-three alpha patients (52.2%) were homozygous for a single variant. In total, 52 different pathogenic variants were found in the *SGCA* gene and three of them were more prevalent than the others: c.229C>T, p.(Arg77Cys) was present in at least one allele in 75 patients (47.2% of all alpha patients), c.850C>T, p.(Arg284Cys) was present in 30 patients (18.9%) and, c.739G>A, p.(Val247Met) in 26 patients (16.4%). Nine of the 53 variants had not been previously described (Fig. 4). Most of the variants were located in exons 3, 6 and 7, with 103 of 159 (64.4%) patients having their two variants in these exons. Most of the patients had two missense mutations (74.8%), while only 3.1% carried two frameshift or nonsense mutations.

Beta patients

Fifty-five beta patients (75.2%) were homozygous for a single variant. In total, 34 different pathogenic variants were found in the *SGCB* gene, but one of them, c.341C>T, p.(Ser114Phe), was the most prevalent, being found in 30 patients (41.1% of all beta patients). Twelve of 34 variants had not been previously described (Fig. 4). Most of the variants were located in exons 3 and 4, with 55 of 73 (75.4%) patients having their two variants in these exons. Fifty-three per cent of the patients had two missense mutations while 28.7% carried two frameshift or nonsense mutations.

Gamma patients

One hundred and thirty-five gamma patients (86%) were homozygous for a single variant. In total, 41 different pathogenic variants were found in the *SGCG* gene and two of them were more prevalent than the others: c.525delT, p.(Phe175Leufs*20) was present in at least one allele in 71 patients (45.2% of all gamma patients) and c.850C>T, p.(Arg284Cys) was present in 38 patients (24.2% of all gamma patients). Thirteen of 41 variants had not been previously described (Fig. 4). Most of the variants were located in exons 6 and 8, with 112 of 157 (71.3%) patients having their two variants in these exons. Most of the patients had two frameshift or nonsense mutations (47.7%) while 33.8% carried two missense mutations. Interestingly, 43.9% of gamma patients carried the mutation c.525delT (known as a Maghrebian founder mutation), while 43.9% carried the c.848G>A mutation (known as a Roma founder mutation).

Delta patients

The seven delta patients were all homozygous for a single variant. Four different pathogenic variants were found in the *SGCD* gene. Five patients (71.4%) were homozygous for a

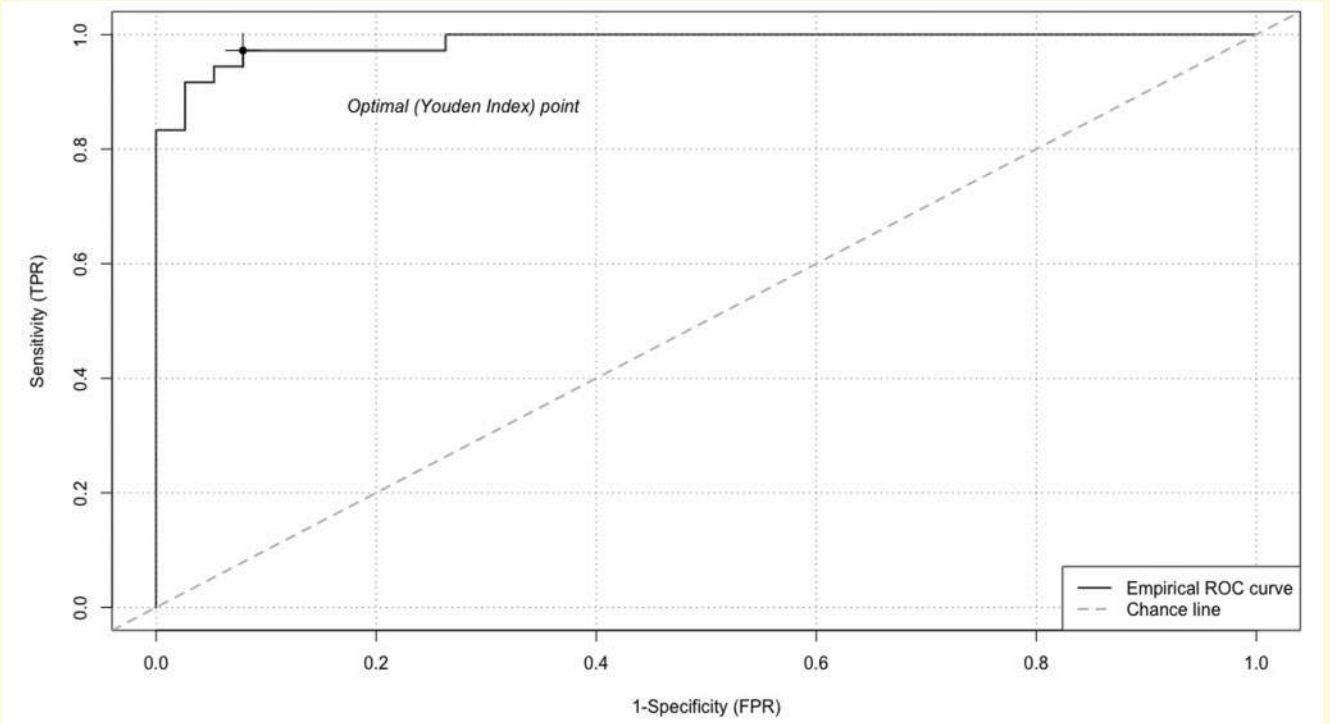

Figure 5 ROC curve of the influence of remaining protein expression for distinguishing patients at risk of losing ambulation before the age of 18 years. The ROC curve analysing remaining protein expression and risk of losing ambulation before 18 years of age, showed an AUC of 0.986 (0.67–1). The Youden's index (optimal point with higher sensitivity and specificity) was 27.5% expression.

deletion mutation. Two of the four variants had not been previously described (Fig. 4).

Genotype-protein expression-phenotype correlation

To analyse the potential genotype-phenotype correlation we studied the impact that the mutation had on the residual protein expression.

A muscle biopsy was performed in 208 patients (101 alpha patients, 42 beta patients and 65 gamma patients). Western blot analysis was performed in 55 (54.5% of patients with muscle biopsy) alpha patients, 20 (47.6%) beta patients and 35 (53.8%) gamma patients. However, because of the high frequency of patients sharing the same mutations and the fact that many patients harboured two out of frame mutations, we were able to predict remaining protein expression in 139 alpha patients, 67 beta and 148 gamma patients. There were 20 (12.6%) alpha patients, six (8.2%) beta patients and nine (5.7%) gamma patients where it was not possible to know the level of protein expression.

To identify if protein expression, analysed using western blot, predicted with high sensitivity and specificity loss of ambulation before 18 years of age, we generated a ROC curve (Fig. 5). We observed that optimal cut-off point was 27.5 expression which had an 83.3% sensitivity and 100% specificity. To compare clinical features depending on the remaining protein expression we categorized all patients in no expression (<1%), <30% expression and >30% expression. We observed significant differences in the age of onset of the disease (ANOVA, $P < 0.001$), the age of loss of ambulation (ANOVA, $P < 0.001$) and the time from onset of symptoms to being wheelchair-bound (ANOVA, $P < 0.001$) between patients with no expression or <30% expression and those patients with expression >30% (Fig. 6). When we performed the analysis by gene subgroups, we observed that age of ambulation loss in alpha patients was significantly influenced by protein expression (Mantel-Cox study, $P < 0.001$) (Fig. 6B). In the case of beta patients, there was a non-significant trend in the age at being wheelchair-bound depending on protein expression levels (Mantel-Cox, $P > 0.05$), although we observed that those expressing >30% of protein had a longer time from onset of symptoms to the loss of ambulation (Fig. 6C). In gamma patients, significant differences were only found between patients having no expression or <30% and patients having >30% expression (Mantel-Cox, $P < 0.05$) (Fig. 6D).

Risk factors associated with rapid disease progression

To determine which risk factors could be associated with early loss of ambulation, before the 18 years of age, we performed a multivariate logistic regression analysis. First,

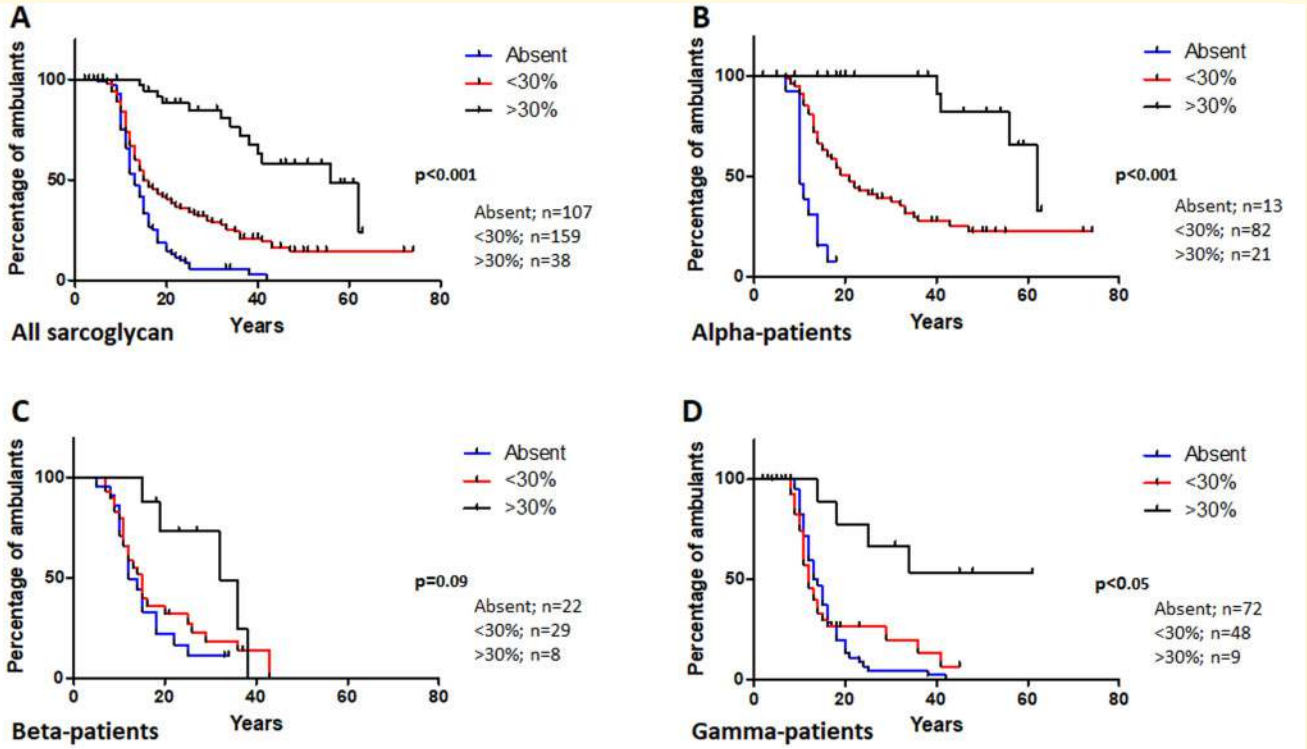

Figure 6 Influence of remaining protein expression on the time to wheelchair. Kaplan-Meier estimates influence of remaining protein expression in age at wheelchair for all sarcoglycan patients (**A**), alpha patients (**B**), beta patients (**C**) and gamma patients (**D**). Patients were stratified into three groups: no protein expression (absent), remaining protein expression lower than 30% (<30%) and remaining protein expression higher than 30% (>30%). SGC = sarcoglycan; SGCA = alpha patients; SGCB = beta patients; SGCG = gamma patients.

we identified which factors could be associated using a univariate analysis including clinical (age of onset, age at diagnosis, gender, scoliosis, need of ventilation, cardiac involvement), genetic data (gene mutated, harbouring two out-of-frame mutations, harbouring two in-frame mutations) and protein expression. This univariate study identified age of onset, protein expression <30% and mutations in the *SGCG* gene as factors with a significant relation with early loss of ambulation. These variables were further included in the multivariable logistic regression model that confirmed that age of onset {odds ratio (OR) = 1.37 [confidence interval (CI):1.18–1.59], $P = 0.001$} and protein expression <30% [OR = 10.7 (CI : 2.04–56.22), $P = 0.020$] were independent risk factors for losing ambulation before age 18 years of age. The ROC curve for the final model, showed an AUC of 0.77 (Supplementary Fig. 3). In addition, we performed a ROC analysis to identify which age of onset cut-off point had the most balanced sensitivity/specificity to predict loss of ambulation before the age of 18 years (Supplementary Fig. 4A). We found that the most balanced cut-off point was age of onset ⩽6 years, which showed a sensitivity of 69.33%, a specificity of 68.63% and an AUC of 0.74 to predict loss of ambulation before 18 years of age. The ROC curve for this age cut-off point is shown in Supplementary Fig. 4B.

Discussion

We report the clinical, genetic and protein expression data of the largest series of patients with mutations in the sarcoglycan genes described so far. The analysis of this international cohort revealed crucial information to establish a prognosis for the diseases as we have observed that onset of symptoms during the first decade of life and protein expression in muscle biopsy lower than 30% were independent risk factors associated with loss of ambulation before 18 years of age. In contrast, onset of symptoms later than 10 years of age and/or protein expression higher than 30% was associated with a slower progression and lower risk of losing ambulation before the age of 18 years. These data are especially relevant at present, as genetic therapies are under development and interventional clinical trials in patients with sarcoglycanopathies are being designed (Israeli *et al.*, 2019; Vita *et al.*, 2019).

Sarcoglycanopathies, as a group, are a common cause of recessive LGMD (Vainzof *et al.*, 1999; Fanin *et al.*, 2009) and the third most common cause of recessive muscular dystrophies after calpainopathies and dysferlinopathies (Ghaoui *et al.*, 2015; Liu *et al.*, 2019). Mutations in these genes have classically been associated with a rapid progression of muscle weakness leading to severe disability, loss of ambulation in the second decade of life and frequently associated with

cardiac and respiratory problems (Semplicini *et al.*, 2015). However, several reports suggested that disease progression is not homogeneous, as there were patients who never lost ambulation or patients in which the onset of symptoms was in the third or fourth decade of life. Our data show that a series of factors may influence clinical progression including the mutated gene, age of onset of symptoms and residual protein expression. For example, progression of the disease was more rapid and severe for beta patients as a group than for alpha patients, as it has previously been suggested (Semplicini *et al.*, 2015). The onset of symptoms for beta patients was during the first decade of life in 87% of cases, and 78.4% of them were wheelchair-bound before 18 years of age. However, we also identified beta patients with milder clinical progression and in all these cases the remaining protein expression was higher than 30%. Previous series had suggested that gamma patients may have a milder progression than beta patients (Guglieri *et al.*, 2008; Ferreira *et al.*, 2011). However, our data show that gamma patients have a more severe clinical phenotype than previously reported: 87.2% of them started with symptoms before 10 years of age and 84.4% of them were wheelchair-bound before 18 years old. In contrast, only 32% of alpha patients had their first symptoms before 10 years of age and just 56.3% were wheelchair-bound by the age of 18 years. In addition, our study supports that remaining protein muscle expression is an independent risk factor for disease progression as previously suggested (Guglieri *et al.*, 2008; Semplicini *et al.*, 2015). It was especially interesting that alpha patients, as a group, needed less remaining protein expression than beta and gamma to maintain ambulation beyond 18 years of age. However, these results should be interpreted carefully, as we have identified patients in which protein expression was >30% who lost ambulation before 18 years of age.

Analysis of mutations can be useful to predict protein expression in many disorders. Harbouring two truncating mutations is generally associated with total or severe loss of protein expression; however, the effect of having one or two missense mutations is not always easy to predict (Guglieri *et al.*, 2008, Winckler *et al.*, 2019). We cannot discount that an apparently missense mutation detected in genomic DNA could create a cryptic splice site that causes a frameshift, only perceptible when analysing mRNA. It is also well known that after protein translation, sarcoglycans are glycosylated in the endoplasmic reticulum where some aberrant proteins could be identified by the ubiquitin-proteasome system and degraded. Consequently, some missense mutations can induce very low or no protein expression (Sandonà and Betto, 2009; Bianchini *et al.*, 2014). Therefore, in our opinion, caution is needed to predict protein expression based on genetic results only. In our study, we had information about protein expression studied by skeletal muscle western blot in a considerable number of patients, which, together with the fact that many patients shared the same mutations, allowed us to predict protein expression in a large proportion of cases. Some of the most common missense mutations, such as c.229C>T, p.(Arg77Cys) in the *SGCA* gene, c.341C>T, p.(Ser114Phe) in the *SGCB* gene and c.848G>A, p.(Cys283Tyr) in the *SGCG* gene were associated with a very reduced protein expression, always <30%, and consequently with a worse prognosis characterized by early onset of symptoms, more rapid progression and early loss of ambulation. In contrast, c.850C>T, p.(Arg284Cys) and c.739G>A, p.(Val247Met) in the *SGCA* gene were associated with a higher protein expression and therefore a better prognosis. It is also important to note that other factors could influence the progression of the disease (apart of the mutated gene and the remaining protein expression), which have not been assessed in this study such as epigenetic factors and modifier genes or even social aspects such as nutrition status, exposition to toxics, or access to physiotherapy and general care. All these aspects could also potentially influence disease's progression.

In our opinion, the data reported here can help in the design of clinical trials in sarcoglycanopathies. These trials should identify two groups of patients: (i) those with two truncating mutations; and/or (ii) those with none or <30% protein expression because these patients were commonly associated with an earlier onset of the disease, a quicker progression and a loss of ambulation before 18 years of age. To determine the effectiveness of gene therapy in these cases, we suggest including children younger than 10 years of age in the clinical trials. In contrast, patients with protein expression >30% were often associated with milder progression, with most of them still ambulant in the fourth decade of life. If these patients were also included in clinical trials, analysis of the effectiveness of the therapy should be performed separately to the other group, as results could be biased by the milder progression of the disease.

Our results can also provide insight into the expected effect of therapeutic approaches that aim to restore protein expression. We have shown that protein expression >30% was associated with a better prognosis. Therefore, gene replacement therapies able to reach almost this range of expression should be effective enough to show a change in the progression of the disease. These data, although hypothetical, are extremely important, as the efficacy of gene replacement therapies could depend on the amount of protein expression levels reached, which are probably influenced by the number of viral genomes infused.

Another interesting finding of our analysis was the low frequency of cardiac and respiratory involvement. Most of the previous cohort descriptions pointed out that >50% of patients developed cardiac and respiratory problems, although another recently published study described the frequency of cardio-respiratory involvement to be <5% in sarcoglycan patients (Melacini *et al.*, 1999; Calvo *et al.*, 2000; Politano *et al.*, 2001; Fanin *et al* 2003; Winckler *et al.*, 2019).

The study also provided information about the delay in the diagnosis of the patients. The mean delay in diagnosis was 14 years for alpha and beta, and 8 years for gamma patients. There are many factors that could increase the delay, such as the lack awareness of the disease among non-specialized services, the difficulties accessing genetic studies

in some countries and the fact that many patients with a Duchenne-like clinical picture could be first assessed for mutations in the dystrophin (*DMD*) gene. We hope that next generation sequencing will allow faster diagnosis in the future and shorten the time to reach a diagnosis. We identified 131 variants in the three genes, but most of these variants were concentrated in two to three exons per gene confirming that there are hot spots in these genes as previously described. It was interesting to see the long delay.

Our study has some limitations because data were collected retrospectively, came from different countries and it is likely that the protocol to assess cardiac and respiratory involvement is different between countries, and they may not be up to date for all patients. Moreover, in the case of respiratory involvement, we only collected data regarding age at which ventilatory support was begun. However, our results show that only 21.6% of the patients had cardiac involvement and 26.2% required ventilatory support. We did not identify any correlation between protein expression, age of onset or age of losing ambulation and the development of cardiac and respiratory involvement. Therefore, it was not possible to predict the development of these symptoms based on protein expression data and periodic assessments of cardiac and respiratory involvement are needed in all cases. Moreover, the data were retrospectively collected and there were missing data for many patients that could have enriched the data analysed. Another limitation is that western blots were performed at local hospitals at the time the muscle biopsies were obtained. Our study covers a long period of time, from the 1990s to the present, and therefore the methods used for western blots were different between laboratories, including commercial antibodies used to detect the expression of sarcoglycans, proteins used as loading controls (GAPDH, b-tubulin, actin or the developing methods used (colorimetric, chemiluminescence, etc). These factors could add a degree of variability to the quantification of sarcoglycans expression. Moreover, there is also an inherent variability in the western blot itself when a protein is quantified. Therefore, we decided not to take into account the exact amount of protein expressed, because we considered that we could not compare an analysis performed in one laboratory with another performed in a different laboratory, many years later and using different technology; instead, we used a range of expression. To our knowledge, there are no reports in the literature that used western blot analysis to quantify the remaining protein expression in sarcoglycanopathies and correlate these results with muscle function in a large cohort of patients. In most previous reports, authors quantified sarcoglycan expression based on immunofluorescence studies and the cohort was divided into two groups: absence or reduction (Guglieri *et al.*, 2008; Semplicini *et al.*, 2015). However, there are some reports describing sarcoglycan patients with milder forms of the disease in which western blot was performed and protein expression was quantified ($n = 7$ cases). The remaining protein expression in these cases is variable, ranging from 18% to 45% (Tarnopolsky *et al.*, 2015; Cantero *et al.*, 2018; Gonzalez-Quereda *et al.*, 2018). Based on these reports, we decided to use 30% protein expression as a threshold to potentially identify milder cases. However, future studies analysing protein expression of a large collection of muscle biopsies in a centralized laboratory would be useful to confirm our observation. Another clear limitation is that we were not able to collect consistent data on respiratory muscle function. Many centres did not perform spirometry until patients began having symptoms of respiratory involvement, and therefore we could not be sure of the real values of forced vital capacity in our cohort. Therefore, we chose to analyse only the needed of ventilatory support. Obviously, not all European patients were included in this analysis and although 62 centres were contacted and invited to participate, not all of them responded and we missed data from some countries such as Turkey, Russia, Romania and Bulgaria. However, the data presented here are still relevant, because they describe the distribution of patients among many European countries, their clinical symptoms and the correlation between protein expression, age of onset and age of lost ambulation.

Conclusion

Our study provides important information about the clinical and genetic features of a large cohort of LGMD patients with mutations in the sarcoglycan genes. We have identified the age of onset of symptoms before 10 years old and a protein expression $<30\%$ as independent risk factors for losing ambulation before the age of 18 years. These data will be useful for the design of clinical trials, including gene replacement therapy studies, that are currently under development.

Acknowledgements

We would like to thank Dr Pol Camps form the Neurology department of the Hospital de la Santa Creu I Sant Pau de Barcelona for his advice about the statistical analysis.

Funding

This investigation was sponsored by a grant from the Spanish Ministry of Health, Fondos FEDER-ISCIII PI18/01525 to J.D-M. G.P.C's research was partially supported by the Italian Telethon Foundation Grant GSP18002B.

Competing interests

All authors report no competing interests.

Supplementary material

Supplementary material is available at *Brain* online.

References

Angelini C, Fanin M, Freda MP, Duggan DJ, Siciliano G, Hoffman EP. The clinical spectrum of sarcoglycanopathies. Neurology 1999; 52: 176–9.

Bianchini E, Fanin M, Mamchaoui K, Betto R, Sandonà D. Unveiling the degradative route of the V247M a-sarcoglycan mutant responsible for LGMD-2D. Hum Mol Genet 2014; 23: 3746–58.

Calvo F, Teijeira S, Fernandez JM, Teijeiro A, Fernandez-Hojas R, Fernandez-Lopez XA. Evaluation of heart involvement in gamma-sarcoglycanopathy (LGMD2C). A study of ten patients. Neuromuscul Disord 2000; 10: 560–6.

Cantero D, Hernández-Lain A, Martínez JFG, Pérez MR, Ruano Y, Lleixà C, et al. Milder forms of alpha-sarcoglycanopathies diagnosed in adulthood by NGS analysis. J Neurol Sci 2018; 394: 63–7.

Chan YM, Bönnemann CG, Lidov HGW, Kunkel LM. Molecular organization of sarcoglycan complex in mouse myotubes in culture. J Cell Biol 1998; 143: 2033–44.

Duclos F, Straub V, Moore SA, Venzke DP, Hrstka RF, Crosbie RH, et al. Progressive muscular dystrophy in α-sarcoglycan-deficient mice. J Cell Biol 1998; 142: 1461–71.

Ervasti JM, Ohlendieck K, Kahl SD, Gaver MG, Campbell KP. Deficiency of a glycoprotein component of the dystrophin complex in dystrophic muscle. Nature 1990; 345: 315–9.

Eymard B, Romero NB, Leturcq F, Piccolo F, Carrié A, Jeanpierre M, et al. Primary adhalinopathy (alpha-sarcoglycanopathy): clinical, pathologic, and genetic correlation in 20 patients with autosomal recessive muscular dystrophy. Neurology 1997; 48: 1227–34.

Fanin M, Melacini P, Boito C, Pegoraro E, Angelini C. LGMD2E patients risk developing dilated cardiomyopathy. Neuromuscul Disord 2003; 13: 303–9.

Fanin M, Nascimbeni AC, Aurino S, Tasca E, Pegoraro E, Nigro V, et al. Frequency of LGMD gene mutations in Italian patients with distinct clinical phenotypes. Neurology 2009; 72: 1432–5.

Ferreira AFB, Carvalho MS, Resende MBD, Wakamatsu A, Reed UC, Marie S. Phenotypic and immunohistochemical characterization of sarcoglycanopathies. Clinics (Sao Paulo) 2011; 66: 1713–9.

Ghaoui R, Cooper ST, Lek M, Jones K, Corbett A, Reddel SW, et al. Use of whole-exome sequencing for diagnosis of limb-girdle muscular dystrophy: outcomes and lessons learned. JAMA Neurol 2015; 72: 1424–32.

Gonzalez-Quereda L, Gallardo E, Töpf A, Alonso-Jimenez A, Straub V, Rodriguez MJ, et al. A new mutation of the SCGA gene is the cause of a late onset mild phenotype limb girdle muscular dystrophy type 2D with axial involvement. Neuromuscul Disord 2018; 28: 633–8.

Guglieri M, Magri F, Angelo MGD, Prelle A, Morandi L, Rodolico C, et al. Clinical, molecular, and protein correlations in a large sample of genetically diagnosed italian limb girdle muscular dystrophy patients. Hum Mutat 2008; 29: 258–66.

Israeli D, Cosette J, Corre G, Amor F, Poupiot J, Stockholm D, et al. An AAV-SGCG dose-response study in a γ-sarcoglycanopathy mouse model in the context of mechanical stress. Mol Ther Methods Clin Dev 2019; 13: 494–502.

Kyriakides T, Angelini C, Vilchez J, Hilton-Jones D. European Federation of the Neurological Societies guidelines on the diagnostic approach to paucisymptomatic or asymptomatic hyperCKemia. Muscle Nerve 2020; 61: E14–E15.

Lim LE, Campbell KP. The sarcoglycan complex in limb-girdle muscular dystrophy. Curr Opin Neurol 1998; 11: 443–52.

Lipshultz SE, Law YM, Asante-Korang A, Austin ED, Dipchand AI, Everitt MD, et al. Cardiomyopathy in children: classification and diagnosis: a scientific statement from the American Heart Association. Circulation 2019; 140: e9–68.

Liu W, Pajusalu S, Lake NJ, Zhou G, Ioannidis N, Mittal P, et al. Estimating prevalence for limb-girdle muscular dystrophy based on public sequencing databases. Genet Med 2019; 21: 2512–20.

Melacini P, Fanin M, Duggan DJ, Freda MP, Berardinelli A, Danieli GA, et al. Heart involvement in muscular dystrophies due to sarcoglycan gene mutations. Muscle Nerve 1999; 22: 473–9.

Nalini A, Gayathri N, Thaha F, Das S, Shylashree S. Sarcoglycanopathy Clinical and histochemical characteristics in 66 patients. Neurol India 2010; 58: 691–6.

Oliveira Santos M, Coelho P, Roque R. Conceição I. Very late-onset limb-girdle muscular dystrophy type 2D: a milder form with a normal muscle biopsy. J Clin Neurosci 2020; 72: 471–3.

Ozawa E, Mizuno Y, Hagiwara Y, Sasaoka T, Yoshida M. Molecular and cell biology of the sarcoglycan complex. Muscle Nerve 2005; 32: 563–76.

Politano L, Nigro V, Passamano L, Petretta V, Comi LI, Papparella S, et al. Evaluation of cardiac and respiratory involvement in sarcoglycanopathies. Neuromuscul Disord 2001; 11: 178–85.

Ponikowski P, Voors AA, Anker SD, Bueno H, Cleland JGF, Coats AJS, et al. 2016 ESC guidelines for the diagnosis and treatment of acute and chronic heart failure: the task force for the diagnosis and treatment of acute and chronic heart failure of the European Society of Cardiology (ESC) developed with the special contribution of the Heart Failure Association (HFA) of the ESC. Eur Heart J 2016; 37: 2129–200.

Sandonà D, Betto R. Sarcoglycanopathies: molecular pathogenesis and therapeutic prospects. Expert Rev Mol Med 2009; 11: 1–27.

Semplicini C, Vissing J, Dahlqvist JR, Stojkovic T, Bello L, Witting N, et al. Clinical and genetic spectrum in limb-girdle muscular dystrophy type 2E. Neurology 2015; 84: 1772–81.

Straub V, Murphy A, Udd B. 229th ENMC International Workshop: limb girdle muscular dystrophies—nomenclature and reformed classification Naarden, the Netherlands, 17-19 March 2017. Neuromuscul Disord 2017; 28: 702–10.

Sveen ML, Thune JJ, Køber L, Vissing J. Cardiac involvement in patients with limb-girdle muscular dystrophy type 2 and Becker muscular dystrophy. Arch Neurol 2008; 65: 1196–201.

Tarakci H, Berger J. The sarcoglycan complex in skeletal muscle. Front Biosci 2016; 21: 744–56.

Tarnopolsky M, Hoffman E, Giri M, Shoffner J, Brady L. Alpha-sarcoglycanopathy presenting as exercise intolerance and rhabdomyolysis in two adults. Neuromuscul Disord 2015; 25: 952–4.

Trabelsi M, Kavian N, Daoud F, Commere V, Deburgrave N, Beugnet C, et al. Revised spectrum of mutations in sarcoglycanopathies. Eur J Hum Genet 2008; 16: 793–803.

Vainzof M, Passos-Bueno MR, Pavanello RCM, Marie SK, Oliveira ASB, Zatz M. Sarcoglycanopathies are responsible for 68% of severe autosomal recessive limb-girdle muscular dystrophy in the Brazilian population. J Neurol Sci 1999; 164: 44–9.

Vita G, Vita GL, Stancanelli C, Gentile L, Russo M, Mazzeo A. Genetic neuromuscular disorders: living the era of a therapeutic revolution. Part 1: peripheral neuropathies. Neurol Sci 2019; 40: 661–9.

Winckler PB, da Silva AMS, Coimbra-Neto AR, Carvalho E, Cavalcanti E, Sobreira C, et al. Clinicogenetic lessons from 370 patients with autosomal recessive limb-girdle muscular dystrophy. Clin Genet 2019; 96: 341–53.

Xie Z, Hou Y, Yu M, Liu Y, Fan Y, Zhang W, et al. Clinical and genetic spectrum of sarcoglycanopathies in a large cohort of Chinese patients. Orphanet J Rare Dis 2019; 14: 13.

clinical neuropathology

ISSN 0722-5091

DOI 10.5414/NP301393
e-pub: July 20, 2021

Muscle inflammatory pattern in alpha- and gamma-sarcoglycanopathies

Chiara Panicucci[1], Serena Baratto[1], Lizzia Raffaghello[1], Paola Tonin[2], Adele D'Amico[3], Giorgio Tasca[4], Monica Traverso[5], Chiara Fiorillo[5], Carlo Minetti[5], Stefano Carlo Previtali[6], Elena Pegoraro[7], and Claudio Bruno[1]

[1]Center of Translational and Experimental Myology, IRCCS Istituto Giannina Gaslini, Genova, [2]Neurological Clinic, University of Verona, Verona, [3]Unit of Neuromuscular and Neurodegenerative Disorders, IRCCS Bambino Gesù Children's Hospital, [4]Unità Operativa Complessa di Neurologia, Fondazione Policlinico Universitario "A. Gemelli" IRCCS, Rome, [5]Pediatric Neurology and Neuromuscular Disorders Unit, IRCCS Istituto Giannina Gaslini and University of Genova, Genova, [6]Neuromuscular Repair Unit, Inspe and Division of Neuroscience, IRCSS San Raffaele ScientificInstitute, Milan, and [7]ERN Neuromuscular Center Department of Neurosciences, University of Padova, Padova, Italy

Key words
sarcoglycanopathy – Duchenne muscular dystrophy – limb-girdle muscular dystrophies – inflammation – DAMPS

Supplemental material is available without charge at: www.clinneuropathol.com
Vol. 40 – ■■■/■■■ 2021

Abstract. Aim: Since the immune system plays a role in the pathogenesis of several muscular dystrophies, we aim to characterize several muscular inflammatory features in α- (LGMD R3) and γ-sarcoglycanopathies (LGMD R5). Materials and methods: We explored the expression of major histocompatibility complex class I molecules (MHCI), and we analyzed the composition of the immune infiltrates in muscle biopsies from 10 patients with LGMD R3 and 8 patients with LGMD R5, comparing the results to Duchenne muscular dystrophy patients (DMD). Results: A consistent involvement of the immune response was observed in sarcoglycanopathies, although it was less evident than in DMD. LGMD R3-R5 and DMD shared an abnormal expression of MHCI, and the composition of the muscular immune cell infiltrate was comparable. Conclusion: These findings might serve as a rationale to fine-tune a disease-specific immunomodulatory regimen, particularly relevant in view of the rapid development of gene therapy for sarcoglycanopathies.

Received
March 4, 2021;
accepted in revised form
April 14, 2021

Correspondence to
Claudio Bruno, MD, PhD
Center of Translational and Experimental Myology, IRCCS Istituto Giannina Gaslini,
Via Gaslini 5,
16147 Genova, Italy
claudio2246@gmail.com

Introduction

Sarcoglycanopathies are a group of recessive inherited limb-girdle muscular dystrophies (LGMDs) due to mutations in sarcoglycan genes that primarily affect proximal skeletal muscles leading to progressive muscle weakness [1]. Among LGMDs, sarcoglycanopathies are classified as LGMD R3 α-sarcoglycan-related, LGMD R4 β-sarcoglycan-related, LGMD R5 γ-sarcoglycan-related, and LGMD R6 δ-sarcoglycan-related [2].

Despite their genetic heterogeneity, muscular dystrophies are characterized by myofiber necrosis and regeneration, reactive fibrosis and adipose tissue substitution, reduced long-term regenerative capacity, and inflammatory infiltrates [3, 4, 5]. Inflammatory processes in muscular dystrophies are triggered by release of danger-associated molecular patterns (DAMPs) in the extracellular space by damaged or necrotic cells [6]. Upon release, DAMPs activate Toll-like receptors (TLRs) and type 2 purinergic receptors (P2s) expressed in non-immune cells, such as endothelial cells and fibroblasts, and innate immune cells, such as neutrophils, macrophages, and dendritic cells (DCs) [7]. DAMPs-activated cells secrete potent pro-inflammatory molecules, such as interleukin 1-β (IL1-β), TNF-α, reactive oxygen species (ROS), and chemokines, thus recruiting and activating other innate and adaptive immune cells. Taken together, these mechanisms establish a chronic inflammatory milieu in muscular tissue, which contributes to worsen the underling dystrophic process [8, 9].

The involvement of the immune system has been illustrated in mouse models and in human muscle samples of different muscular dystrophies such as Duchenne muscular dystrophy (DMD), dysferlinopathies, and facioscapulohumeral muscular dystrophy

Table 1. LGMD R3 and R5 patients' information, gender, age at muscle biopsy (MB), gene mutations, histological parameters evaluated by H&E staining, and clinical features.

Patient ID	Sex	Gene	Mutation(s)	Age MB (yrs)	Fiber size var.	Nuclear Intern.	Necro-sis/ Inflamm.	Fibro-sis	Dystro-phic score	Age and symptoms at onset (yrs)	Age at last visit (yrs)	Wheel chair-bound (yes, no/ yrs)	Cardiac involve-ment (yes, no/ yrs)	Respira-tory insuf-ficiency (yrs)	Muscle MRI (yes, no/ ID in REF 33)
LGMD R3.1	M	SGCA	c. 329C>T/p.Arg77Cys c.1005C>A/p.Cys335X	9.9	2	0	2	2	6	9, difficulties in running and climbing stairs	30	yes, 28	yes, 25	no	Yes IT3_6
LGMD R3.2	F	SGCA	c.409G>A/p.Glu1137Lys c.850C>T/p.Arg284Cys	4.0	2	1	3	1	7	asymptomatic hyperCKemia	7	no	no	no	NA
LGMD R3.3	F	SGCA	c.308T>C/p.Ile103Thr c.850C>T/p.Arg284Cys	19.4	1	1	1	1	4	12, myalgias exercise intolerance	29	no	no	no	Yes IT1_8
LGMD R3.4	F	SGCA	c.329C>T/p.Arg77Cys IVS5:c.584+5G>A	0.8	1	1	1	2	5	4, hyperCKemia difficulties in running	13	no	no	no	Yes IT3_1
LGMD R3.5	M	SGCA	c.409G>A/p.Glu1137Lys c.739G>A/p.Val247Met	26.3	2	2	0	1	5	8, difficulties in climbing stairs	31	no	no	no	Yes IT3_3
LGMD R3.6	M	SGCA	c.329C>T/p.Arg77Cys c.346A>C/p.Thr116Pro	49.6	2	1	0	1	4	6, myalgias, myoglobinuria	50	no	no	no	NA
LGMD R3.7	F	SGCA	c.92T>C/p.Leu31Pro c.739G>A/p.Val247Met	19.2	1	1	0	1	3	18, myalgias	29	no	no	no	NA
LGMD R3.8	F	SGCA	c.739G>A/p.Val247Met c.739G>A/p.Val247Met	9.1	1	0	1	1	3	7, LL myalgias	9	no	no	no	NA
LGMD R3.9	F	SGCA	c.739G>A/p.Val247Met c.739G>A/p.Val247Met	41.8	2	1	0	1	4	38, myalgias hyperCKemia	50	no	no	no	Yes IT5_3
LGMD R3.10	F	SGCA	c.92T>C/p.Leu31Pro c.850C>T/p.Arg284Cys	25.2	2	0	0	1	3	6, difficulties in running and myalgias	28	no	no	no	NA
LGMD R5.1	F	SGCG	c.525delT/p.Phe175Leufs*20 c.525delT/p.Phe175Leufs*20	19.5	3	1	2	3	9	Not known, proximal LL weakness	43	yes, 20	no	no	NA

Table 1. Continuation.

Patient ID	Sex	Gene	Mutation(s)	Age MB (yrs)	Fiber size var.	Nuclear Intern.	Necro-sis/ Inflamm.	Fibro-sis	Dystro-phic score	Age and symptoms at onset (yrs)	Age at last visit (yrs)	Wheel chair-bound (yes, no/ yrs)	Cardiac involve-ment (yes, no/ yrs)	Respira-tory insuf-ficiency (yrs)	Muscle MRI (yes, no/ ID in REF 33)
LGMD R5.2	F	SGCG	c.525delT/p.Phe175Leufs*20 c.525delT/p.Phe175Leufs*20	15.6	3	1	0	2	6	8, proximal LL weakness	28	23	yes, 25	yes, 25	NA
LGMD R5.3	M	SGCG	IVS4:c.385+2T>C c.801_802delTC/p.Pro268Argfs*24	13.4	2	1	1	1	5	7, difficulties in running and climbing stairs	35	20	yes, 19	no	Yes IT3_7
LGMD R5.4	M	SGCG	c.848G>A/p.Cys283Tyr c.848G>A/p.Cys283Tyr	1.5	2	1	3	1	7	asymptomatic hyperCKemia	7	no	no	no	NA
LGMD R5.5	F	SGCG	c.342dupT/p.Ala115Cysfs*41 c.525delT/p.Phe175Leufs*20	2.2	1	1	2	3	7	4, hyperCKemia proximal LL weakness	14	yes, 13	yes, 14	yes, 14	Yes IT1_2
LGMD R5.6	F	SGCG	c.371G>A/p.Gly124Asp c.371G>A/p.Gly124Asp	6.2	2	1	0	1	4	6, myalgias	21	no	no	no	Yes IT5_4
LGMD R5.7	F	SGCG	c.89delG/p.Gly30fs*20 c.307C>G/p.Leu130Val	6	1	1	2	2	6	2, proximal LL weakness	12	no	no	no	NA
LGMD R5.8	M	SGCG	Deletion exon 7 Deletion exon 7	3.5	2	0	3	2	7	4, proximal LL and UL weakness	7	no	no	no	NA

UL = upper limbs; LL = lower limbs; NA = not applicable.

(FSHD) as reviewed by Tidbal et al. [10]. DMD muscle tissue shows an up-regulation of DAMPs-sensing receptors like TLRs and P2 receptors [11, 12], muscle infiltration by macrophages, neutrophils, dendritic cells, and T cells [13], increased muscle transcripts of major histocompatibility complex class I (MHCI) [14] and IL-17 [15]. As such, steroid therapy is a mainstay of treatment for DMD [16].

However, there are no studies unveiling the contribution of the immune system to the onset and progression of sarcoglycanopathies, although muscle biopsies from sarcoglycan-deficient patients often display inflammatory features. Increased transcripts of macrophagic and T-cell markers [17, 18, 19], combined with an up-regulation of the purinergic signal and up-raised levels in pro-inflammatory cytokines, have been shown in Sgca and Sgcg-deficient mice, lacking the α- and the γ-sarcoglycan protein, respectively [19, 20]. Moreover, Sgcg-deficient mice, which represent a suitable LGMD R5 experimental model, showed a reduction of muscle inflammation and membrane damage upon treatment with the immunomodulatory drug FTY720 [20].

To better characterize the inflammatory response in sarcoglycanopathies, we analyzed muscle biopsies of 10 patients with α- and 8 patients with γ-sarcoglycanopathy. The muscle infiltrates were immunophenotyped by the evaluation of CD45, CD68, CD8, CD4 expression, and the detection of MHC class I molecules.

Materials and methods

Patients

Muscle biopsies from 10 LGMD R3 α-sarcoglycan and 8 LGMD R5 γ-sarcoglycan genetically confirmed patients were retrospectively collected from 6 Italian tertiary neuromuscular centers.

Quadricep muscle biopsies were performed for diagnostic purposes. Families of patients gave their consent for research studies in muscle specimens.

As positive controls, we analyzed muscle biopsies from 6 patients with DMD. Six muscle biopsies from patients with not spe-

cific muscle weakness or myalgia and without dystrophic signs at pathological examination served as negative controls.

Histology and immunohistochemistry

8-mm sections from frozen quadricep muscle were cut on a cryostat, collected on poly-L-lysine (0.5 mg/mL) coated glass slides and subsequently stained with Hematoxylin and Eosin (H & E). Muscle biopsies were also stained for the following antibodies according to the manufacturer's instruction and developed in 3,3'-diaminobenzidine (DAB) substrate: CD45 (Clone 2B11, Invitrogen, Carlsbad, CA, USA), MHCI (Clone W6/32, Sigma, St. Louis, MO, USA), CD68 (Clone 514H12, Leica, Newcastle, UK), CD8 (Clone 4B11, Leica), and CD4 (Clone 4B12, Leica). For each staining, muscle sections were scanned with Axioplan Imager M2 microscope software AxioVs40 version 4.8.2.0 (Zeiss, Jena, Germany). Non-overlapping images at × 10 magnification were snapped through the whole section to cover the entire muscle cross-sectional area.

Two blinded examiners performed the histological examinations. H & E staining was evaluated with a "dystrophic score" adapted from Statland et al. [21] and Peverelli et al. [22]. Four dystrophic features were considered: 1) fiber size variability, 2) nuclear internalization, 3) cell necrosis and inflammatory infiltrates, and 4) interstitial fibrosis. The extent of each pathological change was judged by visual inspection and scored between 0 and 3 (0 = normal; 1 = slightly increased; 2 = moderately increased; 3 = severely increased) (Supplementary Table 1). The total score ranged from 0 (normal histological phenotype) up to 12 (severe histological phenotype).

For CD45, CD68, CD8, and CD4 staining, the positive cells were blindly manually enumerated throughout the whole section and reported as density of positive cells to the unit of area (number of cells/number of sections).

For MHC class I staining, the signal was quantified as previously reported [23]. MHCI staining was considered as negative if only capillaries were stained, and positive when both capillaries and sarcolemma were positive for MHCI.

Statistical analysis

Differences of quantitative parameters between the groups were analyzed by the Kruskal-Wallis test for non-parametric data. $p < 0.05$ was considered statistically significant. Graphs show medians +/– 10^{th} and 90^{th} percentiles. Correlations between variables were assessed by Spearman correlation test for non-parametric data. Statistical analysis and graphs were performed with GraphPad8 (Graph-Pad Software, San Diego, CA, USA).

Results

LGMD R3 and R5 patients' information, including gender, gene mutations, histological parameters, and clinical features such as age, symptoms, and serum CK at onset, cardiac involvement, respiratory insufficiency, and MRI study are listed in Table 1.

The H & E staining was performed to assess the overall architecture of the tissues (Figure 1a, b, c, d). In order to quantify the common dystrophic features, a dystrophic score was assigned (Table 1).

MHCI signal was absent in the negative controls and was up-regulated in all the dystrophic patients. Positive MHCI staining was localized both on the surface of inflammatory cells and on the sarcolemma of several myofibers (Figure 1e, f, g, h).

To detect the infiltrating immune cells, muscle tissues were stained for CD45, a panleucocytes marker (Figure 2a, b, c, d). $CD45^+$ cells were significantly higher in DMD and LGMD R3-R5 groups in comparison to the negative controls (Figure 2e).

To characterize the inflammatory infiltrates, muscle samples were stained for markers of the innate and adaptive immune response. Specifically, for the innate immune cells, we checked CD68 (Figure 2f, g, h, i), a surface marker for macrophages; and for the adaptive immunity, we analyzed the $CD8^+$ (Figure 2m, n, o, p) and $CD4^+$ T cells (Figure 2r, s, t, u). $CD68^+$ cells were significantly higher in DMD and LGMD R3-R5 groups in comparison to the negative controls (Figure 2l). $CD8^+$ cells/area of tissue were sig-

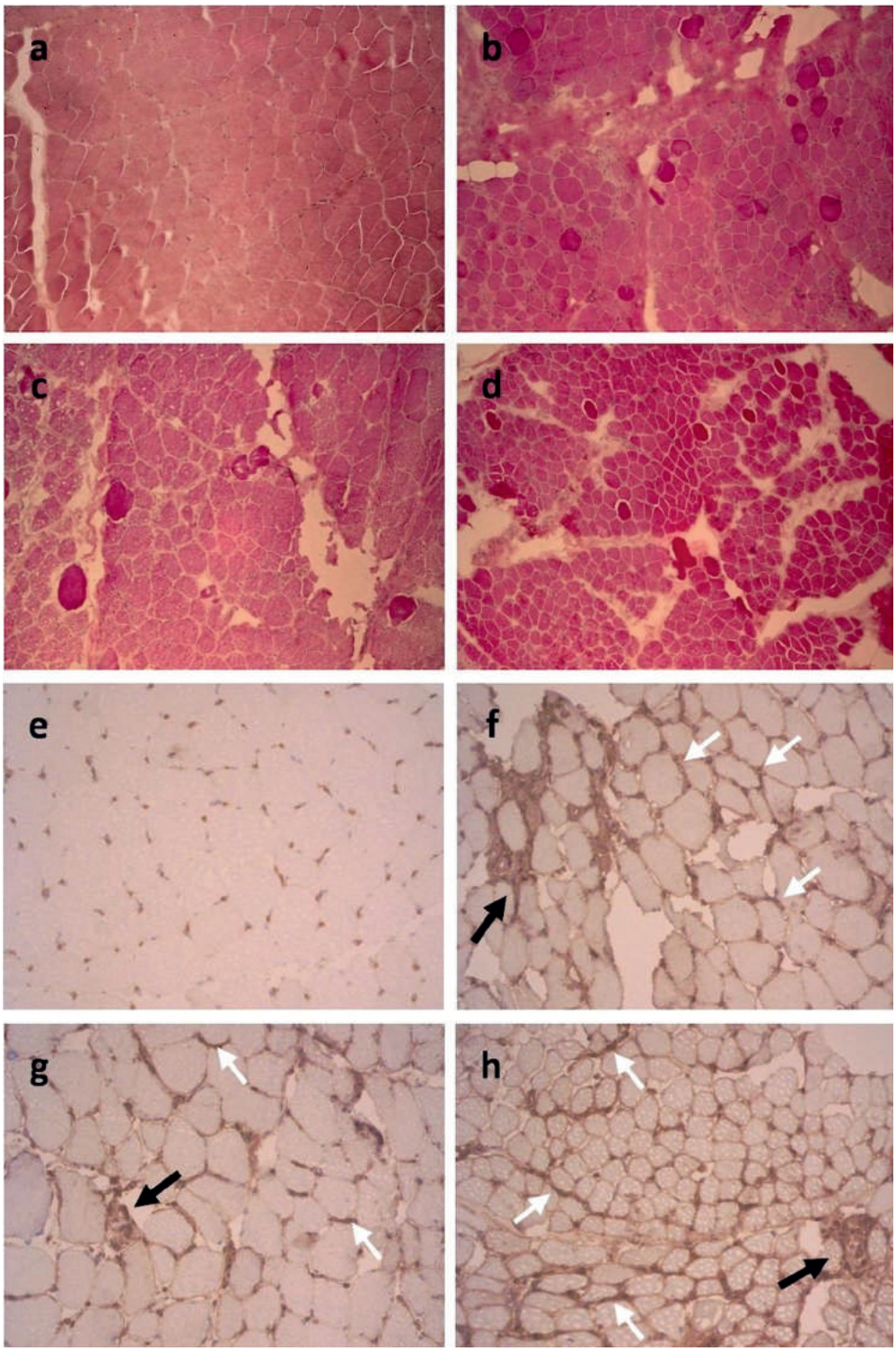

Figure 1. Dystrophic features and MHC class I molecules expression in DMD and LGMD R3-R5. Representative pictures of the H & E staining of negative controls (a), Duchenne muscular dystrophy (b), limb-girdle muscular dystrophy R3 (c), and limb-girdle muscular dystrophy R5 (d). Original magnification × 10. Representative pictures of the MHC class I (MHC I) molecules in negative controls (e), Duchenne muscular dystrophy (f), limb-girdle muscular dystrophy R3 (g), and limb-girdle muscular dystrophy R5 (h). Original magnification × 20. Black arrows show positive staining on the membrane of immune cells, and white arrows show positive staining along the plasma membrane of muscle cells.

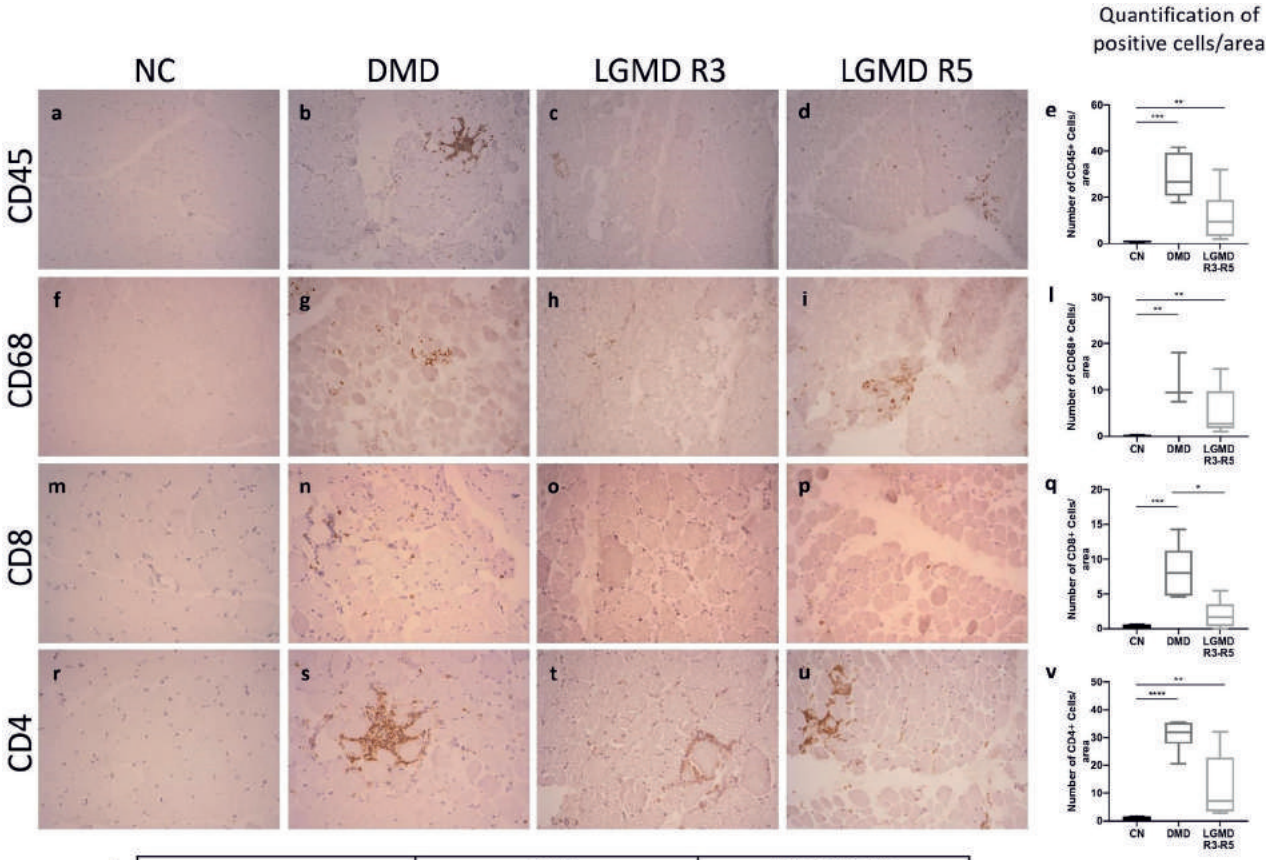

z

	DMD		LGMD R3-R5	
	Spearman r	p-value	Spearman r	p-value
DS vs Age at MB	-0.2	0.7	-0.5	0.07
DS vs CD45+cells	0.39	0.47	0.63	0.09
Age at MB vs CD45+ cells	0.5	0.45	-0.61	0.014

Figure 2. Immunophenotype of the muscle inflammatory infiltrates DMD and LGMD R3-R5. Representative pictures of the CD45 (a, b, c, d), CD68 (f, g, h, i), CD8 (m, n, o, p), and CD4 (r, s, t, u) staining. The muscle biopsies were taken from negative controls (a, f, m, r), Duchenne muscular dystrophy (b, g, n, s), limb-girdle muscular dystrophy R3 (c, h, o, t), and limb-girdle muscular dystrophy R5 (d, i, p, u). Original magnification × 20. Box plots represent the number of CD45+ cells (e), CD68+ cells (l), CD8+ cells (q), and CD4+ cells (v), showing the median, the 10th, and the 90th percentiles. *p-value< 0.05, **p-value < 0.01, ***p-value < 0.001. z: The table shows the results of the Spearman correlation between the number of CD45+ cells, the age at muscle biopsy, and the dystrophic score. DS = dystrophic score. The p-value was considered as statistically significant when < 0.05.

nificantly increased in the DMD compared to the negative controls and to the sarcoglycanopathies (Figure 2q). The amount of CD4$^+$ T-cells was significantly higher in the DMD and LGMD R3-R5 than in the negative control group (Figure 2v).

No significant correlations were found between the dystrophic score and the age at muscle biopsy, although a trend showed the two parameters to be linked by an inverse correlation in sarcoglycanopathies (Figure 2z). A significant inverse correlation was found between the age at muscle biopsy and the number of CD45$^+$ cells in the sarcoglycan group (Figure 2z).

Discussion

We immunophenotyped the intra-muscular inflammatory infiltrates in muscle biopsies from LGMD R3 and R5 patients in parallel with samples from DMD patients, which we used as disease controls for their known inflammatory features.

We found that MHC class I pattern expression was similar throughout all the dystrophic samples. MHCI molecules are not constitutively expressed in skeletal muscle tissue under physiological conditions [8]. It is known that upon exposure to a high concentration of interferons IFN-α, -β, or -γ, myo-

cells markedly increase the transcription of MHCI that binds peptides generated mainly from the degradation of cytosolic proteins by the proteasome. So far, MHCI up-regulation has been considered a diagnostic marker of inflammatory myopathies [23, 24, 25], while its detection in muscular dystrophies is rather inconsistent [14, 23, 26, 27, 28]. In our samples, all dystrophic muscles expressed MHC class I molecules, specifically on the surface of inflammatory cells and on the sarcolemma of almost all muscle fibers.

According to these results, MHCI abnormal expression, besides being a diagnostic marker of inflammatory myopathies, can be considered a sign of the inflammatory activation of dystrophic muscles, likely due to the direct involvement of the muscle cells in promoting the local immune response by antigen presentation.

Nevertheless, further studies are needed to systematically quantify the MHC class I expression in inflammatory myopathies and muscular dystrophies in order to identify possible differential involvement of the antigen-presenting system.

The CD45 staining provided a general view of the muscular immune infiltrates that were evident in LGMD R3-R5, although in both cases less evident than in DMD. In LGMD R3-R5, the density of $CD45^+$ cells inversely correlates with the age at muscle biopsy, mimicking what is already shown in DMD where inflammatory pathways predominate in the early stages, suggesting a stage-specific remodeling of human dystrophic muscle [29].

We immunophenotyped the $CD45^+$ cell infiltrates by checking macrophages, $CD8^+$, and $CD4^+$ T cell markers. All the disease groups showed a predominance of $CD4^+$ T-cells, less macrophages, and occasional $CD8^+$ T cells as previously reported in DMD and dysferlinopathy [26, 27], and to our knowledge, this is the first immuno-characterization of cell infiltrates in LGMD R3 and R5.

Dystrophic patients showed a significantly higher density of $CD45^+$, $CD68^+$, and $CD4^+$ cells compared to the negative controls, without statistically significant differences between DMD and sarcoglycanopathies. The only exception was represented by $CD8^+$ effector T cells, which were significantly up-regulated in DMD compared to sarcoglycanopathies, suggesting that a different regulation of the cell-mediated adaptive immunity might occur in the two groups. Nevertheless, no information about the activation state of the immune cells infiltrating the dystrophic muscles can be assumed from this paper.

Despite the difference in the density of $CD8^+$ T cells, overall, our data show that DMD and α- and γ-sarcoglycanopathies share a common immune response, involving both innate and adaptive response. We hypothesize that the instability and loss of the dystrophin-associated protein complex (DAPC) might be the trigger of the chronic inflammatory response. A possible correlation between the extension of the immune response and the representation of the DAPC on muscle membranes needs to be explored in further studies. DMD therapeutic approach includes low doses of continuative oral steroids, as they proved to slow down disease progression [16], dampening the muscle inflammatory status [13]. Conversely, a placebo-controlled trial assessing the effects of steroids in sarcoglycan-related muscular dystrophies has never been proposed, although the efficacy of immunomodulatory treatments improved muscle repair and performance in α- and γ-sarcoglycan deficient mouse models [30, 31] and in 1 female patient affected by LGMD R3 [32]. Thus, sarcoglycan LGMDs might benefit from an immunomodulatory regimen.

In conclusion, we characterized the intramuscular immune infiltrates in patients with α- and γ-sarcoglycan gene deficiencies. However, we recognize some limitations in our study: the groups were not homogeneous by gender and age at muscle biopsy, given the limited number of patients, and due to the parceling of the muscular immune infiltrates analyzed.

Currently, clinical trials offer different approaches, including gene therapy, which is rapidly developing for many muscular dystrophies. In this scenario, the right immunosuppressant scheme could endorse the efficacy of disease-specific gene therapy by dampening the basal muscular inflammation, and our findings might be useful to fine-tune a disease-specific immunomodulatory regimen.

Acknowledgment

We acknowledge the Telethon Genetic BioBank (GTB12001D), the Eurobiobank network, and Paolo Broda for his technical assistance. GT, CF, EP, and CB are members of the European Reference Network for Neuromuscular Diseases (ERN-NMD).

Data availability

All data generated or analyzed during this study are included in this published article.

Ethics approval

All procedures followed were in accordance with the ethical standards of the responsible committee on human experimentation (institutional and national) and with the Helsinki Declaration of 1975, as revised in 2000.

Consent to participate and for publication

All muscle biopsies were performed for diagnostic purpose, and patients expressed their consent for research studies on muscle specimens.

Funding

This work was supported by Telethon-Italy grant GGP17192, by the Italian Ministry of Health (RF 2016-02364503), and by Fondazione Compagnia di San Paolo grant (ROL 32561).

Conflict of interest

The authors declare that they have no conflict of interest.

References

[1] *Alonso-Pérez J, González-Quereda L, Bello L, Guglieri M, Straub V, Gallano P, Semplicini C, Pegoraro E, Zangaro V, Nascimento A, Ortez C, Comi GP, Dam LT, De Visser M, van der Kooi AJ, Garrido C, Santos M, Schara U, Gangfuß A, Løkken N, et al.* New genotype-phenotype correlations in a large European cohort of patients with sarcoglycanopathy. Brain. 2020; *143:* 2696-2708.

[2] *Straub V, Murphy A, Udd B, Corrado A, Aymé S, Bönneman C, de Visser M, Hamosh A, Jacobs L, Khizanishvili N, Kroneman M, Laflorêt P, Murphy A, Nigro V, Rufibach L, Sarkozy A, Swanepoel S, Torrente I, Udd B, Urtizberea A, et al; LGMD workshop study group.* 229th ENMC international workshop: Limb girdle muscular dystrophies – Nomenclature and reformed classification Naarden, the Netherlands, 17-19 March 2017. Neuromuscul Disord. 2018; *28:* 702-710.

[3] *Kirschner J, Lochmüller H.* Sarcoglycanopathies. Handb Clin Neurol. 2011; *101:* 41-46.

[4] *Mercuri E, Bönnemann CG, Muntoni F.* Muscular dystrophies. Lancet. 2019; *394:* 2025-2038.

[5] *Fanin M, Angelini C.* Regeneration in sarcoglycanopathies: expression studies of sarcoglycans and other muscle proteins. J Neurol Sci. 1999; *165:* 170-177.

[6] *Pétrilli V, Dostert C, Muruve DA, Tschopp J.* The inflammasome: a danger sensing complex triggering innate immunity. Curr Opin Immunol. 2007; *19:* 615-622.

[7] *Chen GY, Nuñez G.* Sterile inflammation: sensing and reacting to damage. Nat Rev Immunol. 2010; *10:* 826-837.

[8] *Rosenberg AS, Puig M, Nagaraju K, Hoffman EP, Villalta SA, Rao VA, Wakefield LM, Woodcock J.* Immune-mediated pathology in Duchenne muscular dystrophy. Sci Transl Med. 2015; *7:* 299rv4.

[9] *Panicucci C, Raffaghello L, Bruzzone S, Baratto S, Principi E, Minetti C, Gazzerro E, Bruno C.* eATP/P2X7R Axis: An orchestrated pathway triggering inflammasome activation in muscle diseases. Int J Mol Sci. 2020; *21:* 5963.

[10] *Tidball JG, Welc SS, Wehling-Henricks M.* Immunobiology of inherited muscular dystrophies. Compr Physiol. 2018; *8:* 1313-1356.

[11] *Chen YW, Donnelly-Roberts DL, Namovic MT, Gintant GA, Cox BF, Jarvis MF, Harris RR.* Pharmacological characterization of P2X7 receptors in rat peritoneal cells. Inflamm Res. 2005; *54:* 119-126.

[12] *Gazzerro E, Baldassari S, Assereto S, Fruscione F, Pistorio A, Panicucci C, Volpi S, Perruzza L, Fiorillo C, Minetti C, Traggiai E, Grassi F, Bruno C.* Enhancement of muscle T regulatory cells and improvement of muscular dystrophic process in mdx mice by blockade of extracellular ATP/P2X Axis. Am J Pathol. 2015; *185:* 3349-3360.

[13] *Kissel JT, Burrow KL, Rammohan KW, Mendell JR; CIDD Study Group.* Mononuclear cell analysis of muscle biopsies in prednisone-treated and untreated Duchenne muscular dystrophy. Neurology. 1991; *41:* 667-672.

[14] *Pescatori M, Broccolini A, Minetti C, Bertini E, Bruno C, D'amico A, Bernardini C, Mirabella M, Silvestri G, Giglio V, Modoni A, Pedemonte M, Tasca G, Galluzzi G, Mercuri E, Tonali PA, Ricci E.* Gene expression profiling in the early phases of DMD: a constant molecular signature characterizes DMD muscle from early postnatal life throughout disease progression. FASEB J. 2007; *21:* 1210-1226.

[15] *De Pasquale L, D'Amico A, Verardo M, Petrini S, Bertini E, De Benedetti F.* Increased muscle expression of interleukin-17 in Duchenne muscular dystrophy. Neurology. 2012; *78:* 1309-1314.

[16] *McDonald CM, Henricson EK, Abresch RT, Duong T, Joyce NC, Hu F, Clemens PR, Hoffman EP, Cnaan A, Gordish-Dressman H; CINRG Investigators.* Long-term effects of glucocorticoids on function, quality of life, and survival in patients with Duchenne muscular dystrophy: a prospective cohort study. Lancet. 2018; *391:* 451-461.

[17] *Pasteuning-Vuhman S, Putker K, Tanganyika-de Winter CL, Boertje-van der Meulen JW, van Vliet L, Overzier M, Plomp JJ, Aartsma-Rus A, van Putten M.* Natural disease history of mouse models for limb girdle muscular dystrophy types 2D and 2F. PLoS One. 2017; *12:* e0182704.

[18] *Verhaart IEC, Putker K, van de Vijver D, Tanganyika-de Winter CL, Pasteuning-Vuhman S, Plomp JJ, Aartsma-Rus AM, van Putten M.* Cross-sectional study into age-related pathology of mouse models for limb girdle muscular dystrophy types 2D and 2F. PLoS One. 2019; *14:* e0220665.

[19] *Gazzerro E, Baratto S, Assereto S, Baldassari S, Panicucci C, Raffaghello L, Scudieri P, De Battista D, Fiorillo C, Volpi S, Chaabane L, Malnati M, Messina G, Bruzzone S, Traggiai E, Grassi F, Minetti C, Bruno C.* The danger signal extracellular ATP is involved in the immunomediated damage of α-sarcoglycan-deficient muscular dystrophy. Am J Pathol. 2019; *189:* 354-369.

[20] *Heydemann A.* Severe murine limb-girdle muscular dystrophy type 2C pathology is diminished by FTY720 treatment. Muscle Nerve. 2017; *56:* 486-494.

[21] *Statland JM, Shah B, Henderson D, Van Der Maarel S, Tapscott SJ, Tawil R.* Muscle pathology grade for facioscapulohumeral muscular dystrophy biopsies. Muscle Nerve. 2015; *52:* 521-526.

[22] *Peverelli L, Testolin S, Villa L, D'Amico A, Petrini S, Favero C, Magri F, Morandi L, Mora M, Mongini T, Bertini E, Sciacco M, Comi GP, Moggio M.* Histologic muscular history in steroid-treated and untreated patients with Duchenne dystrophy. Neurology. 2015; *85:* 1886-1893.

[23] *van der Pas J, Hengstman GJD, ter Laak HJ, Borm GF, van Engelen BG.* Diagnostic value of MHC class I staining in idiopathic inflammatory myopathies. J Neurol Neurosurg Psychiatry. 2004; *75:* 136-139.

[24] *Dalakas MC, Hohlfeld R.* Polymyositis and dermatomyositis. Lancet. 2003; *362:* 971-982.

[25] *Jain A, Sharma MC, Sarkar C, Bhatia R, Singh S, Handa R.* Major histocompatibility complex class I and II detection as a diagnostic tool in idiopathic inflammatory myopathies. Arch Pathol Lab Med. 2007; *131:* 1070-1076.

[26] *Nagappa M, Nalini A, Narayanappa G.* Major histocompatibility complex and inflammatory cell subtype expression in inflammatory myopathies and muscular dystrophies. Neurol India. 2013; *61:* 614-621.

[27] *Yin X, Wang Q, Chen T, Niu J, Ban R, Liu J, Mao Y, Pu C.* CD4+ cells, macrophages, MHC-I and C5b-9 involve the pathogenesis of dysferlinopathy. Int J Clin Exp Pathol. 2015, *8:* 3069-3075.

[28] *Confalonieri P, Oliva L, Andreetta F, Lorenzoni R, Dassi P, Mariani E, Morandi L, Mora M, Cornelio F, Mantegazza R.* Muscle inflammation and MHC class I up-regulation in muscular dystrophy with lack of dysferlin: an immunopathological study. J Neuroimmunol. 2003; *142:* 130-136.

[29] *Chen YW, Nagaraju K, Bakay M, McIntyre O, Rawat R, Shi R, Hoffman EP.* Early onset of inflammation and later involvement of TGFbeta in Duchenne muscular dystrophy. Neurology. 2005; *65:* 826- 834.

[30] *Sciorati C, Buono R, Azzoni E, Casati S, Ciuffreda P, D'Angelo G, Cattaneo D, Brunelli S, Clementi E.* Co-administration of ibuprofen and nitric oxide is an effective experimental therapy for muscular dystrophy, with immediate applicability to humans. Br J Pharmacol. 2010; *160:* 1550-1560.

[31] *Quattrocelli M, Salamone IM, Page PG, Warner JL, Demonbreun AR, McNally EM.* Intermittent glucocorticoid dosing improves muscle repair and function in mice with limb-girdle muscular dystrophy. Am J Pathol. 2017; *187:* 2520-2535.

[32] *Angelini C, Fanin M, Menegazzo E, Freda MP, Duggan DJ, Hoffman EP.* Homozygous alpha-sarcoglycan mutation in two siblings: one asymptomatic and one steroid-responsive mild limb-girdle muscular dystrophy patient. Muscle Nerve. 1998; *21:* 769-775.

[33] *Tasca G, Monforte M, Díaz-Manera J, Brisca G, Semplicini C, D'Amico A, Fattori F, Pichiecchio A, Berardinelli A, Maggi L, Maccagnano E, Løkken N, Marini-Bettolo C, Munell F, Sanchez A, Alshaikh N, Voermans NC, Dastgir J, Vlodavets D, Haberlová J, et al.* MRI in sarcoglycanopathies: a large international cohort study. J Neurol Neurosurg Psychiatry. 2018; *89:* 72-77.

pharmaceuticals

Article

P2X7 Receptor Antagonist Reduces Fibrosis and Inflammation in a Mouse Model of Alpha-Sarcoglycan Muscular Dystrophy

Lizzia Raffaghello [1], Elisa Principi [1], Serena Baratto [1], Chiara Panicucci [1], Sara Pintus [1], Francesca Antonini [2], Genny Del Zotto [2], Andrea Benzi [3], Santina Bruzzone [3], Paolo Scudieri [4,5], Carlo Minetti [5,6], Elisabetta Gazzerro [7,*,†] and Claudio Bruno [1,5,*,†]

1 Center of Translational and Experimental Myology, IRCCS Istituto Giannina Gaslini, 16147 Genoa, Italy; lizziaraffaghello@gaslini.org (L.R.); elisaprincipi@gaslini.org (E.P.); serenabaratto@gaslini.org (S.B.); chiarapanicucci@gaslini.org (C.P.); sarapintus@gaslini.org (S.P.)
2 Core Facilities, Department of Research and Diagnostics, IRCCS Istituto Giannina Gaslini, 16147 Genoa, Italy; francescaantonini@gaslini.org (F.A.); gennydelzotto@gaslini.org (G.D.Z.)
3 Section of Biochemistry, Department of Experimental Medicine (DIMES), University of Genoa, 16132 Genoa, Italy; andreeabenzi@gmail.com (A.B.); santinabruzzone@unige.it (S.B.)
4 Medical Genetic Unit, IRCCS Istituto Giannina Gaslini, 16147 Genoa, Italy; paoloscudieri@unige.it
5 Department of Neuroscience, Rehabilitation, Ophtalmology, Genetics, Maternal and Child Health—DINOGMI, University of Genoa, 16147 Genoa, Italy; carlominetti@gaslini.org
6 Pediatric Neurology Unit, IRCCS Istituto Giannina Gaslini, 16147 Genoa, Italy
7 Unit of Muscle Research, Experimental and Clinical Research Center Charité Universitätsmedizin and Max Delbrück Research Center, 10627 Berlin, Germany
* Correspondence: elisabetta.gazzerro@charite.de (E.G.); claudiobruno@gaslini.org (C.B.); Tel.: +49-030-540450046 (E.G.); +39-010-56362756 (C.B.)
† These authors contributed equally to this work.

Citation: Raffaghello, L.; Principi, E.; Baratto, S.; Panicucci, C.; Pintus, S.; Antonini, F.; Zotto, G.D.; Benzi, A.; Bruzzone, S.; Scudieri, P.; et al. P2X7 Receptor Antagonist Reduces Fibrosis and Inflammation in a Mouse Model of Alpha-Sarcoglycan Muscular Dystrophy. *Pharmaceuticals* **2022**, *15*, 89. https://doi.org/10.3390/ph15010089

Academic Editor: Qian Chen

Received: 14 December 2021
Accepted: 11 January 2022
Published: 13 January 2022

Abstract: Limb-girdle muscular dystrophy R3, a rare genetic disorder affecting the limb proximal muscles, is caused by mutations in the α-sarcoglycan gene (Sgca) and aggravated by an immune-mediated damage, finely modulated by the extracellular (e)ATP/purinoceptors axis. Currently, no specific drugs are available. The aim of this study was to evaluate the therapeutic effectiveness of a selective P2X7 purinoreceptor antagonist, A438079. Sgca knockout mice were treated with A438079 every two days at 3 mg/Kg for 24 weeks. The P2X7 antagonist improved clinical parameters by ameliorating mice motor function and decreasing serum creatine kinase levels. Histological analysis of muscle morphology indicated a significant reduction of the percentage of central nuclei, of fiber size variability and of the extent of local fibrosis and inflammation. A cytometric characterization of the muscle inflammatory infiltrates showed that A438079 significantly decreased innate immune cells and upregulated the immunosuppressive regulatory T cell subpopulation. In α-sarcoglycan null mice, the selective P2X7 antagonist A438079 has been shown to be effective to counteract the progression of the dystrophic phenotype and to reduce the inflammatory response. P2X7 antagonism via selective inhibitors could be included in the immunosuppressant strategies aimed to dampen the basal immune-mediated damage and to favor a better engraftment of gene-cell therapies.

Keywords: muscular dystrophy; limb girdle muscular dystrophy; purinergic receptors

1. Introduction

Limb girdle muscular dystrophy R3 (LGMD R3), an autosomal recessive primary myopathy characterized by progressive involvement of the pelvic and shoulder girdles, is caused by mutations in the α-sarcoglycan gene (*SGCA*) [1,2]. *SGCA* encodes a transmembrane protein, α-sarcoglycan (α-SG), which, together with other 3 SG members (β, γ and δ), interacts with dystrophin, forming the dystrophin-glycoprotein complex (DGC) [3]. The DGC is crucially responsible for connecting the muscle fiber cytoskeleton to the extracellular matrix, preventing damage to the muscle fiber sarcolemma through shearing forces [4].

As other muscular dystrophies [5], LGMD R3 muscle histology is characterized by myofiber necrosis and regeneration, reactive fibrosis and adipose tissue substitution, reduced long-term regenerative capacity and inflammatory infiltrates [6–8]. In physiological conditions, skeletal muscle is considered a privileged immunological site characterized by few immune cells, poorly able to generate localized immune responses. In contrast, the dystrophic muscle presents a high level of inflammation associated with the activation of an innate and adaptive immune response [9,10]. In LGMD R3, the DGC disruption causes fragile muscle fibers and unstable sarcolemma, which, in turn, leads to muscle necrosis and to the release of damage-associated molecular pattern molecules (DAMPs), such as ATP, thus initiating a well-orchestrated immune reaction. Specifically, in α-SG-deficient muscle cells, the effect of ATP release can be further amplified since the ecto-ATPase activity of sarcoglycan, responsible for extracellular ATP (eATP) hydrolysis, is lost [11,12]. Once in the extracellular space, eATP binds and activates ionotropic (P2X) or metabotropic (P2Y) receptors [13]. Among P2X receptors, P2X7 has attracted vivid interest since it plays a relevant role in the induction of immune cell responses via inflammasome activation [14], and the consequent release of interleukin-1β (IL-1β) by mononuclear and polymorphonuclear phagocytes [14–17]. P2X7 is also over-expressed in dystrophic muscle cells [18–21], where it contributes to exacerbate myofiber injury by increasing sarcolemma permeability [22] and participates in the amplification of the inflammatory process by releasing IL-1β [20]. From these observations, P2X7 is an attractive therapeutic target, not only for reducing inflammation but also for decreasing myofiber damage and supporting the regenerative potential of dystrophic myoblasts [23]. In this respect, genetic ablation and pharmacological inhibition of the eATP-P2X7 axis by the broad-spectrum antagonist oxidized ATP (oATP) alleviated dystrophic phenotypes in mouse models of dystrophinopathy and sarcoglycanopathy [18,24,25]. In this study, we performed a long-term treatment in *Sgca null* mice with A438079, a potent and selective P2X7 antagonist. Functional, biochemical, cytofluorimetric and histological analysis are shown, providing evidence that A438079 improved muscle force and morphology by dampening the extent of muscle fibrosis and local inflammation.

2. Results

2.1. P2X7 Targeting by A438079 Improves Functional, Biochemical and Morphological Parameters in Sgca Mice

In order to evaluate the therapeutic efficacy of a selective P2X7-targeting compound in an experimental model of α-sarcoglycanopathy, we treated four-week-old male *Sgca* knockout mice (also termed *Sgca-null*) mice with A438079, a specific antagonist of P2X7 [26]. The drug was administered to *Sgca-null* (here from referred as *Sgca*) mice by i.p. injections at the dose of 3 mg/kg every other day for 24 weeks (Figure 1a). *Sgca* mice injected with PBS (*Sgca* CTR) and Wild-Type (WT) mice served as controls.

The animals were weighted and followed once a week for signs of toxicity until the sacrifice. As shown in Supplementary Figure S1, the weight gain curve of *Sgca* mice treated with A438079 (*Sgca* A438079) was not significantly different from that of *Sgca* CTR mice. In addition, no signs of toxicity, including ruffled fur, vomiting, hyperactivity or loss of ambulation and breathing depression, were observed (data not shown). At the beginning (0 time) and after 6, 12, 18 and 24 weeks of treatment, animals were evaluated for muscle strength by the four-limb hanging test. Figure 1b shows that *Sgca* CTR mice progressively lost muscle strength up to 18 weeks (*Sgca* CTR vs. WT at 12 week $p < 0.001$, at 18 week $p < 0.0001$). At 24 weeks, they still showed significantly lower strength when compared to WT mice ($p < 0.0001$). The apparent slight recovery between 18 and 24 weeks was not significant. On the contrary, *Sgca* A438079 initially showed reduced functional performance, similarly to *Sgca* CTR mice, but after 6 weeks of treatment, muscle strength began to recover, almost reaching the performance of WT animals up to 24 weeks. The difference between *Sgca* CTR and *Sgca* A438079 mice at 12, 18 and 24 weeks was highly significant ($p < 0.05$ at 12, $p < 0.0001$ at 18 and 24 weeks). Accordingly, muscle strength in WT and *Sgca* A438079 mice was not significantly different at any time point. The efficacy of A438079 was confirmed by

the analysis of serum levels of CK, a marker of muscle degeneration. As shown in Figure 1c, CK serum levels of *Sgca* CTR mice measured >10 times more than the WT levels (mean value of WT mice: 406 UI/l, $n = 9$; mean value of *Sgca* CTR mice: 5537 UI/l, $n = 12$, $p < 0.05$). Interestingly, A438079 treatment significantly reduced (by 76%) serum CK in *Sgca* mice after 12 weeks of treatment (mean value in *Sgca* A438079 mice: 1338 UI/l, $n = 8$ vs. *Sgca* CTR mice $p < 0.05$). After 24 weeks of treatment serum CK levels of *Sgca* CTR mice were 6.3 times higher than the WT levels and A438079 led to a serum CK decrease in the treated mice, although it did not reach statistical significance, likely due to increased variability of the measurements (mean value of WT mice: 829 UI/l, $n = 12$; mean value of *Sgca* CTR mice: 5235 UI/l, $n = 10$, $p < 0.05$).

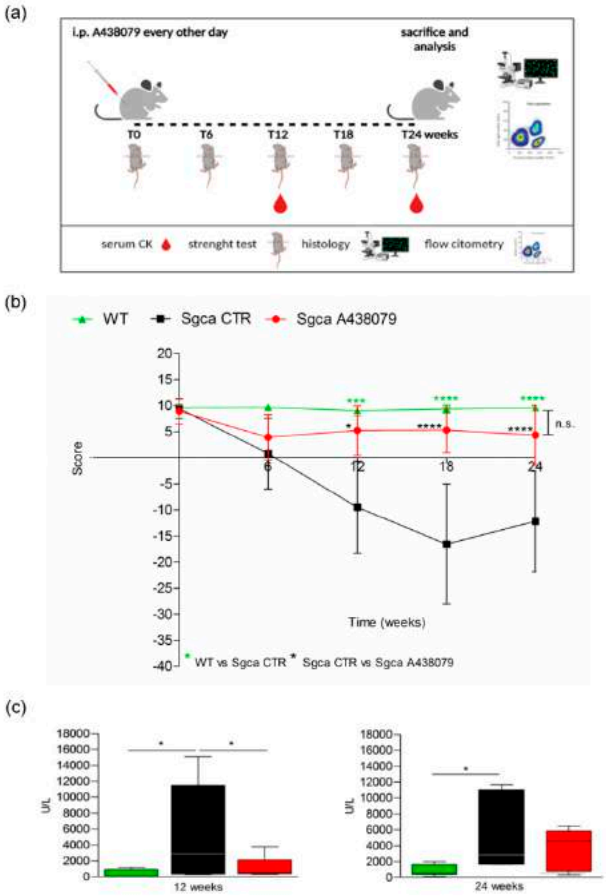

Figure 1. A438079 improves functional, biochemical and histological parameters in *Sgca* mice. (**a**): Experimental design: Four-week-old male *Sgca* mice were treated with PBS vehicle (*Sgca* CTR, $n = 12$) and A438079 (*Sgca* A438079 $n = 8$) that was administered intraperitoneally at the dose of 3 mg/Kg every other day for 24 weeks. Age-matched male C57BL/6 Wild Type (WT $n = 12$) mice were used as negative control; (**b**): four-limb hanging test was performed before treatment and at the end of 6, 12, 18 and 24 weeks of treatment. Each value represents the mean ± SD of animals evaluated. Statistical analysis was performed by one-way ANOVA followed by Tukey's multiple comparison test. Green asterisks indicate statistical significance between WT and *Sgca* CTR ***, $p < 0.001$, ****, $p < 0.0001$). Black asterisks indicate statistical significance between *Sgca* CTR and *Sgca* A438079 (*, $p < 0.05$; ****, $p < 0.0001$). No statistical significance (n.s.) was identified between WT and *Sgca* A438079 mice; (**c**): serum creatine kinase (CK) levels were evaluated at the end of the twelfth and the twenty-fourth week of treatment. Blood samples were obtained by retro orbital withdraw from WT, *Sgca* CTR and *Sgca* A438079 mice. Data are expressed as mean ± SD of animals evaluated. Statistical analysis was performed by one-way ANOVA followed by Tukey's multiple comparison test. Asterisks indicate statistical significance (*, $p < 0.05$).

To investigate whether the improved functional performance of *Sgca* A438079 mice correlated with decreased inflammation and muscle degeneration, we performed histological analysis by H&E staining of quadriceps from WT, *Sgca* CTR and *Sgca* A438079 mice.

Quadriceps from *Sgca* CTR mice presented areas of necrotic cells surrounded by reactive macrophage infiltration (Figure 2a) which were reduced upon A438079 treatment (Figure 2a). According to the histological analysis (Figure 2b), the percentage of centrally nucleated myofibers dramatically increased in quadriceps of *Sgca* mice in comparison to WT animals ($p < 0.001$) and was reduced by 12% in A438079-treated animals ($p < 0.001$) (Figure 2c). As expected, the fiber size variability, calculated as coefficient variance Z of minimal Feret's diameter, was wider in *Sgca* CTR compared to WT mice ($p < 0.001$) but was significantly down-modulated by A438079 treatment ($p < 0.05$) (Figure 2d).

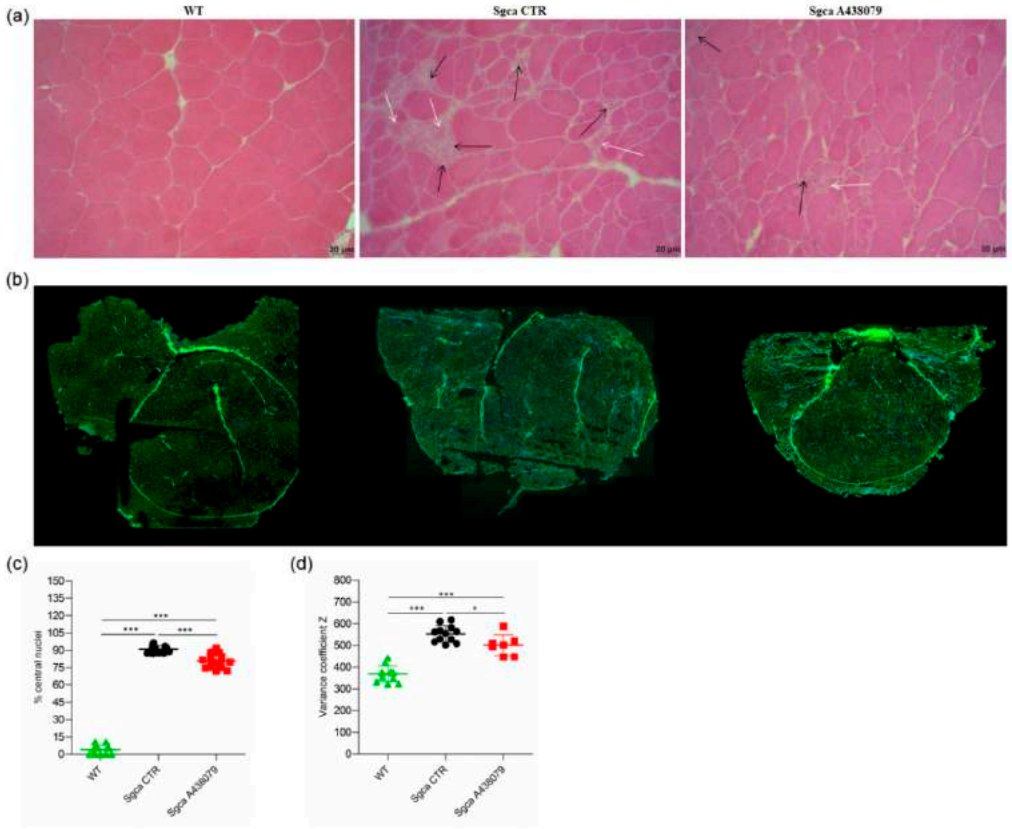

Figure 2. A438079 ameliorates the muscle morphology of *Sgca* mice. (**a**): frozen quadriceps tissue sections from WT, *Sgca* CTR and *Sgca* A438079 mice were collected at the end of the twenty-fourth week of treatment and stained with standard H&E technique. A representative image is shown. Black arrows indicate inflammatory infiltrates, white arrows indicate degenerating muscle fibers. Final magnification, 20×; (**b**): frozen quadriceps tissue sections from WT, *Sgca* CTR and *Sgca* A438079 mice were collected at the end of the twenty-fourth week of treatment and stained with wheat germ agglutinin (WGA) and DAPI. The whole quadricep section has been re-constructed; (**c**): percentage of central nuclei was quantified in four consecutive fields for each muscle section stained with wheat germ agglutinin (WGA) and DAPI and normalized for the fiber number of each field (WT n= 4; *Sgca* CTR n = 4; *Sgca* A438079 n = 4); (**d**): muscle fiber diameter variability from WT, *Sgca* CTR and *Sgca* A438079 mice was calculated in the whole area as variance coefficient Z of minimal Feret's diameter (WT n= 12; *Sgca* CTR n = 12; *Sgca* A438079 n = 7). In panels (**c**,**d**), data are expressed as mean ± SD. Statistical analysis was performed by one-way ANOVA followed by Tukey's multiple comparison test. Asterisks indicate statistical significance (*, $p < 0.05$; ***, $p < 0.001$,).

2.2. A438079 Reduces Muscular Fibrosis and Inflammation in Sgca Mice

Fibrosis as characterized by replacement of muscle tissue with collagen deposits is the histopathological hallmark of end-stage muscular dystrophies, including alfa-sarcoglycanopathy [27]. In order to establish whether A438079 might impact collagen deposits, we performed a Masson trichrome staining on quadriceps of WT, *Sgca* CTR and *Sgca* A438079 mice and evaluated the fraction area of fibrotic reactions. As shown in Figure 3a, *Sgca* CTR quadriceps accumulated abundant extracellular matrix deposits which were increased in comparison to WT mice (mean value of WT mice: 1.47, $n = 7$; mean value of *Sgca* CTR mice: 2.92, $n = 11$, $p < 0.05$). A438079 treatment led to a 37% reduction of extracellular matrix deposition fraction area as compared to *Sgca* CTR mice (mean of *Sgca* A438079 mice: 1.85, $n = 7$, $p < 0.05$). No significant difference was observed between WT and *Sgca* A438079 animals.

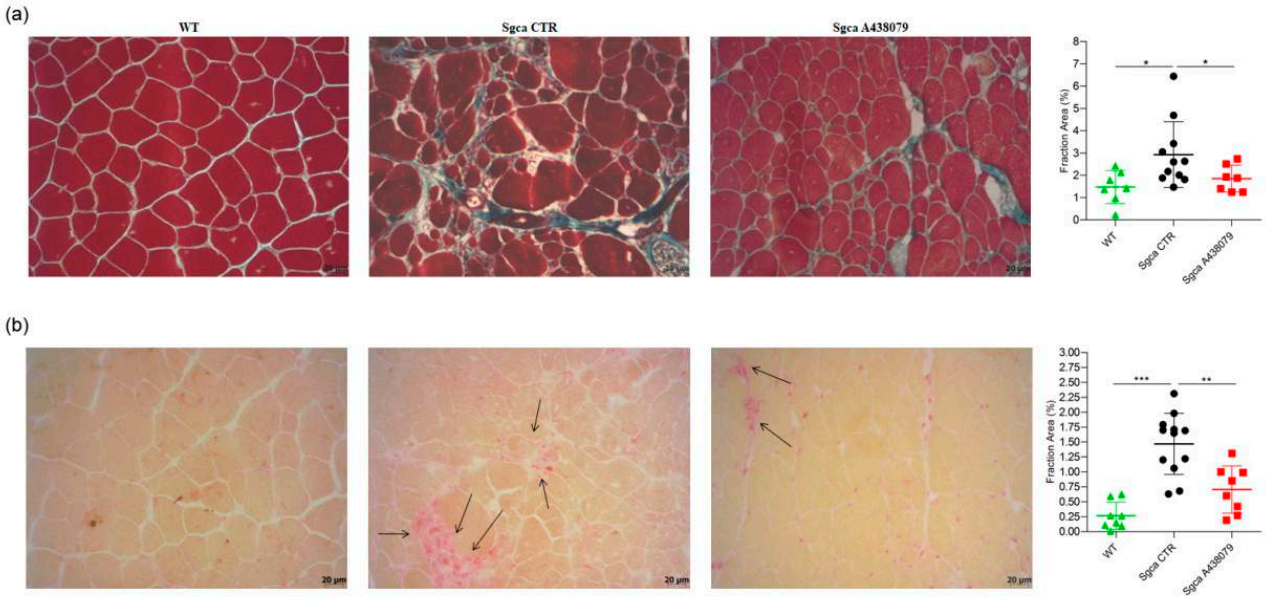

Figure 3. A438079 reduces muscle fibrosis and inflammatory infiltrates in *Sgca* mice. (**a**): frozen sections of quadriceps from WT ($n = 7$), *Sgca* CTR ($n = 11$) and *Sgca* A438079 ($n = 7$) were collected after 24 weeks and stained with a standard Masson trichrome stain protocol. A representative image is shown. Final magnification, 20×. In the right part of the panel (**a**) a graph of the fraction areas of fibrotic green positive signal/fraction area (%) of total section area of muscles evaluated is shown. Data are expressed as mean ± SD. Statistical analysis was performed by one-tailed ANOVA followed by Tukey's multiple comparison test. Asterisks indicate statistical significance (*, $p < 0.05$); (**b**): frozen sections of quadriceps from WT ($n = 8$), *Sgca* CTR ($n = 12$) and *Sgca* A438079 ($n = 8$) were collected after 24 weeks and stained with an acid phosphatase technique. A representative image is shown. Black arrow indicates inflammatory infiltrates. Final magnification, 20×. In the right part of panel (**b**), a graph of the fraction areas of inflammatory red positive signal/fraction area (%) of total section area of muscles evaluated is shown. Data are expressed as mean ± SD. Statistical analysis was performed by one-way ANOVA followed by Tukey's multiple comparison test. Asterisks indicate statistical significance (**, $p < 0.01$; ***, $p < 0.001$).

To evaluate the anti-inflammatory effect of A438079, quadricep sections of WT, *Sgca* CTR and *Sgca* A438079 mice were stained with acid phosphatase, which provides a red positive signal in activated macrophages and degenerative myofibers. As shown in Figure 3b, the acid phosphatase-positive area fraction of quadriceps from *Sgca* CTR mice was increased in comparison to that of WT mice (mean value of WT mice: 0.26, $n = 8$; mean value of *Sgca* CTR mice: 1.47, $n = 12$, $p < 0.001$). Interestingly, A438079 led to 52% reduction of

inflammatory area fraction of *Sgca* mice (mean of *Sgca* A438079 mice: 0.70, $n = 8$, $p < 0.01$). In contrast, no significant difference was observed between WT and *Sgca* A438079 animals.

2.3. A438079 Reduces Innate Inflammatory Cells and Increases T Regulatory Lymphocytes in Limb Muscles of Sgca Mice

In order to better characterize the phenotype of inflammatory muscle infiltrates, we performed a cytometric analysis of a pool of limb muscles, including gastrocnemius, quadriceps and anterior tibialis, isolated from WT, *Sgca* CTR and *Sgca* A438079 mice. As shown in Figure 4a, limb muscles of *Sgca* CTR mice were characterized by the presence of $CD45^+$ hematopoietic immune cells which, in contrast, were not detected in WT mice (WT vs. *Sgca* CTR, $p < 0.01$).

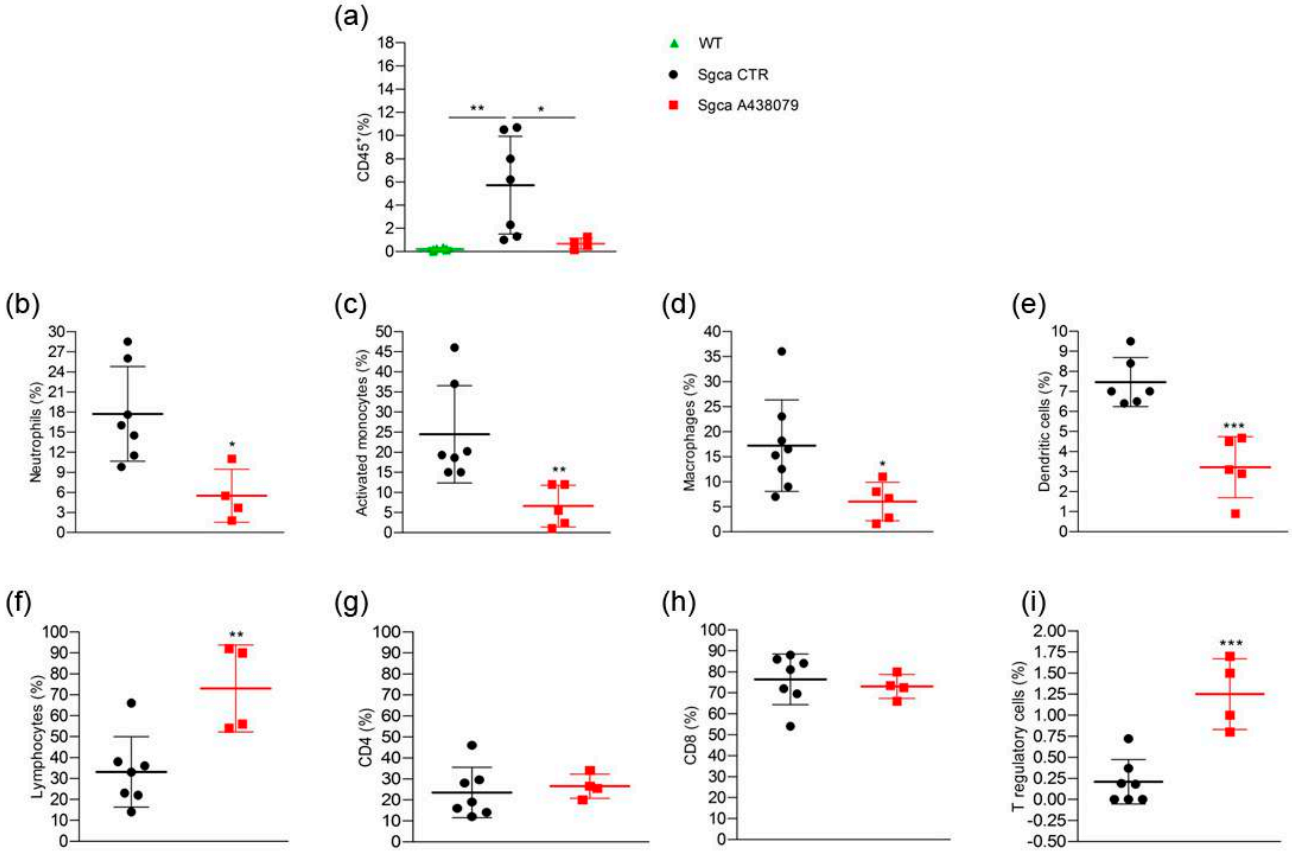

Figure 4. A438079 reduces innate inflammatory cells and increases T regulatory lymphocytes in muscles of *Sgca* mice. Flow cytometric analysis of immune cells isolated from a pool of gastrocnemius, quadriceps, anterior tibialis excised from WT ($n = 6$), *Sgca* CTR ($n = 7$) and *Sgca* A438079 ($n = 5$) mice and stained with specific anti-surface markers mAbs are shown; (**a**): percentage of $CD45^+$ cells gated on alive cells; (**b**): percentage of $Ly6G^+/CD11b^+$neutrophils gated on $CD45^+$ alive cells; (**c**): percentage of $Ly6G^-/Ly6C^+/CD11b^+$ activated monocytes gated on $CD45^+$ alive cells; (**d**): percentage of $Ly6G^-/F480^+/CD11b^+$ macrophages gated on $CD45^+$ alive cells; (**e**): percentage of $Ly6G^-/F480^-/CD11c^+$ dendritic cells gated on $CD45^+$ alive cells; (**f**): percentage of $CD3^+$ T cells gated on $CD45^+$ alive cells; (**g**): percentage of $CD3^+/CD4^+$ T cells gated on $CD45^+/CD3^+$ alive cells. (**h**): percentage of $CD3^+/CD8^+$ T cells gated on $CD45^+/CD3^+$ alive cells; (**i**): percentage of $CD3^+/CD4^+CD25^+/Foxp3^+$ T cells gated on $CD3^+$ alive cells. Data are expressed as mean ± SD. Statistical analysis was performed by one-way ANOVA followed by Tukey's multiple comparison test Panel (**a**) and unpaired *t*-test Panels (**b**–**i**). Asterisks indicate statistical significance (*, $p < 0.05$; **, $p < 0.01$; ***, $p < 0.001$).

A438079 treatment significantly reduced the percentage of $CD45^+$ cells infiltrating the limb muscles of *Sgca* mice (*Sgca* CTR vs. *Sgca* A438079, $p < 0.05$). The further characterization of $CD45^+$ cells was only performed for *Sgca* animals since the amount of $CD45^+$ cells was negligible in the muscle of WT mice. *Sgca* A438079 mice presented a significant reduction of muscle infiltrating innate inflammatory cells, including $Ly6G^+/CD11b^+$ neutrophils (Figure 4b, *Sgca* CTR vs. *Sgca* A438079, $p < 0.05$), $Ly6G^-/CD11b^+/Ly6C^+$ activated monocytes (Figure 4c, *Sgca* CTR vs. *Sgca* A438079, $p < 0.01$), $Ly6G^-/CD11b^+/F480^+$ macrophages (Figure 4d, *Sgca* CTR vs. *Sgca* A438079, $p < 0.05$) and $Ly6G^-/CD11c^+/F480^-$dendritic cells (DC) (Figure 4e, *Sgca* CTR vs. *Sgca* A438079, $p < 0.001$) in comparison to *Sgca* CTR animals. In contrast, the percentage of $CD3^+/CD4^+/CD25^+/Foxp3^+$ T regulatory (Treg) was significantly increased in the muscles of A438079 *Sgca* mice in comparison to *Sgca* CTR mice (Figure 4i, *Sgca* CTR vs. *Sgca* A438079, $p < 0.001$).

Furthermore, the analysis of the peripheral blood (PB) immune cell populations of WT, *Sgca* CTR and *Sgca* A438079 mice showed that the dystrophic animals presented significantly higher percentages of DC compared to WT animals (Figure 5c, WT vs. *Sgca* CTR, $p < 0.001$ for DC). Treatment with A438079 significantly reduced the percentage of DC, $CD8^+$ lymphocytes and T reg cells (Figure 5c,f,g, *Sgca* CTR vs. *Sgca* A438079, $p < 0.05$ for DC; $p < 0.001$ for $CD8^+$ lymphocytes and $p < 0.001$ for Treg).

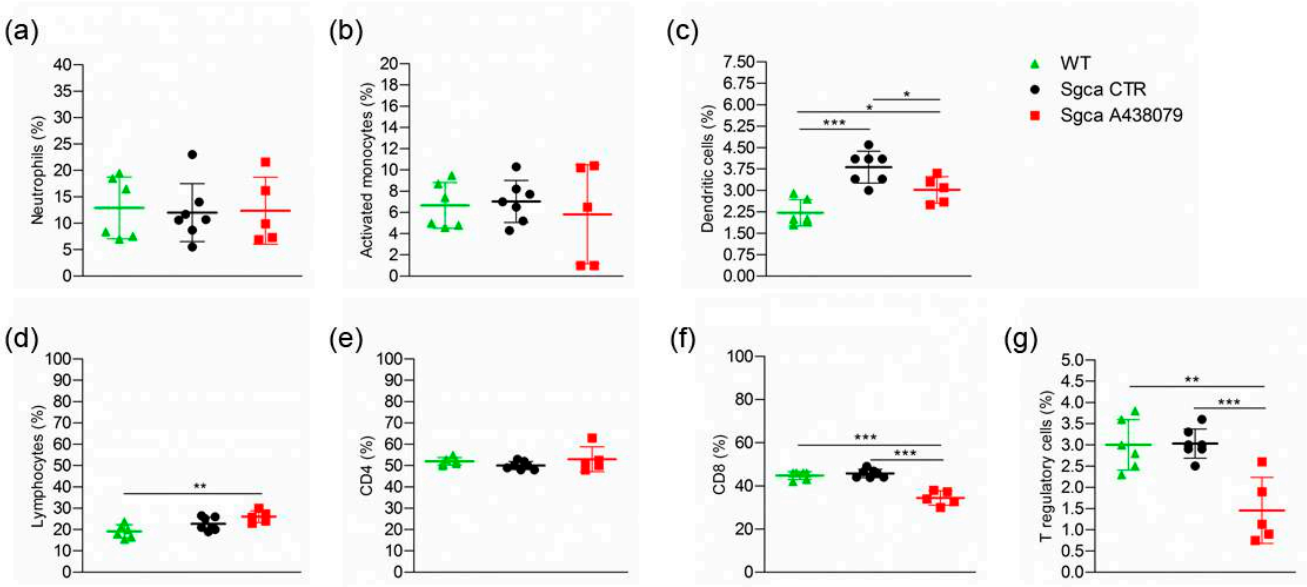

Figure 5. A438079 reduces peripheral cytotoxic and T regulatory cells in *Sgca* mice. Flow cytometric analysis of peripheral blood immune cells isolated from WT ($n = 6$), *Sgca* CTR ($n = 7$) and *Sgca* A438079 ($n = 5$) mice and stained with specific anti-surface markers mAbs are shown; (**a**): percentage of $Ly6G^+/CD11b^+$neutrophils gated on $CD45^+$ alive cells; (**b**): percentage of $Ly6G^-/Ly6C^+/CD11b^+$ activated monocytes gated on $CD45^+$ alive cells; (**c**): percentage of $Ly6G^-/F480^-/CD11c^+$ dendritic cells gated on $CD45^+$ alive cells; (**d**): percentage of $CD3^+$ T cells gated on $CD45^+$ alive cells; (**e**): percentage of $CD3^+/CD4^+$ T cells gated on $CD45^+/CD3^+$ alive cells; (**f**): percentage of $CD3^+/CD8^+$ T cells gated on $CD45^+/CD3^+$ alive cells; (**g**): Percentage of $CD3^+$ $/CD4^{+/}CD25^+/Foxp3^+$ T cells gated on $CD3^+$ alive cells. Data are expressed as mean ± SD. Statistical analysis was performed by one-way ANOVA followed by Tukey's multiple comparison test. Asterisks indicate statistical significance (*, $p < 0.05$; **, $p < 0.01$; ***, $p < 0.001$).

No significant changes were observed in the spleen of WT, *Sgca* CTR and *Sgca* A438079 mice, with the only exception of $CD3^+$ T lymphocytes, which were slightly increased in *Sgca* A43879 mice vs. Sgca CTR (Supplementary Figure S2e, *Sgca* CTR vs. *Sgca* A438079, $p < 0.01$).

3. Discussion

In the present study, we provide evidence that the pharmacological inhibition of P2X7 by the selective antagonist A438079 attenuated the dystrophic phenotype of *Sgca* mice by reducing fibrosis and inflammation and improved muscle performance. P2X7 is an ATP receptor belonging to the ionotropic purinergic P2X subfamily, which is expressed on virtually all cell types of the immune system and regulates the innate and adaptive immune responses [28]. Alongside its expression on immune cells, P2X7 expression and function are upregulated in the dystrophic muscle [18,21,25,29–31]. In this context, we and other groups demonstrated that the genetic ablation of P2RX7 and its pharmacological inhibition by oATP, an irreversible, broad-spectrum P2X7 antagonist [17], produced significant improvements in key functional and molecular disease parameters in *mdx* and *Sgca* mice [18,24,25,30]. However, oATP can also interact with other P2X receptors, including P2X4 [32–34], and appears to exert anti-inflammatory effects, modulating the immune response independently of P2X7 blockage [33,35,36]. Therefore, experiments using oATP cannot unambiguously establish a role in inflammatory diseases for a specific member of the P2X family. Neurotoxicity has been described for oATP, likely due to the low specificity of the drug [37]. In order to overcome the above-described limitations, and to define the therapeutic effect of P2X7 targeting approaches in α-sarcoglycan-deficient muscular dystrophy, we specifically inhibited P2X7 using the A438079 molecule, one of the most potent and selective antagonists that competitively blocks P2X7 receptor in vitro activation and produces anti-nociceptive effects in in vivo settings [38–40]. In addition to nociception, A438079 has already been successfully used in in vivo models of hyperalgesia [41], epilepsy [42,43], Parkinson's disease [44], salivary gland exocrinopathy [45], and Charcot-Marie-Tooth 1A disease [46]. Our results clearly show that, by targeting P2X7, A438079 ameliorated functional and morphological parameters in *Sgca* mice. In particular, A438079 improved muscle morphology by reducing the percentage of centralized nuclei and the coefficient variance Z of minimal Feret's diameter (Figure 2c,d), which are typical signs of dystrophic damage [47]. Furthermore, according to previous studies [24], a relevant therapeutic effect exerted by A438079 was the reduction of muscle fibrosis (Figure 3a). P2X7 has been described to play a nodal role in triggering fibrosis through activation of multiple intracellular pathways that converge in inducing the collagen biosynthetic machinery in various organs [48]. As such, P2X7 blockade may interfere with the main pro-fibrotic pathways, thus possibly representing a target for the pharmacological modulation of fibrotic processes. The most evident beneficial effect of A438079 in *Sgca* animals was a significant modulation of muscle inflammation, a key feature of muscular dystrophies participating in the disease progression but also mediating muscle repair. The dichotomous role of inflammation has been extensively studied in Duchenne muscular dystrophy (DMD), in which $CD4^+$ and $CD8^+$ T cells, macrophages, eosinophils and natural killer T cells infiltrated both human and mouse dystrophic muscle [9,49]. In particular, proinflammatory monocytes $CD11b^+/Ly6G^-/Ly6c^+$ have been reported to be the first innate immune cells to be mobilized from the bone marrow into the circulation and recruited to the site of tissue injury [50], such as dystrophic muscles, where they differentiated into inflammatory macrophages [51,52]. Different studies demonstrated that neutrophils actively participated in the exacerbation of muscular dystrophy and their specific depletion reduced muscular necrosis and inflammation in *mdx* mice [53–55]. Moreover, neutrophil-derived elastase impaired myoblast proliferation, survival and differentiation [56]. In line with this notion, we found that A438079 caused a significant reduction of innate immune cells, including neutrophils, activated monocytes and dendritic cells infiltrating the limb muscles of *Sgca* mice. The downregulation of innate immune response by P2X7 blockade was also observed in dystrophic mice (*mdx* and *Sgca*) treated with other P2X7 antagonists, i.e., oATP or zidovudine (AZT) [18,25,57]. However, the mechanism underlying the latter effect is still unclear. P2X7 antagonists could directly inhibit P2RX7 expressed by inflammatory innate immune cells infiltrating the dystrophic muscle. Alternatively, these agents might reduce inflammatory cell migration into the injured tissue. In favor of the first hypothesis,

innate immune cells are known to express functional P2X7, which in turn triggers inflammasome activation [17,28,58–60]. The second hypothesis is sustained by data showing P2X7-dependent release of chemotactic factors by macrophages. These factors, including CXCL2/macrophage inflammatory protein-2 (MIP-2), were involved in the recruitment of neutrophils into the injured tissue [61]. The immune phenotype of limb muscle from *Sgca* mice treated with A438079 also showed that the pharmacological treatment significantly increased Foxp3$^+$ Treg without affecting CD4$^+$ and CD8$^+$ T lymphocytes. These findings are consistent with previous studies in which P2X7 blockade by oATP or P2X7 genetic ablation in dystrophic mice resulted in a significant increase of Foxp3$^+$ Treg [18,24,25]. Treg have been described to play a dual beneficial role in dystrophic muscles. On one side, they suppress type 1 inflammation by secreting IL-10; on the other side, Treg may also have direct effects on muscle growth and regeneration through secretion of amphiregulin, an epidermal growth factor family member whose receptors are expressed on muscle satellite cells that are critical for muscle regeneration [62,63]. Interestingly, our results showed that A438079 exerted not only a local but also a systemic anti-inflammatory effect by reducing circulating CD8$^+$ cytotoxic T lymphocytes in *Sgca* mice. Currently, physical therapy and prevention of secondary cardiac, pulmonary or orthopedic complications are the only possible care interventions. Although a chronic inflammatory response is documented in muscle specimens from LGMD R3 patients, no trials assessing the effects of immunosuppressive therapies have been proposed in alpha-sarcoglycan deficiency. However, two unrelated LGMD R3 patients treated with steroids showed clinical improvement [64–66]. In light of these considerations, strategies aimed at reducing muscle inflammation, increasing the amount of Treg infiltrating an injured muscle and exerting a systemic anti-inflammatory effect, i.e., antagonists of P2X7, might represent a therapeutic approach for LGMD R3. Immunomodulatory regimens become even more relevant as new gene therapies or gene editing approaches are being developed for alpha-sarcoglycanopathy [67–69], with gene therapy being in Phase I/II clinical trials for LGMD R3 patients (NCT01976091; NCT00494195). Since the success of gene therapy in the muscle tissue has to challenge the pre-existing status of chronic tissue inflammation typically identified in this diseases [67–71], our data suggest that P2X7 antagonism might represent a good strategy to dampen chronic inflammation, possibly leading to a better delivery of gene therapy. To date P2X7 selective antagonists have already been tested in Phase I/II clinical trials for the treatment of Crohn's disease, rheumatoid arthritis, basal cell carcinoma with an overall good tolerability and variable efficacy [72] and a new trial is currently ongoing assessing the effects of JNJ-54175446, a potent, brain-penetrant, selective P2X7 antagonist [73] in patients with major depressive disorder (ClinicalTrials.gov Identifier: NCT04116606).

4. Materials and Methods

4.1. In Vivo Experiments

C57BL/6 wild-type (WT) and *Sgca* knockout mice (also termed *Sgca-null*) were bred in the Animal Facility at Policlinico San Martino, Genova. All mice were housed under standard specific pathogen–free conditions and allowed access to food and water ad libitum. All experimental protocols were approved by the Policlinico San Martino Animal Welfare Body and by the Italian Ministry of Health (Authorization n° 215–2018-PR). *Sgca* mice were previously described [74]. The study design defined a minimum goal of a $n = 8$ animals per genotype and experimental group. According amounts of the drug A438079 was acquired from Tocris Bioscience Bristol, UK. Four week old *Sgca* male mice were randomly divided into two groups: one treated by i.p. injections with A438079 at 3 mg/Kg every other day in the morning between 10–12 for 24 weeks (*Sgca* A438079) and one treated with the same volume of phosphatase-buffered saline (PBS, Sigma Aldrich, St. Louis, MO, USA) every other day for 24 weeks (*Sgca* Control: Sgca CTR). In consideration of the high variability of the histological markers in mouse models of muscular dystrophies [18,25], and in order to increase the statistical power of the study a n of 12 WT mice and a n of 12 *Sgca* CTR were included. The dose of 3 mg/kg of A438079 proved to be well tolerated

by wild-type rats [46]. A438079 was reconstituted at a final concentration of 1 mg/mL in PBS and stored at −20 °C; the reconstituted drug was thawed and immediately used at a final concentration of 3 mg/Kg. All animals were euthanized at the end of treatment by carbon dioxide inhalation and muscles were collected for histological and cytofluorimetric analysis. A group of age-matched WT C57Bl/6 male mice was used as internal control. All animals were weighed and followed for any sign of toxicity, including ruffled fur, vomiting, hyperactivity or loss of deambulation and breathing depression once a week. Blood samples from *Sgca* CTR and *Sgca* A438079 mice were obtained from the saphenous vein (90 µL) before treatment and 12 and 24 weeks after treatment. The samples were centrifuged at 3600× *g* for 30 min and immediately after centrifugation the serum was isolated and stored at −80 °C. Serum creatine kinase (CK) levels were measured using a clinical-standard automatic chemistry analyzer (BS-380 Mindray, Milan, Italy).

4.2. Four-Limb Hanging Test

Before treatment and at the end of the sixth, twelfth, eighteenth and twenty-fourth week of treatment, the muscle strength of WT, *Sgca* CTR and *Sgca* A438079- mice was scored through the four-limb hanging test. Mice were subjected to a 180-s lasting hanging test, during which a falling score was recorded. The animals had to hang for three trials, and the average maximum hanging time of the three trials was measured (standard operating procedure, https://treat-nmd.org/research-overview/preclinical-research/experimental-protocols-for-dmd-animal-models, last accessed on September 2021.

4.3. Histological Studies, Imaging and Analysis

Quadriceps isolated from WT, *Sgca* CTR and *Sgca* A438079 mice were cut on cryostat, and 7-µm-thick sections were stained with standard hematoxylin and eosin (H&E) (reagents from Sigma Aldrich), acid phosphatase (reagents from Sigma Aldrich) to detect inflammatory reactions and Masson trichrome (reagents from Sigma Aldrich) to evaluate muscle fibrosis. Representative pictures were taken at 20× magnification. To quantify the extension of the inflammatory response and fibrotic area, images of stained sections were acquired using a Nikon Ti Eclipse microscope equipped with a 20× objective. Whole sections were imaged with an automated tile scan acquisition (usually over a 45 mm^2-surface) by using the perfect focus system (PFS) to control the focal plane. Quantification of acid phosphatase and trichrome staining was performed using semi-automated measurement tools in NIS-Elements AR software version 4.20 and expressed in terms of fraction area (the ratio between total section area and the area of the stained objects that were detected by HSI thresholding mode). All the histological analyses were performed blind to experimental group identity. The Masson Trichrome and acid phosphatase staining were completely negative in WT mice; therefore, the n was reduced to 7 animals.The histological sections of *Sgca* CTR and *Sgca* A438079 treated mice displaying freezing artifacts were not analyzed and are excluded from the results.

4.4. Immunofluorescence

The wheat germ agglutinin (WGA)/DAPI (WGA Alexa Fluor™ 488 Conjugate Invitrogen, Thermo Fisher Scientific, Waltham, MA, USA; DAPI, Fluoromount-G® Southern Biotech, Birmingham, USA) staining was performed on quadricep 5-µm-thick sections, in order to calculate the Minimum Feret's Diameter and the percentage of centralized nuclei. Briefly, unfixed quadriceps sections were incubated with a blocking solution containing 0.2% TritonX-100 (Sigma Aldrich), 2% bovine serum albumin (Sigma Aldrich), 5% fetal bovine serum (GIBCO, Thermo Fisher Scientific), 2% goat serum (GIBCO) in PBS for 1 h at room temperature (RT) and then with WGA Alexa Fluor 488 conjugated diluted 1:200 in Hank's Balanced Salt Solution (HBSS) (GIBCO) for 2 h at RT. Finally, sections were mounted with Fluoromount G. Images were acquired by Axioplan Imager M2 miscroscope software AxioVs40 version 4.8.2.0 (Zeiss, Oberkochen, Germany) and manually overlapped using Adobe Photoshop CS6 to generate whole cross-section. Image analysis was performed

using Fiji, ImageJ 1.52i (NIH, Bethesda, MA, USA). A plugin (Muscle Morphometry) developed as described in [24] was used to quantify the muscle fiber diameter (minimal Feret's diameter) and the percentage of centralized nuclei, as described in TREAT-NMD-recommended protocol (https://treat-nmd.org/research-overview/preclinical-research/experimental-protocols-for-dmd-animal-models, last accessed on 10 September 2021). All the analyses were performed blind to experimental group identity.

4.5. Flow Cytometry

Hematopoietic cells were collected from different districts, namely PB, spleen and limb muscles. Cells collected from PB were first incubated with 2 µL/sample of TruStainFcX™ anti-mouse CD16/32 for 5 min in order to block Fc receptor and then with cocktails of antibodies specific for CD45, CD3, CD4, CD8, CD11b, CD11c, CD25, F4/80, Ly-6C, Ly-6G and Foxp3 for 30 min. The intracellular staining of transcription factor Foxp3 was performed using the Foxp3/Transcription factor staining buffer set (Thermo Fisher) as described by the manufacturer. After antibody incubation, samples were lysed (Becton Dickinson Pharm Lyse TM, San Josè, CA, USA), washed and resuspended in 300 ul of PBS. All the antibodies were purchased from Biolegend (San Diego, CA, USA). Gastrocnemius, quadriceps and anterior tibialis excised from WT, *Sgca* CTR and *Sgca* A438079 mice were resuspended in RPMI 1640 base medium (Euro Clone, Milan, Italy), mechanically and enzimatically digested using Skeletal Muscle Dissociation Kit (Miltenyi Biotec, Bologna, Italy) and filtered through 100- and 70-µm mesh filters (BD Bioscience, San Jose, CA, USA) (Supplementary Method). After filtration, cells were purified using gradient centrifugation by Percoll solution (GE Healthcare Bio-sciences, Uppsala, Sweden) and stained with Live/Dead™ Fixable Yellow Dead Cell Stain Kit (Invitrogen, Thermo Fisher Scientific) and the antibodies listed above. The spleen from WT, *Sgca* CTR and *Sgca* A438079 mice was mechanically digested, filtered through 100- and 70-µm mesh filters, counted and stained as described for PB and muscle. All acquisitions were performed with a three laser LSR Fortessa X20 (Becton Dickinson) and obtained FSC files were analysed with Kaluza Software (version 2.1, Beckman Coulter). The immune profile of the peripheral blood, spleen and muscles was performed in the same animals (WT $n = 6$, *Sgca* CTR $n = 7$ and *Sgca* A438079 $n = 5$).

4.6. Statistical Analysis

Statistical parameters, including the exact value of n and statistical significance, are reported in the figures and their associated legends. Results were analyzed using a one-way ANOVA followed by Tukey's multiple comparison test or unpaired t-test, where indicated, using GraphPad Prism 3.0 software (GraphPad Software, El Camino Real, San Diego, CA, USA). Asterisks indicate statistical significance (*, $p < 0.05$; **, $p < 0.01$; ***, $p < 0.001$, ****, $p < 0.0001$).

5. Conclusions

In conclusion, A438079 ameliorated the dystrophic phenotype of *Sgca* mice by reducing muscle fibrosis and inflammation and by improving functional muscle performance. In the current scenario of clinical trials including gene therapy, selective P2X7 antagonists could represent candidates for a combinatory therapy to endorse the efficacy of disease-specific gene therapy by dampening the basal muscular inflammation.

Supplementary Materials: The following are available at https://www.mdpi.com/article/10.3390/ph15010089/s1. Figure S1: Weight of *Sgca* mice treated (not) with A438079; Figure S2: A438079 modulation of splenic immune cells of *Sgca* mice and Supplementary Methods.

Author Contributions: Conceptualization, C.B., L.R., E.G.; methodology, S.B. (Serena Baratto), E.P., S.P., F.A., G.D.Z., A.B., P.S.; software C.P., P.S.; validation, S.B. (Serena Baratto), E.P., S.P., F.A., G.D.Z., A.B., P.S., C.P.; formal analysis, L.R., E.G., S.B. (Santina Bruzzone); investigation, S.B. (Serena Baratto), E.P., C.P., L.R.; resources, C.B., L.R.; data curation, S.B. (Serena Baratto), E.P., S.B. (Santina Bruzzone), C.P.; writing—original draft preparation, L.R.; writing—review and editing, E.P., S.B. (Serena Baratto), L.R., C.B., E.G., S.B. (Santina Bruzzone), C.P., C.M.; visualization, L.R., S.B. (Serena Baratto), E.P., S.B. (Santina Bruzzone), C.P.; supervision, L.R., E.G., C.B., C.M.; project administration, E.G., C.B.; funding acquisition, L.R., C.B. All authors have read and agreed to the published version of the manuscript.

Funding: This research was funded by by Telethon-Italy grant GGP17192 (to C.B.), by the Italian Ministry of Health RF 2016–02364503 (to C.B.), and by Fondazione Compagnia di San Paolo grant ROL 32561 (to L.R.).

Institutional Review Board Statement: The animal study was conducted according to the Ethical Guidelines for the Use of Animals in Research (3Rs) and approved by the Policlinico San Martino Animal Welfare Body, Genova, Italy and by the Italian Ministry of Health (Authorization n° 215–2018-PR).

Informed Consent Statement: Not available.

Data Availability Statement: The data presented in this study are available in the main text and Supplementary Material.

Acknowledgments: The authors thank C.B. and C.M. They are members of the European Reference Network for Neuromuscular Disorders.

Conflicts of Interest: The authors declare no conflict of interest. The funders had no role in the design of the study; in the collection, analyses, or interpretation of data; in the writing of the manuscript, or in the decision to publish the results.

References

1. Alonso-Pérez, J.; González-Quereda, L.; Bello, L.; Guglieri, M.; Straub, V.; Gallano, P.; Semplicini, C.; Pegoraro, E.; Zangaro, V.; Nascimento, A.; et al. New genotype-phenotype correlations in a large European cohort of patients with sarcoglycanopathy. *Brain A J. Neurol.* **2020**, *143*, 2696–2708. [CrossRef] [PubMed]
2. Vainzof, M.; Souza, L.S.; Gurgel-Giannetti, J.; Zatz, M. Sarcoglycanopathies: An update. *Neuromuscul. Disord.* **2021**, *31*, 1021–1027. [CrossRef] [PubMed]
3. Sandona, D.; Betto, R. Sarcoglycanopathies: Molecular pathogenesis and therapeutic prospects. *Expert Rev. Mol. Med.* **2009**, *11*, e28. [CrossRef]
4. Petrof, B.J.; Shrager, J.B.; Stedman, H.H.; Kelly, A.M.; Sweeney, H.L. Dystrophin protects the sarcolemma from stresses developed during muscle contraction. *Proc. Natl. Acad. Sci. USA* **1993**, *90*, 3710–3714. [CrossRef]
5. Tidball, J.G.; Welc, S.S.; Wehling-Henricks, M. Immunobiology of Inherited Muscular Dystrophies. *Compr. Physiol.* **2018**, *8*, 1313–1356.
6. Kirschner, J.; Lochmüller, H. Sarcoglycanopathies. *Handb. Clin. Neurol.* **2011**, *101*, 41–46. [CrossRef] [PubMed]
7. Mercuri, E.; Bönnemann, C.G.; Muntoni, F. Muscular dystrophies. *Lancet* **2019**, *394*, 2025–2038. [CrossRef]
8. Fanin, M.; Angelini, C. Regeneration in sarcoglycanopathies: Expression studies of sarcoglycans and other muscle proteins. *J. Neurol. Sci.* **1999**, *165*, 170–177. [CrossRef]
9. Rosenberg, A.S.; Puig, M.; Nagaraju, K.; Hoffman, E.P.; Villalta, S.A.; Rao, V.A.; Wakefield, L.M.; Woodcock, J. Immune-mediated pathology in Duchenne muscular dystrophy. *Sci. Transl. Med.* **2015**, *7*, 299rv294. [CrossRef]
10. Panicucci, C.; Baratto, S.; Raffaghello, L.; Tonin, P.; D'Amico, A.; Tasca, G.; Traverso, M.; Fiorillo, C.; Minetti, C.; Previtali, S.C.; et al. Muscle inflammatory pattern in alpha- and gamma-sarcoglycanopathies. *Clin. Neuropathol.* **2021**, *40*, 310–318. [CrossRef]
11. Betto, R.; Senter, L.; Ceoldo, S.; Tarricone, E.; Biral, D.; Salviati, G. Ecto-ATPase activity of alpha-sarcoglycan (adhalin). *J. Biol. Chem.* **1999**, *274*, 7907–7912. [CrossRef]
12. Sandona, D.; Gastaldello, S.; Martinello, T.; Betto, R. Characterization of the ATP-hydrolysing activity of alpha-sarcoglycan. *Biochem. J.* **2004**, *381*, 105–112. [CrossRef]
13. Di Virgilio, F.; Adinolfi, E. Extracellular purines, purinergic receptors and tumor growth. *Oncogene* **2017**, *36*, 293–303. [CrossRef]
14. Di Virgilio, F.; Sarti, A.C.; Grassi, F. Modulation of innate and adaptive immunity by P2X ion channels. *Curr. Opin. Immunol.* **2018**, *52*, 51–59. [CrossRef] [PubMed]
15. Munoz-Planillo, R.; Kuffa, P.; Martinez-Colon, G.; Smith, B.L.; Rajendiran, T.M.; Nunez, G. K(+) efflux is the common trigger of NLRP3 inflammasome activation by bacterial toxins and particulate matter. *Immunity* **2013**, *38*, 1142–1153. [CrossRef]
16. MacKenzie, A.; Wilson, H.L.; Kiss-Toth, E.; Dower, S.K.; North, R.A.; Surprenant, A. Rapid secretion of interleukin-1beta by microvesicle shedding. *Immunity* **2001**, *15*, 825–835. [CrossRef]

17. Karmakar, M.; Katsnelson, M.A.; Dubyak, G.R.; Pearlman, E. Neutrophil P2X7 receptors mediate NLRP3 inflammasome-dependent IL-1beta secretion in response to ATP. *Nat. Commun.* **2016**, *7*, 10555. [CrossRef]
18. Gazzerro, E.; Baldassari, S.; Assereto, S.; Fruscione, F.; Pistorio, A.; Panicucci, C.; Volpi, S.; Perruzza, L.; Fiorillo, C.; Minetti, C.; et al. Enhancement of Muscle T Regulatory Cells and Improvement of Muscular Dystrophic Process in mdx Mice by Blockade of Extracellular ATP/P2X Axis. *Am. J. Pathol.* **2015**, *185*, 3349–3360. [CrossRef] [PubMed]
19. Yeung, D.; Zablocki, K.; Lien, C.F.; Jiang, T.; Arkle, S.; Brutkowski, W.; Brown, J.; Lochmuller, H.; Simon, J.; Barnard, E.A.; et al. Increased susceptibility to ATP via alteration of P2X receptor function in dystrophic mdx mouse muscle cells. *FASEB J.* **2006**, *20*, 610–620. [CrossRef]
20. Rawat, R.; Cohen, T.V.; Ampong, B.; Francia, D.; Henriques-Pons, A.; Hoffman, E.P.; Nagaraju, K. Inflammasome up-regulation and activation in dysferlin-deficient skeletal muscle. *Am. J. Pathol.* **2010**, *176*, 2891–2900. [CrossRef]
21. Young, C.N.; Brutkowski, W.; Lien, C.F.; Arkle, S.; Lochmuller, H.; Zablocki, K.; Gorecki, D.C. P2X7 purinoceptor alterations in dystrophic mdx mouse muscles: Relationship to pathology and potential target for treatment. *J. Cell. Mol. Med.* **2012**, *16*, 1026–1037. [CrossRef]
22. Cea, L.A.; Puebla, C.; Cisterna, B.A.; Escamilla, R.; Vargas, A.A.; Frank, M.; Martinez-Montero, P.; Prior, C.; Molano, J.; Esteban-Rodriguez, I.; et al. Fast skeletal myofibers of mdx mouse, model of Duchenne muscular dystrophy, express connexin hemichannels that lead to apoptosis. *Cell. Mol. Life Sci.* **2016**, *73*, 2583–2599. [CrossRef] [PubMed]
23. Gorecki, D.C. P2X7 purinoceptor as a therapeutic target in muscular dystrophies. *Curr. Opin. Pharmacol.* **2019**, *47*, 40–45. [CrossRef]
24. Sinadinos, A.; Young, C.N.; Al-Khalidi, R.; Teti, A.; Kalinski, P.; Mohamad, S.; Floriot, L.; Henry, T.; Tozzi, G.; Jiang, T.; et al. P2RX7 purinoceptor: A therapeutic target for ameliorating the symptoms of duchenne muscular dystrophy. *PLoS Med.* **2015**, *12*, e1001888. [CrossRef] [PubMed]
25. Gazzerro, E.; Baratto, S.; Assereto, S.; Baldassari, S.; Panicucci, C.; Raffaghello, L.; Scudieri, P.; De Battista, D.; Fiorillo, C.; Volpi, S.; et al. The Danger Signal Extracellular ATP Is Involved in the Immunomediated Damage of alpha-Sarcoglycan–Deficient Muscular Dystrophy. *Am. J. Pathol.* **2019**, *189*, 354–369. [CrossRef] [PubMed]
26. Nelson, D.W.; Gregg, R.J.; Kort, M.E.; Perez-Medrano, A.; Voight, E.A.; Wang, Y.; Grayson, G.; Namovic, M.T.; Donnelly-Roberts, D.L.; Niforatos, W.; et al. Structure-activity relationship studies on a series of novel, substituted 1-benzyl-5-phenyltetrazole P2X7 antagonists. *J. Med. Chem.* **2006**, *49*, 3659–3666. [CrossRef]
27. Pozsgai, E.R.; Griffin, D.A.; Heller, K.N.; Mendell, J.R.; Rodino-Klapac, L.R. β-Sarcoglycan gene transfer decreases fibrosis and restores force in LGMD2E mice. *Gene Ther.* **2016**, *23*, 57–66. [CrossRef]
28. Di Virgilio, F.; Dal Ben, D.; Sarti, A.C.; Giuliani, A.L.; Falzoni, S. The P2X7 Receptor in Infection and Inflammation. *Immunity* **2017**, *47*, 15–31. [CrossRef] [PubMed]
29. Young, C.N.; Sinadinos, A.; Lefebvre, A.; Chan, P.; Arkle, S.; Vaudry, D.; Gorecki, D.C. A novel mechanism of autophagic cell death in dystrophic muscle regulated by P2RX7 receptor large-pore formation and HSP90. *Autophagy* **2015**, *11*, 113–130. [CrossRef]
30. Young, C.N.J.; Chira, N.; Rog, J.; Al-Khalidi, R.; Benard, M.; Galas, L.; Chan, P.; Vaudry, D.; Zablocki, K.; Gorecki, D.C. Sustained activation of P2X7 induces MMP-2-evoked cleavage and functional purinoceptor inhibition. *J. Mol. Cell. Biol.* **2017**, *10*, 229–242. [CrossRef]
31. Panicucci, C.; Raffaghello, L.; Bruzzone, S.; Baratto, S.; Principi, E.; Minetti, C.; Gazzerro, E.; Bruno, C. eATP/P2X7R Axis: An Orchestrated Pathway Triggering Inflammasome Activation in Muscle Diseases. *Int. J. Mol. Sci.* **2020**, *21*, 5963. [CrossRef]
32. Savio, L.E.B.; de Andrade Mello, P.; da Silva, C.G.; Coutinho-Silva, R. The P2X7 Receptor in Inflammatory Diseases: Angel or Demon? *Front. Pharmacol.* **2016**, *9*, 52. [CrossRef] [PubMed]
33. Di Virgilio, F. Novel data point to a broader mechanism of action of oxidized ATP: The P2X7 receptor is not the only target. *Br. J. Pharmacol.* **2003**, *140*, 441–443. [CrossRef]
34. De Marchi, E.; Orioli, E.; Dal Ben, D.; Adinolfi, E. P2X7 Receptor as a Therapeutic Target. *Adv. Protein Chem. Struct. Biol.* **2016**, *104*, 39–79.
35. Beigi, R.D.; Kertesy, S.B.; Aquilina, G.; Dubyak, G.R. Oxidized ATP (oATP) attenuates proinflammatory signaling via P2 receptor-independent mechanisms. *Br. J. Pharmacol.* **2003**, *140*, 507–519. [CrossRef] [PubMed]
36. Figliuolo, V.R.; Chaves, S.P.; Santoro, G.F.; Coutinho, C.M.; Meyer-Fernandes, J.R.; Rossi-Bergmann, B.; Coutinho-Silva, R. Periodate-oxidized ATP modulates macrophage functions during infection with Leishmania amazonensis. *Cytom. A* **2014**, *85*, 588–600. [CrossRef]
37. Craighead, M.W.; Middlehurst, K.M.; LeFeuvre, R.; Kimber, I.; Rothwell, N.J. Oxidised adenosine 5′-triphosphate, a P2X(7) antagonist, is toxic to rat cerebellar granule neurones in vitro. *Neurosci. Lett.* **2001**, *311*, 77–80. [CrossRef]
38. Donnelly-Roberts, D.L.; Namovic, M.T.; Han, P.; Jarvis, M.F. Mammalian P2X7 receptor pharmacology: Comparison of recombinant mouse, rat and human P2X7 receptors. *Br. J. Pharmacol.* **2009**, *157*, 1203–1214. [CrossRef]
39. Honore, P.; Donnelly-Roberts, D.; Namovic, M.T.; Hsieh, G.; Zhu, C.Z.; Mikusa, J.P.; Hernandez, G.; Zhong, C.; Gauvin, D.M.; Chandran, P.; et al. A-740003 [N-(1-{[(cyanoimino)(5-quinolinylamino)methyl]amino}-2,2-dimethylpropyl)-2-(3,4-dimethoxyphenyl)acetamide], a novel and selective P2X7 receptor antagonist, dose-dependently reduces neuropathic pain in the rat. *J. Pharmacol. Exp. Ther.* **2006**, *319*, 1376–1385. [CrossRef] [PubMed]
40. McGaraughty, S.; Chu, K.L.; Namovic, M.T.; Donnelly-Roberts, D.L.; Harris, R.R.; Zhang, X.F.; Shieh, C.C.; Wismer, C.T.; Zhu, C.Z.; Gauvin, D.M.; et al. P2X7-related modulation of pathological nociception in rats. *Neuroscience* **2007**, *146*, 1817–1828. [CrossRef]

41. Teixeira, J.M.; Oliveira, M.C.; Parada, C.A.; Tambeli, C.H. Peripheral mechanisms underlying the essential role of P2X7 receptors in the development of inflammatory hyperalgesia. *Eur. J. Pharmacol.* **2010**, *644*, 55–60. [CrossRef] [PubMed]
42. Jimenez-Pacheco, A.; Mesuret, G.; Sanz-Rodriguez, A.; Tanaka, K.; Mooney, C.; Conroy, R.; Miras-Portugal, M.T.; Diaz-Hernandez, M.; Henshall, D.C.; Engel, T. Increased neocortical expression of the P2X7 receptor after status epilepticus and anticonvulsant effect of P2X7 receptor antagonist A-438079. *Epilepsia* **2013**, *54*, 1551–1561. [CrossRef]
43. Mesuret, G.; Engel, T.; Hessel, E.V.; Sanz-Rodriguez, A.; Jimenez-Pacheco, A.; Miras-Portugal, M.T.; Diaz-Hernandez, M.; Henshall, D.C. P2X7 receptor inhibition interrupts the progression of seizures in immature rats and reduces hippocampal damage. *CNS Neurosci. Ther.* **2014**, *20*, 556–564. [CrossRef]
44. Marcellino, D.; Suárez-Boomgaard, D.; Sánchez-Reina, M.D.; Aguirre, J.A.; Yoshitake, T.; Yoshitake, S.; Hagman, B.; Kehr, J.; Agnati, L.F.; Fuxe, K.; et al. On the role of P2X(7) receptors in dopamine nerve cell degeneration in a rat model of Parkinson's disease: Studies with the P2X(7) receptor antagonist A-438079. *J. Neural Transm.* **2010**, *117*, 681–687. [CrossRef] [PubMed]
45. Khalafalla, M.G.; Woods, L.T.; Camden, J.M.; Khan, A.A.; Limesand, K.H.; Petris, M.J.; Erb, L.; Weisman, G.A. P2X7 receptor antagonism prevents IL-1β release from salivary epithelial cells and reduces inflammation in a mouse model of autoimmune exocrinopathy. *J. Biol. Chem.* **2017**, *292*, 16626–16637. [CrossRef]
46. Sociali, G.; Visigalli, D.; Prukop, T.; Cervellini, I.; Mannino, E.; Venturi, C.; Bruzzone, S.; Sereda, M.W.; Schenone, A. Tolerability and efficacy study of P2X7 inhibition in experimental Charcot-Marie-Tooth type 1A (CMT1A) neuropathy. *Neurobiol. Dis.* **2016**, *95*, 145–157. [CrossRef] [PubMed]
47. Folker, E.S.; Baylies, M.K. Nuclear positioning in muscle development and disease. *Front. Physiol.* **2013**, *4*, 363. [CrossRef] [PubMed]
48. Gentile, D.; Natale, M.; Lazzerini, P.E.; Capecchi, P.L.; Laghi-Pasini, F. The role of P2X7 receptors in tissue fibrosis: A brief review. *Purinergic Signal.* **2015**, *11*, 435–440. [CrossRef]
49. Villalta, S.A.; Rosenberg, A.S.; Bluestone, J.A. The immune system in Duchenne muscular dystrophy: Friend or foe. *Rare Dis.* **2015**, *3*, e1010966. [CrossRef]
50. Ingersoll, M.A.; Platt, A.M.; Potteaux, S.; Randolph, G.J. Monocyte trafficking in acute and chronic inflammation. *Trends Immunol.* **2011**, *32*, 470–477. [CrossRef]
51. Mojumdar, K.; Liang, F.; Giordano, C.; Lemaire, C.; Danialou, G.; Okazaki, T.; Bourdon, J.; Rafei, M.; Galipeau, J.; Divangahi, M.; et al. Inflammatory monocytes promote progression of Duchenne muscular dystrophy and can be therapeutically targeted via CCR2. *EMBO Mol. Med.* **2014**, *6*, 1476–1492. [CrossRef]
52. Villalta, S.A.; Nguyen, H.X.; Deng, B.; Gotoh, T.; Tidball, J.G. Shifts in macrophage phenotypes and macrophage competition for arginine metabolism affect the severity of muscle pathology in muscular dystrophy. *Hum. Mol. Genet.* **2009**, *18*, 482–496. [CrossRef]
53. Kranig, S.A.; Tschada, R.; Braun, M.; Patry, C.; Poschl, J.; Frommhold, D.; Hudalla, H. Dystrophin deficiency promotes leukocyte recruitment in mdx mice. *Pediatr. Res.* **2019**, *86*, 188–194. [CrossRef]
54. Hodgetts, S.; Radley, H.; Davies, M.; Grounds, M.D. Reduced necrosis of dystrophic muscle by depletion of host neutrophils, or blocking TNFalpha function with Etanercept in mdx mice. *Neuromuscul. Disord.* **2006**, *16*, 591–602. [CrossRef] [PubMed]
55. Tulangekar, A.; Sztal, T.E. Inflammation in Duchenne Muscular Dystrophy-Exploring the Role of Neutrophils in Muscle Damage and Regeneration. *Biomedicines* **2021**, *9*, 1366. [CrossRef]
56. Arecco, N.; Clarke, C.J.; Jones, F.K.; Simpson, D.M.; Mason, D.; Beynon, R.J.; Pisconti, A. Elastase levels and activity are increased in dystrophic muscle and impair myoblast cell survival, proliferation and differentiation. *Sci. Rep.* **2016**, *6*, 24708. [CrossRef] [PubMed]
57. Al-Khalidi, R.; Panicucci, C.; Cox, P.; Chira, N.; Róg, J.; Young, C.N.J.; McGeehan, R.E.; Ambati, K.; Ambati, J.; Zabłocki, K.; et al. Zidovudine ameliorates pathology in the mouse model of Duchenne muscular dystrophy via P2RX7 purinoceptor antagonism. *Acta Neuropathol. Commun.* **2018**, *6*, 27. [CrossRef]
58. Pelegrin, P. Targeting interleukin-1 signaling in chronic inflammation: Focus on P2X(7) receptor and Pannexin-1. *Drug News Perspect.* **2008**, *21*, 424–433. [CrossRef] [PubMed]
59. Pelegrin, P.; Barroso-Gutierrez, C.; Surprenant, A. P2X7 receptor differentially couples to distinct release pathways for IL-1beta in mouse macrophage. *J. Immunol.* **2008**, *180*, 7147–7157. [CrossRef]
60. Pizzirani, C.; Ferrari, D.; Chiozzi, P.; Adinolfi, E.; Sandonà, D.; Savaglio, E.; Di Virgilio, F. Stimulation of P2 receptors causes release of IL-1beta-loaded microvesicles from human dendritic cells. *Blood* **2007**, *109*, 3856–3864. [CrossRef]
61. Kawamura, H.; Kawamura, T.; Kanda, Y.; Kobayashi, T.; Abo, T. Extracellular ATP-stimulated macrophages produce macrophage inflammatory protein-2 which is important for neutrophil migration. *Immunology* **2012**, *136*, 448–458. [CrossRef]
62. Villalta, S.A.; Rosenthal, W.; Martinez, L.; Kaur, A.; Sparwasser, T.; Tidball, J.G.; Margeta, M.; Spencer, M.J.; Bluestone, J.A. Regulatory T cells suppress muscle inflammation and injury in muscular dystrophy. *Sci. Transl. Med.* **2014**, *6*, 258ra142. [CrossRef] [PubMed]
63. Burzyn, D.; Kuswanto, W.; Kolodin, D.; Shadrach, J.L.; Cerletti, M.; Jang, Y.; Sefik, E.; Tan, T.G.; Wagers, A.J.; Benoist, C.; et al. A special population of regulatory T cells potentiates muscle repair. *Cell* **2013**, *155*, 1282–1295. [CrossRef]
64. Quattrocelli, M.; Zelikovich, A.S.; Salamone, I.M.; Fischer, J.A.; McNally, E.M. Mechanisms and Clinical Applications of Glucocorticoid Steroids in Muscular Dystrophy. *J. Neuromuscul. Dis.* **2021**, *8*, 39–52. [CrossRef] [PubMed]

65. Connolly, A.M.; Pestronk, A.; Mehta, S.; Al-Lozi, M. Primary alpha-sarcoglycan deficiency responsive to immunosuppression over three years. *Muscle Nerve* **1998**, *21*, 1549–1553. [CrossRef]
66. Angelini, C.; Fanin, M.; Menegazzo, E.; Freda, M.P.; Duggan, D.J.; Hoffman, E.P. Homozygous alpha-sarcoglycan mutation in two siblings: One asymptomatic and one steroid-responsive mild limb-girdle muscular dystrophy patient. *Muscle Nerve* **1998**, *21*, 769–775. [CrossRef]
67. Griffin, D.A.; Pozsgai, E.R.; Heller, K.N.; Potter, R.A.; Peterson, E.L.; Rodino-Klapac, L.R. Preclinical Systemic Delivery of Adeno-Associated α-Sarcoglycan Gene Transfer for Limb-Girdle Muscular Dystrophy. *Hum. Gene Ther.* **2021**, *32*, 390–404. [CrossRef] [PubMed]
68. Turan, S.; Farruggio, A.P.; Srifa, W.; Day, J.W.; Calos, M.P. Precise Correction of Disease Mutations in Induced Pluripotent Stem Cells Derived From Patients With Limb Girdle Muscular Dystrophy. *Mol. Ther. J. Am. Soc. Gene Ther.* **2016**, *24*, 685–696. [CrossRef]
69. Pozsgai, E.; Griffin, D.; Potter, R.; Sahenk, Z.; Lehman, K.; Rodino-Klapac, L.R.; Mendell, J.R. Unmet needs and evolving treatment for limb girdle muscular dystrophies. *Neurodegener. Dis. Manag.* **2021**, *11*, 411–429. [CrossRef] [PubMed]
70. Chu, M.L.; Moran, E. The Limb-Girdle Muscular Dystrophies: Is Treatment on the Horizon? *Neurotherapeutics* **2018**, *15*, 849–862. [CrossRef] [PubMed]
71. Escobar, H.; Krause, A.; Keiper, S.; Kieshauer, J.; Müthel, S.; de Paredes, M.G.; Metzler, E.; Kühn, R.; Heyd, F.; Spuler, S. Base editing repairs an SGCA mutation in human primary muscle stem cells. *JCI Insight* **2021**, *6*, e145994. [CrossRef] [PubMed]
72. Shokoples, B.G.; Paradis, P.; Schiffrin, E.L. P2X7 Receptors: An Untapped Target for the Management of Cardiovascular Disease. *Arterioscler. Thromb. Vasc. Biol.* **2021**, *41*, 186–199. [CrossRef] [PubMed]
73. Recourt, K.; van der Aart, J.; Jacobs, G.; de Kam, M.; Drevets, W.; van Nueten, L.; Kanhai, K.; Siebenga, P.; Zuiker, R.; Ravenstijn, P.; et al. Characterisation of the pharmacodynamic effects of the P2X7 receptor antagonist JNJ-54175446 using an oral dexamphetamine challenge model in healthy males in a randomised, double-blind, placebo-controlled, multiple ascending dose trial. *J. Psychopharmacol.* **2020**, *34*, 1030–1042. [CrossRef]
74. Duclos, F.; Straub, V.; Moore, S.A.; Venzke, D.P.; Hrstka, R.F.; Crosbie, R.H.; Durbeej, M.; Lebakken, C.S.; Ettinger, A.J.; van der Meulen, J.; et al. Progressive muscular dystrophy in alpha-sarcoglycan-deficient mice. *J. Cell. Biol.* **1998**, *142*, 1461–1471. [CrossRef] [PubMed]